The fate of platinum-group elements during weathering processes

- with a special focus on the pristine and weathered Platreef ore at the Mogalakwena Mine in the Bushveld Complex -

Von der Naturwissenschaftlichen Fakultät der
Gottfried Wilhelm Leibniz Universität Hannover

zur Erlangung des Grades

Doktor der Naturwissenschaften (Dr. rer. nat.)

genehmigte Dissertation
von
Malte Junge, M.Sc. (Niederlande)

[2017]

Referent: [Prof. Dr. François Holtz]
Koreferent: [Prof. Dr. Frank Melcher]
Tag der Promotion: [17.03.2017]

Keywords: Platreef, Bushveld Complex, platinum-group elements, platinum-group minerals, near-surface platinum-group element deposits, pentlandite

Schlagwörter: Platreef, Bushveld Komplex, Platingruppenelemente, Platingruppenminerale, oberflächennahe Platingruppenelement-Lagerstätten, Pentlandit

Table of Contents

List of Figures

List of Tables

Abstract

All main sources for economically relevant platinum-group elements (PGE) are associated with sulfide and chromite in mafic-ultramafic rocks. The Bushveld Complex of South Africa hosts the world's largest reserves and resources of PGE with the major PGE-ores being the Merensky Reef, the UG-2 chromitite, and the Platreef. Mining operations of the UG-2 and the Merensky Reef are mainly underground, but several open pits exist in the Bushveld Complex, most notably for the Platreef. The Platreef is an up to 400 m thick mineralized feldspathic pyroxenite with Pt and Pd contents of about 1 to 4 g/t. Pristine sulfide ores are processed by conventional crushing, grinding and froth flotation with recovery rates of Pt and Pd of up to 90%. Surface weathering in the area of the Bushveld Complex is 10 to 40 m from the surface. Attempts to recover Pt and Pd from these oxidized ore resulted in recoveries of «50%, despite the fact that Pt and Pd concentrations are similar in pristine and weathered ore. In general, weathered Platreef ores have a huge potential as total resources of 26 Moz PGE are estimated. In this study three boreholes covering a sequence of pristine into oxidized Platreef ore are studied in order to investigate the behavior of PGE during weathering.

Platinum-group elements are bimodally distributed in the pristine ore, occurring as discrete platinum-group minerals (PGM) or in the crystal lattice of sulfide and chromite. Platinum forms discrete PGM. Palladium occurs in a variety of discrete PGM and is incorporated in pentlandite. Rhodium is found in the form of discrete PGM but is also hosted in pentlandite. The IPGE (Os, Ir and Ru) are mainly hosted in laurite, PGE-sulfarsenides and in the chromite lattice (hundreds ppb-range). The differences between typical PGM assemblages in chromite-rich (dominant PGE-sulfarsenides, -arsenides and -sulfides; (Pt,Pd)-bismuthotellurides are largely absent) and sulfide-rich (dominant (Pt,Pd)-bismuthotellurides) ores indicate different behavior of Te, Bi, S, As during ore forming processes (fO_2 and fS_2, partition coefficient $D_{MSS/liquid}$, atomic radii). Sulfur saturation at the Platreef is partly caused by contamination with the country rocks as shown by $\delta^{34}S$ values ranging from 2 to 5‰ and late stage hydrothermal overprint is observed in the Platreef along strike. The sulfide mineralogy in the Platreef is dominated by pyrrhotite, chalcopyrite, pentlandite and minor pyrite. Along strike, sulfide mineralogy and the textures vary locally. The PGE mineralogy at the Platreef is similar along strike and is largely dominated by (Pt,Pd)-bismuthotellurides, cooperite-braggite and laurite.

The whole rock Pt and Pd contents remain in a similar range despite the fact that the Pt/Pd ratio increases from pristine to weathered ore due to the larger mobility of Pd. During weathering sulfide are destroyed and pyroxene and plagioclase break down to secondary minerals, such as kaolinite, smectite, Fe-oxy/hydroxides, Mn-phases and various clay minerals. Only relict PGM are present in the oxidized ore, being sperrylite and cooperite-braggite, whereas (Pt,Pd)-bismuthotellurides are rare. This indicates different stabilities of PGM during weathering processes, i.e. (Pt,Pd)-bismuthotellurides are less stable than cooperite-braggite and sperrylite. Altered and newly formed PGM are observed within weathered Platreef, UG-2, Merensky Reef and LG-MG chromitites. In general, PGE are polymodally distributed in the oxidized ore, i.e. PGE occurring in relict PGM, in iron- and manganese-oxides/hydroxides, or in secondary silicates. Secondary silicates and iron- and manganese oxides/hydroxides contain concentrations of Pt, Pd and Rh in the 100s ppm range. Platinum-group elements are not loosely attached to interstitial sites of clay minerals but are rather incorporated in the mineral structure or form stronger bonds in clay minerals.

Kurzfassung

Wirtschaftlichrelevante Vererzung von Platingruppenelementen (PGE) ist ausschließlich assoziiert mit mafisch-ultramafischen Gesteinen. Die weltweit größten Reserven und Ressourcen von PGE treten im Bushveld Komplex in Südafrika auf, wo die wichtigsten PGE-Erze das Merensky Reef, der UG-2 Chromitit und das Platreef sind. Diese Erze werden hauptsächlich im Untertagebergbau gefördert, allerdings gibt es auch diverse Tagebaubetriebe (insbesondere das Platreef). Das Platreef ist ein 400 m mächtiger feldspatreicher Pyroxenit mit durchschnittlichen Pt- und Pd-Gehalten von 1 bis 4 g/t. Unverwitterte sulfidische Erze werden mittels konventioneller Abbaumethoden und anschließender Flotation aufbereit. Ausbringraten liegen bei diesem Erztyp bei über 90%. Im Bushveld Komplex reicht die oberflächennahe Verwitterung bis zu einer Tiefe von 10 bis 40 m. Aufbereitungsversuche dieser verwitterten Erze erbrachte Ausbringraten von «50%. Allerdings wird dem verwitterten Platreef ein enormes Potential zugesprochen, da Berechnungen zufolge die gesamten Ressourcen dieser Erze bei 26 Moz PGE liegen. In dieser Arbeit wurden drei Bohrkerne, die frisches und verwittertes Platreeferz durchteufen untersucht, um die Verwitterungsprozesse von PGE Erze besser zu verstehen.

Im frischen, unverwitterten Erz, sind die PGE bimodal verteilt und treten sowohl als diskrete Platingruppenminerale (PGM) als auch eingebaut im Sulfid- und Chromitgitter auf. Platin bildet lediglich diskrete PGM. Palladium und Rh tretten in verschieden PGM und auch eingebaut im Pentlandit auf. Laurit und PGE-sulfarsenide bilden die Hauptträger für die IPGE (Os,Ir,Ru). Zusätzlich treten IPGE im Chromitgitter auf. Die Unterschide zwischen der PGM-Verteilung in chromitreichen (hauptsächlich PGE- Sulfarsenide, -Arsenide und -Sulfide; (Pt,Pd)-Bismuthotelluride fehlen) und sulfidreichen Erzen (hauptsächlich (Pt,Pd)-Bismuthotelluride) deuten auf unterschiedliches Verhalten von Te, Bi, S und As während erzbildener Prozesse hin (fO_2, fS_2, $D_{MSS/liquid}$, Atomradius). Im Platreef ist die Schwefelsättigung zumindest teilweise durch Kontamination mit dem Nebengestein hervorgerufen, wie anhand der Schwefelisotopie ersichtlich ist (δ^{34}S variiert von 2 bis 5‰). Spätere hydrothermale Überprägung wird entlang des Streichens vom Platreef beobachtet. Die Sulfidmineralisation im Platreef besteht hauptsächlich aus Pyrrhotin, Chalcopyrit, Pentlandit und geringere Anteile von Pyrit. Die Sulfidmineralisation und texturelle Unterschiede variieren entlang des Streichens vom Platreef. (Pt,Pd)-Bismuthotelluride, Cooperit-Braggit und Laurit bilden die häufigsten PGM im Platreef.

Die Gesamtgesteinskonzentrationen von Pt und Pt sind im primären und verwitterten Erz ähnlich, wobei das Pt/Pd Verhältnis im verwitterten Erz geringer ist als im primären. Dies ist auf die leichtere Mobilisation von Pd während der Verwitterung zurückzuführen. Während der Verwitterung werden Sulfide zerstört und Pyroxen und Plagioklas zerfallen zu sekundären Mineralphasen (z.B. Fe-Oxy/Hydroxide und diverse Tonminerale). Im verwitterten Erz werden lediglich geringe Anteile von PGM beobachtet. Diese sind hauptsächlich Cooperit-Braggit und Sperrylith, wohin gegen (Pt,Pd)-Bismuthotelluride selten sind. Dies weist auf unterschiedliche Stabilitäten von PGM während der Verwitterung hin. Verwitterte und neugebildete PGM treten im Platreef, UG-2, Merenky Reef und in den LG-MG Chromititen auf. Zusammenfassend, sind die PGE im verwitterten Erz sind polymodal verteilt und kommen als reliktische PGM, in Eisen- und Manganoxiden/hydroxiden oder in sekundären Silikaten vor. Sekundäre Silikate und Eisen- und Manganoxide/hydroxide haben Pt, Pd und Rh Konzentrationen im Bereich von mehreren 100 ppm. PGE sind nicht schwach in den Zwischengitterschichten von Tonmineralen gebunden, sondern absorptiv an Tonminerale oder sind direkt in die Mineralphasen eingebaut.

Abbreviations

ACTLABS	Activation Laboratories Limited (ACTLABS) in Ontario/Canada
AMS	(ultra-sensitive accelerator mass spectrometry)
BGR	Bundesanstalt fuer Geowissenschaften und Rohstoffe
	(German Federal Institute for Geosciences and Natural Resources)
BSE	Back-Scattered Electrons
CEC	Cation exchange capacity
EDX	Energy-Dispersive X-ray Spectroscopy
EELS	electron energy-loss spectroscopy
EPD	Electric-Pulse Disaggregation
EPMA	Electron probe microanalysis
FA-MS	Fire Assay Metallic Screen
FFT	Fourier transformation
FIB	Focussed Ion Beam
FTIR	Fourier transform infrared spectroscopy
GFZ	GeoForschungsZentrum
GST	Glass Separation Tube
HAADF	high-angle annular dark field imaging
HREM	high-resolution images
HS	Hydroseparation
ICP-MS	Inductively coupled plasma mass spectrometry
ICP-OES	Inductively Coupled Plasma Optical Emission Spectrometry
IMA	International Mineralogical Association
INAA	Instrumental Neutron Activation Analysis
IPGE	Iridium-Group-PGE
IR	Infrared spectroscopy
ISS	intermediate sulfide solid solution
LA-ICP-MS	Laser Ablation Inductively Coupled Plasma Mass Spectrometry

LG	Lower Group Chromitite
LOI	lost of ignition
MG	Middle Group Chromitite
MLA	Mineral liberation analysis
MSS	monosulfide solid solution
MSZ	Main sulfide zone
NFG	naturally floating gangue
nPGM	nanometersized platinum-group minerals
oz	Ounces Troy = 31.1034768 g
PGE	Platinum-group elements
PGM	Platinum-group minerals
PIXE	particle-induced X-ray emission
PPGE	Palladium-Group-PGE
SEM	Scanning Electron Microscope
SF-ICP-MS	sector field-inductively coupled plasma-mass spectrometer
SIMS	secondary ion mass spectrometry
STEM	scanning transmission mode
TD-ICP-MS	total digestion combined with inductively coupled plasma-mass spectrometer
TEM	Transmission Electron Microscopy
UG	Upper Group Chromitite
VCDT	Vienna Canyon Diablo Troilite
WDX	Wavelength Dispersive X-ray Spectroscopy
XAFS	X-ray absorption fine structure
XANES	X-ray absorption near edge structure
XRD	X-ray diffraction
XRF	X-ray fluorescence

Acknowledgments

I would like to thank Prof. Dr. François Holtz and Prof. Dr. Frank Melcher for their support during the last years. I thank them in particular for all the constructive and good discussions and advices. I would like to specially thank Dr. Thomas Oberthür for all his advices in the last years in Hannover and during field trips in South Africa and on various conferences. I am very grateful for his mentoring and for his thoroughly reviews of my work. I would also like to thank my colleagues Anna and Simon for reviewing my manuscripts and for the helpful discussions at various locations and moments. Many thanks also to Dr. Dennis Krämer and Prof. Dr. Michael Bau for the very nice sampling campaign in South Africa at the beginning of this project and for various discussions on conferences and meetings. I am very grateful to Jacques Roberts and Robert Schouwstra for giving me access to the Mogalakwena Mine and to the sample material.

This work highly benefited by the excellent polished sections which were prepared by Peter Rendschmidt, Donald Henry, Manfred Frey and Ulf Hemmerling. Electron probe microanalysis was ably performed by Jerzy Lodziak, Christian Wöhrl, and Dr. Simon Goldmann. Many thanks also to Dominic Göricke for his support during my SEM work. I also gratefully acknowledge the support of Dieter Weck, Dr. Kristian Ufer, Dr. Stephan Kaufhold and Dr. Reiner Dohrmann from the BGR for XRD and IR analysis.

Finally, many thanks to my colleagues at the BGR and the PhD students at the Institute for Mineralogy for a very nice time and last but definitely not least I would like to thank my family and friends for all their support and understanding during the last years.

Outline

This thesis contains four publications which are included as separate chapters (Chapter 4, 6, 7 and 8). The first chapters describe the aim of the study and summarize the previous work on pristine and weathered PGE deposits and the general knowledge about platinum-group elements and associated deposits (Chapter 1). A brief review about the geology and mineralization of the Bushveld Complex forms Chapter 2. The samples used in this study and the analytical methods are summarized in Chapter 3. The subsequent chapters are split into a general part about the distribution of PGE in pristine Platreef and UG-2 ores with a special focus on the distribution of PGE in pentlandite (Chapter 4), followed by a the results of the studied drill cores of the Platreef ore, including the overall petrography, mineralogy, mineral chemistry of pentlandite as well as a comparison between sulfur isotopes and S-Se ratios (Chapter 5). More detailed results of the distribution of PGE in pristine and near-surface Platreef ores are presented and discussed in Chapter 6. These chapters - describing the distribution of PGE in pristine and near-surface Platreef ore - are followed by a section about the UG-2 chromitite (Chapter 7). The third main results part describes and discusses the chromitites of the Lower and Middle Group of the Bushveld Complex (Chapter 8). A general discussion with additional arguments which have not been discussed in the previous chapters is presented as Chapter 9 and all data are summarized in Chapter 10. Chapter 11 gives some ideas about further research needed related to pristine and near-surface PGE ores.

Chapter 1

Introduction

In this chapter the aim of this thesis is explained. Additionally, the previous work on near-surface PGE ores, experiments on the mobility of PGE, and attempts of processing oxidized PGE ores are summarized.

1.1 Aim of the study

All economic sources of platinum-group elements (PGE) are associated with mafic-ultramafic rocks in either a sulfide or chromite environment. The major deposits are regionally limited as the world's PGE production only originates from South Africa, Zimbabwe, Russia, Canada, the United States of America, Finland and Colombia. The Bushveld Complex of South Africa hosts the world's largest reserves and resources of PGE with resources of Pt and Pd of about 68% Pt and 39% Pd (Vermaak 1995). New estimations of the contained metal in mineral resources by Zientek et al. (2014) show for Pt 38 kt and for Pd 13 kt. The major PGE ores of the Bushveld Complex are the Merensky Reef, the UG-2 chromitite, and the Platreef. Mining operations at the UG-2 and the Merensky Reefs are mainly underground, whereas several large open pits are in operation, most notably for the Platreef which is an up to 400 m thick rock package. Pristine sulfide ores are processed by conventional crushing, grinding and froth floatation with recovery rates of Pt and Pd of up to 90% (Liddell et al. 1986, Rule 1998, Bulatovic 2003). The mafic-ultramafic rocks in the Bushveld Complex are strongly weathered down to 10 to 40 m from surface (Wagner 1929, Hey 1999). Sulfides and platinum-group minerals (PGM) are largely

destroyed during weathering processes, but PGE contents remain in a similar range as in the pristine ores (Locmelis 2005, Locmelis et al. 2010). Early attempts to recover Pt and Pd from oxidized ore by flotation resulted in recoveries of considerably less than 50% (Prendergast 1988, Evans 2002, Becker et al. 2014). At present, on active open mining sites at the Platreef, near surface PGE ore is stockpiled (Evans 2002, Buchholz & Foya 2015). A huge potential for the oxidized PGE ore of the Bushveld Complex has been calculated, with about 337 Mt containing 517 t of 4E (Pt, Pd, Rh and Au) (Buchholz & Foya 2015). So far, detailed knowledge about the mobility of PGE during weathering processes and a characterization of the distribution of PGE in the oxidized ore is lacking. However, this knowledge is essential to design an extraction method for recovery of PGE from oxidized ore.

The aim of this study is to characterize the distribution of PGE in pristine and oxidized PGE ores and to evaluate the incorporation or adsorption of PGE to secondary mineral phases. Oxidized PGE ores from the Bushveld Complex are a potential new resource for low-cost production once new extraction methods have been designed based on the mineralogical characterization of these ores.

In order to characterize pristine and oxidized PGE ores, the following methods were employed: whole rock geochemistry, ore microscopy, X-ray diffraction (XRD), scanning electron microscopy (SEM), mineral liberation analysis (MLA), electron probe microanalysis (EPMA), laser ablation-inductively coupled plasma-mass spectrometry (LA-ICP-MS) and transmission electron microscopy (TEM).

1.2 Physical and chemical properties of platinum-group elements

The six transition metals ruthenium (Ru), rhodium (Rh), palladium (Pd), osmium (Os), iridium (Ir) and platinum (Pt) are grouped together to PGE due to their similar physical and chemical properties. Platinum-group elements have high melting points, excellent electrical conductivities, unique catalytical properties and great resistance to chemical attack. Especially the catalytical properties lead to high interest of the automotive sector for the use in autocatalysts.

Platinum-group elements together with Fe, Co and Ni belong to the group VIII transition elements (Figure 1.1). Together with Ag and Au, PGE are often named as precious metals. The PGE are subdivided according to their specific densities (Figure 1.1 and Table 1.1) into light PGE (Ru, Rh and Pd with densities of 12.10 g/cm^3, 12.41 g/cm^3 and 12.02 g/cm^3, respectively) and heavy PGE (Os, Ir and Pt with densities of 22.59 g/cm^3, 22.56 g/cm^3 and 21.45 g/cm^3, respectively). A further more common subdivision is based on the differences in melting temperatures: Iridium group PGE (IPGE) (Ru, Os and Ir with melting temperatures of 2334°C, 3033°C and 2446°C, respectively) and the Palladium group PGE (PPGE) (Rh, Pd and Pt with melting temperatures of 1964°C, 1555°C and 1768°C, respectively).

Goldschmidt (1937), in his classic work on the laws of element distribution, showed that the PGE are predominantly siderophile but may also show chalcophile affinities. The siderophile character of the PGE favors the formation of metallic bonds over ionic bonds. The chalcophile character of PGE indicates that PGE together with Cu, Ag and Au form covalent bonds with sulfur in preference to ionized bonds with oxygen.

Table 1.1 also shows the relative abundances of the naturally occurring PGE isotopes and the electron configuration of the respective PGE.

25 Mn 1246°C ~7.21 g/cm³	26 Fe 1538°C 7.87 g/cm³	27 Co 1495°C 8.90 g/cm³	28 Ni 1455°C 8.90 g/cm³	29 Cu 1085°C 8.96 g/cm³
43 Tc 2157°C 11.50 g/cm³	44 Ru 2334°C 12.10 g/cm³	45 Rh 1964°C 12.41 g/cm³	46 Pd 1555°C 12.02 g/cm³	47 Ag 962°C 10.50 g/cm³
75 Re 3185°C 20.80 g/cm³	76 Os 3033°C 22.59 g/cm³	77 Ir 2446°C 22.56 g/cm³	78 Pt 1768°C 21.45 g/cm³	79 Au 1064°C 19.30 g/cm³

Figure 1.1 – Physical properties of PGE in the periodic table with atomic number, melting temperature and density (at 20°C). The IPGE (Ru, Os and Ir) are highlighted in blue and the PPGE (Rh, Pd and Pt) in green. The heavy PGE are marked with red font and the light PGE white font. Data taken from Lide (2010).

Table 1.1 – Physical properties of PGE (Lide 2010), isotope data obtained from Rosman & Taylor (1998) and atomic radii from Slater (1964).

	Ru	**Rh**	**Pd**	**Os**	**Ir**	**Pt**
Atomic number	44	45	46	76	77	78
Atomic weight	101.07	102.91	106.42	109.23	192.22	195.08
Density [g/cm^3]	12.10	12.41	12.02	22.59	22.56	21.45
Melting temp.(25°C)	2334	1964	1555	3033	2446	1768
Atomic radius m	1.30	1.35	1.40	1.30	1.35	1.35
electron configuration	[Kr]4d^{7}5s	[Kr]4d^{8}5s	[Kr]4d^{10}	[Xe]4f^{14}5d^{6}6s^2	[Xe]4f^{14}5d^{7}6s^2	[Xe]4f^{14}5d^{10}6s
Isotopes (relative abundance)	^{96}Ru (5.54%)	^{103}Rh (100%)	^{102}Pd (1.02%)	^{184}Os (0.02%)	^{191}Ir (37.3%)	^{190}Pt (0.01%)
	^{98}Ru (1.87%)		^{104}Pd (11.1%)	^{186}Os (1.59%)	^{131}Ir (62.7%)	^{192}Pt (0.78%)
	^{99}Ru (12.8%)		^{105}Pd (22.3%)	^{187}Os (1.96%)		^{194}Pt (33.0%)
	^{100}Ru (12.6%)		^{108}Pd (26.5%)	^{188}Os (13.2%)		^{195}Pt (33.8%)
	^{101}Ru (17.1%)		^{110}Pd (11.7%)	^{189}Os (16.1%)		^{196}Pt (25.2%)
	^{102}Ru (31.6%)			^{190}Os (26.3%)		^{198}Pt (7.16%)
	^{104}Ru (18.6%)			^{192}Os (40.8%)		

1.3 Platinum-group minerals

Platinum-group elements generally occur as discrete PGM or in solid solution in the crystal lattice of sulfide and chromite (Wagner 1929, Cabri et al. 1981, Cabri 2002, Oberthür et al. 1997a, Locmelis et al. 2011, Osbahr et al. 2013, 2014, Junge et al. 2014, 2015b, Pagé & Barnes 2016). The atomic or ionic radii of elements play a particularly important role for their ability to enter into the lattice of other minerals (Goldschmidt 1926). Platinum-group minerals occur as a wide range of different minerals, such as sulfides, arsenides, tellurides, bismuthides, antimonides, selenides and as alloys (Cabri 2002). Reviews of PGM have been published by Cabri (1976, 1981), Tarkian & Bernhardt (1984) and Daltry & Wilson (1997). Daltry & Wilson (1997) reviewed the until 1996 approved PGM (96 in total) and minerals which contain varying concentrations of one or more of the six PGE. Cabri (2002) describes all 109 PGM being recognized by the Commission on New Minerals and Mineral Names, International Mineralogical Association until 2002. However, new PGM have been and are continuously being discovered and described afterwards (e.g. garutiite [Ni,Fe,Ir] as presented by McDonald et al. (2010) and palladosilicide [Pd_2Si] as reported by Cabri et al. (2015)). Table 1.3 shows the 138 PGM which have been approved by the International Mineralogical Association (IMA) until November 2016.

Decay systems such as ^{190}Pt-^{186}Os and ^{190}Pt-^{4}He have been successfully applied for dating PGE mineralization including PGM from the Bushveld Complex (Nowell et al. 2008, Coggon et al. 2011, 2012, Shukolyukov et al. 2012a,b, Yakubovich et al. 2015). These systems also allow the determination of the formation age of PGM in placer deposits, which is otherwise difficult to constrain. These information can give ideas about the source of PGM and also about deformation events effecting PGE mineralization such as at the Platreef in the Bushveld Complex.

Table 1.2 – List of all the 138 PGM approved by the IMA with ideal formulae and crystal system. Data taken from Cabri (2002), MinDat.org (2016) and IMA (2016). hex=hexagonal, iso=isometric, mono=monoclinic, ortho=orthorhombic, tri=triclinic.

name	**formulae**	**system**	**name**	**formulae**	**system**
anduoite	$RuAs_2$	ortho	irarsite	(Ir,Ru,Rh,Pt)AsS	iso
arsenopalladinite	$Pd_8As_{2.5}Sb_{0.5}$	tri	iridarsenite	$(Ir,Ru)As_2$	mono
atheneite	$(Pd,Hg)_3As$	hex	iridium	Ir	iso
atokite	$(Pd,Pt)_3Sn$	iso	isoferroplatinum	Pt_3Fe	iso
borishanskiite	$Pd^{+x}(As,Pb)_2$	ortho	isomertieite	$Pd_{11}Sb_2As_2$	iso
borovskite	Pd_3SbTe_4	iso	jacustingaite	Pt_2HgSe_3	tri
bortnikovite	Pd_4Cu_3Zn	tetra	jagueite	$Cu_2Pd_3Se_4$	mono
bowieite	$(Rh,Ir,Pt)_2S_3$	ortho	kalungaite	PdAsSe	iso
braggite	(Pt,Pd,Ni)S	tetra	kashinite	$(Ir,Rh)_2S_3$	ortho
cabriite	Pd_2CuSn	ortho	keithconnite	$Pd_{20}Te_7$	tri
changchengite	IrBiS	iso	kharaelakhite	$(Cu,Pt,Pb,Fe,Ni)_9S_8$	ortho
chengdeite	Ir_3Fe	iso	kingstonite	$(Rh,Ir,Pt)_3S_4$	mono
cherepanovite	RhAs	ortho	kitagohaite	Pt_7Cu	iso
chrisstanleyite	$Ag_2Pd_3Se_4$	mono	kojonenite	$Pd_{7-x}SnTe_2$	tetra
coldwellite	Pd_3Ag_2S	iso	konderite	$Cu_3Pb(Rh,Pt,Ir)_8S_{16}$	hex
cooperite	PtS	tetra	kotulskite	Pd(Te,Bi)	hex
crerarite	$Pt_{2-x}(BiPb)_{11}(S,Se)_{11}$	tri	laflammeite	$Pd_3Pb_2S_2$	mono
cuproiridsite	$(Cu,Fe)Ir_2S_4$	iso	laurite	RuS_2	iso
cuprorhodsite	$(Cu,Fe)Rh_2S_4$	iso	lisiguangite	$PtCuBiS_3$	ortho
damiaoite	$PtIn_2$	iso	luberoite	Pt_5Se_4	mono
daomanite	$CuPtAsS_2$	ortho	lukkulaisvaaraite	$Pd_{14}Ag_2Te_9$	tetra
erlichmanite	OsS_2	iso	majakite	PdNiAs	hex
ferhodsite	$(Fe,Rh,Ni,Ir,Cu,Pt)_9S_8$	tetra	malanite	$Cu(Pt^{3+},Ir^{3+})_2S_4$	iso
ferronickelplatinum	Pt_2FeNi	tetra	malyshevite	$PdCuBiS_3$	ortho
ferrorhodsite	$(Fe,Cu)(Rh,Ir,Pt)_2S_4$	iso	maslovite	PtBiTe	iso
froodite	$PdBi_2$	mono	mayingite	IrBiTe	iso
gaotaiite	Ir_3Te_8	iso	menshikovite	$Pd_3Ni_2As_3$	hex
garutiite	(Ni,Fe,Ir)	hex	merenskyite	$(Pd,Pt)(Te,Bi)_2$	tri
genkinite	$(Pt,Pd,Rh)_4Sb_3$	tetra	mertieite I	$Pd_{11}(Sb,As)_4$	hex
geversite	$PtSb_2$	iso	mertieite II	$Pd_8(Sb,As)_3$	tri
hexaferrum	(Fe,Os,Ru,Ir)	hex	miasseite	$Rh_{17}S_{15}$	iso
hexamolybdenium	(Mo,Ru,Fe,Ir,Os)	hex	michenerite	PdBiTe	iso
hollingworthite	(Rh,Pt,Pd)AsS	iso	miessiite	$Pd_{11}Te_2Se_2$	iso
hongshiite	PtCu	tri	milotaiite	PdSbSe	iso
inaglyite	$Cu_3Pb(Ir,Pt)_8Sb_{16}$	hex	moncheite	$(Pt,Pd)(Te,Bi)_2$	tri
insizwaite	$Pt(Bi,Sb)_2$	iso	naldrettite	Pd_2Sb	ortho

nielsenite	$PdCu_3$	tetra	ruthenium	Ru	iso
niggliite	PtSn	hex	shuangfengite	$IrTe_2$	tri
norilskite	$(Pd,Ag)_2Pb$	tri	skaergaardite	PdCu	iso
omeiite	$(Os,Ru)As_2$	ortho	sobolsevskite	Pd(Bi,Te)	hex
oosterboschite	$(Pd,Cu)_7Se_5$	ortho	sopcheite	$Ag_4Pd_3Te_4$	ortho
osarsite	(Os,Ru)AsS	mono	sperrylite	$PtAs_2$	iso
osmium	Os	iso	stannopalladinite	$(Pd,Cu)_3Sn_2$	hex
oulankaite	$(Pd,Pt)_5(Cu,Fe)_4SnTe_2S_2$	tetra	stibiopalladinite	Pd_5Sb_2	hex
padmaite	PdBiSe	iso	stillwaterite	Pd_8As_3	tri
palarstanide	$Pd_5(Sn,As)_2$	hex	stumpflite	Pt(Sb,Bi)	hex
palladinite	(Pd,Cu)O	tetra	sudburyite	(Pd,Ni)Sb	hex
palladium	Pd	iso	sudovikovite	$PtSe_2$	tri
palladoarsenide	Pd_2As	mono	taimyrite	$(Pd,Cu,Pt)_3Sn$	ortho
palladobismutharsenide	$Pd_2(As,Bi)$	ortho	tatyanaite	$(Pt,Pd,Cu)_9Cu_3Sn_4$	ortho
palladodymite	$(Pd,Rh)_2As$	ortho	telargpalite	$(Pd,Ag)_3(Te,Bi)$	iso
palladosilicide	Pd_2Si	hex	telluropalladinite	Pd_9Te_4	mono
palladseite	$Pd_{17}Se_{15}$	iso	temagamite	Pd_3HgTe_3	tri
paolovite	Pd_2Sn	ortho	testibiopalladite	PdTe(Sb,Te)	iso
pasavaite	$Pd_3Pb_2Te_2$	ortho	tetraferroplatinum	PtFe	tetra
platarsite	PtAsS	iso	tischendorfite	$Pd_8Hg_3Se_9$	ortho
platinum	Pt	iso	tolovkite	IrSbS	iso
plumbopalladinite	Pd_3Pb_2	hex	toernroosite	$Pd_{11}As_2Te_2$	iso
polarite	Pd(Bi,Pb)	ortho	tulameenite	Pt_2CuFe	tetra
polkanovite	$Rh_{12}As_7$	hex	ungavaite	Pd_4Sb_2	tetra
potarite	PdHg	tetra	urvantsevite	$Pd(Bi,Pb)_2$	tetra
prassoite	$Rh_{17}S_{15}$	iso	vasilite	$(Pd,Cu)_{16}(S,Te)_7$	iso
rhodarsenide	$(Rh,Pd)_2As$	ortho	verbeekite	$PdSe_2$	mono
rhodium	Rh	iso	vincentite	Pd_3As	tetra
rhodplumsite	$Rh_3Pb_2S_2$	tri	vysotskite	(Pd,Ni)Sb	tetra
ruarsite	(Ru,Os)AsS	mono	xingzhongite	$(Cu,Pb,Fe)Ir_2S_4$	iso
rustenburgite	$(Pt,Pd)_3Sn$	iso	yixunite	Pt_3In	iso
ruthenarsenite	(Ru,Ni)As	ortho	zvyagintsevite	$(Pd,Pt,Au)_3(Pb,Sn)$	iso
rutheniridosmine	(Ir,Os,Ru)	hex	zaccariniite	RhNiAs	tetra

1.4 Primary ores and the formation of PGE ores

Platinum-group element mineralisation within ultramafic rocks is controlled by the presence of base metal sulfides. In these ores, the PGEs are bimodally distributed, occurring both as discrete platinum-group minerals and hosted by sulfides. Especially, pentlandite [$(Fe,Ni)_9S_8$] is known to contain elevated concentrations of Pd and Rh (Cabri & Laflamme 1981, Todd et al. 1982, Cabri et al. 1984, Oberthür et al. 1997a, 2003, Gervilla et al. 2004, Godel et al. 2007, Holwell & McDonald 2010, Osbahr et al. 2013, 2014, Junge et al. 2014). Platinum-group minerals are usually associated with sulfides and occur either enclosed in sulfides or at the grain boundaries (Figure 1.2A,B,D). In rare cases PGM occur enclosed in chromite grains (Figure 1.2C).

In general, and in in particular the Platreef, sulfide assemblages are typically made up of pyrrhotite, pentlandite and chalcopyrite (Holwell & McDonald 2006). Platinum-group minerals are mostly (Pt,Pd)-tellurides with some (Pt,Pd)-sulfides, sperrylite [PtA_2] and Pd bismuthides (Holwell et al. 2005, Holwell & McDonald 2006).

The six PGE generally occur together in rocks and ores, mostly associated with Ni-Cu and Cr-deposits. The average PGE contents in the Earth's crust are about 1 to 7 ppb (Clarke & Washington 1924, McDonough & Sun 1995, Smith & Huyck 1999, Ridley 2013) and concentrations of PGE in ore deposits are in the range of 1 to 15 ppm.

A good correlation exists between rock types and metals for the formation of certain metal ore deposits: ultramafic rocks are associated with Ni, Cr and PGE, gabbro and norites with Cu, Co, Ni, Fe, Ti and V, andesite and intermediate intrusive rocks with Cu and Au and granites with Be, Li, Sn and W (Pohl 2011). The association of rock type and certain metals is understood as a result of the geochemical behaviour of the different metals during fractional crystallization of silicate melt bodies (Goldschmidt 1954). All major PGE deposits on Earth are associated with mafic-ultramafic intrusions and occur in three major groups as (i) stratiform mineralisation within mafic-ultramafic intrusions, often referred to as reefs, (ii) as a by-product of major Ni-Cu sulfide deposits and in minor amounts in (iii) placer deposits (Weiser 2002, Naldrett 2004a, Cawthorn et al. 2005, Maier 2005, Godel 2015).

In order to form magmatic sulfide deposits, it is essential to reach sulfide saturation, the point when the magma cannot hold sulfur anymore in solution (Naldrett 2004a, Holwell & Mc-

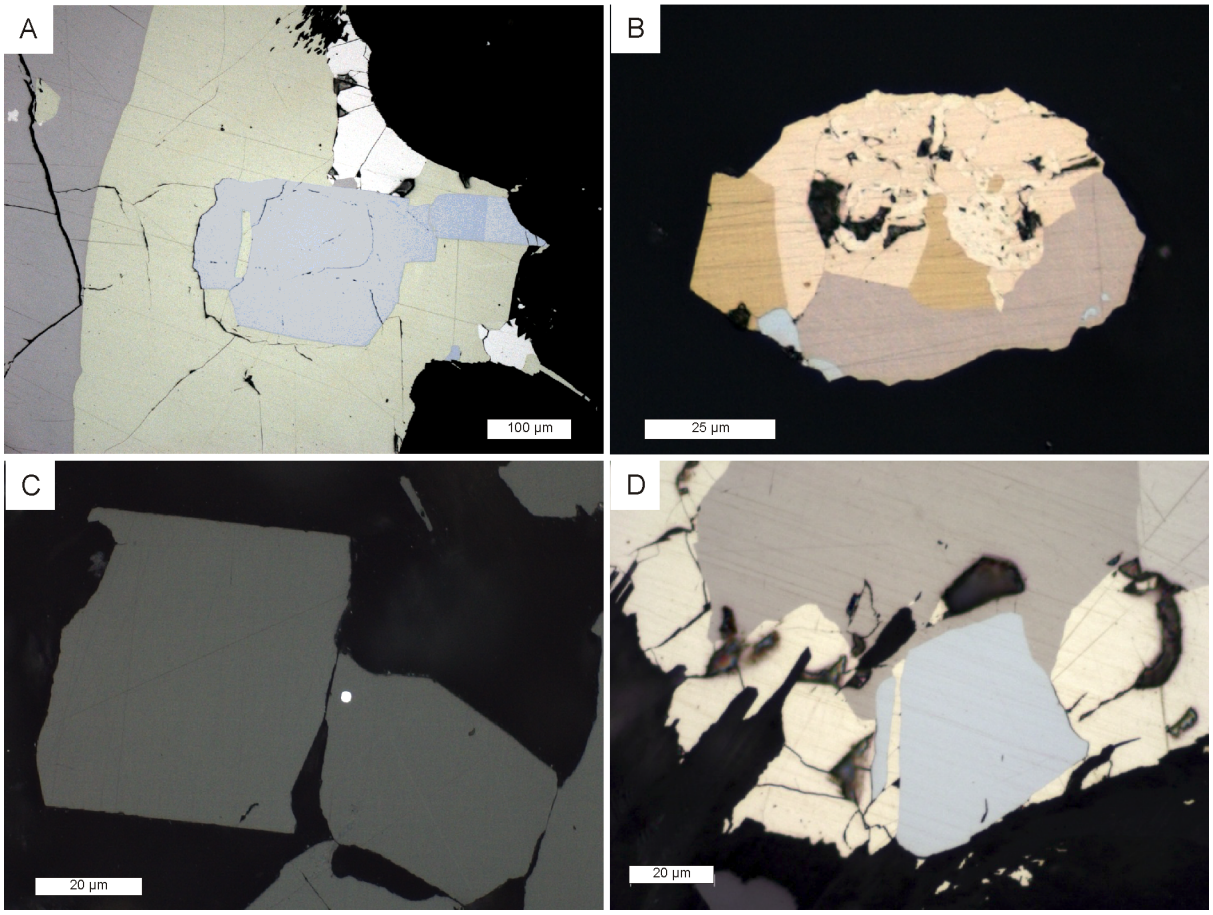

Figure 1.2 – Photomicrographs of platinum-group minerals in oil. A. Braggite (blue) in sulfide assemblage consisting of chalcopyrite (yellow), pyrrhotite (red-brown) and pentlandite (creme). Note the anisotropy of braggite. Merensky Reef, western Bushveld Complex (AS887b). B. Braggite in sulfide assemblage. UG-2, western Bushveld Complex (AS8917a). C. Laurite (white) in chromite (grey). Platreef, northern Bushveld Complex (AS10432). D. Braggite in sulfide assemblage. Merensky Reef, western Bushveld Complex (AS8890).

Donald 2010). Sulfur is incompatible in the crystallizing silicate phases and the sulfur concentration therefore steadily increases during magma fractionation until the sulfur concentration reaches the point where an immiscible sulfide liquid is formed which then can segregate through the crystallizing magma. The sulfide saturation (Figure 1.3) depends on various factors, i.e. temperature, pressure, oxygen fugacity, melt composition and in particular the Fe content of the melt (Naldrett & von Gruenewaldt 1989). In addition sulfide saturation may be caused by external factors such as mixing of magma with different composition and assimilation of the country rocks by primitive magmas (Godel 2015).

Two main mechanisms of PGE concentration in mafic-ultramafic rocks are under debate, i.e. chromite and sulfur control. For chromitite systems, various studies about the mechanism of PGE concentration and in particular their mode of occurrence (in the lattice of chromite or associated sulfide, as metal clusters, or as discrete PGM) exist (Tredoux et al. 1995, Cawthorn 1999a, Mathez 1999, Maier 2005, Finnigan et al. 2008, Mungall 2010). Scoon & Teigler (1994) defined the term "chromite control" as "*a process thought to involve a combination of direct nucleation of PGMs and localized S saturation*".

The close association between PGE enrichment and sulfide has always dominated the hypotheses about the genesis of PGE ores such as the Merensky Reef (Vermaak 1976, Campbell et al. 1983, Naldrett et al. 1986, 2009). Naldrett et al. (2009) defined two different models for the formation of the Merensky Reef, (i) the PGE concentration took place from below ("Uppers") and (ii) from the overlying magma ("Downers"). It is argued that the concentration and association of PGE with sulfide-rich rocks is controlled by the partition coefficient "D" which relates the concentration of an element in the sulfide and silicate liquids. This partition coefficient is in the order of at least 10^4 and possibly as high as 10^7 which makes sulfide melts an excellent collector of PGE (Campbell et al. 1983, Fonseca et al. 2009). The association of PGE with sulfide is explained by the fact that the heavy sulfide droplets migrate through the magma chamber and during migration these droplets collect chalcophile elements such as PGE. In addition to the high distribution coefficient factor, the time period for how long the sulfide droplets migrate through the silicate melt as well as the amount of available silicate melt itself, affect the concentrations of PGE in the sulfide droplets. Besides PGE there are also various other chalcophile elements (semimetals such as Bi, Te, As) which may later act as a partner for the formation

of discrete PGM. Campbell & Naldrett (1979) defined the "R-factor" as a silicate/sulfide liquid mass ratio and described the partition coefficient between sulfide and silicate melt and the bulk metal concentrations by Equation 3.4:

$$C_{Sul} = C_0 D^{Sul/Sil} \frac{R+1}{R+D^{Sul/Sil}} \tag{1.1}$$

where C_0 equals the concentration of a given metal in the original silicate liquid, $D^{Sul/Sil}$ is the partition coefficient between sulfide and silicate liquid and R is the mass ratio of silicate to sulfide liquid. A high R-factor describes the situation in which an immiscible sulfide droplet migrates through a large portion of silicate magma from which it derived and could therefore collect a large amount of PGE. This situation is an analogue to a turbulent flow or where a immiscible sulfide droplet sinks through a large magma column, which both allows an effective interaction with the silicate melt. A low R-factor, on the other hand, rather describes the situation in which a sulfide droplet is static or in which the sulfide droplet is removed early from the silicate melt and could therefore not collect any further PGE.

Thus, in the case of PGE deposits with a high R-factor, if small amounts of sulfide in a magma chamber are formed the PGE concentration in sulfides will be high (Campbell et al. 1983). When the R-factor is low for the case if the amount of sulfide formed is larger relative to the host magma, the PGE concentration in the sulfide will be diluted and may not be to sufficient to form economic deposits.

The PGE may occur as metal clusters within the sulfide liquid as proposed by Tredoux et al. (1995) and Ballhaus & Sylvester (2000), and illustrated in Figure 1.4. The sulfide droplets are enriched in PGE and other chalcophile elements (like Ni, Cu, Au and Co), but differences in the compatibilities exist in the newly formed monosulfide solid solution (MSS) and intermediate sulfide solid solution (ISS) and fractionation takes place (Barnes & Maier 1999, Barnes et al. 2001, Fleet & Stone 1991, Fleet et al. 1999b,a, Mungall et al. 2005). At high temperatures (>1100°C) the first phase crystallizing from the immiscible sulfide liquid is MSS and partitioning of elements such as Ni, Cu and Co takes place due to their different compatibilities. In general, Ni is compatible with MSS and will partition into it at the early stage (Holwell & McDonald 2010). A residual Cu-rich liquid remains which crystallizes to ISS at around 900°C

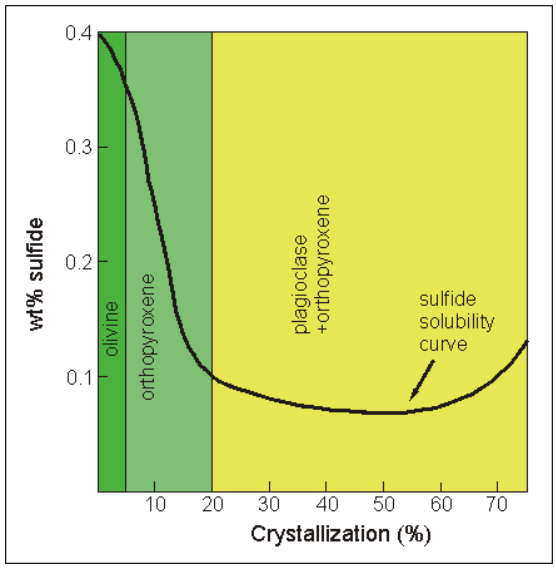

Figure 1.3 – Schematic diagram showing the sulfide solubility curve and illustrating sulfur saturation. Modified after Naldrett & von Gruenewaldt (1989).

(Holwell & McDonald 2010). During further cooling, recrystallization of ISS and MSS takes place forming pentlandite and pyrrhotite from the MSS and chalcopyrite from the ISS forming the characteristic magmatic sulfide assemblages (Figure 1.4). The precise temperature range of the recrystallisation of the MSS largely depends on the amount of sulfur in the MSS (Naldrett 2004b). The PGE - in particular Pt - may dissolve from the sulfide liquid to form discrete PGM depending on the availability of semimetals. The crystallization of MSS and ISS and the subsequent recrystallisation to pentlandite, pyrrhotite and chalcopyrite also affects the distribution of PGE which occur either incorporated in the sulfide lattices or as discrete PGM at the grain boundaries of the sulfide aggregates. Various studies investigated the partitioning of PGE during cooling of a sulfide liquid to magmatic sulfide assemblages via MSS and ISS (Fleet & Stone 1991, Fleet et al. 1993, Li et al. 1996, Barnes et al. 1997, Fleet et al. 1999a,b, Barnes et al. 2001, Mungall et al. 2005).

Magmatic sulfide deposits can be divided into two major groups, (i) Ni and Cu ores with PGE as byproducts (e.g., Noril'sk, Kambalda, Voisey's Bay, Pechenga) and (ii) those of value primarily because of PGE (e.g., UG-2, Merensky Reef, Platreef, JM reef of the Stillwater, Main Sulfide Zone of the Great Dyke, Lac des Iles) (Naldrett 2004a). Layered intrusions, such as the Bushveld Complex and the Skaergard intrusions are of particular interest for the study of PGE deposits. Detailed review books on layered intrusions were edited by Cawthorn (1996), Charlier

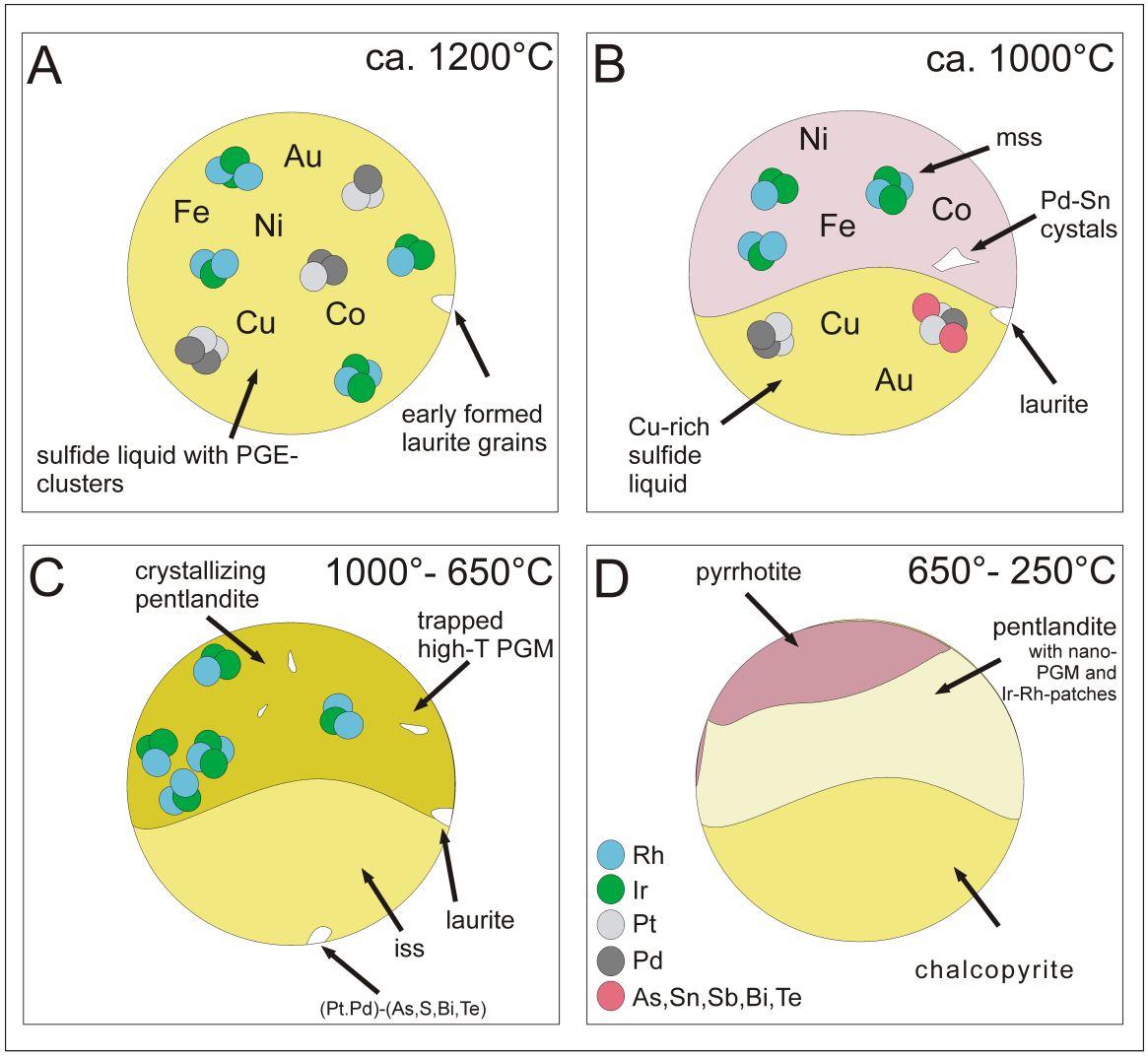

Figure 1.4 – Collection of PGE by magmatic sulfide droplets in the form of metal clusters, discrete PGM or in solid solution in the sulfide minerals. Modified after Holwell & McDonald (2010).

et al. (2015) and early work by Wager & Brown (1968). Secondary, hydrothermal redistribution and concentrations of PGE from zones with lower grade disseminated sulfides may also cause the development of a PGE deposit (Naldrett et al. 2008).

Fractionation of PGE is often demonstrated by using the Pt/Pd ratio and by normalizing the data to primitive mantle or chondrite, which is thought to represent the primordial material from which the Earth was formed. In ophiolites PGE concentrations are roughly chondritic (0.1 to 1) for the IPGE but only 0.01 times chondritic for Pt and Pd. The contrary is shown on the chondrite normalized PGE distribution pattern for the stratiform deposits of the Bushveld Complex as Pt and Pd reach four times chondrite concentrations (Figure 1.5). In general, IPGE are enriched in the early crystalline phases which were formed in mafic melts, whereas Pt, Pd and Au rather segregate into residual liquids (Pohl 2011).

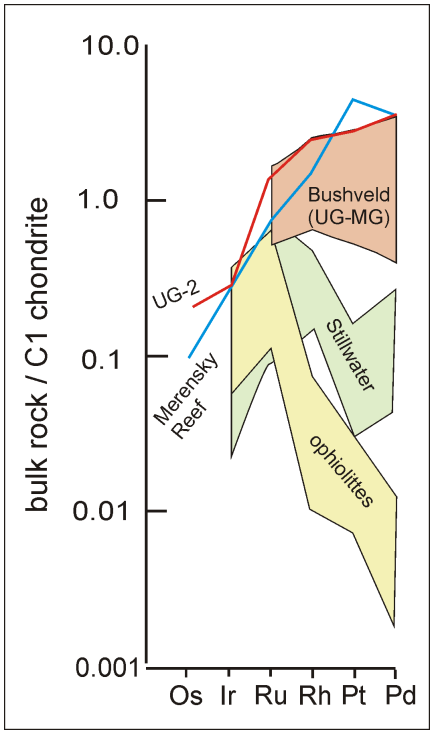

Figure 1.5 – Chondrite-normalized distribution pattern of ophiolites and major PGE deposits. Modified after Naldrett & von Gruenewaldt (1989).

Platinum-group element deposits exist in various associations in mafic-ultramafic rocks, showing similarities and different characteristics. Table 1.3 summarizes these typical PGE mineralisation types.

Merensky-type mineralization is characterized by the presence of disseminated base-metal

sulfides (<5 vol.%). The host rocks have various compositions from harzburgite, pyroxenite, troctolite, norite to anorthosite (Godel 2015). Deposits of this type include the Merensky Reef of the Bushveld Complex, the JM Reef of the Stillwater Complex and the Main Sulfide Zone of the Great Dyke of Zimbabwe. The Merensky Reef (Figure 1.6A) is a pegmatoidal pyroxenite usually bordered by two thin chromitite layers forming a narrow PGE reef that constitutes, after the UG-2 chromitite, the second largest PGE resource in the world and occurs 15 to 400 m above the UG-2 chromitite in the Bushveld Complex (Lee 1996). The Merensky Reef has average PGE grades of 4 to 9 g/t (Von Gruenewaldt et al. 1986, Von Gruenewaldt & Merkle 1995, Cawthorn 1999a).

Chromitite-type mineralization is usually enriched in all PGE compared to the hosting silicate rocks in the PGE deposits and PGE ores such as the Great Dyke, Bushveld Complex, Rum intrusion (Hiemstra 1979, Von Gruenewaldt et al. 1986, Lee & Parry 1988, Teigler & Eales 1993, Naldrett 2009, 2011, Naldrett et al. 2011, O'Driscoll et al. 2014). In the Bushveld Complex all chromitite layers (Figure 1.6B-C) are enriched in PGE but the UG-2 chromitite has the highest PGE grades and currently is the only chromitite layer mined for PGE in the Bushveld Complex and elsewhere in the world. The UG-2 chromitite has average PGE contents of 4 to 8 g/t (Von Gruenewaldt et al. 1986, Von Gruenewaldt & Merkle 1995, Cawthorn 1999a). For the association of IPGE with chromite different ideas exist. (i) IPGE partition into the chromite grains forming solid solution (Capobainco & Drake 1990, Locmelis et al. 2011, Brenan et al. 2012, Pagé et al. 2012, Pagé & Barnes 2016) and (ii) IPGE exhibit low solubility in mafic magma and crystalize as IPGE-rich minerals during chromite crystallization.

Contact-type mineralizations are located at or near the base of the sidewall of a layered intrusion. Examples for contact-type PGE mineralization are the Platreef in the Bushveld Complex as shown for example by McDonald & Holwell (2011), Yudovskaya et al. (2011) and Chapter 2.3, the Portimo Complex in northern Finland (Alapieti & Lahtinen 2002), various orebodies at the base of the Duluth Complex in the USA (Miller et al. 2002) and the Feodorov-Panski intrusion in Russia (Dubrovsky & Rundqvist 2009). Sulfide contents are in general higher than in other PGE mineralizations with contents of 5 to 10%. Generally, various amounts of xenoliths of the country rocks generally occur within the mineralization. Various studies describe the crustal contamination using isotopes affecting the sulfur signature and PGE distribution in

contact-type mineralization (Barnes & Maier 2002a, Holwell et al. 2007, Penniston-Dorland et al. 2008, Pronost et al. 2008, Reisberg et al. 2011, Roelofse 2012, Sharman et al. 2013). The Platreef is an up to 400 m thick ore deposit mined by open pit methods. The PGE grades average 1 to 3 ppm in the Platreef (Cawthorn et al. 2002b) and are lower than in the Merensky Reef and the UG-2 chromitite but due to the large thickness of the mineralization the Platreef represents one of the most economically important PGE deposits on Earth.

Dunite pipes in the Bushveld Complex (Figure 1.6D-E) may contain extraordinary high concentrations of PGE of up to 200 g/t but are now mined out. Four major PGE-rich dunite pipes are known in the eastern Bushveld Complex: Onverwacht, Mooihoek, Driekop and Twyfelaar (Wagner 1929, Stumpfl & Tarkian 1982, Viljoen 1985, Scoon & Mitchell 2004, Melcher & Lodziak 2007).

Alaskan-type complexes, also Ural-Alaskan-type complexes, are pipe-like concentrically zoned ultramafic-mafic complexes whose size is generally less than 80 km^2 (Taylor 1967, Johan 2002). The core is dunitic surrounded successively by olivine-clinopyroxenite, biotite and hornblende clinopyroxenite, hornblendite, and a monazonite-gabbro rim (Johan 2002, Naldrett 2004a). Typical alaskan-type complexes are in Russia (the Urals), United States (Alaska), Canada (British Columbia), Ethiopia (Yubdo area), Australia (New South Wales) and Colombia (Choco district) (Johan 2002). These types of ultramafic-mafic complexes were the major source for PGE before the discovery of the PGE reefs in the Bushveld Complex. Alaskan-type complexes are extremely enriched in Pt with respect to Ru and Ir (Johan 2002). Platinum concentrations in silicate rocks of the Nizhny Tagil are normally <200 ppb but in the chromitites vary from 40 to 20,000 ppb (Ivanov 1996, Naldrett 2004a).

Besides the main types of Merensky, chromitite, contact and dunite-pipe ores, PGE are also processed as by-products from Ni-Cu deposits in Sudbury, Canada (*meteorite impact type*) and at Noril'sk, Russia and Jinchuan, China (*rift and continental-flood basalts-type*), as well as from *komatiite-types* as in Kambalda, Australia.

Before the discovery of the major PGE deposits as described above, PGE were mainly recovered from placer deposits in Russia and Colombia (Cabri et al. 1996, Weiser 2002). Nowadays, production from placer as for example at Kondyor in eastern Russia (Figure 1.6F) constitutes a minor supply of the World's PGE production.

Table 1.3 – Main characteristics and examples for PGE deposits types. Modified after Gunn (2014).

	characteristics	**Pt+Pd [g/t]**	**examples**
PGE-dominant			
Merensky type	extensive, laterally continuous, thin layers of ultramafic rocks in large layered mafic-ultramafic intrusions	5 to 7	Merensky Reef, Bushveld Complex; Main Sulfide Zone, Great Dyke; J-M Reef, Stillwater Complex
Chromitite type	similar to Merensky type with low sulfide contents	4 to 8	UG-2, Bushveld Complex; Lower chromitites, Stillwater Complex
Contact type	extensive, discontinuous mineralisation with low-grade Ni and Cu (by-product Ni and Cu; major PGE resources)	1 to 4	Platreef, Bushveld Complex; Duluth Complex; Portimo, Finland
Dunite pipes	very high-grade PGE mineralisation in discordant pipe-like dunite bodies of up to 1 km in diameter	3 to 2000	Onverwacht, Driekop, Mooihoek, Bushveld Complex
Alaskan-type	pipe-like concentrically zoned ultramafic-mafic complexes whose size is generally less than 80 km^2. The highest Pt concentration is associated with the chromitites	locally up to 20 g/t	Nizhny Tagil, Urals; Kondyor, Eastern Siberia; Tulameen Complex, British Columbia; Yubdo, Ethiopia
Ni and Cu dominant			
Meteorite impact	deposit in impact melt rocks and underlying radial and concentric fracture and breccia zones	1 to 10;	Sudbury
Rift and continental-flood basalts	in sub-volcanic sills feeding flood basalts associated with intercontinental rifting	2 to 100;	Noril'sk; Jinchuan
Komatiite	komatiitic volcanic and intusive rocks of Archean and Palaeoproterozoic	100s ppb	Kambalda; Pechenga; Thompson Belt; Ungava Belt

Figure 1.6 – Field exposures of different types of PGE mineralization. A: Outcrop of the Merensky Reef at the discovery site of Hans Merensky. B: UG-2 outcrop at Smoky Hills. C: Outcrop of the UG-1 at Dwars Rivers. D: Onverwacht pipe with magnesite veins. E: Driekop pipe. F: PGE placer deposit at Kondyor, Russia.

1.5 Mobility of platinum-group elements at supergene conditions

The recovery of oxidized PGE ore was problematic from the beginning of the exploitation of PGE deposits in South Africa. The Merensky Reef dips very shallow and therefore extend throughout the oxidation zone in which almost no sulfides are present and recovery rates were only about 50% (Schneiderhöhn 1931). Research work on PGE ores has been carried out for the Main Sulfide Zone in the Great Dyke of Zimbabwe (Evans 2002, Locmelis 2005, Oberthür & Melcher 2005, Locmelis et al. 2010, Oberthür et al. 2013a), the UG-2 chromitite (Hey 1999), the Merensky Reef (Korges 2014), the Stillwater Complex in Montana (Fuchs & Rose 1974) and the Lac de Iles deposit in Canada (Hattori & Cameron 2004). Furthermore, the distribution and mobility of PGE was studied in laterites in Sierra Leone, (Bowles 1986, 1994, Bowles et al. 1995), Madagascar, (Salpéteur & Jezequel 1992, Salpéteur et al. 1995), Cuba and the Dominican Republic (Aiglsperger et al. 2015b,a, 2016). Figure 1.7 shows field exposures of oxidized PGE ores in the LG and MG chromitites (Figure 1.7A), the UG-2 chromitite (Figure 1.7B), the Merensky Reef (Figure 1.7C) and the Platreef (Figure 1.7D). Within the oxidized PGE ores of the MSZ, the PGE are polymodally distributed, occurring in relict PGM and sulfides and unspecified amounts of the PGE are redistributed and either form secondary PGMs, are found in chemically and mineralogically badly characterized (Pt/Pd)-oxides or hydroxides, or in iron-hydroxides, Mn-Co-hydroxides, and in secondary silicates (Oberthür et al. 2013a). The sulfides are largely destroyed, partly releasing their base metal and PGE contents, and are replaced by iron oxides or hydroxides (Locmelis 2005, Oberthür & Melcher 2005, Locmelis et al. 2010, Oberthür et al. 2013a).

1.5.1 Geochemical behavior of platinum-group elements during weathering

The aqueous geochemistry regarding the solubility and mobility of PGE was studied as a geochemical exploration tool for PGE deposits and therefore experimental studies on the behaviour of PGE in surficial environments exist. Similarly, environmental studies on roadside dust, river

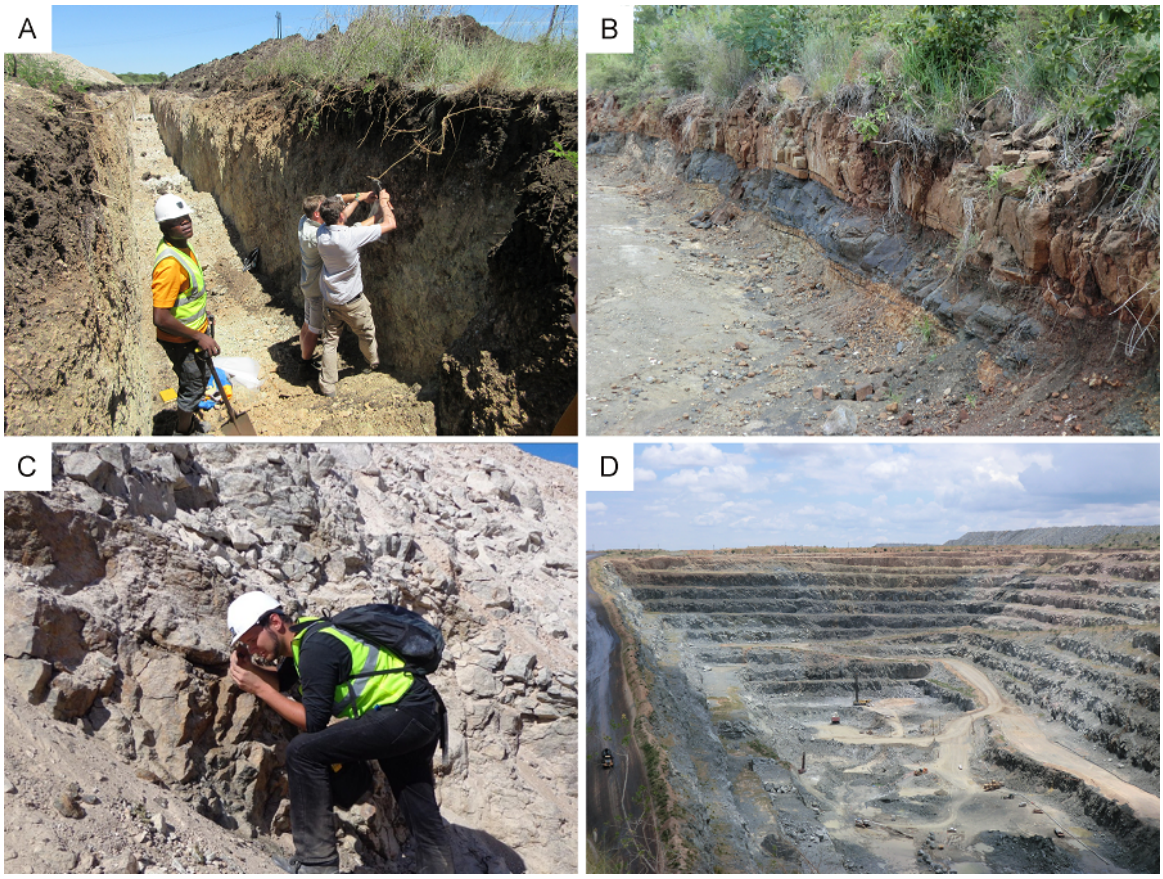

Figure 1.7 – Field exposures of oxidized PGE deposits. A: Soil sampling of oxidized LG- and MG-chromitites of the western Bushveld Complex at the Thaba Chrome Mine. B: Outcrop of oxidized UG-2 at Smokey Hills Mine, eastern Bushveld Complex. C: Outcrop of the Merensky Reef at Der Brochen eastern Bushveld Complex. D: Overysel open-pit at the Mogalakwena Mine indicating the weathering horizon (reddish colored rocks).

sediments and waste waters of hospitals due to the use of PGE as automobile catalysts and medical applications increased the current knowledge about PGE in near-surface and low temperature environments (Zereini et al. 1998, Ely et al. 2001, Jarvis et al. 2001, Tabler 2007, Prichard et al. 2009).

Schneiderhöhn & Moritz (1939) already pointed out that chlorine possibly is the best agent to extract Pt from oxidized sulfide-rich pyroxenite of the Merensky Reef since they were able to extract up to 65% of the Pt from flotation tailings using dilute HCl at 75°C for 5 h. Several studies showed that the Pt/Pd-ratio in the oxidized zone is higher than in the sulfide ore, arguing that Pd easily partitions into solution and can be transported out of the system (Wagner 1929, Hall 1932, Schneiderhöhn & Moritz 1939, Goldschmidt 1954, Ottemann & Ausustithis 1967, Fuchs & Rose 1974, Hey 1999, Locmelis 2005, Traore et al. 2006, Locmelis et al. 2010). Hattori & Cameron (2004) observed that near the Lac des Iles deposit in Canada, Pd migrates into solution from mineralization. Surface waters are typically pure and dilute in the Canadian Shield environment, which reflects high precipitation and low evaporation in cool climate (Cameron & Hattori 2005). For the case of the Platreef and the MSZ in southern Africa the climatic conditions and also the behavior of PGE during weathering are different to those in the Canadian Shield environment.

Fuchs & Rose (1974) studied the geochemical behavior of Pt and Pd in the weathering cycle in the area of the Stillwater Complex, Montana, USA. They worked on two different locations, where soils overlay PGE enrichments in small chromitite bodies and in sulfide-bearing ultramafic rocks. Fuchs & Rose (1974) observed that the depletion of Pd increases with the amount of weathering. Eh-pH relations demonstrate that Pd is more mobile in acid soils, probably being transported as chloride complexes. Platinum, in contrast, is only transported under very acidic conditions or within high-chloride complexes (Fuchs & Rose 1974). Figure 1.8 shows the Eh-pH relation of the system Pd-Pt-H_2O-Cl at 25°C, in which the aqueous platinum chloride field is much more restricted than the aqueous palladium chloride field. Fuchs & Rose (1974) concluded that the most important factors for behavior of PGE during weathering processes are pH, Eh, chloride concentrations and how the PGE occur in the primary ore. Figure 1.9 shows a logfO_2-pH diagram, indicating the lower solubility of Pt. Platinum displays a solubility in pure water only under highly oxidizing conditions and limited pH values (pH <1 for Pt^{2+} and pH>8

for platinum hydroxyl complexes). Palladium is soluble over the pH range found in most near surface environments (4<pH<9) (Cabral et al. 2007). Solubility will be increased by inorganic and organic ligands (e.g. chloride and humic and fulvic acids).

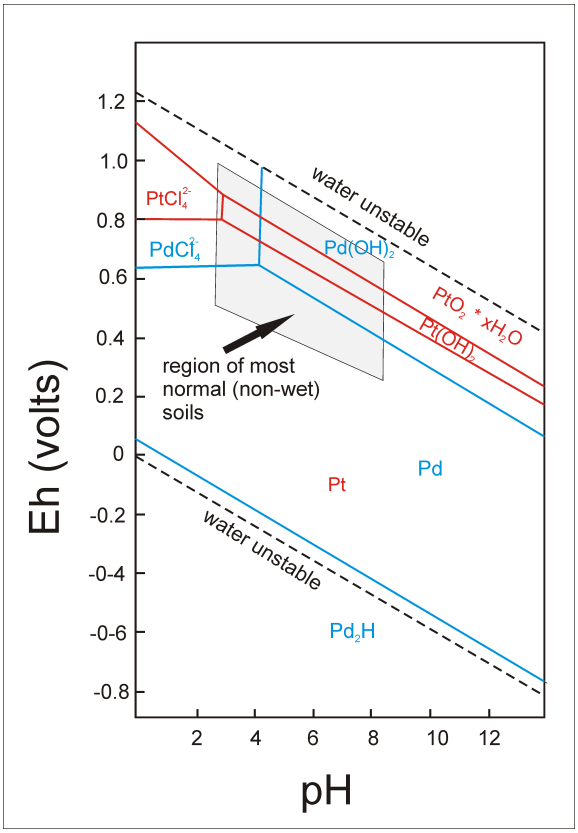

Figure 1.8 – Eh-ph diagram of the system Pd-Pt-H_2O-Cl at 25°C after Fuchs & Rose (1974).

When sulfides are being oxidized, PGE may also be mobilized in the form of thiosulfates and polysulfides in low-temperature environments (Wood et al. 1992). Hey (1999) argued that for the UG-2, channeling of permeating water through the inert chromite grains most of the sulfides are in contact with the percolating meteoric waters causing the mobilisation of PGE along the chromite grains.

Mountain & Wood (1988) conducted experimental studies in bisulfide-bearing systems at low temperatures and showed that in reduced, neutral pH, low temperature hydrothermal systems the bisulfide ion is an important ligand for PGE transport. Platinum-group elements may be also mobilized as hydroxides in the Pirogues ophiolite of New Caledonia (Augé & Legendre 1994).

Palladium is the most mobile PGE under hydrothermal and supergene conditions. Experiments on the solubility of Pd and complexation in chloride and bisulfide-rich fluids was

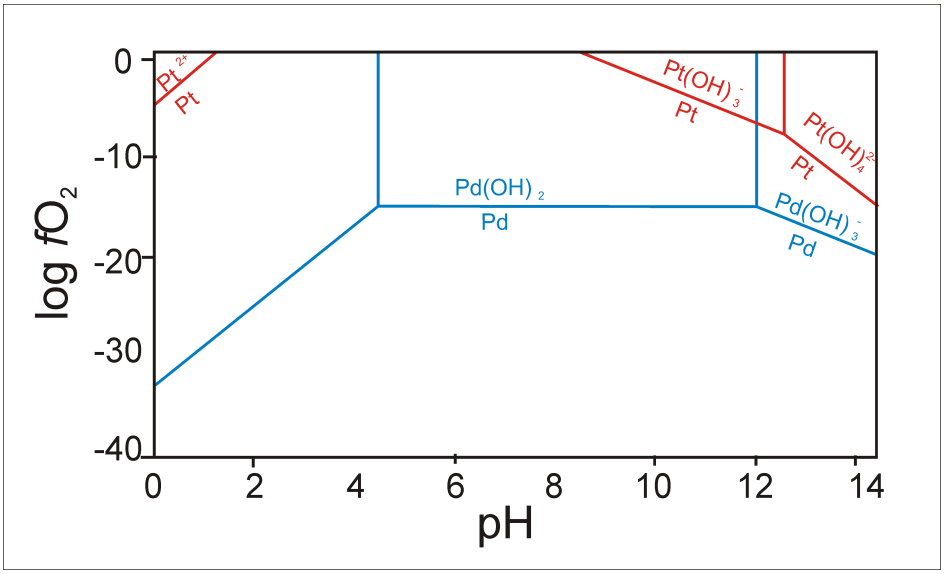

Figure 1.9 – Log fO_2-pH diagram of the system Pd-Pt-H_2O at 25°C after Cabral et al. (2007).

investigated Mei et al. (2015). Several studies describe the behavior of PGE under hydrothermal conditions; however, in low-temperature near-surface environments hydroxides, thiosulfates, sulfates and organic complexes are more likely to be the dominant carrier of PGE (Wood 2002).

1.5.2 The influence of organic matter

Various authors pointed out that organic ligands mobilized PGE (Cousins & Kinloch 1976, Bowles 1986, Wood & Vlassopoulos 1990, Bowles 1994, Bowles et al. 1995, Wood 1996, Reith et al. 2016). Experimental and theoretical studies showed that substances such as humic and fulvic acids increase the solubility of amorphous $Pt(OH)_2$ or $Pd(OH)_2$ (Wood 1990, Wood et al. 1994). Additionally, amino acids form strong bonds with Pt^{2+} and Pd^{2+} (Wood 1990, Wood & Van Middlesworth 2004) and carboxylic acids increase the solubility of $Pd(OH)_2$ and strongly bounded Pd^{2+} and Pd-oxalate complexes can therefore account for a large proportion of organic-bound Pd in acidic soils (Wood 2002). Another mechanism for the solubility of Pd^{2+} are siderophores which are naturally occurring ligands segregated by microbes in order to matabolize Fe (Normand & Wood 2005).

Platinum and Pd dissolve in solutions with fulvic, humic and other organic acids (Wood 1990, Wood et al. 1994, Bowles et al. 1995). Soluble organic complexes with humic acid, fulvic

acid, amino acid, acetate and oxalate exist for Pd in addition with hydroxyl complexes (Li & Byrne 1990, Wood 2002). For Pt, it is argued that the most important effect of humic and fulvic acids is to stabilize colloids (Wood 2002). The behavior of PGE in soils has been studied by Wood & Vlassopoulos (1990), Hattori & Cameron (2004) and Oppermann (2016). Oppermann (2016) studied soils at the Thaba chromite mine in the western Bushveld Complex and observed differences in the Pt and Pd contents in humic and fulvic acids; Pt concentrations are higher in the fulvic acids compared to humic acids, whereas no differences in the concentrations of Pd between these two acids were observed. Further, amino acids (with up to 50% of soil-hosted nitrogen) form strong complexes with Pt^{2+} and Pd^{2+} (Wood 1990, Wood & Van Middlesworth 2004) and carboxylic acids such as oxalate, acetate, malonate and citrate increase the solubility of amorphous $Pd(OH)_2$ and bounded strongly to Pd^{2+}, whereas Pd-oxalate complexes are accounting for a relevant part of organic-bound Pd in acidic soils (Wood 2002).

The influence of microorganism on the mobility of PGE was investigated by Reith et al. (2016). They studied PGM grains from Brazil, Australia and Columbia by SEM and showed that PGM grains are covered by biofilms. These biofilms contain nanoparticles of PGM and microcrystalline aggregates. It was suggested that some PGM grains are of biogenic origin.

1.5.3 Neoformation of platinum-group minerals

Schneiderhöhn (1931) proposed that within the oxidation zone of the Platreef, the PGM assemblage does not change on a large scale but that during the oxidation process Pt-bearing sulfides are destroyed and Pt precipitates as native metal grains. Platinum-group minerals have different stabilities, i.e. sperrylite is more stable than cooperite/braggite and PGE-bismuthotellurides are very unstable during weathering (Hey 1999, Oberthür et al. 1999, Evans 2002). Goldschmidt (1954) already described that laurite and sperrylite are fairly resistant to weathering.

Locmelis et al. (2010) studied oxidized MSZ ore and showed that PGE occur as relict primary PGM (e.g., sperrylite, cooperite-braggite), in solid solution in relict sulfide minerals, as secondary, neo-formed Pt-Fe alloys, PGE-oxides/hydroxides and as substituting or adsorbed cations in Fe- and Mn-oxides/hydroxides. Oberthür & Melcher (2005) estimated that circa 50% of Pt occurs as discrete PGM, 45% by hydroxides and 5% by relict sulfides.

The existence of newly formed PGM in low-temperature and near-surface environments

is still debated. Some studies argued that PGM are only formed under hypogene conditions (Cabri & Harris 1975, Brenan & Andrews 2001, Traore et al. 2006), whereas other authors propose that PGM can from in-situ after the mobilisation and re-deposition of PGE (Wagner 1929, Augusthitis 1965, Cousins & Kinloch 1976, Bowles 1986, Bowles et al. 2000, Garuti et al. 2012). Traore et al. (2006) studied the effects of weathering on Pt and Pd in a supergene environment in New Caledonia. Using SEM and EPMA they argue that the PGM are residual and are affected by dissolution processes and not the result of neoformations. Wagner (1929) described the occurrence of newly formed PGM in supergene rocks overlying the Merensky Reef. Bowles (1986) and Bowles et al. (2000) suggested that PGE nuggets in alluvial deposits have grown in-situ, partly as a result of precipitation from aqueous solutions.

Only limited knowledge exists about PGE oxides and PGE hydroxides (Weiser 1991, Augé & Legendre 1994, Jedwab 1995, Hey 1999, Melcher et al. 2005). Hey (1999) mentioned that some PGM of the oxidized UG-2 showed signs of alteration and that silicates in the vicinity of PGM have a brighter appearance than usually expected caused by the incorporation of PGE in the vicinity of altered PGM. Figure 1.10 shows backscattered electron images of various altered PGM and PGE-oxides. Platinum-group minerals in near-surface environments can show unweathered cores with rims of oxides.

The mineralogical identity of oxygen-bearing PGM has been investigated using X-ray micro-beam adsorption of oxygen-bearing Pt-Fe grains by Hattori et al. (2010). The adsorption spectra of the oxygen-bearing Pt-Fe grains have an additional peak caused by the presences of an Fe^{3+}-bearing phase such as ferrihydrite (Fe^{3+}-O-OH)). Thus, some grains, chemically resembling oxygen bearing Pt-Fe grains, are a mixture between ferrihydrite and relict isoferroplatinum.

Cousins & Kinloch (1976) pointed to the larger size of PGM in alluvial PGM samples compared to those in primary deposits. They investigated alluvial samples from the Urals (Nizhnii Tagil), Colombia (Rio Quito, Choco) and British Colombia (Discovery, Atlin, Bullion) as well as eluvial samples from Ethiopia (Yubdo). Besides the large size of these PGM, also the remarkable, almost perfect crystal shapes of PGM found in alluvial and eluvial locations are special for these PGM.

Formation of Pd hydroxide species as well as mixed hydroxyl-chloride species in oxidized,

near neutral to alkaline surface waters are of general interest in environments where the amount of available organic matter is extremely low (Hanley 2005). In the UG-2 chromitite Hey (1999) identified various PGE-oxides and PGE-hydroxides.

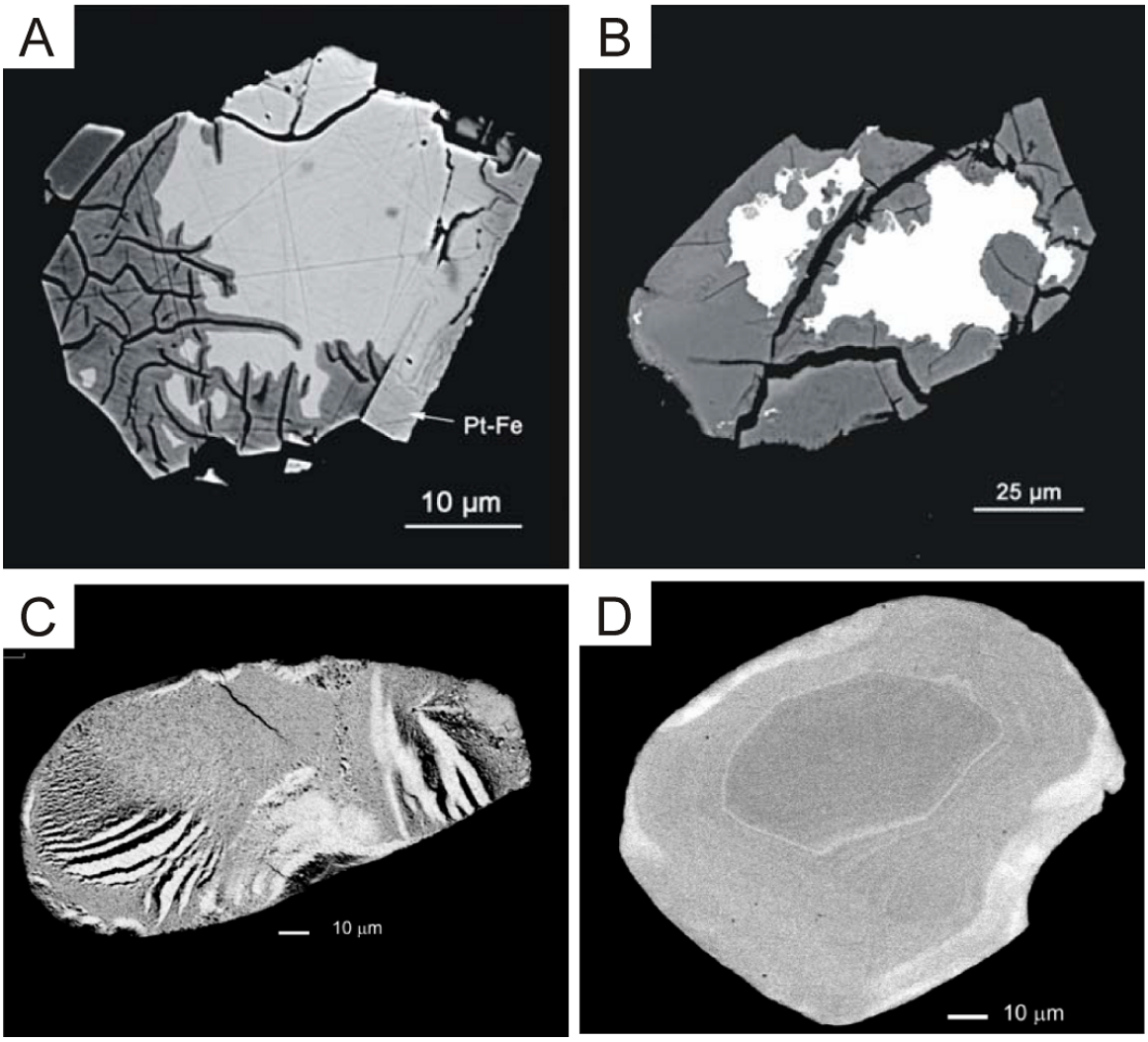

Figure 1.10 – Backscattered electron images of PGE-oxides. A. Pt-bearing sobolevskite [PdBi] (light gray) being replaced by Pd-Pt-Bi-oxide. Note attached Pt-Fe grain. Ngezi Mine, Great Dyke, Zimbabwe, Oberthür & Melcher (2005). B. Relict core of michenerite (white) surrounded by Pd-Bi-Cu-oxide (medium gray). Hartley Mine, Great Dyke, Zimbabwe Oberthür & Melcher (2005). C. Porous oxygen-bearing Pt-Fe. Pirogues Ophiolite, New Caledonia, Hattori et al. (2010). D. Concentrically zoned Pt-Fe-oxide. Pirogues Ophiolite, New Caledonia, Augé & Legendre (1994) and Hattori et al. (2010).

1.6 Supply and demand of platinum-group elements

The use of PGE is dominated by applications in the automobile industry as autocatalysts but also in jewellery and medicine (dental alloys and cancer treatments). Further uses are in hydrogen fuel cells and electronic components.

Global PGE production is limited to a few countries. The largest PGE producing countries are South Africa (in particular Pt) and Russia (mainly Pd). Before the discovery of the major ore deposits in southern Africa, PGE were mainly produced from placers in Colombia and the Urals in Russia. Figure 1.11 visualizes the annual production of PGE by country from 1900 to 2009. It shows that in the beginning of the 20th century production was largely limited to USSR (Russia) and Colombia were PGE are produced from placer deposits. Figure 1.11 also shows the beginning of the mining period of the UG-2 chromitite after optimizing benefication processes of the chromite ore and the major discovery of the PGE deposits in the Bushveld Complex and Sudbury in Canada in the 1920s.

Estimated PGE resources in these main PGE deposits are large and future supply of PGE is secure (Vermaak 1995, Cawthorn 1999a, Zientek et al. 2014). However, concerns exist for potential supply risks of PGE. For this reason the European Commission defined PGE as critical metals (European-Commission 2004, Gordon et al. 2006, Yang 2009). In general the current metal prices of PGE largely affect the mining industry in South Africa, however, the demand for PGE will steadily increase in the next decades as soon as countries such as China and India increase automobile production and improve environmental regulations which can affect the metal prices again. However, higher metal prices in the past caused large investments in exploration for new PGE deposits and junior companies carried out exploration programs. Exploration in the last decade resulted in the discoveries of new potential ore types in the Bushveld Complex. Ivanhoe Platinum started to build a mine in the western part of the current Platreef operations (Buchholz & Foya 2015). In the northern part of the Bushveld Complex intensive drilling campaign resulted in the new Waterberg deposit (Kinnaird et al. 2014, Buchholz & Foya 2015). Large proportions of PGE (in particular Pt, Pd and Rh) on the metal market originate also from recycling of autocatalysts and jewellery (up to 24% from the demand of Pt and 25% of Pd) and stock sales (Cowley 2013, Schmidt 2015).

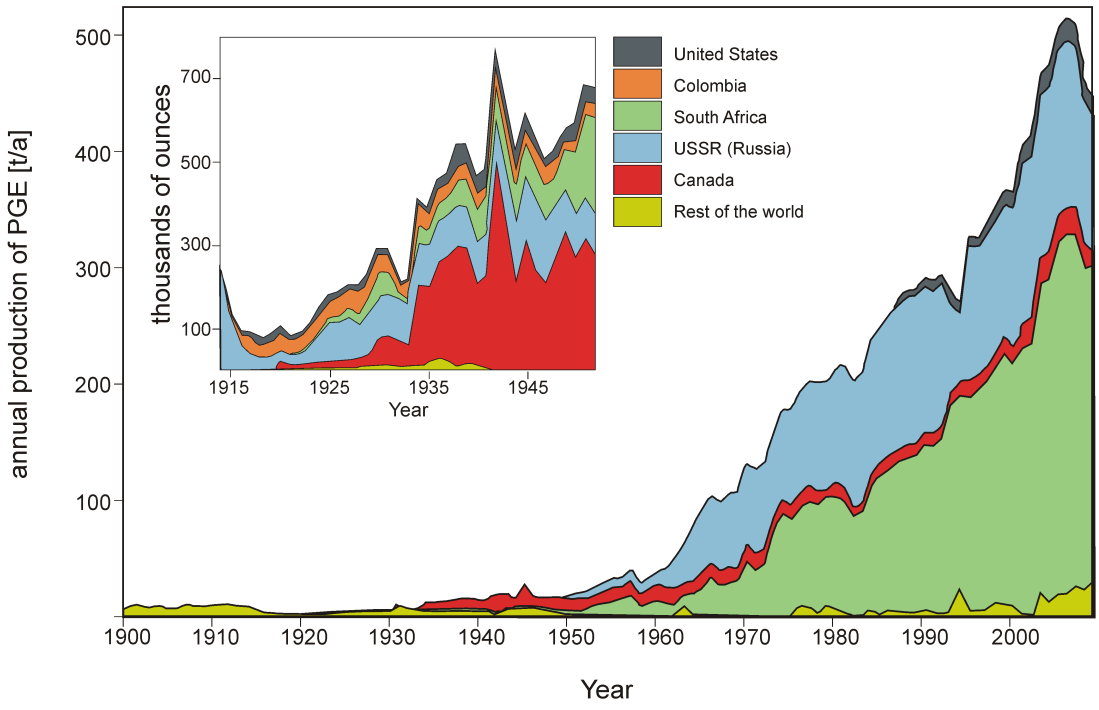

Figure 1.11 – Annual production of PGE by country from 1900 to 2010 showing the discoveries and start of main production of the individual deposits in the countries. The inset shows the first decades of PGE production of the 20th century indicating that the world's production was obtained mainly from placer deposits in Colombia and the Ural mountains in Russia before mining started in Sudbury (Canada) and the Bushveld Complex. Modified after Mudd (2012) and Zientek et al. (2014).

In the last years PGE producers in South Africa experienced various problems as the Pt price further decreased and labor costs increased after several miners strikes. In addition underground mining becomes significantly more expensive as depths of more than 2000 meters are reached. Low-cost open pit mining therefore becomes of greater importance and mining of the Platreef will significantly increase in the near future. The Pt and Pd price development is shown in Figure 1.12.

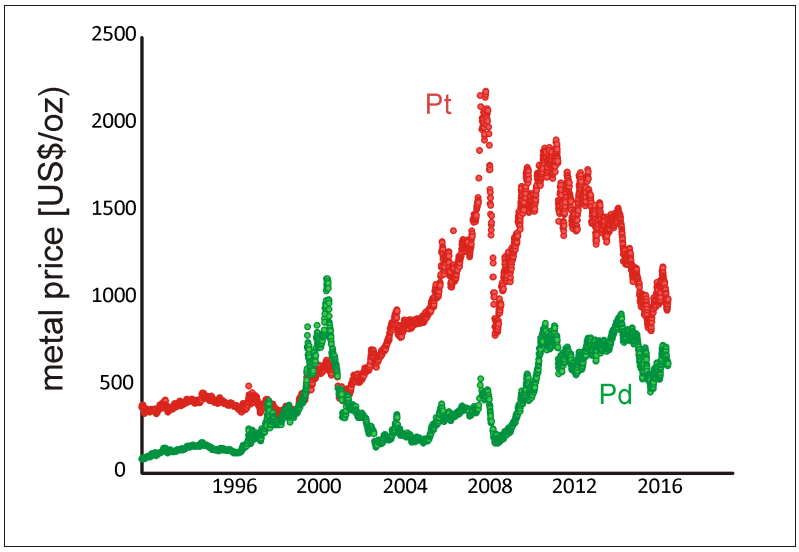

Figure 1.12 – Price development of Pt and Pd from July 1992 to November 2016. Data taken from Johnson Matthey (2016).

1.7 Recovery of platinum-group elements

The recovery of PGE and the grade of the concentrate largely depends on the mineralogy of the ore (Bulatovic 2003). Platinum-group elements occur in different types of ore deposits and type of mineralisation. In PGE deposits which are associated with base metal sulfides (the main source of PGE production), the amount of sulfides in these deposits may vary significantly. In these deposits naturally occurring gangue material exists representing a major problem in achieving a high-grade PGE concentrate (Bulatovic 2003). Platinum-group elements mineralisation associated with chromium deposits has different processing characteristics. A general process which is largely applied for the recovery of PGE is flotation. Flotation is a beneficiation process to concentrate fine-grained ore particles by transporting them attached to air bubbles to

the surface forming foam from which the ore can be separated (Penberthy et al. 2000). Sulfides are in particular well suited for this extraction since their surface properties have the ability to adhere to chemical reagents, which can then be removed (Penberthy et al. 2000). The small PGM grains usually float together with the sulfide minerals. The floatability of PGM has a large influence on the recovery by flotation. Platinum-group elements are hosted either in discrete PGM or in solid solution or as nanometersized platinum-group mineral (nPGM) inclusions in sulfides (Cabri & Laflamme 1981, Todd et al. 1982, Cabri et al. 1984, Oberthür et al. 2003, Gervilla et al. 2004, Godel et al. 2007, Holwell & McDonald 2010, Osbahr et al. 2013, 2014, Wirth et al. 2013, Junge et al. 2014, 2015b). The concentrate is further treated by smelting and refining in order to recover Ni, Cu, Co and PGE. Processing procedures differ between Merensky Reef and UG-2 due to the variation in the major gangue minerals, grain sizes of sulfide minerals and noble metal minerals (Liddell et al. 1986). Processing of PGE from placer deposits makes up only a minor contribution to the World's PGE production. Concentrating PGE from these deposit types is made by simple crushing and density separation in larger machines, or by artisanal panning.

An attempt to mine oxidized MSZ ores was undertaken at the Old Wedza Mine at the Great Dyke of Zimbabwe between 1926 and 1928, however, the results were uneconomic (Oberthür et al. 2013a). At the Smokey Hills mine in the eastern Bushveld Complex, oxidized UG-2 ore has been added to the conventional flotation process which resulted in low PGE recoveries (Mines online, 2014). Becker et al. (2014) studied oxidized Merensky Reef from the Pilanesberg Platinum mine in the western Bushveld Complex, where recovery rates of oxidized PGE ore are <40%, and tried to improve recoveries by flotation but without success. Therefore alternative technologies are required for processing oxidized PGE ore since flotation is not a successful technique for achieving significant recoveries.

Batch leaching experiments on PGE ores from the Great Dyke were carried out by Kraemer et al. (2015) using siderophores. These are biogenic complexing agents produced by bacteria and plants. In combination with a hydrochloric acid pre-treatment an extraction of Pt up to 80% was achieved.

Processing test work of oxidized PGE ore from the Great Dyke was done by Becker & Wotruba (2008). They used density (distributing jigger) and magnetic susceptibility as major properties for as separation techniques. However, their results showed that neither density nor

the magnetic susceptibility was useful in producing PGE concentrate from oxidized PGE ore. The highest contents of Pt and Pd are always concentrated in the fine fraction (<63 μm). In the case of the Hartley mine, Great Dyke (HOP 201 to 209; 1.39 ppm Pt, 0.83 ppm Pd), Becker & Wotruba (2008) showed that after conventional crushing and grinding 25% of a mix of the sample is in the fine fraction which contains 45% and 44% of Pt and Pd, respectively. At least this test work showed that mechanical processing of oxidized PGE ore is not possible since PGE are usually enriched in the fine fraction which makes mechanical processing impossible.

Locmelis et al. (2010) also used electric pulse disaggregation in order to get a mechanical separation of PGM and PGE-bearing phases. The bulk of the PGE is also present in the finest fraction.

Becker et al. (2012) demonstrated that hydroxamate co-collector AM 28 (a potassium hydrogen n-octanohydroxamate) increases recovery rates of oxidized Merensky Reef ore by flotation. The addition of NaHS and AM 28 in the presence of 500 g/t depressant resulted in recovery rates of up to 40%; highest Pt recovery was 52%, highest Pd: 20% (Becker et al. 2014).In order to decrease naturally floating gangue (NFG) it was shown that a depressant dosage of ca 300 g/t is sufficient to depress all the NFG in the Merensky Reef (Wiese et al. 2007). For oxidized Merensky Reef, Becker et al. (2014) used a depressant dosage of 750 g/t in order to fully depress all NFG. Competitive bubble loading may cause lower recovery rates by flotation since the attachment of PGM to the bubbles may be reduced if competitive bubble loading exists (Becker et al. 2014). Controlled potential sulfidization is a process whereby a non-sulfide mineral surface is converted to a sulfide-like surface (Becker et al. 2014). However, sulfidization usually only works on a laboratory scale but not in the processing plant due to various factors such as conditioning time, type of collector, preparation procedures (Bulatovic 2010).

Chapter 2

The Bushveld Complex

The ultramafic-mafic rocks of the Bushveld Complex in South Africa (Figure 2.1), were emplaced into the Paleoproterozoic sediments of the Transvaal Supergroup and Archean basement of the Kaapvaal craton about 2,055 $\pm$ 3.9 Ma ago (Scoates & Friedman 2008). Emplacement and cooling took probably less than one million years (Zeh et al. 2015) and the rocks of the Bushveld Complex have remained extraordinarily well preserved from deformation and metamorphism (Hall 1932, Scoates & Friedman 2008, Cawthorn 2015). The Bushveld Complex is the largest layered mafic-ultramafic intrusion on Earth covering an area of circa 66,000 km^2 with a thickness of about 7 to 9 km and inward dipping layers (Cawthorn 2015). In general, the Bushveld Complex is subdivided into a northern, eastern and western limb, and some larger faults (as the Thabazimbi-Murchison lineament) intersect the entire layered intrusion which are shown in Figure 2.1. Apart from containing the largest resources of PGE on Earth, the Bushveld Complex also hosts economically important resources of Cr and V (Vermaak 1995, Wilson 1998, Zientek et al. 2014, Buchholz & Foya 2015). Zientek et al. (2014) estimated the resources for the Bushveld Complex to be 33,850 t Pt, 19,690 t Pd, 5,110 t Rh, 1,248 t Ru, 281 t Ir and 1,678 t Au, which are in accordance with earlier estimations by Vermaak (1995).

In 2013, South Africa produced 4,020 Moz (125 t) of Pt and 2,350 Moz (73 t) of Pd equaling 70% and 35% of the global supply of Pt and Pd, respectively (Loferski 2016). The Bushveld Complex and in particular its PGE deposits are extensively studied since decades. After the discovery of the Merensky Reef by Andries Lombaard and Hans Merensky on the farm Maandagshoek near Steelpoort, early studies on the Bushveld Complex and its PGE deposits

were done by Wagner (1925a,b, 1926a,b), Merensky (1926) and Reuning (1927). An extensive compilation of the first period of work on the geology and exploration in the Bushveld Complex was carried out by Wagner (1929) and Hall (1932), however for circa 50 years little information was available due to confidentiality of the mining industry (Vermaak 1976). Mining production in South Africa increased significantly after the 1970s (Figure 2.2).

Economic concentrations of PGE mainly occur in three ore bodies, namely the Merensky Reef, the UG-2 chromitite, and the Platreef, whereby the UG-2 chromitite is the largest resource of PGE (Vermaak 1995, Zientek et al. 2014) and is nowadays the predominant source of PGE from the Bushveld Complex with a total global production of Pt 43.5%, Pd 29.5% and Rh 64% (Cawthorn 1999a,b, Mungall & Naldrett 2008). However, also due to metal price development, mining at the Platreef as open-pit production will steadily increase in the next years and will make the Platreef the most important PGE deposit worldwide.

The similarity between the rocks of the eastern and western limbs led Hall (1932) to the conclusion that they are connected. Recent petrological and geophysical studies by Cawthorn & Webb (2001) and Webb et al. (2004) support the connection of the eastern and western Bushveld Complex.

The layered igneous rocks of the Bushveld Complex are defined by South African Committee on Stratigraphy (1980) as the Rustenburg Layered Suite (Figure 2.3). Abundant evidence for open-system behaviour forming the cumulates of the Rustenburg Layered Suite exists. This includes multiple injections and mixing of different parental magmas, assimilation of significant amounts of crustal rocks (Harris et al. 2005), as well as loss of large volumes of evolved magma in volcanic eruptions (Eales & Cawthorn 1996, VanTongeren et al. 2010).

Studies on comagmatic sills associated with the Rustenburg Layered Suite suggest three distinct types of parental magma referred to as B1, B2 and B3 (Barnes et al. 2010, Godel et al. 2011, Maier et al. 2013). Estimations of the compositions of the parental magma vary but a common feature is that one of the magmas corresponds to Si-rich picrite or Mg-rich basaltic andesite (SiO_2 about 55 wt.% and MgO about 12 wt.%, respectively), and the other two magmas having almost identical major element characteristics corresponding to tholeiitic basalt (50 to 51 wt.% SiO_2 and 6 to 7.5 wt.% MgO). All three magma compositions contain a significant crustal component and are not in equilibrium with a residual mantle mineral assemblage (Veksler et al.

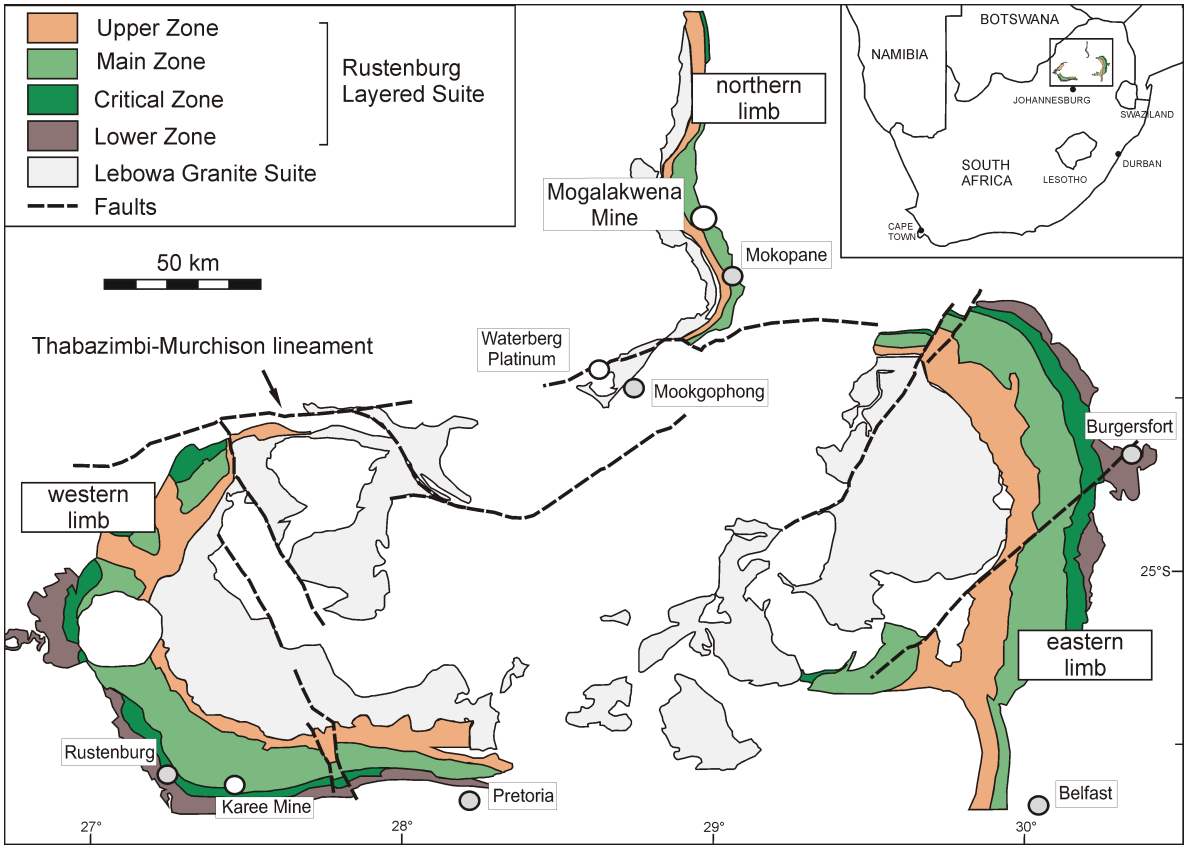

Figure 2.1 – Geological map of the Bushveld Complex with sample location of the Mogalakwena mine in the northern Bushveld Complex. Based on the geological map by Vorster (2007).

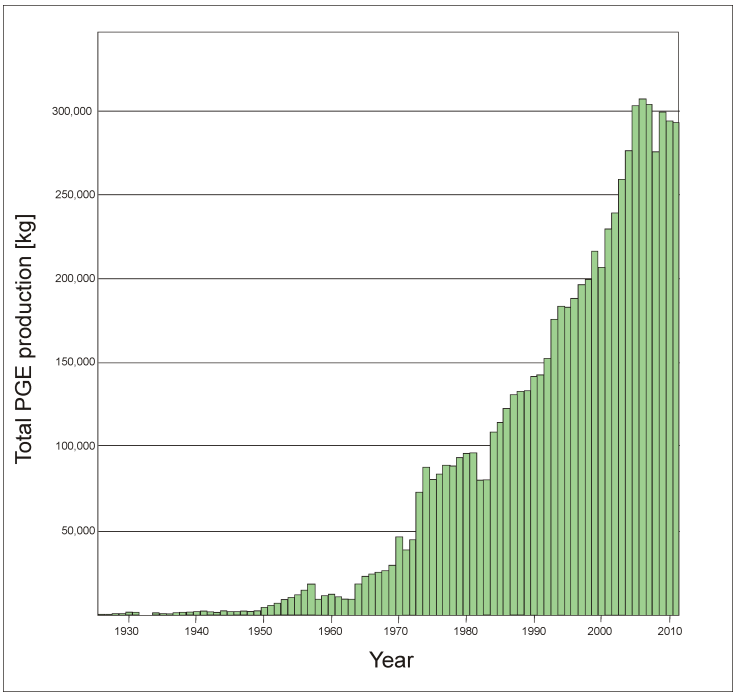

Figure 2.2 – Histogram showing annual production of platinum-group elements in South Africa from 1926 to 2011. Modified after Zientek et al. (2014).

2015).

Traditionally, the stratigraphy of the Rustenburg Layered Suite can be subdivided into five principal zones which are described below: Marginal Zone, Lower Zone, Critical Zone, Main Zone and Upper Zone (Hall 1932).

The *Marginal Zone* (not outlined in Figure 2.3) comprises a sequence up to 800 m of heterogenous norites and minor pyroxenites, which form the base of the complex (Eales & Cawthorn 1996). In this zone the norites are medium-grained and unlayered, interpreted as composite sills or cumulates rather than chilled parental margins (Cawthorn et al. 1981).

The *Lower Zone* has a thickness of 800 to 1700 m and is mainly composed of pyroxenites, harzburgites and dunites (Cameron 1978). Furthermore, the thickness of this zone was influenced by basement topography and structure (Cawthorn et al. 2002a). The Lower Zone has a limited lateral extent and is poorly exposed and not continuous around the entire intrusion. Its best exposure occurs in the eastern limb at the Olifants River (Cameron 1978, Cawthorn & Walraven 1998). At this location the Lower Zone was subdivided by Cameron (1978) into basal pyroxenite, a harzburgite and an upper pyroxenite sequence. In the northern limb the Lower Zone

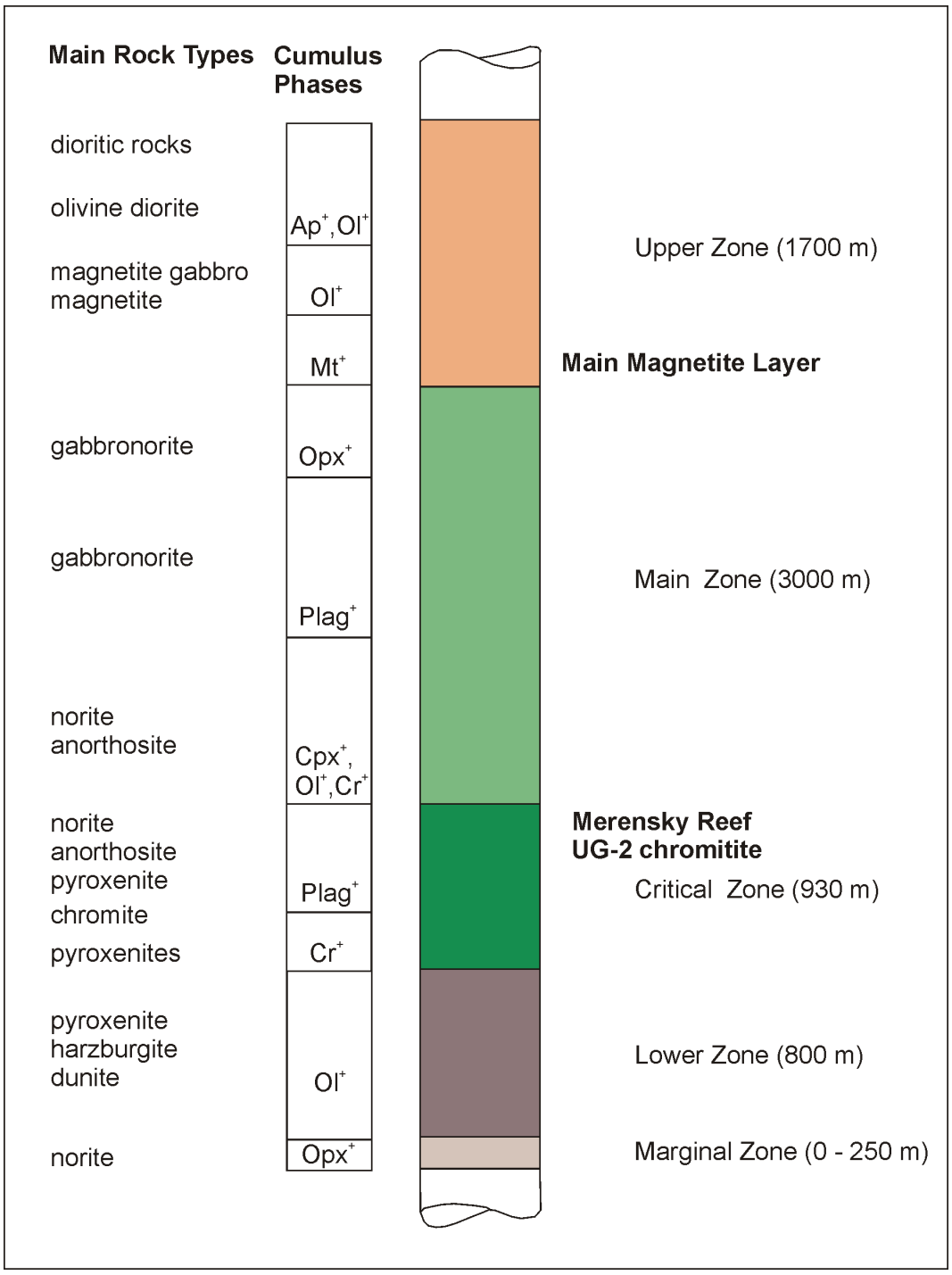

Figure 2.3 – Stratigraphy of the Rustenburg Layered Suite. Modified after Mitchell (1990).

contains chromitite layers with significant PGE contents (Hulbert & Von Gruenwald 1985).

The *Critical Zone* has a thickness varying from 1300 to 1800 m and is subdivided into the Lower and the Upper Critical Zone (Cameron 1980, 1982). The base of the Critical Zone is marked by the appearance of cumulus chromitite. The Lower Critical Zone comprises orthopyroxenite, chromitite and some harzburgite, whereas the Upper Critical Zone contains chromitite, orthopyroxenite, norite and anorthosite with very minor harzburgite (Cameron 1980, 1982). The Upper Critical Zone contains the world's largest platinum-bearing ore bodies, which are the Merensky Reef and the UG-2. In addition, huge reserves of chromium are present and mined in the Lower Critical Zone (Hatton & von Gruenewaldt 1987, Eales & Cawthorn 1996). These massive chromitite layers are numbered sequentially from the base upwards and are subdivided into three major groups, i.e. Lower Group (LG), Middle Group (MG) and Upper Group (UG) (Cousins & Feringa 1964, Cameron 1977, Hatton & von Gruenewaldt 1985, Scoon & Teigler 1994). The Lower Group comprising the LG-1 to LG-7; the Middle Group comprising the MG-0 to MG-4 and the Upper Group comprising the UG-1, UG-2 and UG-3. Most of the layers can be traced over large distances in the eastern limb as well as the western limb (Hatton & von Gruenewaldt 1987). The Upper Group consists usually of two chromitites, the UG-1 and UG-2, in the western limb, but in the eastern limb the UG-3 has been recognized. Gain (1985) argued that the UG-3 in the western limb is locally merged with the UG-2 chromitite. The thickest chromitite layer of the Critical Zone ranges up to several meters and there are numerous thin chromitite stringers of only a few centimeters in between the massive chromitite seams. Figure 2.4 shows the average PGE concentrations form LG-1 stratigraphically upwards to the Merensky Reef indicating the increase of PPGE over IPGE with stratigraphic height.

The *Main Zone* is a 3000 to 3400 m thick unit of homogenous norite, gabbro, gabbronorite, and anorthosite devoid of olivine and chromian spinel (Mitchell 1990). Only minor amounts of anorthosite and pyroxenite layers occur. The concentrations of PGE in the Main Zone are low and only limited data about the distribution of PGE in the Main Zone exists (Barnes et al. 2007). The Bellevue drill core in the northern limb covers a sequence of the entire Upper Zone and half of the Main Zone (Ashwal et al. 2005, Barnes et al. 2007).

The *Upper Zone* is 2000 to 3000 m thick and the base is generally defined by the appearance of cumulus magnetite (Eales & Cawthorn 1996) but other studies locate the boundary between

Main and Upper Zone rather at the pyroxenite marker (600 to 700 m below) where significant petrological and isotopical changes are recorded (Kruger et al. 1987, Kruger 1990).

Isotope studies indicate strong evidences that the magmas of the Rustenburg Layered Suite experienced high degree of crustal contamination (Sr: Hamilton (1977), Kruger & Marsh (1982), Kruger (1994), Sharpe (1985); Nd: Maier et al. (2000); Os: Hart & Kinloch (1989), McCandless et al. (1999), McCandless & Ruiz (1991), Schoenberg et al. (1999), Reisberg et al. (2011); O: Harris et al. (2005)). Especially for the case of Sr-isotope studies it can be observed that the initial Sr-isotope ratios change abruptly at certain stratigraphic heights, which has been interpreted to be caused by the injection of new magmas with distinctly different isotopic composition compared to the fractionated magma already present in the chamber (Kruger & Marsh 1982). One abrupt change in the Sr-isotope ratio can be observed at the level of the Merensky Reef, which Kruger & Marsh (1982) explained by the injection of new magma which is more contaminated by crustal material. The interaction with crustal material is also evident by Nd-isotope ratios, roughly anti-correlating the Sr-isotope data (Maier et al. 2000). This anti-correlation may be obvious since the continental crust has high $^{87}Sr/^{86}Sr$ ratios coinciding with low $^{143}Nd/^{144}Nd$ ratios relative to mantle values. Both Sr- and Nd-isotopic data indicate increasingly crustal signatures with increasing stratigraphic height from Lower to Main Zone (Kruger & Marsh 1982, Maier et al. 2000).

2.1 Merensky Reef

The Merensky Reef is a circa 1 m thick stratiform PGE reef in the eastern and western Bushveld Complex, occurs 15 to 400 m above the UG-2 chromitite (Lee 1996) and is continuous over 100s of kilometres (Berg 1928). The Merensky Reef usually is limited by a lower and an upper few millimeter thin chromitite layer. Nevertheless, the thickness, the amount of chromitite stringers, PGE grades and the lithology of hanging and footwall varies within the Bushveld Complex. The hanging wall and footwall of the Merensky Reef generally consist of pyroxenite, norite and anorthosite (Vermaak 1976).

The Merensky Reef is generally described as a pegmatoidal pyroxenite. Rock-forming minerals consist of pyroxene (about 75%), plagioclase (about 20%), phlogopite (about 5%) and

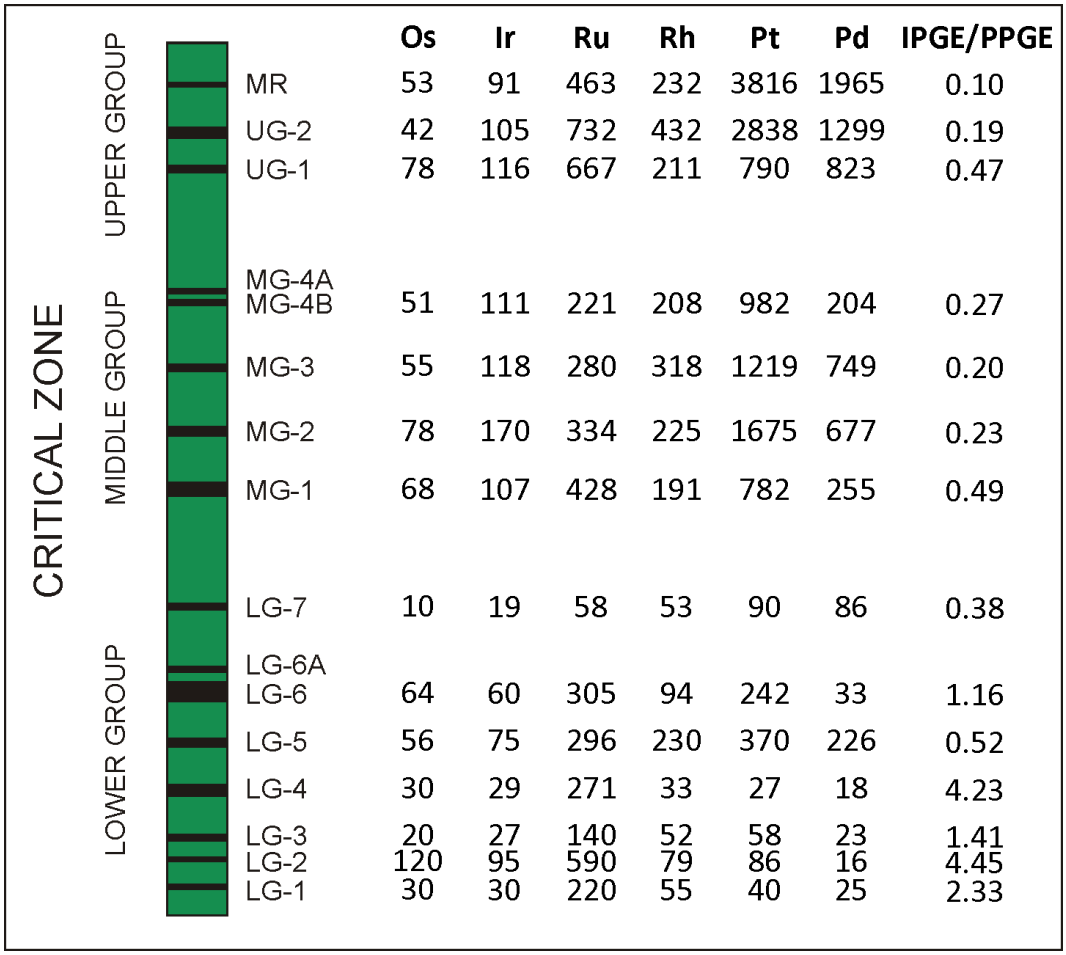

	Os	Ir	Ru	Rh	Pt	Pd	IPGE/PPGE
MR	53	91	463	232	3816	1965	0.10
UG-2	42	105	732	432	2838	1299	0.19
UG-1	78	116	667	211	790	823	0.47
MG-4A							
MG-4B	51	111	221	208	982	204	0.27
MG-3	55	118	280	318	1219	749	0.20
MG-2	78	170	334	225	1675	677	0.23
MG-1	68	107	428	191	782	255	0.49
LG-7	10	19	58	53	90	86	0.38
LG-6A							
LG-6	64	60	305	94	242	33	1.16
LG-5	56	75	296	230	370	226	0.52
LG-4	30	29	271	33	27	18	4.23
LG-3	20	27	140	52	58	23	1.41
LG-2	120	95	590	79	86	16	4.45
LG-1	30	30	220	55	40	25	2.33

Figure 2.4 – The PGE concentrations and IPGE/PPGE ratios in the Critical Zone of the western Bushveld Complex. Data of the LG-1 to MG-4A is taken from Scoon & Teigler (1994) and from the UG-2 and the Merensky Reef (MR) rom Vermaak (1995).

occasionally olivine. Secondary minerals are mainly serpentine, talc, chlorite and magnetite. Sulfides are in general <5% and typically occur as polyphase sulfide assemblages of pyrrhotite (about 40%), pentlandite (about 30%), chalcopyrite (about 15%) and minor amounts of pyrite, millerite and cubanite. The Merensky Reef has average sulfide contents of 1 to 3 wt% and typically contains of one to more thin chromite seams (Barnes & Maier 2002b).

The average PGE grade of the Merensky Reef has been estimated to 6.16 g/t, being 3.43 g/t Pt, 1.98 g/t Pd, 0.19 g/t Rh, 0.43 g/t Ru, 0.08 g/t Ir, and 0.05 g/t Os (Vermaak 1995).

A few meeters above the Merensky Reef, a petrographically similar sulfide-bearing lithology is commonly present, which, however, does not contain economic contents of PGE, is therefore termed the Bastard Reef (Schneiderhöhn 1931).

The distribution of PGE within the Merensky Reef is very variable (Wagner 1929, Viljoen 1999). The Merensky Reef is located close to the boundary between Critical and Main Zone and most models for the formation of the Merensky Reef indicate a mixing process between the distinct magmas which correspond to these two zones (Barnes & Maier 2002b).

Platinum-group minerals in the Merensky Reef are typically PGE-sulfides (laurite, cooperite, braggite) and PGE-bismuthotellurides and minor amounts of sperrylite and PGE-alloys (Kinloch 1982, Ziaja et al. 2007, Osbahr et al. 2013, Osbahr 2012). The PGM mainly occur associated with sulfides or as inclusions in chromite (laurite). Grain sizes of PGM are in average some 10 μm.

2.2 UG-2 chromitite

The UG-2 chromitite occurs in the Upper Group of the Critical Zone, between 15 to 400 m below the Merensky Reef and has a general thickness of about one meter, varying between 0.4 and 2.5 m (Wagner 1929, Cousins & Kinloch 1976, Hiemstra 1979, 1985, 1986, McLaren & De Villiers 1982).

Various hypotheses exist on the formation of the chromitite, i.e. chromitite layers are formed as a result of magma addition of different composition (Irvine 1975, 1977, Eales et al. 1986), changes in oxygen fugacity (Ulmer 1969), or total pressure (Lipin 1993).

The UG-2 has the largest estimated resources of PGE worldwide: 20 kt Pt, 13 kt Pd, 3.7 kt

Rh, 0.94 kt Ru, 0.23 kt Ir and 0.42 kt Au (Zientek et al. 2014). Platinum-group element grades are always restricted to the chromitite and only rarely occur in the footwall (mainly caused by chromitite schlieren). The average PGE grade of the UG-2 has been estimated to 5 to 7 g/t with 2.66 g/t Pt, 1.71 g/t Pd, 0.44 g/t Rh, 0.71 g/t Ru, 0.15 g/t Ir, and 0.07 g/t Os (Vermaak 1995). However, average grades of the reefs mined today are generally lower. Comparing the average PGE grade of the UG-2 with the Merensky Reef it can be demonstrated that the IPGE in the UG-2 are generally higher than in the Merensky Reef since the IPGE are traditionally associated with chromite and often occur as discrete PGM (mainly laurite [RuS_2]) inside chromite grains. The sulfide content of the UG-2 (<1%) is significantly lower than that of the Merensky Reef and the Platreef.

Platinum-group elements within the UG-2 are bimodally distributed, occurring both as discrete PGM and within sulfide. Especially pentlandite is known to hold high contents of PGE, as outlined by a number of authors from different mafic-ultramafic intrusions (Cabri et al. 1981, Cabri 2002, Oberthür et al. 1997a, Godel et al. 2007, Holwell & McDonald 2010, Osbahr et al. 2013, 2014, Junge et al. 2014, 2015b). The PGE distribution is generally limited to the UG-2 itself (McLaren & De Villiers 1982, Hiemstra 1985, 1986, Lee 1996).

Figure 2.5 shows that PGE are generally enriched directly at the base or the upper contact of the chromitite layer or in the center of the seam (Von Gruenewaldt et al. 1986, Maier & Barnes 2008, Junge et al. 2014).

The UG-2 chromitite has sharp basal and upper contacts. The footwall generally consists of a pegmatoidal pyroxenite containing schlieren of chromitite, or less commonly an anorthositic footwall (Cawthorn et al. 2005). Chromites in the UG-2 have average Cr/Fe ratio between 1.26 and 1.4 (Lee 1996). The mineralogy of the chromitite is characterized by chromite (about 70%), interstitial pyroxene (about 15%) and plagioclase (about 15%). Rutile and ilmenite can be quite abundant in some UG-2 sections occurring within individual chromite grains or interstitial to chromite. Secondary minerals existing only in minor amounts are phlogopite, talc, chlorite and serpentine. In general, the UG-2 contains <1% sulfides; the major base metal sulfides are pentlandite and chalcopyrite whereas pyrrhotite is a minor phase.

Mining of the UG-2 chromitite did not began until the 1970s as the chromitite ore could not be processed due to the fact that the too high melting point of chromite exceeded operational

temperatures for furnaces (Nel & Theron 2004, Zientek et al. 2014).

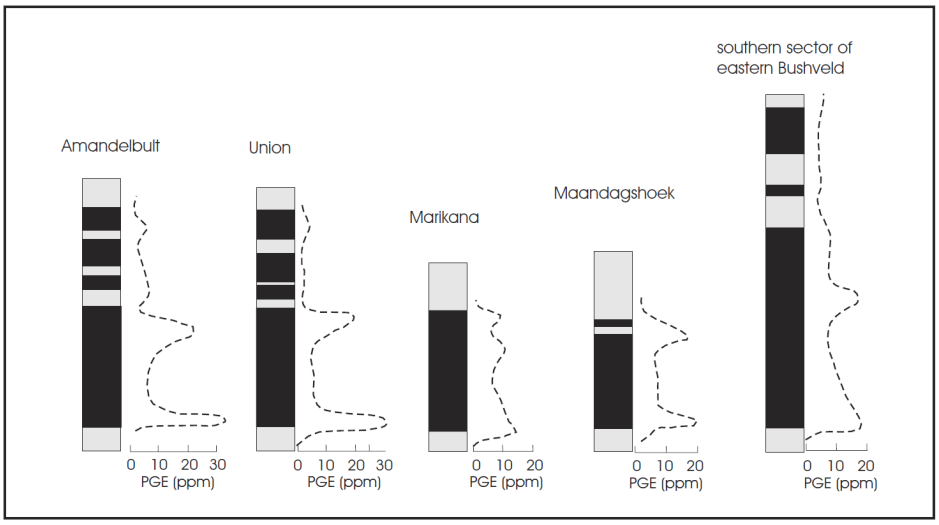

Figure 2.5 – Distribution of PGE in the UG-2. After Von Gruenewald & Hatton (1986) and Maier et al. (2008).

2.3 The Platreef

The Platreef in the northern limb of the Bushveld Complex (Figure 2.6) extends from Mokopane northwards for about 110 km until it is covered by younger Waterberg sediments (Van der Merwe 1976). The northern limb is separated from the rest of the Bushveld Complex by the Thabazimbi-Murchison lineament, which may have acted as a barrier during and after the formation of the northern limb and the rest of Bushveld Complex (Figure 2.1). The Thabazimbi-Murchison lineament is a pre-Bushveld collisional suture zone which formed at around 2.9 Ga and experienced repeated reactivation (Good & Wit 1997, McDonald et al. 1999b, Armitage et al. 2007).

The Platreef provides one of the most import sites for PGE production and represents the most extensively exploited PGE deposit by open-pit mining on Earth with significant associated reserves of Ni and Cu, amounting to about 30% of the in-situ value (Naldrett 2010). Open-pit mining of the Platreef takes place on the farms Sandsloot, Zwartfontein, and Overysel (Figure 2.8), and further exploration projects exist along the strike of the Platreef (e.g. Ivanhoe Platinum). Large scale mining operations started at Sandsloot (1992), Zwartfontein (2002) and

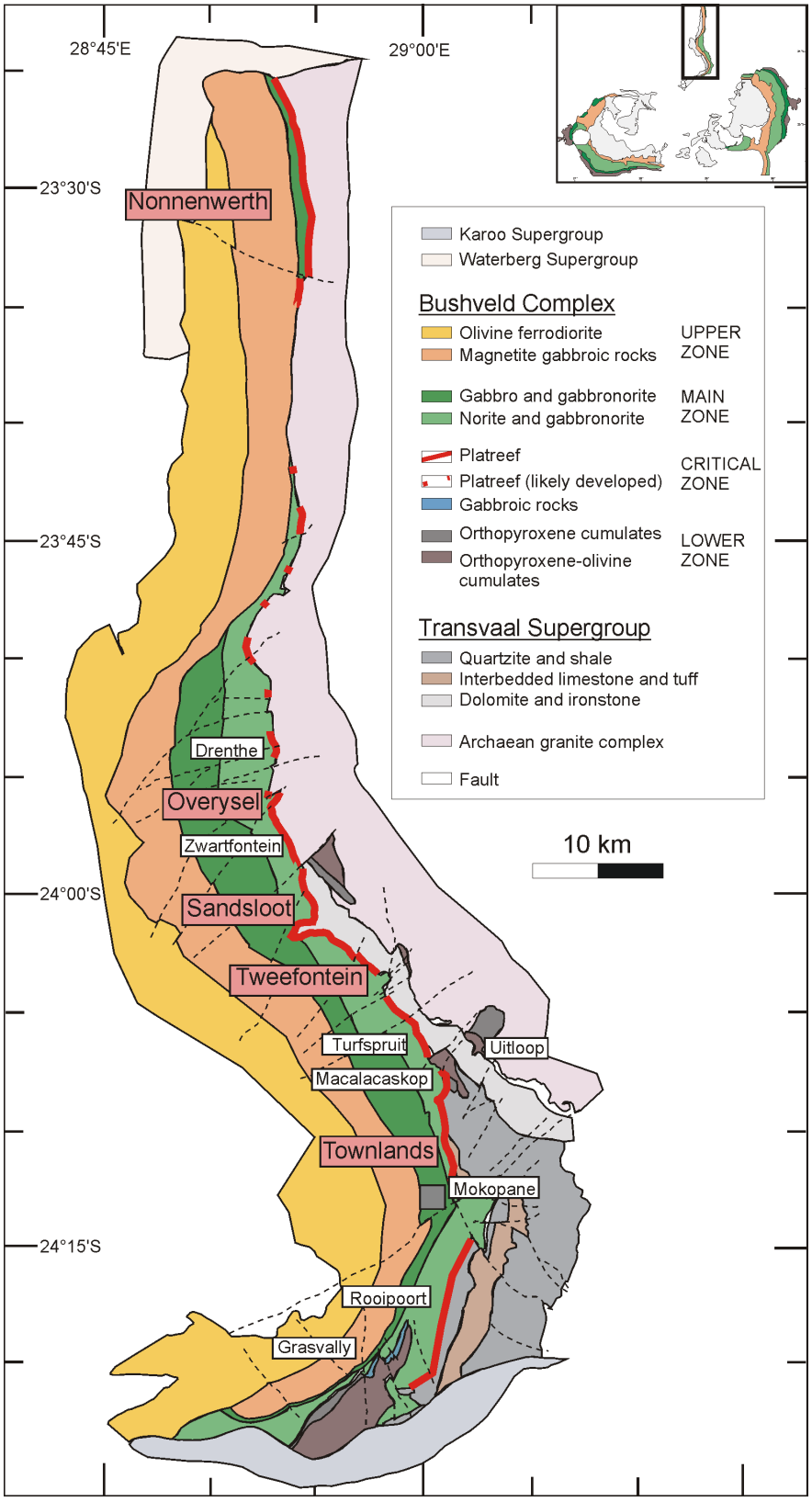

Figure 2.6 – Simplified geological map of the northern limb of the Bushveld Complex. Modified after Ashwal et al. (2005) and Maier et al. (2008).

Overysel (2006) causing extensive development of open-pits in the last decades (Figure 2.7). The Platreef dips to the southwest, west-southwest or west at 20 to 75°(Wagner 1929). The first description of the lithologies and the mineralisation of the Platreef was published by Wagner (1929), who noted that the deposit consists of pyroxenites and norites, which were variably mineralised with sulfides, with a footwall composed of metamorphosed sediments and granite. The Platreef consists generally of pyroxenitic units with PGE-Ni-Cu mineralization and varies up to 400 m in thickness (Wagner 1929, McDonald & Holwell 2011, Yudovskaya et al. 2011).

Kinnaird & McDonald (2005) proposed the following working definition for the Platreef as *"mafic units enriched in Ni-Cu-PGE that occur between the Archaean granite-gneiss basement or the Transvaal Supergroup and the gabbros-gabbronorites of the Main Zone, north of the Planknek Fault"*. However, this working definition excludes the Ni-Cu-PGE occurrences of the Grasvally Norite-Pyroxenite-Anorthosite (GNPA) member, which is located south of Mokopane (Von Gruenewaldt et al. 1989, Smith et al. 2011, 2014).

The Platreef is generally classified as contact-style mineralization, characterized by accumulations of magmatic sulfides associated with xenoliths and brecciation, as well as coarse pegmatitic textures (Maier 2005). Other major examples of contact-style mineralization are described from the Duluth Complex in the USA, the Lac des Illes deposit in Canada, the Portimo Complex in Finland, the Federov Pansky intrusion in Russia, and the East Bull Lake in Canada.

The sulfide contents are generally higher in the Platreef (about 3%) than in the Merensky Reef and UG-2. However, the mineralization within the Platreef is less continuous than in the Merensky Reef and UG-2, and also PGE contents (circa 1 to 4 g/t) are generally lower. However, due to the large thickness of the Platreef, mining of this comparable lower grade ore is still highly economic. The total average PGE concentrations in the Platreef are 4.12 g/t, with 1.77 g/t Pt, 2.01 g/t Pd, 0.114 Rh, 0.164 Ru, 0.037 g/t Ir and 0.033 g/t Os (Vermaak 1995).

Lithological units in the Platreef are mainly pyroxenites, gabbronorites, norites, periodites, chromitites, serpentinites, and a variety of hybrid lithological units (McDonald & Holwell 2011, Yudovskaya & Kinnaird 2010). Chromitite seams can occur as disseminated and massive seams and form two main chromitite-bearing zones in the Platreef: the Upper chromitite and the Lower chromitite (Yudovskaya & Kinnaird 2010). The Platreef is overlain by norites and gabbronorites of the Main Zone (McDonald & Holwell 2011). The geology of the Platreef at the Sandsloot

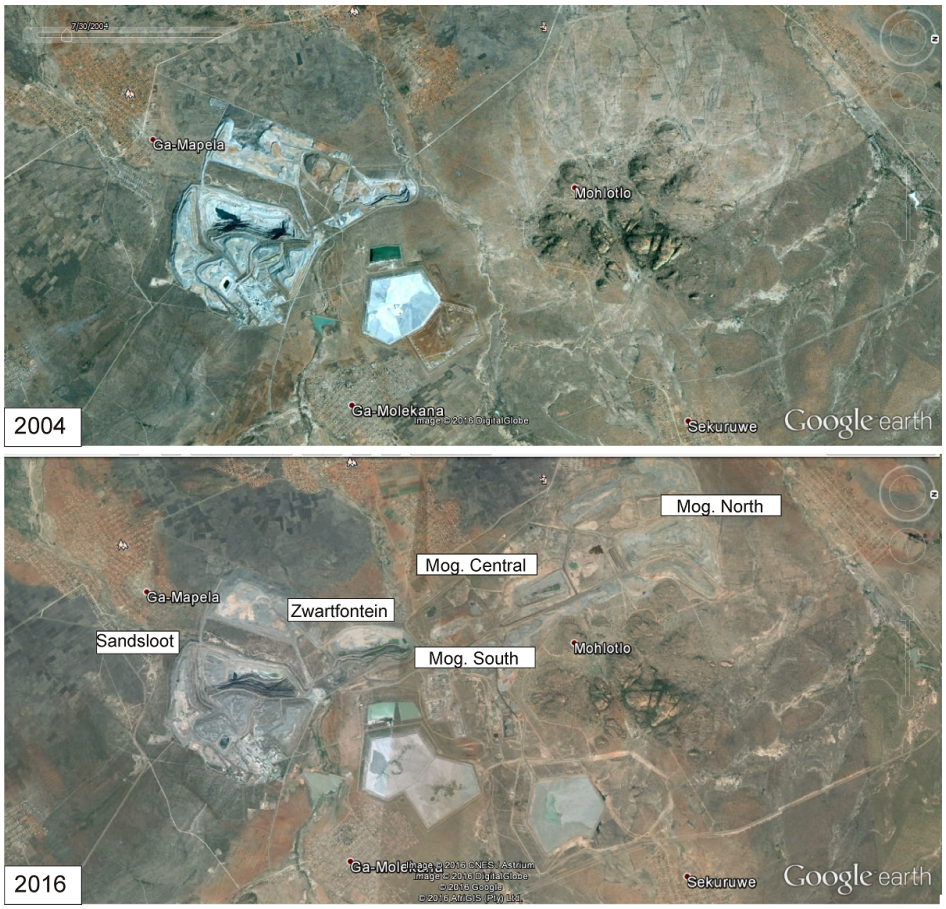

Figure 2.7 – Google Earth image of the Mogalakwena Mine in 2004 and 2016.

open-pit has been described in more detail by several authors (Harris & Chaumba 2001, Armitage et al. 2002, McDonald et al. 2005, Holwell et al. 2005, 2006).

The footwall to the Platreef becomes progressively older from south to north, with metasedimentary rocks of the Paleoproterozoic Transvaal Supergroup (including quartzites and shales of the Silverton and Timeball Hill formations, shales of the Duitsland formation, the Penge banded iron formation, dolomites of the Malmani Subgroup) and, from the farm Zwartfontein northwards, on Archean granites and gneisses (Merensky 1926, Wagner 1929, Holwell et al. 2006, McDonald & Holwell 2011, Roelofse 2012). Based on the footwall lithology Kinnaird et al. (2005) divided the Platreef into three sectors: the Southern Sector (footwall of Transvaal Supergroup shales, banded ironstones, calc silicates, mudstones and siltstones), the Central Sector (dolomitic footwall) and the Northern Sector (Archean granite).

The Platreef contains richer sulfide mineralization than the UG-2 and the Merensky Reef. A stratigraphic relationship between the Platreef and the PGE reefs of the eastern and western Bushveld Complex, the UG-2 chromitite and the Merensky Reef, is unclear. Van der Merwe (1976) equated the Platreef to the base of the Main Zone. More recent studies by McDonald et al. (2005) argue that is not possible to correlate the Platreef with the Critical Zone. A continuous set of detailed data on boreholes in the northern limb where gathered on the Bellevue borehole and the Moordkopje (Ashwal et al. 2005, Roelofse 2012).

Syn- and postmagmatic alteration effected the Platreef (Buchanan 1981, Holwell & McDonald 2006, Hutchinson & Kinnaird 2005) and Gain & Mostert (1982) proposed that devolatilization of dolomitic footwall and xenoliths added CO_2, H_2O and S into the magma, which lowered the sulfur solubility, resulting in the formation of an immiscible sulfide melt. Different studies showed that the Platreef exhibits enriched initial Sr, ϵ-Nd and γ-Os isotopes arguing for syn- and postmagmatic alteration of the Platreef (Barnes & Maier 2002a, Pronost et al. 2008, Reisberg et al. 2011, Roelofse 2012) and in particular at Overysel, Cawthorn et al. (1985) argues that the contamination of the Platreef magma occurred via a granite-derived fluid based on the Sr-isotopes data. Pronost et al. (2008) studied the Nd-isotopic system of samples from the Platreef and the overlying hanging wall and argued that due to the similarity in isotope composition the Platreef and the hanging wall have the same magma source. Their data are in accordance with local contamination of an already contaminated magma of Main Zone composition.

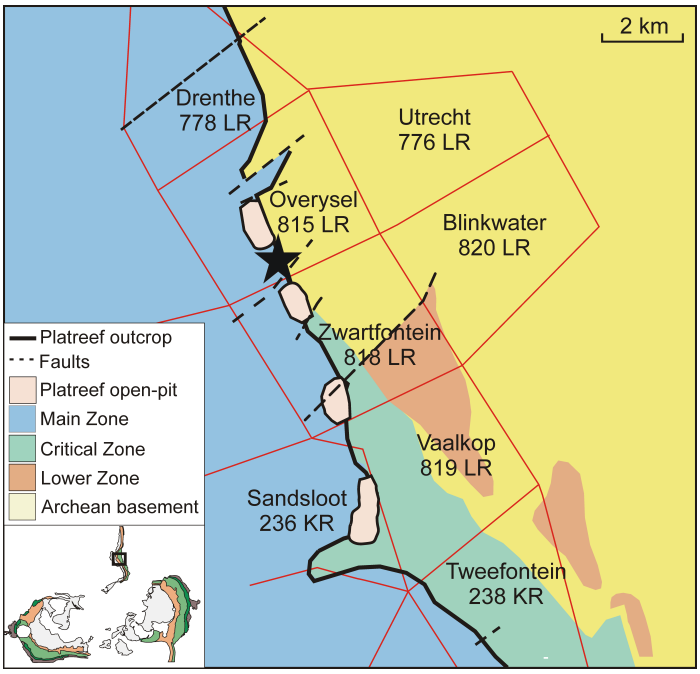

Figure 2.8 – Simplified Geological Map of the mining area of the Platreef. Modified after McDonald & Holwell (2011).

Various conventional and mass independent sulfur isotope studies exist for the Platreef (Buchanan 1981, Manyeruke et al. 2005, Sharman-Harris et al. 2005, Holwell et al. 2007, Penniston-Dorland et al. 2008, 2012, Sharman et al. 2013, Smith et al. 2014, 2016). A sulfur isotope study at Tweefontein by Buchanan (1981) showed that the sulfide mineralisation involves assimilation of sedimentary-derived sulfur into the Platreef magma. Holwell et al. (2007) argued that the sulfide mineralization in the Platreef has a mantle source of sulfur and local overprint of crustal sulfur occurred where the Platreef intruded pyrite-rich shales. Based on these findings Holwell et al. (2007) proposed that assimilation and introduction of external S is rather viewed as an ore-modifying process than as the primary trigger for mineralization. Sharman et al. (2013) indicated on their multiple sulfur isotope study that the Duitschland formation, a stratigraphic horizon in the footwall of the Platreef, contributed largely to the crustal sulfur isotope signature of the Platreef and this addition of crustal sulfur caused a dilution of pre-existing PGE-rich sulfide melt.

Stable isotope studies on mineral separates of pyroxene and plagioclase in the northern limb were carried out by Harris & Chaumba (2001) and Sharman-Harris et al. (2005). Both studies showed differences between plagioclase and pyroxene δ^{18}O values which indicates exchange

with fluids causing additional contamination.

Chapter 3

Materials and Methods

3.1 Origin of studied samples

Three drill cores were sampled at the Mogalakwena Mine on the Platreef (Fig. 2.8). The mine is located in the Limpopo province 30 km northwest of the town of Mokopane. Within the Mogalakwena Mine four open pits exist, namely Sandsloot, Zwartfontein, Mogalakwena Central and Mogalakwena North pits (Figure 2.8). The depths of the open pits vary from 110 m at the Mogalakwena North pit down to 245 m at the Sandsloot pit.

The three bore holes (Oymetox 1, 2 and 3) were drilled between the Mogalakwena Central and Mogalakwena North pits (Figure 2.8) at the Overysel farm in the norther Bushveld Complex. The bore holes were drilled using the triple tube method, enabling good preservation of the weathered and oxidized ore. The drill cores are covering sequences of oxidized to pristine Platreef ore.

Additionally to the drill cores at Overysel, samples from the farms at Townlands, Tweefontein, Sandsloot, and Nonnenwerth were used for a mineralogical (sulfides and PGM) and for S-isotope study. For the study of the Sandsloot, two feldspathic pyroxenite samples (Pr3, Pr5) are investigated for the mineralogical characterization and the S-isotope study. The drill core TN 181 (Tweefontein) intersects different lithologies (feldspathic pyroxenite, hornfels, BIF and black shale) and 13 polished sections from this core are used for the mineralogical characterisation and 9 for S-isotope data. At Townlands the 230 m drill core TL01-3 intersected varies portion of the reef and 18 polished sections are studied in total and from the two drill cores at

Nonnenwerth (B2121 and B2199) 17 polished sections were used for S-isotope study and the mineralogical characterization. All sample numbers and results are given in the Appendix.

3.2 Whole-rock geochemistry

Major and trace elements were analyzed by ACTLABS in Ontario/Canada using a combination of FA-MS (Fire Assay Metallic Screen), INAA (Instrumental Neutron Activation Analysis) and TD-ICP-MS (total digestion combined with inductively coupled plasma-mass spectrometry).

For the INAA method three different Merensky Reef reference materials from the African Mineral Standards (AMIS0254, AMIS0367 and AMIS0396) were used. Nickel and Cu concentrations are determined by ICP/MS and S contents by ICP applying a sodium peroxide fusion procedure. For Ni and Cu a jasperoid (GXR-1) and a porphyry copper ore (GXR-4) from the US Geological Survey and for S analysis a zinc-tin-copper-lead ore from Mount Pleasant mine (MP-1b) from the Canadian Certified Reference Materials Project were used as reference material.

For measurement of noble metals, a sample mass of 50 g is required and is mixed with soda ash (sodium carbonate), borax (sodium borate), litharge (PbO), flour (baking flour used to add carbon as a reductant), silica, and possible nitre (potassium nitrate) (Hoffman et al. 1998, Hoffman & Dunn 2002). Furthermore, Ag is added as a collector and the entire mixture is heated at temperatures ranging from 1000°C to 1200°C (Hoffman et al. 1978, Hoffman & Dunn 2002). As the Ag in the melt settle to the bottom of the crucible, it scavanges the Au (+/- Pd, Pt) from the melt (Hoffman et al. 1998). The lead button is cupelled at 950°C to a magnesia cupel. A tiny Ag bead which contains Au, Pt and Pd can be dissolved and analyzed. This method is rapid and has better sensitives for noble metals compared to other analytical methods (Hoffman et al. 1978). Using Au instead of Ag enables also the analysis of Rh by fire assay, as Rh forms insoluble alloys in the Ag collector matrix which cannot be dissolved quantitatively (Hoffman & Dunn 2002).

Instrumental Neutron Activation Analysis is an analytical technique which is dependent on measuring gamma radiation induced on the sample by irradiation with neutrons (Hoffman et al. 1998, Hoffman & Dunn 2002). The primary source of neutrons for irradiation is usually a

nuclear reactor. Each element which is activated emits a "fingerprint" of gamma radiation which can be measured and quantified (Hoffman et al. 1998).

Major and trace elements were additionally analyzed with X-ray fluorescence spectroscopy (XRF) at the BGR in Hannover, Germany. The X-ray fluorescence analyses were performed on a Philips PW 1480 with a chromium X-ray tube and a Philips PW 2400 with a rhodium X-ray tube. X-ray fluorescence is a method for the quantitative and qualitative analysis of elements with an atomic number between 11 (Na) and 92 (U) (Rollinson 1993). Before applying this method, specific sample preparation is required first. Therefore, samples were finely ground and about 1 g of the powder is heated for ten minutes at 1030°C in a muffel furnace in order to release volatile phases like water, carbon dioxide and sulphur dioxide. The lost weight which is produced during annealing is called "loss on ignition" (LOI). Afterwards, the annealed sample is added to 5 g lithiummetaborate ($LiBO_2$) and 25 mg lithiumbromide (LiBr). Then the sample is smelted for twenty minutes at 1200°C on a permanent moving melt tablet which guarantees a homogenous dispersion of the elements for the following analysis.

In order to investigate the correlation between the elements, as detected by the described analytical methods, a correlation matrix was calculated for the geochemical analysis of INAA and ICP-MS. A correlation matrix is a geostatistical method in which the correlation is a measurement of the relationship between two variables on a number of individuals (Rollinson 1993). With the correlation matrix it is possible do determine the statistic significance of a correlation between two variables. Therefore the coefficient of correlation "r" shows the linear relation for two variables which are calculated out of "n" number of individuals as expressed in equation 3.1 by Lonzán (1992).

$$r = \sqrt{\frac{(\sum xy)^2}{\sum xx * \sum yy}} \tag{3.1}$$

The calculated coefficient of correlation ranges from -1 to +1 and whether a correlation is considered statistically significant (positive or negative) depends on the degree of freedom which can be calculated using equation 3.2, where "n" equals the numbers of individuals.

$$\text{degrees of freedom} = n - 2 \tag{3.2}$$

3.3 X-ray diffraction

The mineralogical composition of a powder is identified by X-ray diffraction (XRD). The diffraction of X-rays by a lattice plane can be described by the Bragg equation:

$$n * \lambda = 2 * d * sin(\theta) \tag{3.3}$$

with λ being the wavelength of the X-rays (Cu-radiation used in this study), d as the interplanar spacing between the individual parallel lattice planes and 2θ is the angle between the diffracted and undeviated X-ray (Reynolds 1989). Using the Bragg equation for XRD patterns the interplanar spacing d can be calculated and minerals can be determined.

Powders are polycrystalline materials containing a large amount of differently orientated crystals. Further, by adding glycerin to the sample it can be determined if swellable phases exist. Addition of glycerin causes a shift in the peaks of the diffraction pattern to lower 2θ angles (coinciding with increasing d-spacing) the spacing between parallel lattice planes increases.

In this study, a PANalytical MPD PRO diffractometer (Cu-Kα radiation generated at 40 kV and 30 mA) was used. This diffractometer is equipped with a variable divergence slit (20 mm irradiated length), Scientific X'Celerator detector (active length 0.59°), and a sample changer (sample diameter 28 mm). The samples were investigated from 3° to 84° 2θ with a step size of 0.0167° 2θ and a measuring time of 10 sec per step. The weighted mean wavelength used for Cu radiation (Kα) is 1.541838.

3.4 Cation exchange capacity

Cations are electrostatically bound at negatively charged soil particles. These cations can be exchanged with other cations of equivalent charge. For example, Ca^{2+} and K^{+} can be exchanged (desorbed) with Al^{3+} and then analyzed in the soil solution.

For the cation exchange capacity (CEC) investigation, ammoniumacetat (77.08 g/mol; EMSURE) was used on selected samples of oxidized Platreef ore (five from Oy1, four from Oy2, and one from Oy3).

The samples were treated with ammoniumacetat-solutions and initially analyzed without

any treatment using XRD. After centrifugation, the supernatant was decanted and fresh solution was added. This procedure was performed three times. After that samples were transferred to porous ceramic tiles and washed three times with deionized water and analyzed via XRD. The samples were then analyzed by Inductively Coupled Plasma Optical Emission Spectrometry (ICP-OES).

3.5 Infrared spectroscopy

For infrared spectroscopy analysis a Thermo-Electron iS50 FTIR Advanced Flex Gold coupled with a IR-microscope Continuum (Figure 3.1) at the BGR, Hannover was used. The IR microscope enables space-resolved imaging. The IR microscopy is usually used in addition to XRD analysis for mineralogical investigations.

Figure 3.1 – Photo of the infrared spectroscopy used for the analysis carried out at the BGR, Hannover. Photo taken from BGR (2016).

3.6 Scanning electron microscopy with mineral liberation analysis

A FEI Quanta 650 FEG scanning electron microscope (SEM) equipped with two Bruker Quantax X-Flash 5030 energy dispersive X-ray spectrometers (EDX) is used to identify mineral phases at BGR in Hannover, Germany (Figure 3.2). The source for the electron beam is a field emission gun in a high-vacuum environment. The electron beam is focused by condenser lens and scans over a a selected area of the sample. These primary electrons interact with the sample creating secondary electrons (SE), backscattered electrons (BSE) and X-rays (Bremsstrahlung and characteristic X-rays). The characteristic X-rays provide chemical information of the sample and are detected by EDX. Secondary electrons are used to display the surface morphology of the sample whereas BSE display chemical information as they result from the mean atomic number of the individual phases.

Scanning electron microscopy based image analysis systems becomes more frequently used for automated phases analysis (Gu 2003, Fandrich et al. 2007, Oberthür et al. 2008, O'Driscoll et al. 2014, Gu et al. 2014, Little et al. 2015, Osbahr et al. 2015). Several SEM-based image analysis softwares such as Mineral liberation analysis (MLA, FEI, Hillsboro, Oregon, USA) and Quantitative Evaluation of Minerals (QEMSCAN, FEI, Hillsboro, Oregon, USA), Tescan Integrated Mineral Analyzer (TIMA; TESCAN Orsay Holding, Brno, Czech Republic), or RoqSCAN (Carl Zeiss AG, Oberkochen, Germany) are commercially available. The MLA system uses the chemical information obtained from the EDX analysis combined with BSE imaging to automatically identify mineral phases (Gu 2003, Fandrich et al. 2007). For each mineral phase identified by BSE, the respective X-ray spectrum of each mineral phase is compared with the X-ray spectra of known phases in a database. After comparison each phase on the sample surface is classified and displayed on a MLA image. Besides the total mineralogical composition in area and weight percentage, the MLA software provides additional information which are in particular of interest for ore processing, such as grain size distributions and intergrowths of single mineral phases.

A polished section was produced from a PGM flotation concentrate originating from the

Mogalakwena Mine. The quantitative mineralogical analysis on the concentrate was carried out using a FEI-Quanta 650 F field emission scanning electron microscope (FE-SEM) equipped with two Bruker Quantax X-Flash 5030 energy dispersive X-ray spectroscopy (EDS) detectors and FEIs MLA suite 3.1.4 software for data acquisition, at the Helmholtz Institute Freiberg for Resource Technology, Germany.

For MLA analysis the analytical parameters used for PGM identification are given in Table 3.1.

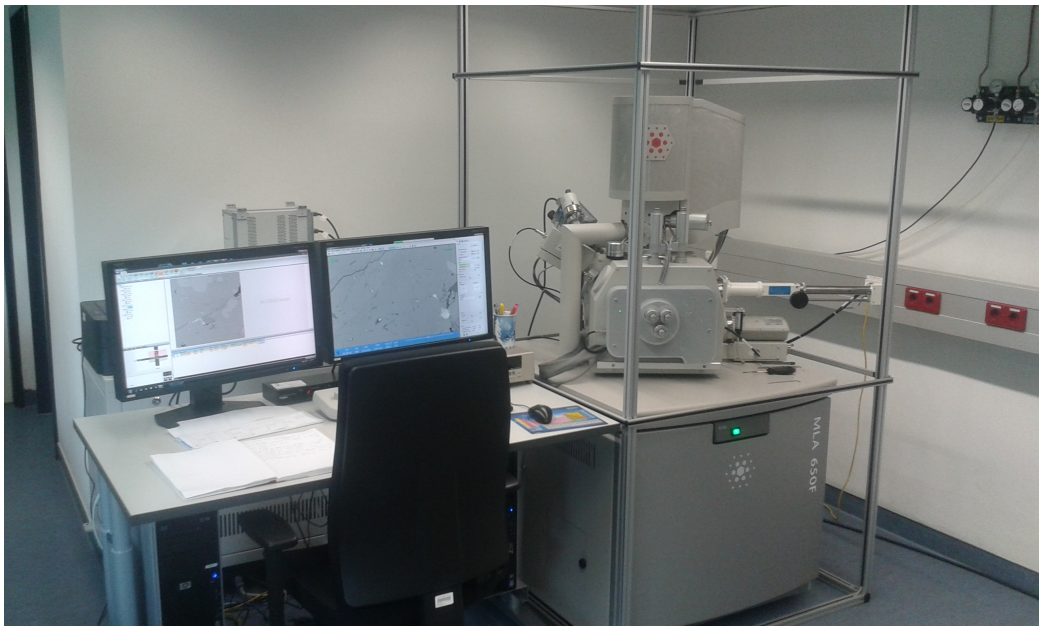

Figure 3.2 – Scanning electron microscope FEI MLA 650F at the BGR.

Table 3.1 – Analytical SEM and MLA parameters for PGM. Spot size is different at the Helmholtz Institute Freiberg for Resource Technology (5.704) and the BGR, Hannover (5.9). The parameters are the same as used in Osbahr et al. (2015).

SEM parameters		MLA parameters	
Voltage (kV)	25	Scan speed	16
Working distance (mm)	13	Resolution	1000 x 1000
Probe current (nA)	10	Pixel size (μm)	0.6
Spot size	5.704/5.9*	Acq. time (ms)	5
Horizontal Field Width (μm)	600	SPL BSE trigger	95-255
Brightness	93.77	Minimum grain size (px)	2
Contrast	19.40		
BSE calibration	Au 245		

3.7 Electron probe microanalysis

For analyses of sulfide, PGM and weathered minerals a CAMECA SX 100 electron probe microanalysis (EPMA) at the BGR (Hannover/Germany) was used (Figure 3.3). Electron probe microanalysis measures element concentrations of materials on a micrometer scale. It is a non-destructive method using a focused electron beam which bombards the sample with a specific acceleration voltage (10 to 50 keV). The interaction of electrons with the sample causes formation of characteristic X-rays which are detected by wavelength dispersive X-ray spetrometers (WDX). The wavelengths of these X-rays are element characteristic and are thus used to identify the elemental composition of the respective sample. Based on this method, elements with an atomic number between 5 (Boron) and 92 (Uranium) can be identified. The WDX measures the amount of X-rays of a specific wavelength which is diffracted by a crystal. Compared to EDX, WDX counts only the amount of X-rays of a single wavelength at time. The crystal, which is necessary for the measurement of the wavelengths of the emitted X-rays, has known lattice values at a precise angle. Based on this procedure the WDX has a higher spectral resolution than the EDX in order to obtain precise chemical analysis of the sample. The sample needs to be coated with carbon. Generally, an EMPA has several different WDX spectrometers in order to measure multiple elements at the same time. At the time when the characteristic X-rays meet the analytical crystal at a specific angle Θ, just the wavelengths which obey the Bragg's Law (Equation 3.3) are reflected and just a single wavelength is passed to the detector. The CAMECA SX 100 works with a tungsten filament as cathode which emits the electrons for the electron bombardment of the sample. The emitted electrons from the cathode are focused with by Wehnelt cylinder and are accelerated up to 50 keV (typically 15 to 25 kev). Further, the electron beam runs through an electromagnetic lens system where it is focused. In the same manner as with the SEM, backscattered electrons can be used to obtain a BSE image.

For the analysis of pentlandite (Table 3.2), chalcopyrite (Table 3.3), pyrite (Table 3.4), pyrrhotite (Table 3.5), and for the analysis of PGE contents in secondary minerals (Table 3.6) different analytical procedures were followed.

Figure 3.3 – The electron microprobe CAMECA SX 100 at the BGR, Hannover. Photo taken from BGR (2016).

Table 3.2 – Analytical parameters including measured lines, measurement time (meas. time) in seconds, used standards, and median detection limits (det. lim.) in ppm at 120 nA and 20 kV for each element during analysis of pentlandite at the Cameca SX 100 electron microprobe.

element	line	meas. time [s]	reference material	median det. lim. [ppm]
Al	Ka	20	chromite	76
Si	Ka	10	metal	163
S	Ka	10	pentlandite	282
Cr	Ka	20	metal	61
Fe	Ka	10	pentlandite	309
Co	Ka	100	metal	72
Ni	Ka	10	pentlandite	442
Cu	Ka	40	chalcopyrite	171
As	La	60	galliumarsenide	181
Se	La	100	metal	91
Rh	La	60	metal	117
Pd	La*	130	metal	147
Ag	Ka	180	metal	156
Pt	La	190	metal	301

Table 3.3 – Analytical parameters including measured lines, measurement time (meas. time) in seconds, used standards, and median detection limits (det. lim.) in ppm at 120 nA and 20 kV for each element during analysis of chalcopyrite at the Cameca SX 100 electron microprobe.

element	line	meas. time [s]	reference material	median det. lim. [ppm]
Al	Ka	20	chromite	75
Si	Ka	10	metal	160
S	Ka	10	chalcopyrite	288
Cr	Ka	20	metal	72
Fe	Ka	10	chalcopyrite	311
Co	Ka	100	metal	71
Ni	Ka	10	pentlandite	127
Cu	Ka	10	chalcopyrite	304
As	La	60	galliumarsenide	180
Se	La	100	metal	90
Rh	La	60	metal	125
Pd	La*	130	metal	147
Ag	Ka	180	metal	155
Pt	La	190	metal	297

Table 3.4 – Analytical parameters including measured lines, measurement time (meas. time) in seconds, used standards, and median detection limits (det. lim.) in ppm at 120 nA and 20 kV for each element during analysis of pyrite at the Cameca SX 100 electron microprobe.

element	line	meas. time [s]	reference material	median det. lim. [ppm]
Al	Ka	20	chromite	63
Si	Ka	10	metal	135
S	Ka	10	pyrite	312
Cr	Ka	20	metal	70
Fe	Ka	10	pyrite	322
Co	Ka	80	metal	79
Ni	Ka	40	pentlandite	125
Cu	Ka	40	chalcopyrite	155
As	La	60	galliumarsenide	148
Se	La	100	metal	75
Rh	La	60	metal	114
Pd	La*	130	metal	145
Ag	Ka	180	metal	156
Pt	La	190	metal	288

Table 3.5 – Analytical parameters including measured lines, measurement time (meas. time) in seconds, used standards, and median detection limits (det. lim.) in ppm at 120 nA and 20 kV for each element during analysis of pyrrhotite at the Cameca SX 100 electron microprobe.

element	line	meas. time [s]	reference material	median det. lim. [ppm]
Al	Ka	20	chromite	69
Si	Ka	10	metal	148
S	Ka	10	pyrrhotite	289
Cr	Ka	20	metal	68
Fe	Ka	10	pyrrhotite	368
Co	Ka	80	metal	83
Ni	Ka	40	pentlandite	129
Cu	Ka	40	chalcopyrite	159
As	La	60	galliumarsenide	164
Se	La	100	metal	82
Rh	La	60	metal	113
Pd	La*	130	metal	144
Ag	Ka	180	metal	153
Pt	La	190	metal	293

3.8 Laser ablation-inductively coupled plasma-mass spectrometry

Laser ablation-inductively coupled plasma-mass spectrometry (LA-ICP-MS) is used as micro-analytical tool for quantitative in-situ analysis of solid samples for determination of major and trace element concentrations or isotope ratios with a high spatial resolution and spot sizes of 10 μm to several 10s μm (Heinrich et al. 2003, Longerich 2008). Figure 3.4B shows the mass spectrometer used in this study which is a ThermoScientific Element XR double-focusing sector field-inductively coupled plasma-mass spectrometer (SF-ICP-MS). The SF-ICP-MS is coupled to a UP193-HE (New Wave Research) femtosecond solid-state Ti-sapphire laser (Figure 3.4A). The system was tuned using a NIST610 reference material. Spot size diameters were 20 to 30 μm. Total measuring time was 120 s with 60 s for the background and 60 s for the signal on the sample/reference material. For external standardisation a NIST610 (Jochum et al. 2011) and a Lombard (Gilbert et al. 2012) reference material were used. Analyses were carried out in

Table 3.6 – Analytical parameters including measured lines, measurement time (meas. time) in seconds, used standards, and median detection limits (det. lim.) in ppm at 120 nA and 20kV for each element during analysis of secondary PGE-bearing phases at the Cameca SX 100 electron microprobe.

element	line	meas. time [s]	reference material	median det. lim. [ppm]
Mg	Ka	10	chromite	129
Al	Ka	10	chromite	101
Si	Ka	10	metal	99
S	Ka	10	pentlandite	170
Ca	Ka	10	kaersutite	127
Cr	Ka	30	metal	79
Mn	Ka	10	metal	158
Fe	Ka	10	metal	254
Co	Ka	60	metal	93
Ni	Ka	30	metal	144
Cu	Ka	30	metal	147
As	La	80	galliumarsenide	105
Se	La	80	metal	87
Rh	La	120	metal	91
Pd	Lb	180	metal	53
Ag	Lb	200	metal	317
Pt	La	360	metal	205

packages of 20 analyses with 4 times NIST610 and 4 times Lombard followed by 12 analyses on the samples. The following isotopes were measured: ^{25}Mg, ^{27}Al, ^{29}Si, ^{34}S, ^{43}Ca, ^{47}Ti, ^{55}Mn, ^{57}Fe, ^{60}Ni, ^{63}Cu, ^{77}Se, ^{89}Y, ^{99}Ru, ^{101}Ru, ^{103}Rh, ^{105}Pd, ^{108}Pd, ^{111}Cd, ^{137}Ba, ^{139}La, ^{140}Ce, ^{147}Sm, ^{153}Eu, ^{172}Yb, ^{175}Lu, ^{185}Re, ^{189}Os, ^{193}Ir, ^{194}Pt, ^{195}Pt, ^{197}Au, ^{205}Tl. Ablation was done mostly as lines and smooth spectra were obtained. The raw data were exported to a data-handling software tool implemented in JAVA using the libraries JFreeChart (JFree 2009), commons Math (Commons 2009) and POI (POI 2009). A normalization of MgO, Al_2O_3, SiO_2, CaO, MnO, FeO to 100% was used, because these oxides comprise the major compounds of the analyzed phases.

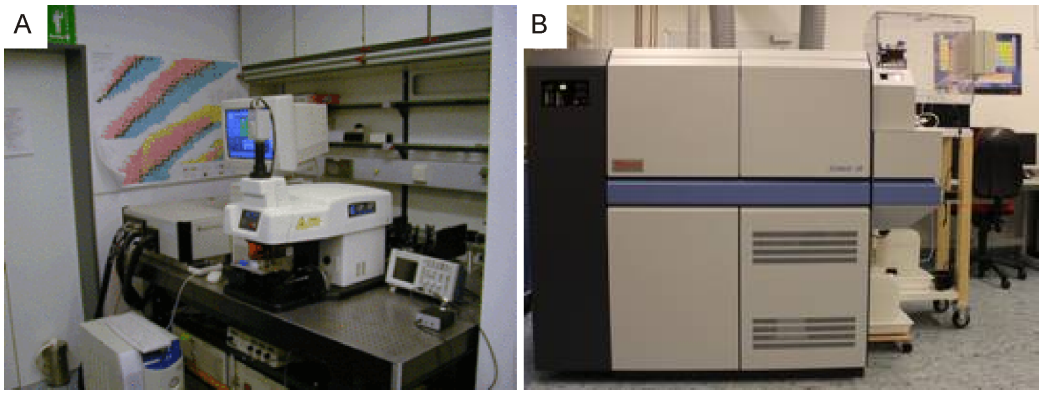

Figure 3.4 – The LA-ICP-MS system in operation at the Leibniz University, Hannover. A. The New Wave Research UP193-HE femtosecond unit. B: The ThermoScientific Element XR mass spectrometer. Photo taken from Institute for Mineralogy - University Hannover (2016).

The principle of a laser ablation (LA) system is the emission of highly focused laser light pulses to remove material at a spatial resolution of a few micrometers in diameter from a solid sample. The sample is contained in a gastight cell of the laser ablation system. The sample is transformed by the laser into an aerosol of small particles which is transported in a flow of gas (Longerich 2008) to the inductively coupled plasma. The aerosol from the ablation of the sample is carried into the plasma where it is vaporized, atomized and ionized. In the mass spectrometer the ions are separated based on their mass and the intensity (ions per second) of the ion beam is transformed in to an electrical signal. This electrical signal can then be measured.

Three major types of configurations for an ICP-MS system exist, time of flight, quadropole, and magnetic sector field (single collector sector and multi collector). The differences between these configuration is mainly in the speed (time to change from one selected mass to another),

the sensitivity (signal per unit concentration) and the installation cost (Longerich 2008). The requirement for the each configuration depends on the application (general use for elemental and isotopic analysis or a high precision isotope ratios).

3.9 Transmission electron microscopy and focused ion beam

The investigation of solids by transmission electron microscopy (TEM) allows the unique combination of information about chemical composition and structural crystallographic information (e.g., crystal structure on the nanometre scale). Chemical information about a solid may be obtained with TEM using three different analytical techniques: energy dispersive X-ray analysis (EDX); electron energy-loss spectroscopy (EELS); and high-angle annular dark field imaging (HAADF) (Wirth 2004, 2009).

High-energy electrons (e.g. 200 keV) penetrate and interact with the sample emitting Bremstrahlung X-rays and characteristic X-rays. The use of the EDX system provides chemical information of the sample using the excited characteristic X-rays of the specimen caused by the interaction of the accelerated electrons with the sample. For the use of the TEM in combination with FIB, thin foils with homogeneous thicknesses, element mapping and line scans with very high spatial resolution (few nanometers) can be generated (Wirth 2004, 2009). Besides the described generated X-rays which are used for an EDX analysis, the interaction of incident high-energy electrons also results in elastic and inelastic scattering of the electrons within the sample. Elastic scattering is an electron-nucleus interaction without energy loss but with a change in momentum and scattering direction. On the other hand, inelastic scattering is primarily an electron-electron interaction and involves a loss of energy as well as a change in momentum (Wirth 2009). The inelastically scattered electrons may be used for elemental mapping with very high spatial resolution. Both elastically and inelastically scattered electrons are detected by the HAADF detectors which are used for imaging in the scanning transmission mode (STEM) of the microscope (Wirth 2009).

For TEM investigations electron transparent samples with a thickness usually less than

200 nm is required. A nowadays largely used sample preparation technique in geoscience is the focused ion beam (FIB). The FIB is a site-specific sample preparation technique that can produce thin foils with the dimensions 15 to 20 μm wide, 10 to 15 μm high and approximately 100 to 150 nm thick from metals, alloys, ceramics, minerals, glasses and organic materials (Wirth 2004, 2009). For the preparation of FIB foils, atoms are sputtered from the target material by bombarding the target with accelerated heavy ions. For this study foils with a size of 15 x 10 x 0.15 μm were sputtered with Ga ions accelerated to 30 keV from chosen locations within the sample material (Figure 3.5). For the preparation of FIB foils a FEI FIB200TEM (Figure 3.6A) was used.

For the TEM study a FEI F20 X-Twin transmission electron microscope (Figure 3.6B) with a Schottky field emitter as electron source at the GFZ Potsdam was used. The TEM is equipped with a Gatan Tridiem imaging filter, a Fishione high-angle annular dark field detector allowing for Z-contrast sensitive imaging, and an EDX (Wirth 2004, 2009, Wirth et al. 2013).

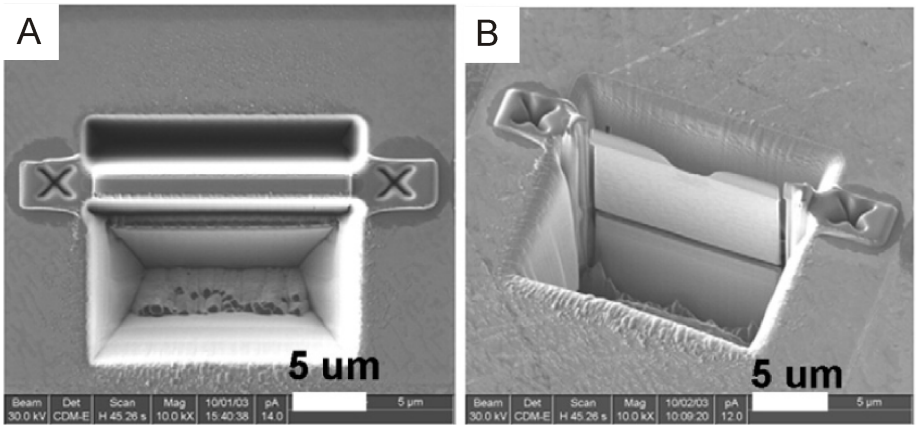

Figure 3.5 – Secondary electron image of a FIB foil modified after Wirth (2009). A. Platinum strip deposited on the surface with two reference crosses milled. Two trenches, one in the front of the foil and one smaller behind it, are already sputtered. B. The FIB foil is ready to be taken out.

Crystallographic information of nano-crystals and host minerals were obtained from fast Fourier transformation (FFT) which has been calculated from high-resolution images (HREM). Therefore, single crystal diffraction patterns were compared with calculated spacing from the literature (e.g., American Mineralogist Crystal Structure Database) by measuring the distance between Bragg reflections and the angles between the individual reflections. Chemical compositions of phases are measured with a EDX in the STEM. Low Ga-concentrations in the EDX

measurements of pentlandite may be present due to the preparation method of foils using FIB. More detailed descriptions of the FIB sample preparation are given by Wirth (2004, 2009) and Wirth et al. (2013).

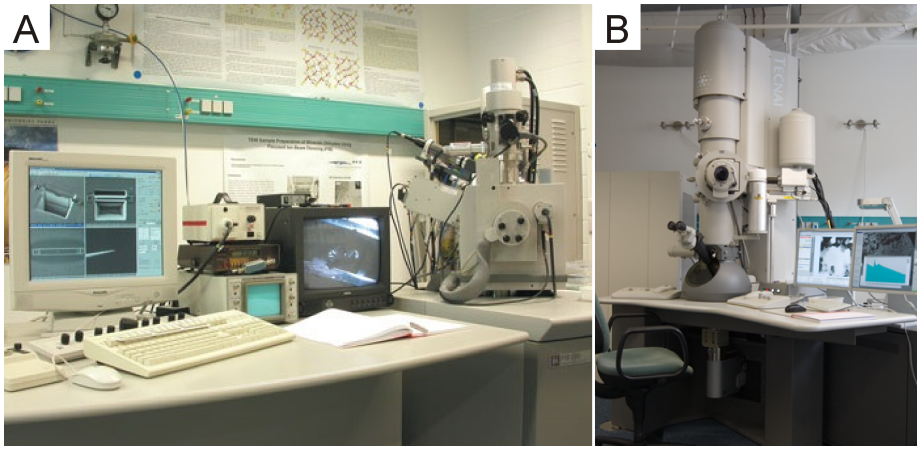

Figure 3.6 – A. For the preparation of FIB foils an FEI FIB200TEM scanning electron microscope equipped with a focus ion beam was used. B. FEI F20 X-Twin transmission electron microscope at the Geoforschungszentrum (GFZ), Potsdam.

3.10 Sulfur isotopes

Sulfur isotopic measurements ($\delta^{34}S$) were carried out using a ThermoFinniganMat DELTA Plus mass spectrometer coupled to an elemental analyzer (Carlo Erba) at the Geologisch-Palaeontologisches Institut, Westfaelische Wilhelms-Universitaet Muenster, Germany.

The four stable sulfur isotopes are ^{32}S, ^{33}S, ^{34}S and ^{36}S with approximate abundances of 95.02, 0.75, 4.21, and 0.002% (Macnamara & Thoede 1950). The variation of sulfur isotopes are in a relatively small range as most fractionation processes typically cause variations in the ratios in the fifth or sixth decimal places (Seal 2006). Therefore, the isotopic composition of substances is expressed in the delta (δ) notation as parts per thousands variation relative to a reference material. The typically used reference material is the Vienna Canyon Diablo Troilite (VCDT) with $\delta^{34}S = 0.0$. A meteoritic sulfide mineral as the reference material is used because it is assumed that meteoritic sulfide represents the primordial sulfur isotope composition of the

Earth (Nielsen et al. 1991). The δ - notation is defined as:

$$\delta^{34}S = \left(\frac{\frac{^{34}S}{^{32}S\,sample} - \frac{^{34}S}{^{32}S\,reference}}{\frac{^{34}S}{^{32}S\,reference}} \right) x1000 \tag{3.4}$$

3.11 Electric pulse disaggregation and hydroseparation

The distributions of PGM within two samples (one oxidized and one pristine ore sample) of drill core Oymetox 2 were determined by Electric pulse disaggregation (EPD) and hydroseparation (HS) and additional SEM work. The EPD and HS analyses were carried out by CNT-Mineral Consulting Inc. in St. Petersburg.

Electric pulse disaggregation and HS are techniques for extraction of specific minerals such as PGM, and are also methods for the recovery of undamaged crystals (Cabri et al. 2008). Electric pulse disaggregation is a mineral separation technique that uses an electric current from a high-voltage power source greater than 100 kV, which induces the explosive breakdown of the solids (Andres et al. 2001, Cabri et al. 2008). This high voltage is achieved by the use of capacitors which are charged in a parallel way but discharged in series (Cabri et al. 2008). The sample is placed in a water bath and rapid distribution of electric pulses leads to explosions, where the breakdown preferentially occurs along grain boundaries since these represent zones of weakness. Individual mineral grains of interest can be recovered by EPD from a rock in their original shape and undamaged, which in contrast to conventional mechanical crushing allows the study and analysis of individual rock-forming and ore minerals.

The breakdown occurs along the grain boundaries as a result of electrical breakdown and radial expansion of the plasma streamers occurring along the boundaries of minerals with different permittivity and electrical conductivity. An unbalanced electrical charge occurs at the grain boundaries of different minerals (Andres et al. 2001). Individual and undamaged mineral grains can be extracted from rock samples by this method. Usual mechanical crushing of whole-rock samples is not necessary, since EPD allows more precise separations (Cabri et al. 2008, Oberthür et al. 2008).

The products of EPD are particularly well suited to further handling with HS resulting in representative concentrates of all heavy minerals including the fines particles (5 to 10 μm) (Cabri et al. 2008). The HS is a water-based mineral separation technique which can be applied for various rock and ore types (Rudashevsky et al. 2002). The drawback of this method is that the settling velocity depends on the grain size (radius) squared and the density only by the power of one (Rudashevsky et al. 2002). Hydroseparation is used to produce representative heavy-mineral concentrates which are produced by applying a carefully controlled upward pulsating water stream. Following Stokes' law, heavy minerals are settled in the glass separation tube (GST) and light fractions are moved upward in the GST and are collected in a beaker under the GST. The concentrated heavy minerals remain in the GST and can be extracted for further investigations. Using the HS technique the nugget effect can be overcome even if only limited sample material (e.g., drill core, museum specimens) is available (Oberthür et al. 2008). From the heavy mineral concentrates a monolayer polished sections is prepared which can then further be studied by SEM, MLA and EPMA.

Using a combined method of EPD and HS, the crystal morphology, mineralogy and mineral chemistry of PGM can be studied in rocks which contain only low concentrations of valuable minerals.

Chapter 4

Mineralogical siting of platinum-group elements in pentlandite from the Bushveld Complex, South Africa

This chapter is published as: Junge, M., Wirth, R., Oberthür, T., Melcher, F., Schreiber, A. (2015): Mineralogical siting of platinum-group elements in pentlandite from the Bushveld Complex, South Africa. Mineralium Deposita: 50, 41-54.

4.1 Introduction

Platinum-group element (PGE) mineralization is mainly associated with mafic-ultramafic intrusions such as the Bushveld Complex in South Africa. In these ores, the PGEs are usually bimodally distributed, occurring both as discrete platinum group minerals (PGMs) and hosted by sulfides. Especially, pentlandite [$(Fe,Ni)_9S_8$] is known to contain elevated concentrations of Pd and Rh (Cabri & Laflamme 1981, Todd et al. 1982, Cabri et al. 1984, Oberthür et al. 1997a, 2003, Gervilla et al. 2004, Godel et al. 2007, Holwell & McDonald 2010, Osbahr et al. 2013, 2014, Junge et al. 2014).

So far, PGE contents of sulfides were studied using different analytical methods such as

electron probe microanalysis (EPMA), particle-induced X-ray emission (PIXE), secondary ion mass spectrometry (SIMS), and laser ablation induced coupled plasma mass spectrometry (LA-ICP-MS) (Cabri et al. 1984, Cabri 1988, Oberthür et al. 1997a, 2003, Osbahr et al. 2013, 2014, Junge et al. 2014). EPMA provides chemical information with detection limits of tens of ppm at a spatial resolution of about 1 μm. LA-ICP-MS enables analysis in the ppb range but at inferior resolution due to the relative wide laser beam (10 to 50 μm). Junge et al. (2014) studied pentlandite grains from the UG-2 (Karee Mine, western Bushveld Complex, South Africa) with EPMA and LA-ICP-MS and analyzed maximum values of 2.2 wt% Pd and 3.0 wt% Rh (average contents in the hundreds of ppm range) and elevated contents of Ir (30 to 500 ppm), unparalleled by Os and Ru, and therefore not reflecting inclusions of laurite [(Ru,Os,Ir)S_2]. Preparation of focused ion beam (FIB) foils for transmission electron microscopy (TEM) studies with applications in geosciences exists since about 15 years (Wirth 2004, 2009). However, this technique has only occasionally been applied to problems related to ore genesis (Ciobanu et al. 2011, Wirth et al. 2013).

In the present study, pentlandite grains with elevated concentrations of PGEs from the UG-2 (Karee Mine) and the Platreef (Mogalakwena Mine, Sandsloot pit) were investigated. Following ore microscopy and scanning electron microscopy (SEM) studies, high-resolution element maps and line scans were acquired using TEM in order to reveal the distribution of PGEs in pentlandite on the nanometer-scale. The purposes of this study are to gather insight into the deportment of PGEs in pentlandite from the Bushveld.

4.2 Geological background

The Bushveld Complex in South Africa (Figure 2.1) is the largest layered mafic-ultramafic intrusion on Earth covering an area of 66,000 km^2 and has an age of 2,055 $\pm$ 3.9 Ma (Scoates & Friedman 2008). Apart from containing the largest resources of PGEs on Earth (about 70% of the Pt and 40% of the Pd; Vermaak (1995)), the Bushveld Complex also hosts economically important resources of Cr and V. Economic PGE deposits within the Bushveld Complex mainly occur in three ore bodies, namely the Merensky Reef, the UG-2 chromitite, and the Platreef. Notably, the UG-2 chromitite is the largest resource of PGEs on Earth (Vermaak 1995).

The UG-2 chromitite occurs in the Upper Group of the Critical Zone, between 15 to 400 m below the Merensky Reef and has a general thickness of about 1 m, varying between 0.4 and 2.5 m (Hiemstra 1979, 1985, 1986, McLaren & De Villiers 1982, Schouwstra et al. 2000). Regional studies indicate that the Merensky Reef and the UG-2 are laterally continuous over hundreds of kilometers (Von Gruenewaldt et al. 1986, Hatton & von Gruenewaldt 1987, Scoon & Teigler 1994). In the UG-2, PGE concentrations typically range from 4 to 8 g/t and the distribution of the PGE is generally limited to the UG-2 chromitite itself, as essentially no PGEs are present above or below the chromitite layer (McLaren & De Villiers 1982, Hiemstra 1985, 1986, Lee 1996, Cawthorn 2011). Copper and Ni contents are generally below 0.05 wt%, and S is below 0.1 wt%, indicating low sulfide contents (Von Gruenewaldt et al. 1986, Lee 1996, Cawthorn 2011). Indeed, sulfides (pentlandite, chalcopyrite, and minor pyrrhotite) are rare (<1 vol%) in the UG-2 and generally occur interstitial to chromite grains. The PGMs (grain sizes <5 to 50 μm) in the UG-2 are locked within or more commonly occur at the peripheries of sulfide grains, and the suite of PGMs is dominated by laurite [RuS_2], cooperite/ braggite [(Pt,Pd)S], Pt-Fe alloy, and sperrylite [$PtAs_2$] (Kinloch 1982, McLaren & De Villiers 1982, Penberthy & Merkle 1999, Schouwstra et al. 2000, Kuhlmann et al. 2006, Junge et al. 2014). Platinum and the IPGEs (Os, Ir, Ru) are dominantly present as discrete PGMs, whereas large proportions of the Pd and Rh are hosted in pentlandite which may contain up to 2 wt% of Pd and 3 wt% of Rh as outlined by Junge et al. (2014).

The Platreef in the northern Bushveld Complex varies up to 400 m in thickness with sulfide contents of approximately 3 vol% and PGE contents ranging between 1 and 4 g/t (Vermaak 1995, Kinnaird & McDonald 2005, McDonald & Holwell 2011). The floor rocks of the Platreef show lithological variation, including shale, BIF, dolomite, granite gneiss, and quartzite (Manyeruke et al. 2005, Holwell et al. 2006, McDonald & Holwell 2011). The Platreef is currently the most extensively exploited PGE deposit by open-pit mining worldwide. Platinum-group elements within the Platreef are bimodally distributed, occurring both as discrete PGMs and within sulfides. Again, pentlandite may hold elevated contents of PGEs (Pd median values (Sandsloot; this study), 390 ppm).

4.3 Samples and analytical techniques

This study focuses on pentlandite from the Platreef at Mogalakwena Mine (Sandsloot pit) in the northern Bushveld Complex and from the UG-2 chromitite at the Karee Mine, western Bushveld Complex (2.1). Following conventional methods of study, namely ore microscopy, scanning electron microscopy (SEM), and electron probe microanalysis (EPMA), seven electron transparent foils from three pentlandite grains of the UG-2 with the largest concentrations of Pd and Rh (Table 4.1) were sputtered out of one polished section (AS 8918b; Table 4.2). From the Platreef, eight electron transparent foils (four from AS10340, three from AS7368, and one from AS7372) were sputtered out of pentlandite with FIB. Pentlandite grains of the Platreef contain several 100s ppm of Pd (median value, Pd, 390 ppm). In total, 15 TEM foils of pentlandite were analyzed for the distribution of PGEs on the nanometer scale.

Pentlandite grains were analyzed with a CAMECA SX 100 electron microprobe using the following analytical conditions: 20-kV acceleration voltage, 120-nA sample current, and up to 180-s measuring time. Synthetic metals (Pd, Rh, Pt, Ag, Co, Cu, Se) and natural sulfides (pentlandite) were used as standards. Mean detection limits were 75 ppm for Co, 100 ppm for Se, 120 ppm for Rh, 140 ppm for Pd, 160 ppm for Ag, and 300 ppm for Pt. Laser Ablation Inductively Coupled Plasma Mass Spectrometry (laser wavelength 193 nm, Agilent 7500i) measurements were conducted using a spot size of 10 to 25 μm in diameter, a laser frequency of 20 Hz and 0.95 GW/cm^2, and a fluence of 4.8 J/cm^2. Acquisition time was 20 s for the background and 20 s for the mineral analysis. Signal quantification was carried out by GLITTER (van Achterbergh et al. 2000). The methodology of the LA-ICP-MS is the same as described by Osbahr et al. (2013).

Electron probe microanalysis and LA-ICP-MS are key methods for the in situ analysis of major, minor, and trace elements in geosciences. Electron probe microanalysis is a non-destructive method with an electron beam size down to 1 μm (analytical volume of a few cubic micrometers) emitting X-rays that are analyzed by wavelength dispersive spectrometry. Detection limits of EPMA are in the 10s to 100s ppm range. Laser Ablation Inductively Coupled Plasma Mass Spectrometry is a destructive method creating craters or lines of several 10s to 100s cubic micrometers in volume. The larger analytical volume obtained by LA-ICP-MS and the measurement of isotopes instead of X-rays allow analysis of trace elements in the ppb range.

Both, EPMA and LA-ICP-MS, deliver only chemical data. Time-resolved spectra as obtained by LA-ICP-MS may discern very tiny inclusions when using appropriate analytical conditions; however, no direct confirmation and visualization of such inclusions are possible. In contrast, TEM allows a direct link between the crystal and its chemical composition on the nanometer scale. The preparation of electron transparent foils for the TEM investigation was carried out using a FIB technique, which is a site-specific preparation method. For this study, foils with a size of 15x10x0.15 μm were sputtered with Ga ions accelerated to 30 keV from chosen locations within pentlandite. Electron transparent foils were cut from pentlandite grains previously analyzed by EPMA (Platreef and UG-2; see Table 4.1).

For the TEM study, a FEI F20 X-Twin transmission electron microscope with a Schottky field emitter as electron source was used at the GeoForschungsZentrum in Potsdam. The TEM is equipped with a Gatan Tridiem Imaging Filter, a Fishione high-angle annular dark field detector (HAADF) allowing for Z-contrast sensitive imaging, and an EDAX Xray analyzer (Wirth et al. 2013).

Crystallographic information of nano-crystals and host minerals were obtained from fast Fourier transforms (FFTs) which have been calculated from high-resolution electron microscopy (HREM). For that purpose, measured d-spacings from single crystal diffraction patterns were compared with calculated d-spacings from the literature (American Mineralogist Crystal Structure Database) by measuring the distance between Bragg reflections and the angles between the individual reflections. Chemical compositions of phases were measured with an energy-dispersive X-ray (EDX) analyzer in the scanning transmission electron microscopy (STEM) mode. Low Ga concentrations in the EDX measurements of pentlandite are usually present in the EDX spectra due to Ga ion implantation during FIBs ample preparation. Detailed descriptions of the FIB sample preparation were given elsewhere (Wirth 2004, 2009, Wirth et al. 2013).

4.4 Results

Geochemical data of PGEs within the UG-2 (whole-rock data) are compared to PGE data of pentlandite analyzed by LA-ICP-MS (normalized to C1-chondrite; Fig. 4.1). The whole rock data closely correspond to the average PGE data of the UG-2 as given by Barnes & Maier

Table 4.1 – EPMA measurements of Pd and Rh (in wt%) from of the UG-2 (pn1_UG2 to pn3_UG2) and the Platreef (pn_1Pr to pn_5Pr) and LA-ICP-MS measurements of Pd and Rh (in wt%) and Os, Ir, Ru, and Pt (in ppm) in pentlandite from of the UG-2.

		EPMA (wt.%)		LA-ICP-MS (wt.%)(ppm)						
		Pd	Rh	Pd	Rh	Os	Ir	Ru	Pt	Foils
pn_1UG2		0.65	3.00	0.42	2.18	<1.1	327	3.94	<0.76	#3510
		0.63	2.35	0.65	2.38	<1.4	326	<1.2	1.44	
pn_2UG2		0.02	12.5							#3512,#3516,#3534
		0.05	10.3							
pn_3UG2		0.99	1.38	0.93	1.64	<0.3	471	1.53	3.52	#3514,#3523,#3533
		1.26	1.16	0.50	0.95	0.715	396	1.60	6.47	
		0.87	1.31							
	(n)	(ppm)								
pn_1Pr	5	680	<135							#3502,#3511
pn_2Pr	3	504	<136							#3504,#3509
pn_3Pr	4	360	<135							#3522
pn_4Pr	4	370	<135							#3524
pn_5Pr	4	357	<136							#3503

(2002a). However, the chondrite-normalized pattern for the PGEs in pentlandite shows a distinct fractionation (enrichment) of Rh and Pd as well as Ir. In contrast, Os, Ru, and Pt display minima. Therefore, Junge et al. (2014) proposed that the PGE-in pentlandite pattern largely reflects the capability of pentlandite to host Rh and Pd as well as some Ir in its crystal lattice, and as Pt is not compatible in pentlandite, this element forms discrete PGMs. Ruthenium and Os appear to have undergone a comparable fate as Pt as they are mainly found in laurite [RuS_2]. In samples of the UG-2 and the Platreef, discrete PGMs (grain sizes 1 to 50 μm) were detected by ore microscopy and analyzed using SEM and EPMA. The PGMs in the UG-2 at the Karee Mine are mainly cooperite/braggite [(Pt,Pd)S], laurite, and Pt-Fe alloy (Fig. 4.2a). The suite of PGMs is Pt and IPGE-dominated although the whole-rock analysis of the sample (Junge et al. 2014) indicates elevated contents of Pd (2,290 ppb) and Rh (790 ppb). In the UG-2, Pd, Rh, and Ir are hosted by base metal sulfides, whereas the concentrations of Pt, Os, and Ru in base metal sulfides are low, and therefore, these metals occur as discrete PGMs (Junge et al. 2014). In polished sections from the Platreef, additionally to the identification of discrete PGMs (mainly Pt-Pd-bismuthotellurides, cooperite/braggite; grain sizes 1 to 50 μm; Fig. 4.2b), el-

Table 4.2 – Platinum-group mineral inclusions and PGE incorporation in pentlandite from the UG-2 chromitite and the Platreef.

Foils	Sample no.	nPGM	Grain size	Remarks
Platreef				
AS10340				
#3502	pn1_Pr	PtTe	about 50 nm	Fluid inclusion trails
#3511	pn1_Pr	n.d.		
#3504	pn2_Pr	(Pt,Pd)Sn	about 50 nm	Unorientated relative to host sulfide
#3509	pn2_Pr	n.d.		
AS7368				
#3522	pn3_Pr	Pt(Fe,Cu)	about 1 μm	
#3524	pn4_Pr	Pt-(Fe,Cu)	200 nm	
#3503	pn5_Pr	PtBi	about 50 nm	
AS7372				
#3501	pn6_Pr	n.d.		
UG-2				
chromitite				
#3510	pn1_UG2	n.d.		Patchy solid solution of Rh and Ir
#3512	pn2_UG2	Pt-(Fe,Cu)	about 750 nm	Patchy solid solution of Rh and Ir
#3516	pn2_UG2	PdSn	about 50 nm	Patchy solid solution and lamellae of Rh and Ir
#3534	pn2_UG2	n.d.		Patchy solid solution of Rh and Ir
#3514	pn3_UG2	n.d.		Patchy solid solution of Rh and Ir
#3523	pn3_UG2	n.d.		Patchy solid solution of Rh and Ir
#3533	pn3_UG2	Pt-(Fe,Cu)	<50 nm	Patchy solid solution of Rh and Ir

In the foils of the Platreef, no patchy solid solution of any PGE was detected
nPGM nanometer-sized platinum-group mineral, n.d. not detected

evated concentrations of Pd (median value, Pd, 390 ppm) in pentlandite were measured with EPMA. Additionally, some (Pd,Pt)- germanides [$(Pd,Pt)_2Ge$] were observed, which so far have been rarely described (McLaren & De Villiers (1982), UG-2; Kozyrev et al. (2002), Norilsk-Talnakh; Grokhovskaya et al. (2005), Burakovsk Layered Complex; Holwell et al. (2006), Platreef/Sandsloot; Subbotin et al. (2012), Fedorova-Pana).

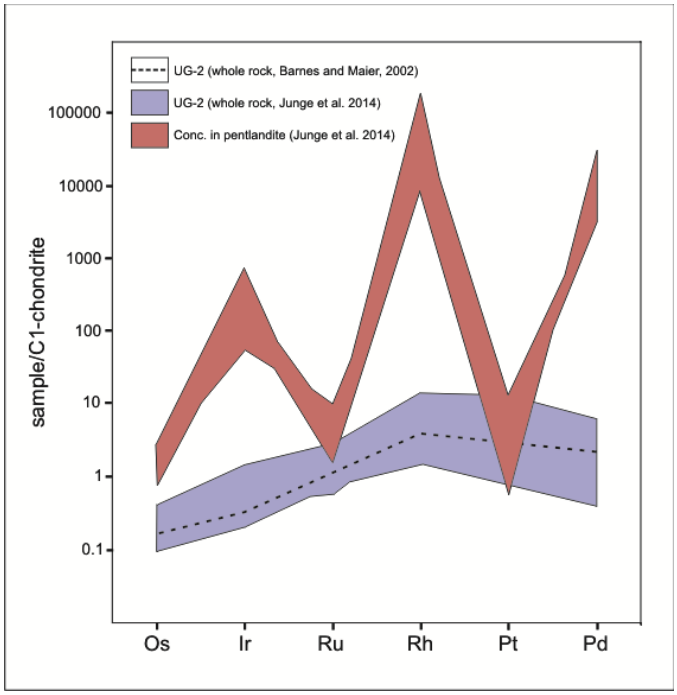

Figure 4.1 – Chondrite-normalized PGE distributions of average UG-2 of the western Bushveld (Barnes & Maier 2002a); stippled line), of DO-24 from the Karee Mine (Junge et al. 2014) whole rock data (red). Platinum-group elements contents of pentlandite analyzed by LA-ICP-MS (range in blue). C1-chondrite values from McDonough & Sun (1995).

4.4.1 Nano-inclusions of platinum-group minerals in pentlandite

In addition to the occurrence of discrete PGM grains (μm-sized), the TEM studies confirm the presence of heterogeneously distributed nm-sized PGM in pentlandite in the FIB foils of both the UG-2 and the Platreef (Figs. 4.2c, d, Table 4.2). These nanometer-sized PGMs (nPGMs) are mainly idiomorphic, with grain sizes <100 nm. Analyses of the nPGM display that these are Pt-Pd-Sn compounds, Pt-bismuthides and Pt-tellurides (Platreef only), a Pd-Sn compound (probably atokite [Pd_3Sn]; UG-2 only), and Pt-(Fe,Cu) alloys (at both localities). The example shown (Fig. 4.2c; TEM dark-field image) demonstrates that the Pt-Pd-Sn-nPGM (Platreef) is

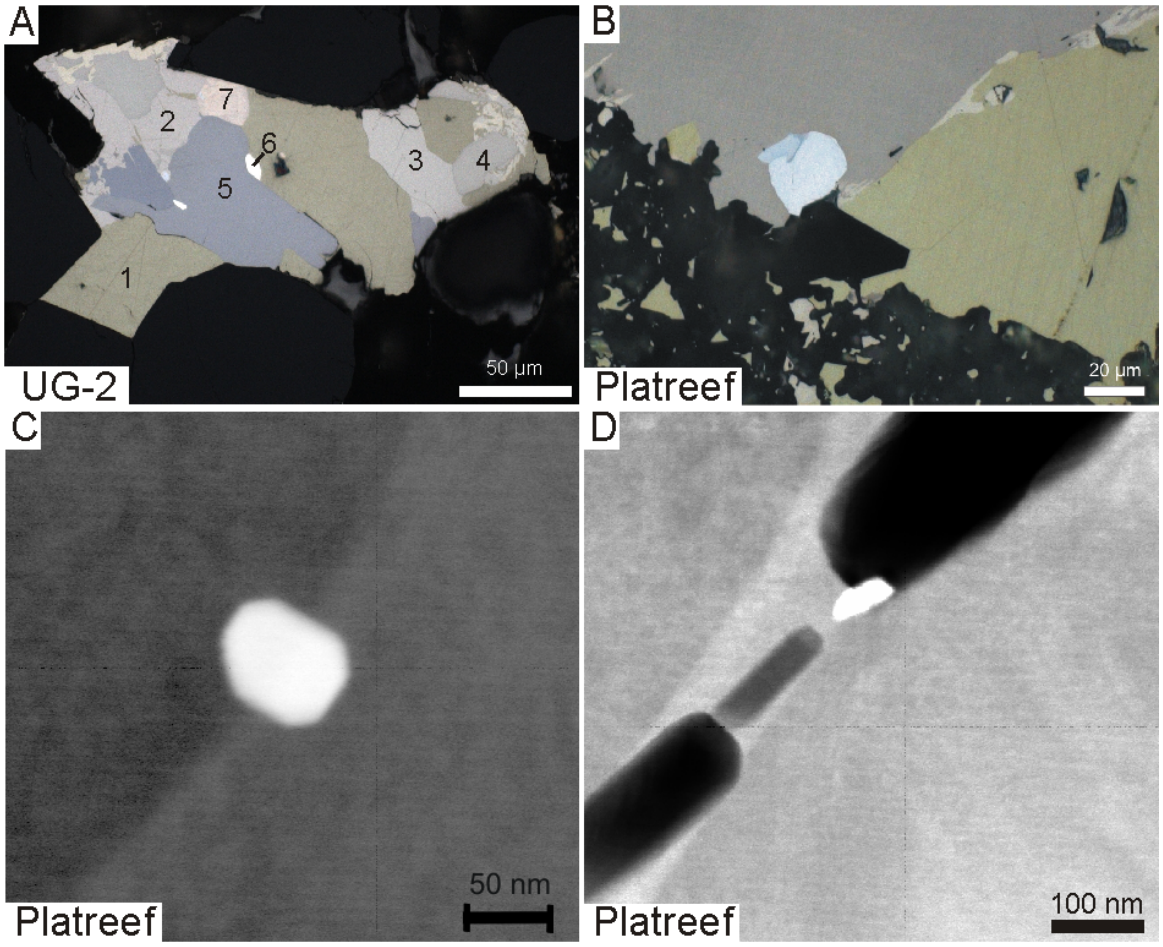

Figure 4.2 – a Chalcopyrite (1), pentlandite (2), millerite (3), pyrite (4), braggite [(Pt,Pd)S] (5), kotulskite [PdTe] (6), and temagamite [Pd_3HgTe_3] (7) (UG-2, Lebowa Mine, Eastern Bushveld Complex; AS7631, from Kuhlmann et al. (2006)). b Pyrrhotite, pentlandite, and chalcopyrite with PGE-bismuthotelluride (white) in reflected light, in oil (Platreef, Mogalakwena Mine; AS10451). c TEM bright-field image of one inclusion of a discrete nPGM [(Pt,Pd)Sn] in pentlandite of the Platreef (foil #3504). d Discrete nPGM [PtTe] within fluid inclusions trail (Platreef, foil #3502).

not oriented relative to the crystal lattice of the host sulfide and therefore is a discrete phase. Notably, some fluid inclusion trails were observed in pentlandite of the Platreef containing a nanometer-sized Pt-telluride with a grain size of approximately 50 nm (foil #3502; Fig. 4.2d).

An approximately 1-μm large Pt-(Fe,Cu) alloy (probably tulameenite [Pt_2FeCu]) is shown in Fig. 4.3a (foil #3512). The diffraction pattern of this PGM is disturbed, indicated by irregular shapes of Bragg reflections especially at higher order reflections (Fig. 4.3b), whereas the diffraction pattern of the surrounding pentlandite is undisturbed. Figure 4.3c shows element maps of the area of the PGMs which reveal that Pt, Fe, and Cu are homogenously distributed within the PGMs.

4.4.2 Platinum-group elements within the crystal lattice of pentlandite

Platinum-group elements within the crystal lattice of pentlandite of the UG-2 (Table 4.2) are substituting for Ni and/or Fe and occur as (i) patchily distributed PGEs (Fig. 4.4a) or (ii) in an ordered arrangement forming oriented lamellar nanostructures (Fig. 4.5). In the Platreef samples analyzed by EDX, however, no random or ordered arrangement of PGE in pentlandite was observed (Table 4.2).

(i) Patchily distributions in pentlandite comprise concentrations of Rh and Ir in the form of small (10 to 100 nm) specks (Fig. 4.4a and Table 4.2). An EDX line profile across one single patch demonstrates that these patches represent an enrichment of Rh and Ir and simultaneous depletion of Fe and Ni (Fig. 4.4c). The heterogeneous and patchy distribution of Rh and Ir can also be observed in the HREM lattice fringe image of pentlandite (Fig. 4.4b). In this image, the dark zones are due to local enrichments of Rh and Ir, causing higher mass adsorption contrast resulting in darker contrasts in the HREM image. Element distribution maps using Pt-L and Rh-L Xray intensities (Fig. 4.3c) further visualize the patchy distribution of PGEs (Pt and Rh). The line scan (Fig. 4.4c) together with the element distribution maps (Fig. 4.3c) confirms that Rh and Ir are heterogeneously distributed in the pentlandite lattice. In electron diffraction patterns of the Rh and Ir-rich zones, only the Bragg reflections of pentlandite are detectable. Note that in case that nanocrystals would be present in pentlandite, additional diffraction spots should be

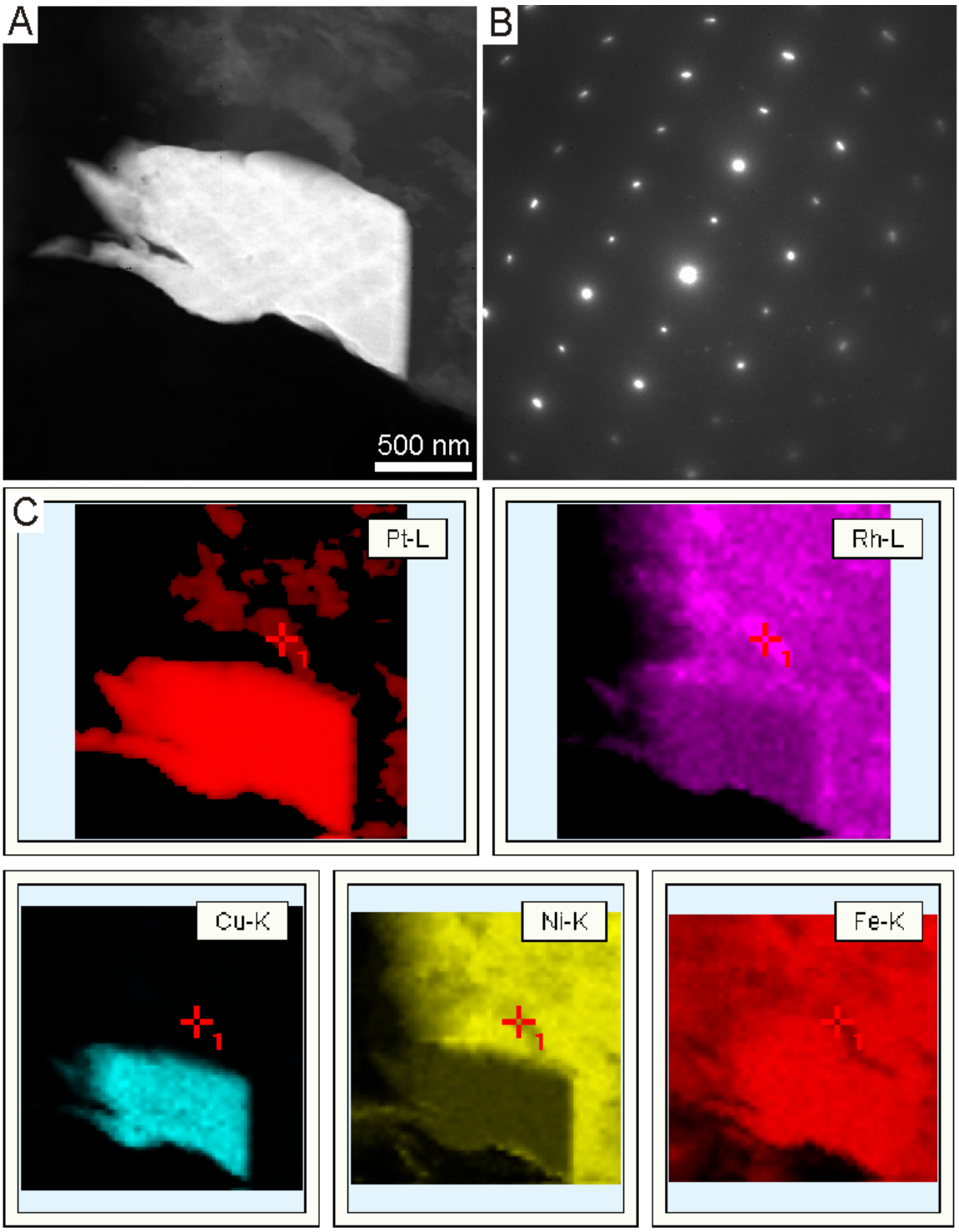

Figure 4.3 – a TEM bright-field image of an inclusion of Pt-(Fe,Cu) in pentlandite (UG-2, foil #3512). b Electron diffraction pattern of the Pt-(Fe,Cu) showing disturbed Bragg reflections at higher order (UG-2, foil #3512). c Element maps showing the distributions of Pt, Rh, Cu, Ni, and Fe and the chemistry of patches (bright gray) in pentlandite (dark gray) and of the Pt(Fe,Cu) alloy (white) in foil #3512.

observed, which is not the case. Therefore, Rh and Ir occur in solid solution and do not reflect any discrete compound or mineral.

(ii) In pentlandite grains from the UG-2 with unusually high concentration of Rh (up to 12.3 wt%) and Pd (up to 0.6 wt%) (foils #3512, #3516, #3534; Table 4.1), Rh and Ir occur in an ordered arrangement within the pentlandite lattice forming orientated lamellar nano-structures (Fig. 4.5). These lamellae, which are visible in the HREM in Fig. 4.5c, have thicknesses of several nanometers. The lamellae and the higher contrasts are a result of the enrichment of Rh and Ir, which cause higher mass adsorption contrasts and therefore darker contrasts in the HREM image. These lamellae follow four different orientations. Detailed analysis of these lamellae revealed that they reflect chemical variations of Rh- and Ir-rich and Ni- and Fe-poor zones (Fig. 4.5e). Measuring the distance between the Bragg reflections in the diffraction pattern of the lamellae and indexing the respective reflections with the calculated (hkl) data from the American Mineralogist Crystal Structure Database demonstrate enrichments of Ir and Rh on the (111) plane of pentlandite (Fig. 4.5d). Additional weak diffraction signals (streaking) between the major Bragg reflections of pentlandite caused by the presence of thin Ir- and Rh-rich lamellae on the (111) plane are also visible in the diffraction pattern (Fig. 4.5d). This periodic structure is defined as a superlattice, suggesting an ordered arrangement of Ir and Rh within the pentlandite crystal lattice. In contrast, solid solution represents random arrangements of element incorporation. The intensive study of superlattices that followed their discovery (e.g., Johansson & Linde (1925)) provided an excellent base for the understanding of order-disorder transformation within a crystal. It should be noted that the present study was sparked off by the identification by EPMA and LA-ICP-MS of elevated contents (in the % range) of Pd and Rh in pentlandite. Nanometer-sized PGMs are mainly Pt bearing (Pt-bismuthides, Pt-tellurides, Pt-(Fe,Cu) alloys) and rarer Pd-Sn and Pt-Pd-Sn compounds. Crystal lattice related PGE concentrations in pentlandite comprise heterogeneous and patchily distributions as well as ordered arrangements within the pentlandite lattice of Rh and Ir. Therefore, our data imply that a large proportion of the Pd is present in solid solution (substituting for Ni or Fe) in the crystal lattice of pentlandite as already suggested by, e.g., Cabri et al. (1984).

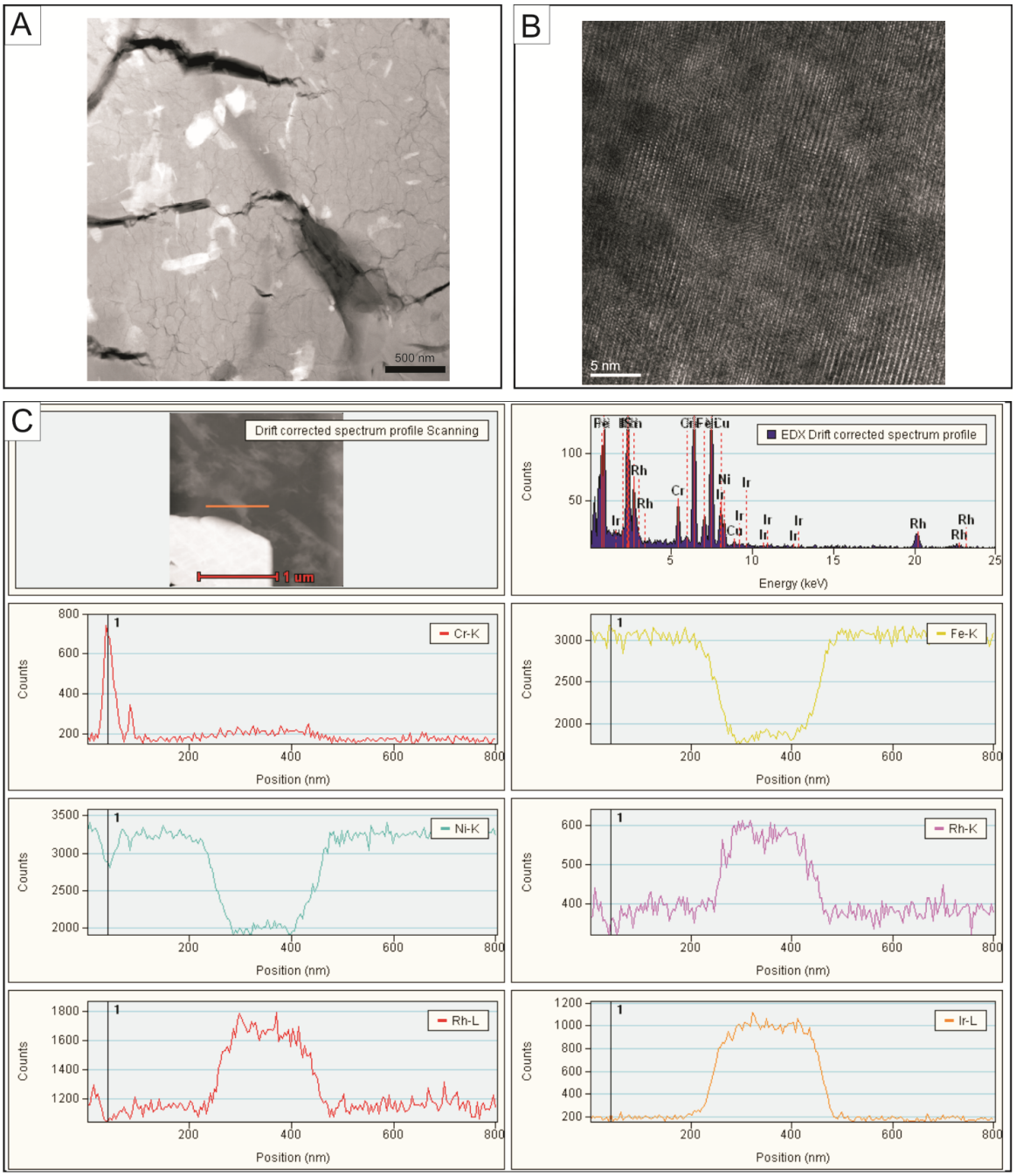

Figure 4.4 – a Patches of Ir- and Rh-rich zones (white) in "normal" pentlandite (gray) (foil #3514). b HREM of patchy distribution of PGEs in pentlandite (foil #3516). c EDX line scan (orange line) showing the distribution of Ir, Rh, Ni, and Fe (foil #3516).

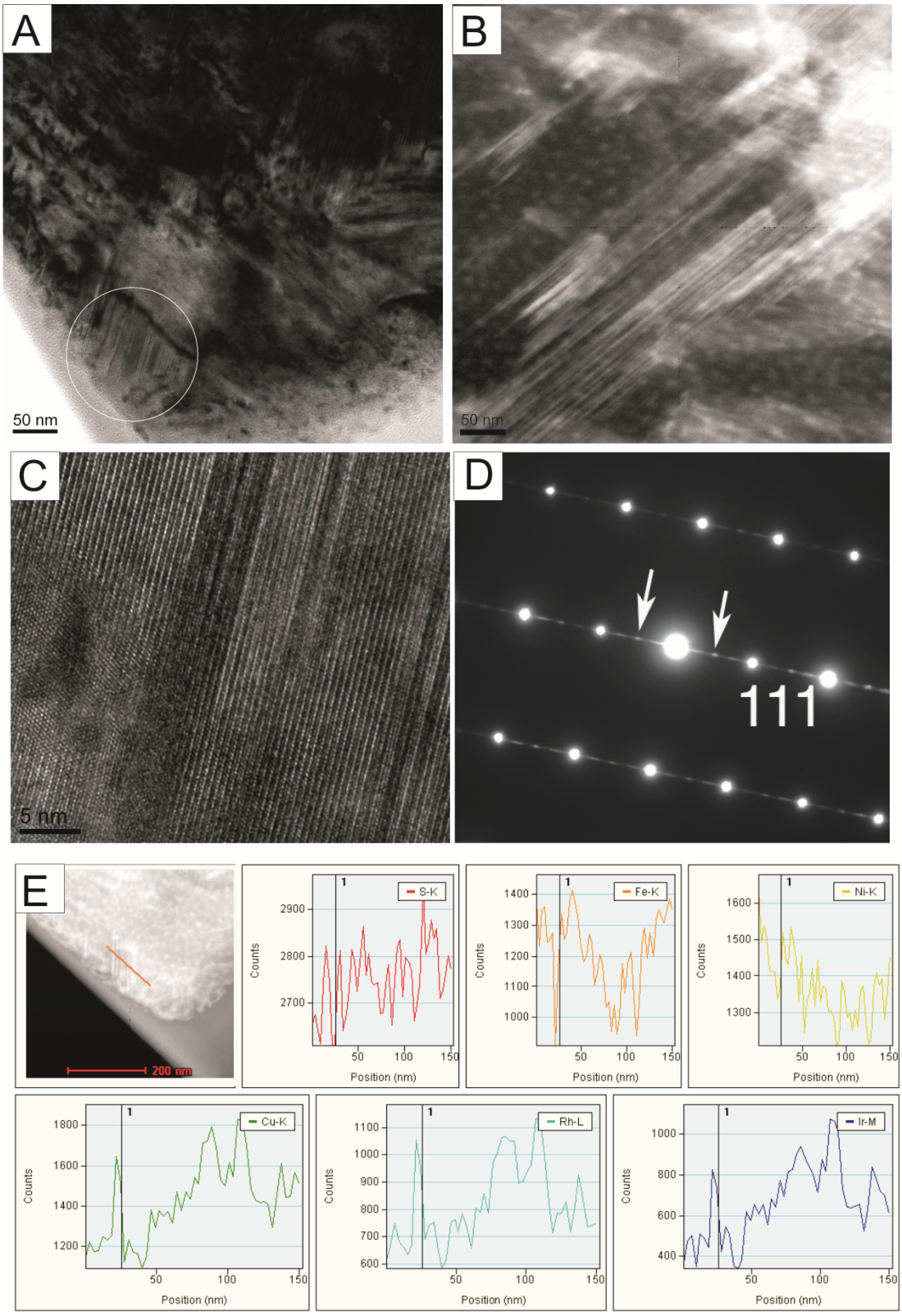

Figure 4.5 – Lamellar structures of pentlandite (foil #3516). a, b Structures in TEM mode. c HREM image of lamellae. d FFT image of c. Note the additional reflections indicating the presence of a superlattice. d Line scan (red line) through lamellae.

4.5 Discussion

State-of-the-art analytical methods, such as EPMA and LA-ICP-MS, are key methods for the in situ analysis of major, minor, and trace elements in modern geosciences. Analyses using EPMA and LA-ICP-MS provide information that sulfides contain PGEs from the ppb to ppm range upward. However, these methods do not allow the determination of their chemical state (PGM, nPGM, or in solid solution) in the crystal lattice. Investigation of the distribution of PGEs in sulfides and the identification of discrete PGMs on a nanometer scale as well as a direct link between the crystal and its chemical composition can be obtained using the TEM. However, the drawback of the method is the comparatively high detection limit of PGEs (about 1,500 ppm; e.g., Wirth et al. (2013), Cabri (2013).

Previous studies by EPMA and LA-ICP-MS have demonstrated that elevated concentrations of Pd and Rh may occur in pentlandite (Cabri et al. 1984, Oberthür et al. 2003, Godel et al. 2007, Holwell & McDonald 2010, Osbahr et al. 2013, Junge et al. 2014). The association of PGEs with sulfides generally points to the fact that the PGEs were originally concentrated by an immiscible sulfide liquid (Naldrett et al. 1979, Naldrett 2004a).

The present TEM study of samples from the UG-2 and the Platreef revealed that the PGEs in pentlandite occur as discrete nPGMs as well as incorporated in the crystal lattice of pentlandite, either heterogeneously distributed, or as an ordered arrangement of lamellar nanostructures. For the Platreef samples, no patchy solid solution was found indicating that the PGEs are homogenously distributed in pentlandite.

4.5.1 nPGMs in pentlandite

Wirth et al. (2013) described nPGMs in sulfides from the Merensky Reef. In the present study, a variety of different nPGMs (Pt-bismuthides, Pt-tellurides, Pt-(Fe,Cu) alloys, and rarer Pd-Sn and Pt-Pd-Sn compounds) was found in pentlandite of both the UG-2 and the Platreef (Table 4.2). These nPGMs are idiomorphic and their crystallographic orientation is not linked to that of the pentlandite lattice, probably indicating that the nPGMs crystallized earlier than pentlandite and are not results of exsolution from pentlandite. The presence of discrete micrometer to nanometer

inclusions of PGMs was already assumed due to distinct parallel peaks of PGE and semimetals in time-resolved analysis (TRA) spectra from LA-ICP- MS studies on Platreef samples (Holwell et al. 2006, Holwell & McDonald 2007, Hutchinson & McDonald 2008). However, TRA spectra cannot directly distinguish between discrete micro- or nano-inclusions and heterogeneously distributed PGEs occurring as solid solution. Definitely, in both the UG-2 and the Platreef, a continuum of discrete micrometersized PGMs to nPGMs is present.

4.5.2 Patchy solid solution distribution of platinum-group elements in pentlandite

Rhodium and Ir were not detected in the form of discrete minerals but are heterogeneously and patchily distributed within pentlandite, as indicated by element maps (Fig. 4.3c), electron diffraction patterns (Fig. 4.4b), and by line scans (Fig. 4.4c). Similar distribution patterns of gold in sulfides and sulfarsenides were reported by Cabri et al. (1989), Oberthür et al. (1997b), and Genkin et al. (1998). It is well known that Rh preferentially forms discrete PGMs like hollingworthite [RhAsS] in chromitite (Merkle 1992) or sulfide environments (Mostert et al. 1982, Oberthür et al. 2003) in case that sufficient quantities of As and S are available in the system.

Mungall et al. (2005) demonstrated that in S-rich systems, IPGE and Rh are highly compatible in monosulfide solid solution (MSS). Monosulfide solid solution is the first phase which crystallizes from a sulfide liquid, and intermediate solid solution (ISS) crystallizes subsequently from the remaining liquid (Li et al. 1996, Mungall et al. 2005). Some authors postulate that all PGEs are primarily collected by sulfide liquid in the magmatic stage due to their high partition coefficients in favor of sulfide (Campbell et al. 1983, Mungall & Naldrett 2008). Within the sulfide liquid, the PGEs may be trapped as single atoms, ions, metal clusters, or precursors of nPGMs (Tredoux et al. 1995). Down-temperature, MSS recrystallizes and since Ir and Rh are more compatible in MSS than Pd and Pt, Ir and Rh are concentrated in MSS, whereas Pd and Pt remain in the Cu-rich sulfide liquid (Mungall et al. 2005).

The heterogeneous and patchy distribution of Rh and Ir in the pentlandite lattice possibly indicates that clusters of Rh and Ir were heterogeneously distributed within the initial sulfide

liquid, at magmatic temperatures, or that Rh/Ir accumulations exsolved down temperature. The absence of possible reaction partners (e.g., Bi, Te, As, and Sn) necessary for the formation of discrete PGM apparently forced Rh and Ir to remain in the crystal lattice of pentlandite.

4.5.3 Lamellar intergrowths of platinum-group elements in pentlandite

Lamellar nano-structures were found within pentlandite from the UG-2. The thicknesses of these lamellae are only several nanometers (Fig. 4.5c). EDX analyses demonstrate that these structures represent Ir- and Rh-rich and relative Ni- and Fe poor zones (Fig. 4.5e). Studying the diffraction pattern of these lamellae shows the presence of additional Bragg reflections besides the regular ones of pentlandite (Fig. 4.5d).

In general, in crystals with a disordered arrangement of atoms, crystallographically equivalent planes of atoms are statistically identical with one another. However, in a superlattice structure, the distance between identical planes may be two times (or manifold) the distance between identical planes of the disordered crystal causing additional Bragg reflections in the diffractions patters. This is visible in the diffraction patterns of the Ir- and Rh-rich lamellae (Fig. 4.5d). Detailed examination revealed that these Ir- and Rh-rich zones occur on the (111) plane of pentlandite. Between the (111) spots, at least one additional diffraction spot is visible that represents a d-spacing of [2xd111]=11.4308 Å. Streaking is due to the narrow thickness of the lamellae. Due to the cubic lattice of pentlandite and the fourfold axis, four different orientations of (111) planes exist and lamellae may show four different orientation patterns within pentlandite.

For example, in the Cu-Au system, Cu and Au are randomly distributed in the temperature range between approximately 890 and 410°C. At temperatures below 410°C, Cu and Au atoms start to order along particular lattice planes, thereby creating ordered superlattices (Toth & Sato 1962, Barrett & Massalski 1980). Superlattices initiate near the compositions Cu_3Au, CuAu, and $CuAu_3$. For the Cu-Au system (face centered cubic crystal system) alloys containing 25 at.% Au (Cu_3Au), Au and Cu are randomly distributed on the cube corners or the face centers at high temperatures. Below a critical temperature of 390°C, ordering takes place and

Au atoms are occupying the cube corners and Cu atoms the face centers (Toth & Sato 1962, Barrett & Massalski 1980). The disorder-order change therefore results in an additional symmetry element, which causes additional Bragg reflections in the electron diffraction patterns. Increasing the concentrations of Au to a composition close to Cu_3Au initiates ordering of the randomly distributed Au and Cu atoms to an ordered arrangement leading to the formation of a superlattice.

In pentlandite grains containing PGE concentrations in the range of some hundreds of ppm, Rh and Ir appear to be distributed in a statistically random manner within the crystal lattice and no preferred atom sites are occupied by Rh and Ir. However, with increasing concentrations of Rh and Ir (at least 12.3 wt% Rh and up to 0.6 wt% Pd), ordering takes place and certain lattice sites are preferentially occupied by only one kind of atom, causing a change in the crystal symmetry of pentlandite, which is visible in the electron diffraction patterns.

In general, the substitution of trace elements into a solid phase is considered to be controlled by the nature of the bonding, the size of the lattice site, and the charge balance. The pentlandite structure represents a pseudo-cubic closest packing with cations (Fe, Ni) occupying the octahedral and tetrahedral sites (Rajamani & Prewitt 1973, 1975). The ionic radii (in Å) of Pd, Fe, and Ni are $^{IV}Pd^{2+}$=0.64, $^{IV}Fe^{2+}$=0.63, and $^{IV}Ni^{2+}$= 0.55 (Shannon 1976), thereby allowing substitution of Pd for Ni and/or Fe as the ionic radii differ by less than 15 % (Goldschmidt 1926). The same is true for $^{VI}Rh^{3+}$=0.665, $^{VI}Ir^{3+}$=0.68, $^{VI}Ni^{2+}$=0.69, and $^{VI}Fe^{2+}$=0.61. The electron configurations of Fe, Os, Ir, Ru, and Rh have a d^2sp^3 preferred hybridization state, suitable for octahedral sites (Evans 1966, Barnes et al. 2001). Iron is consequently preferentially substituted by Os, Ir, Ru, and Rh. Platinum, Pd, and Ni prefer dsp^2 configurations, being suitable for the square planar sites.

4.5.4 Crystal growth of platinum-group minerals and precursors (PGM embryos)

A Pt-(Fe,Cu) alloy with a slightly distorted diffraction pattern indicated by smeared out Bragg reflections visible at the higher order reflections is depicted in Fig. 4.3b. The coalescence of "embryos" or precursors forming nanometer- to micrometersized crystals with minute misorien-

tations at the interfaces causes a slightly disturbed diffraction pattern (Penn & Banfield 1998). In situ experiments have shown that many minerals are preceded by crystalline nanometer-sized particles and noncrystalline nano-phases in low-temperature aqueous solution. Helmy et al. (2013) demonstrated in their high-temperature experiments in the Pt-As system that this also applies for PGEs in magmatic systems. These authors showed that Pt and As selforganize to nano-particles long before the melt had reached Pt-As concentrations sufficient to crystallize and form discrete PGMs. The particular Pt-(Fe,Cu) alloy of the present study (Fig. 4.3a) may thus represent embryos or precursor phases of PGMs that coalesced as described by Helmy et al. (2013).

Teng (2013) reviewed theories of crystal formation and pointed to alternative, cluster-based pathways for crystallization, i.e., aggregation of nanometer-sized clusters, which formed crystalline structures under either an ordered or in initially random patterns (Banfield et al. 2000, Nabrotsky 2004, Gebauer et al. 2008, Pouget et al. 2009, Baumgartner et al. 2013). The above hypothesis challenges the classic theory of thermodynamics and atomic structures of crystal surfaces, i.e., that crystallization is a sequential addition of atoms or ions. Penn & Banfield (1998) further described the process of crystal growth as a result of oriented nano-crystal attachment. The diffraction pattern of the Pt-(Fe,Cu) alloy (Fig. 4.3b) supports the hypothesis of the latter authors, whereby nPGM coalesces with small misorientations causing smeared out Bragg reflections at higher order in the diffraction pattern.

4.6 Conclusions

The presence of PGEs in sulfides is known from EPMA and LA-ICP-MS studies. The present work applied conventional and follow-up high-resolution methods using combined techniques of FIB and TEM to pentlandite from both the UG-2 chromitite and the Platreef. The results indicate that a continuum exists from discrete micrometer- to nanometer-sized PGMs in both the UG-2 and the Platreef. Further, Pd is present as homogenous solid solution in pentlandite. Additionally, in the UG-2 sample, Rh and Ir occur as a patchily distributed solid solution and ordered within the pentlandite crystal structure, substituting for Ni and/or Fe. The major findings of this study are as follows:

1. In the UG-2 samples, the suite of discrete PGMs mainly consists of cooperite/braggite, laurite, and Pt-Fe alloy. In the Platreef samples, discrete PGMs are mainly Pt-Pd bismuthotellurides and cooperite/braggite.

2. Within pentlandite, a variety of nanometer-sized PGMs (Pt-bismuthides, Pt-tellurides, Pt-(Fe,Cu) alloy, Pd-Sn and Pt-Pd-Sn compounds) was detected. These nPGMs do not display any orientation relationship to the host sulfide and therefore probably represent discrete phases which were trapped early during pentlandite growth.

3. The heterogeneous and patchy distributions of Rh and Ir in the pentlandite lattice indicate that Rh and Ir were collected early by a sulfide liquid. The absence of possible reaction partners (e.g., Bi, As, and Sn), necessary for the formation of discrete PGMs, forced Rh and Ir to remain in the crystal lattice of pentlandite and their down temperature exsolution caused patchy distribution patterns of Rh and Ir.

4. In pentlandite grains from the UG-2 with unusually high concentration of Rh (up to 12.3 wt%) and Pd (up to 0.6 wt%), ordering of Rh and Ir within the pentlandite lattice takes place on the (111) plane, forming a superlattice. The lamellae show that above a certain concentration of Rh and Ir (at least 12.3 wt% Rh and 0.6 wt% Pd), Rh and Ir form an ordered arrangement in the pentlandite lattice, causing a change in the crystal symmetry of pentlandite.

5. Slightly disturbed diffraction patterns indicated by diffuse Bragg reflections visible at the higher-order reflections of a Pt-(Fe,Cu) alloy indicate that the formation of PGMs may result from embryos or precursor phases which may coalescence to form discrete PGMs.

6. Our data imply that a large proportion of the Pd, even at elevated concentrations, is present in homogenous solid solution in the crystal lattice of pentlandite.

Chapter 5

Platreef - from pristine to weathered ore

This chapter provides additional results on the pristine Platreef ore which have not been covered by the two publications presented in Chapters 4 and 6. The main focus of this chapter is a more detailed petrographic description and the whole rock geochemistry of the drill cores from the Mogalakwena Mine. Some additional results about PGM and the S/Se ratio are presented.

5.1 Petrography and mineralogy

Figure 5.1 shows selected drill core samples of pristine, partly weathered and more strongly weathered ore. Feldspathic pyroxenite with sulfide mineralisation typically consists of cumulus orthopyroxene and interstitial plagioclase. Sulfides occur disseminated, net-textured or massive and are mainly pyrrhotite, pentlandite, chalcopyrite and minor pyrite. Pristine ores usually contain sulfide aggregates of <1 cm in size but also blebs of a few centimeters are observed (Figure 5.1A,B). During weathering sulfides are largely destroyed and only relict sulfides are observed. Small cracks exist in the near-surface ore and allow the circulation of hydrous fluids and the breakdown of primary minerals and the formation of secondary hydrous minerals, carbonates and Fe-oxy/hydroxides (Figure 5.1C,D). At larger degrees of weathering, orthopyroxene, clinopyroxene and plagioclase break down almost completely to serpentine, smectite and kaolinite and larger degrees of iron oxidation and the formation of Mn-oxides are observed

(Figure 5.1E,F).

5.1.1 Pristine Ore

Within the pristine and unweathered rocks, feldspathic pyroxenite consists of cumulus orthopyroxene (about 60 to 80%) with grain sizes of a few millimeters and interstitial plagioclase (20 to 30%) grains (Figure 5.2A,B). The other major minerals are, clinopyroxene (0 to 20%), phlogopite (<5%) and amphiboles (tremolite and actinolite) with <5%. Orthopyroxene is also observed as elongated grains showing the same orientation (Figure 5.3A,B). Phlogopite occurs associated with sulfide mineralisation (Figure 5.2C,D). Amphiboles seem to partly replace sulfides (Figure 5.2E,F). Minor amounts of olivine, phlogopite, amphibole and quartz are observed along the cores.

5.1.2 Low-degree weathered ore

The low-degree weathered feldspathic pyroxenite shows alteration along smaller cracks (Figure 5.3C,D). Along these cracks primary minerals are partly destroyed and Fe-oxy/ hydroxides formed. In general, within the transition zone from pristine to completely weathered ore, primary minerals such as orthopyroxene, olivine and plagioclase remain relatively well shaped. Sulfides are partly destroyed but are still frequently observed. Chromite grains are typically unaffected by low degree weathering (Figure 5.3D).

5.1.3 Weathered ore

Highly weathered feldspathic pyroxenites showing the breakdown of orthopyroxene and clinopyroxene (Figure 5.4) and the formation of smectite, sericite and kaolinite. Fe-oxy/hydroxides occur in different shapes (larger patches, veins). The major amounts of serpentine, smectite and kaolinite indicate the complete breakdown of pyroxene, olivine and feldspar. Sulfides are almost completely destroyed and only relict grains are observed.

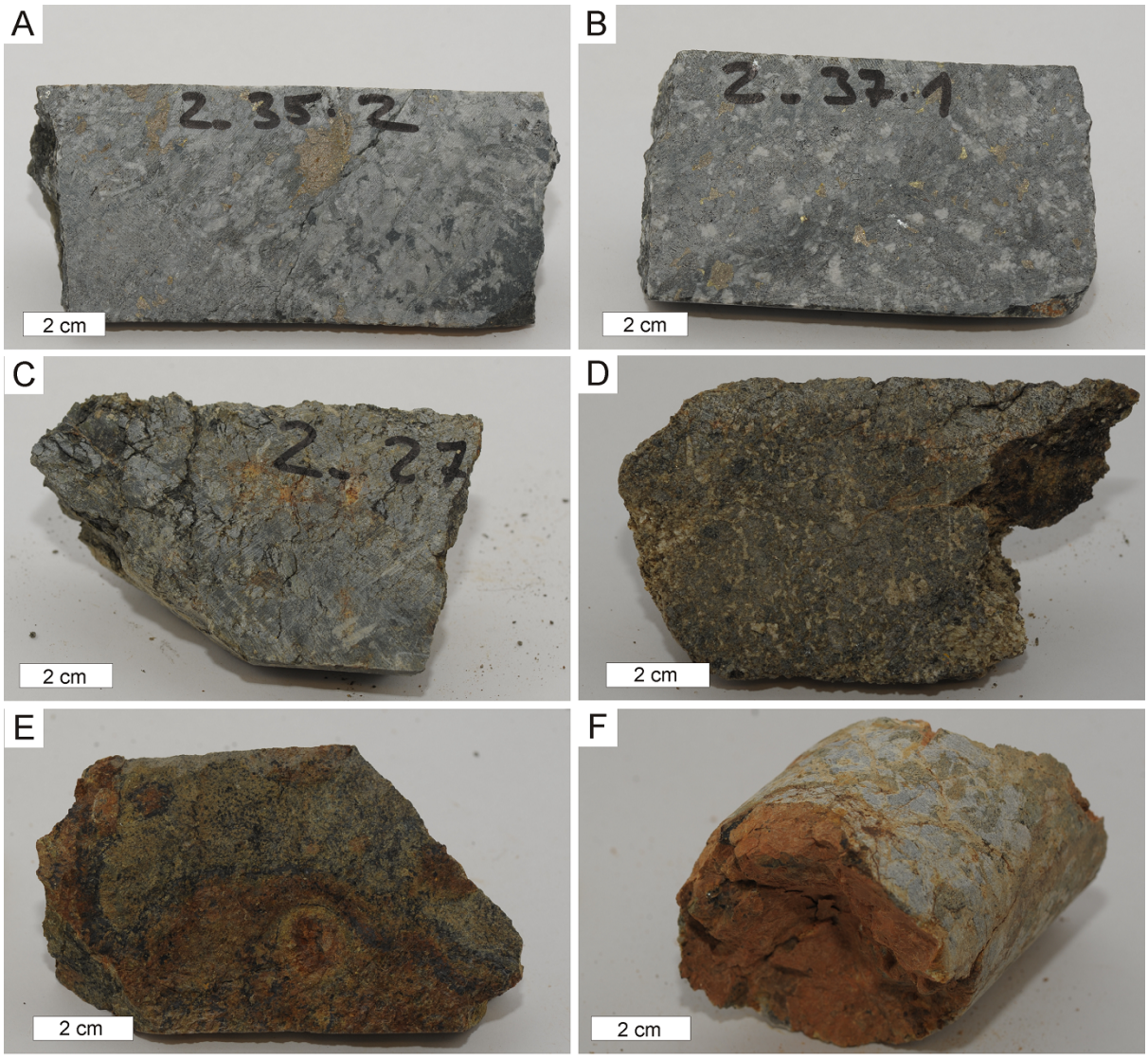

Figure 5.1 – Photos of pristine (A,B), partly weathered (C,D) and more strongly weathered (E,F) Platreef ores from the Mogalakwena Mine. A: Feldspathic pyroxenite with centimeter-sized sulfide aggregates (mainly pyrrhotite). At a depth of 35.2 m; Oy2-15. B: Feldspathic pyroxenite with disseminated sulfide mineralisation. At a depth of 37.1 m; Oy2-17. C: Partly weathered feldspathic pyroxenite with serpentine and Fe-oxy/hydroxides and only limited amounts of relict sulfides. At a depth of 27 m; Oy2-12. D: Partly weathered feldspathic pyroxenite with various secondary minerals including Fe-oxy/hydroxides and Mn-oxides. Sulfides are largely absent. At a depth of 18.6 m; Oy2-8. D: Weathered feldspathic pyroxenite with Mn-oxides. Sulfide are largely absent. At a depth of 10.1 m; Oy1-6. E: Weathered feldspathic pyroxenite with various secondary minerals including Fe-oxy/hydroxides and Mn-oxides. Sulfides are absent. At a depth of 18.6 m; Oy2-8. F: Weathered feldspathic pyroxenite with larger degree of Fe-alteration. At a depth of 13 m; Oy2-5.

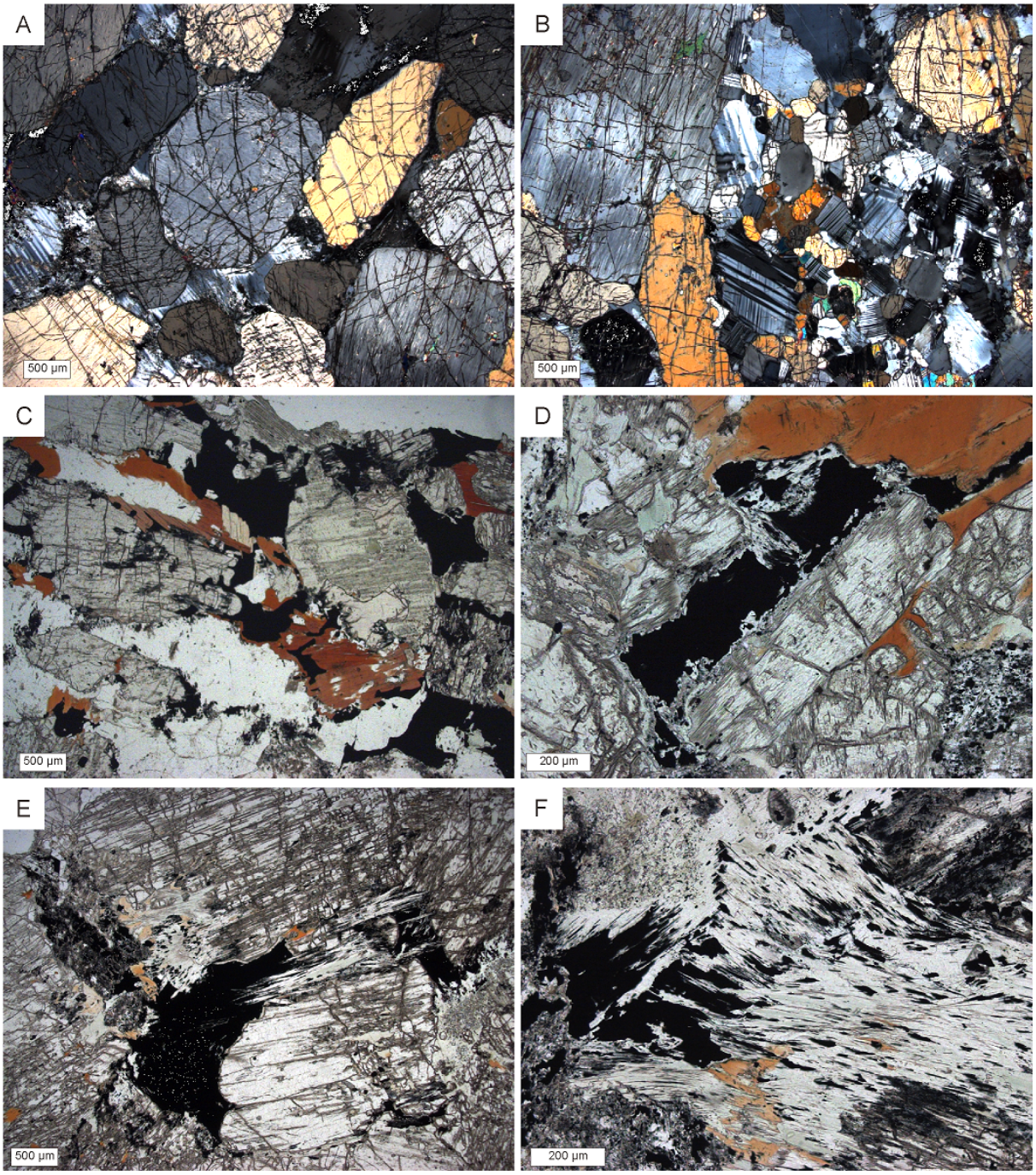

Figure 5.2 – Photomicrographs of pristine feldspathic pyroxenites in transmitted light. A,B: Orthopyroxene and interstitial plagioclase. Crossed polarized light; Oy2-21b. C: Orthopyroxene and interstitial plagioclase with phlogopite and associated sulfide mineralisation. Plane polarized light; Oy3-3a. D: Orthopyroxene with phlogopite and associated sulfide mineralisation. Plane polarized light; Oy3-16b. E,F: Orthopyroxene and amphibole replacing sulfide mineralisation. Plane polarized light; Oy2-21b.

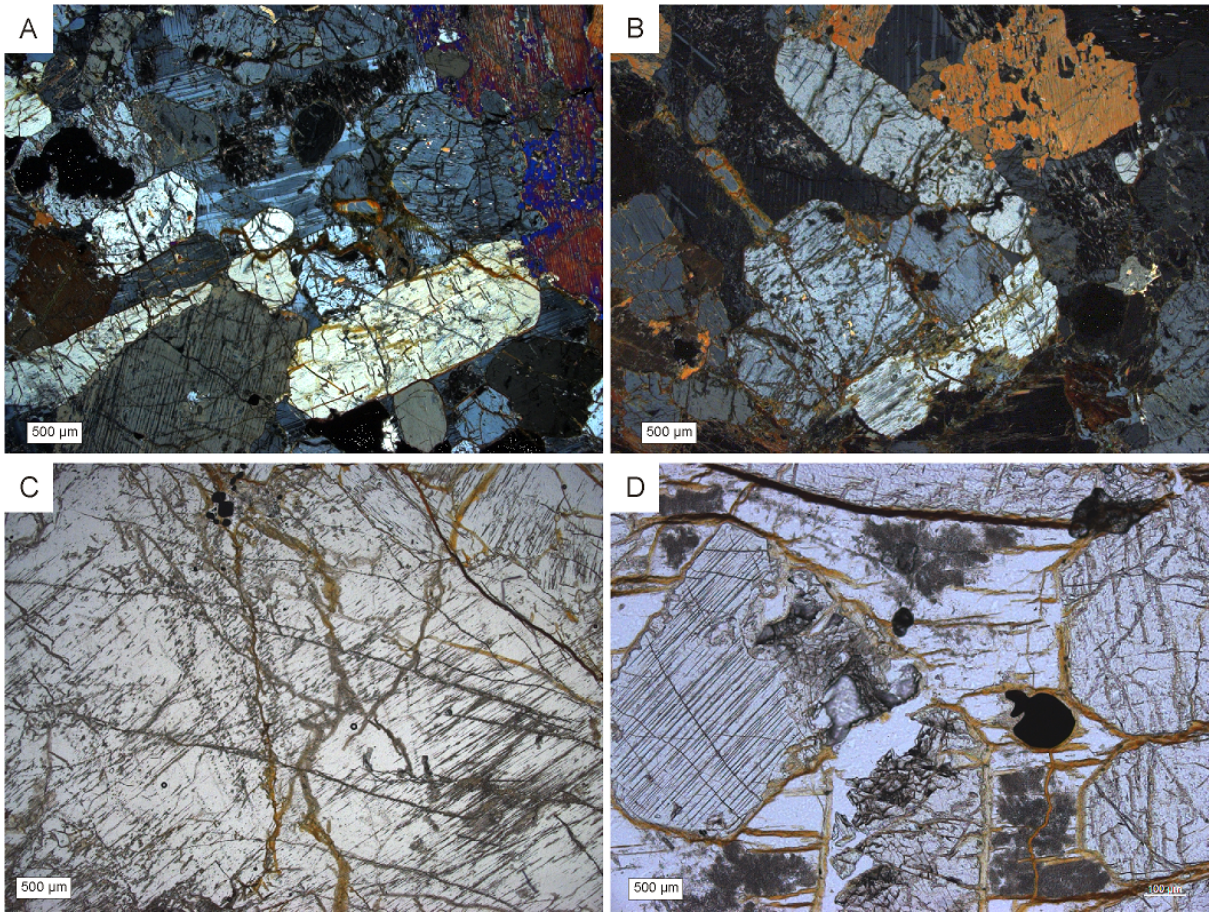

Figure 5.3 – Photomicrographs of pristine ore with first indications of weathering in transmitted light. A,B: Ortho- and clinopyroxene and interstitial plagioclase. Crossed polarized light; Oy2-6b. C: . Ortho- and clinopyroxene, interstitial plagioclase and chromite. Plane polarized light; Oy2-6b´. D: Ortho- and clinopyroxene, interstitial plagioclase and chromite. Plane polarized light; Oy2-8.

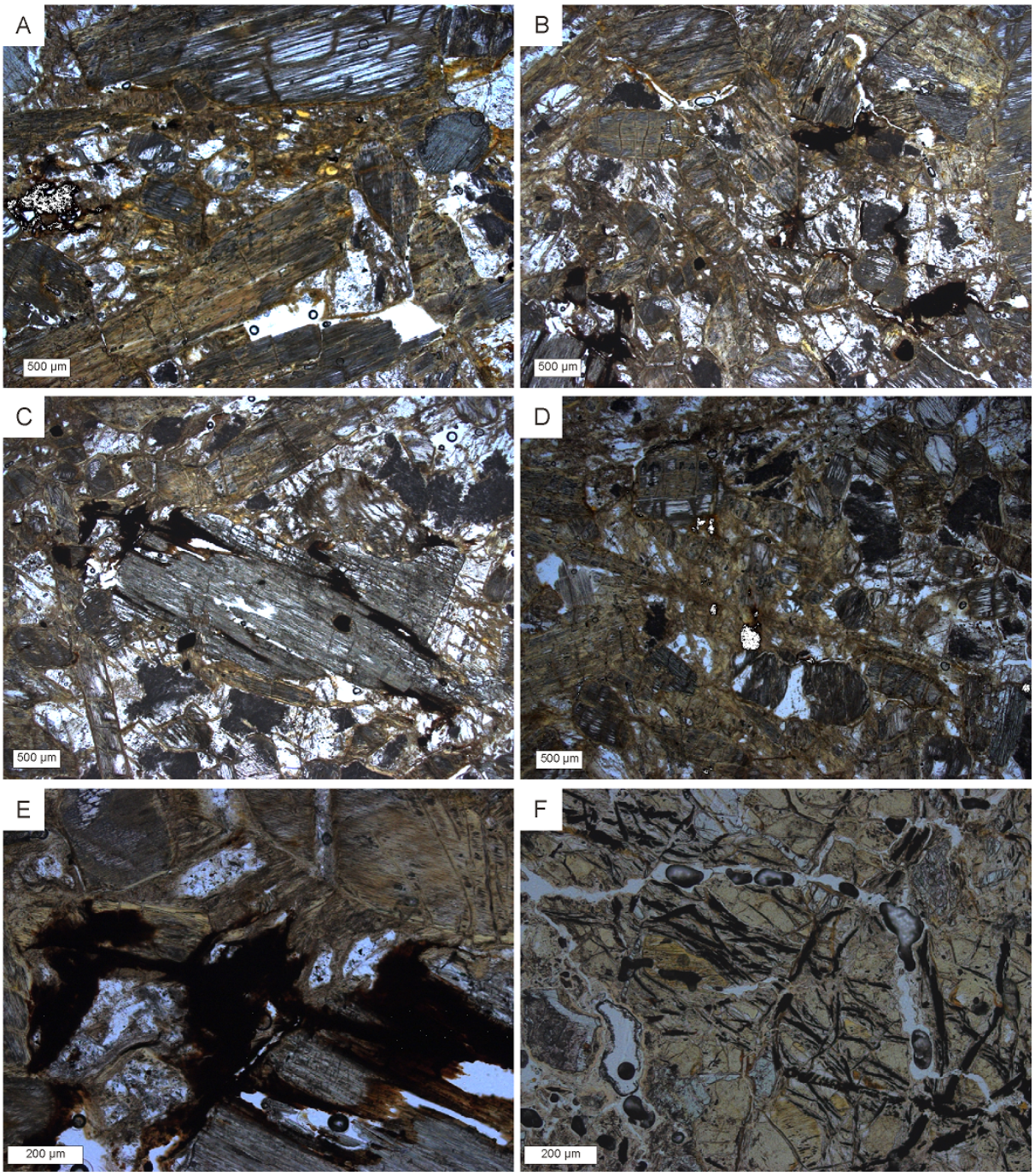

Figure 5.4 – Photomicrographs of weathered ore in transmitted light. A-E: Weathered orthopyroxene with Fe-oxy/hydroxides. Plane polarized light; Oy1-9a. F: Plane polarized light; Oy2-2.

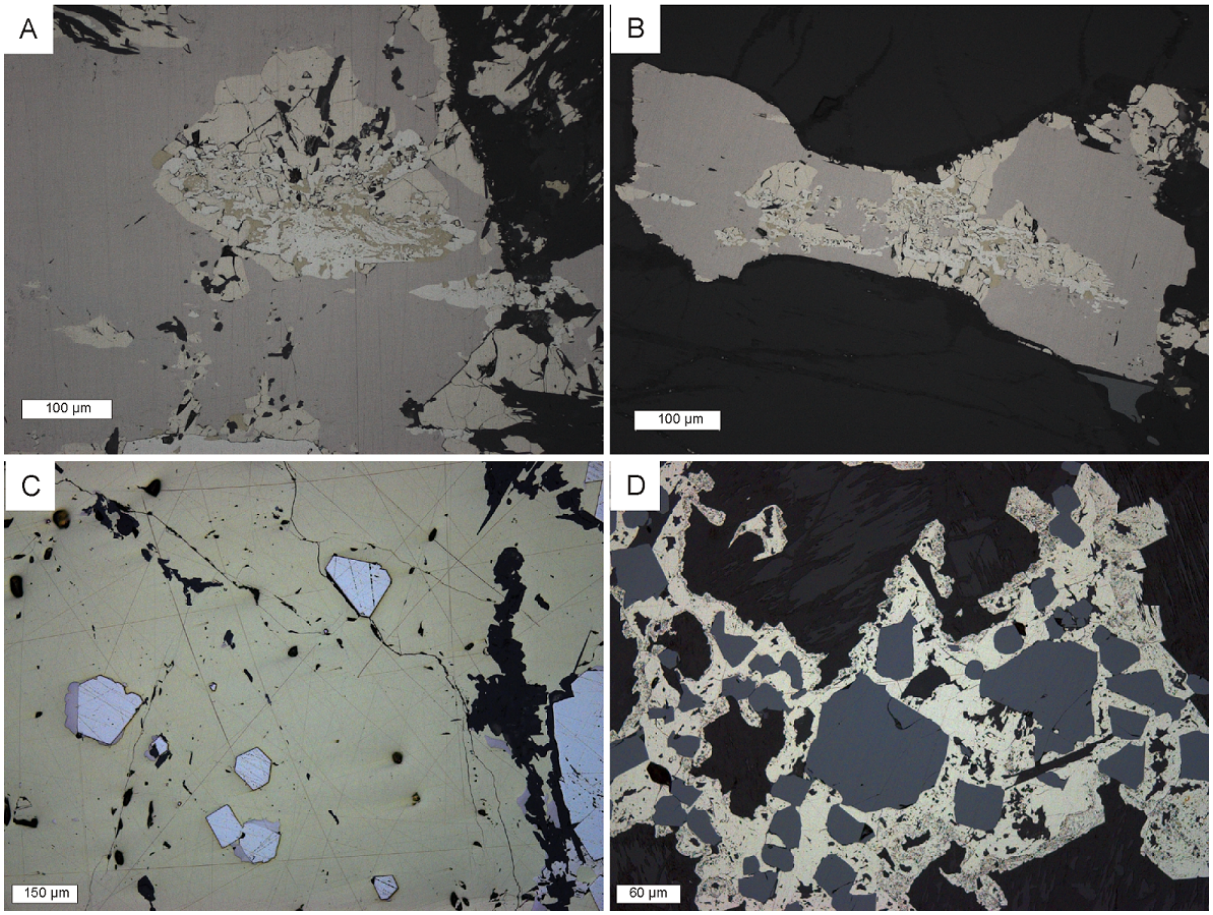

Figure 5.5 – Photomicrographs of sulfide assemblages at Overysel. All in air. A,B: Pyrrhotite (red-brown), with pentlandite (creme) at the rims and a symplectic intergrowth of chalcopyrite (yellow) with pyrite (white). Oy2-21. C: Massive sulfide with chalcopyrite and inclusions of pyrite with pyrrhotite. Oy1-26a. D: Pyrite surround chromite grains. Oy1-22.

5.2 Whole rock geochemistry

Two approaches were applied for sampling the drill cores: (i) a selective sampling by taking representative samples of each lithology and (ii) an incremental approach in which the cores were separated by lithological boundaries into 3 to 5 m intervals, crushed and homogenized (see Appendix). The total amount of composite and selective ore samples is shown in Table 5.1.

Table 5.1 – Number of drill core samples of composite and selective samples.

drill core	no. composite	no selective
Oymetox 1	12	26
Oymetox 2	15	21
Oymetox 3	15	17

In the soil, weathered and pristine part of the drill cores, differences in the element distribution are observed. Figure 5.6 shows the whole rock data of the composite analysis for Cu, Ni, Co, Pt, Pd, Au and the Pt/Pd ratio. At all three drill cores, Cu, Ni and Co have low concentrations in the soil horizon, whereas no pronounced differences between weathered and pristine ore are visible for these metals. Copper, Ni and Co largely reflect the presence of sulfides in the pristine ore. Platinum, Pd and Au are heterogeneously distributed within the cores. The Pt/Pd ratio in the pristine ore is roughly 1:1, but decreases in the weathered ore and the soil.

Figure 5.7 shows the whole-rock XRF data for SiO_2, Al_2O_3, MgO, MnO, CaO and loss of ignition (LOI) of the selectively sampled ores. The soil of Oymetox 1 and 2 (Figure 5.7) has enriched values of SiO_2 and Al_2O_3, whereas MgO, MnO, CaO are depleted. A similar observation can be made for Oymetox 3, except that here the Al_2O_3 concentrations in the soil are not distinctly different. The LOI show highest values in the soil and weathered part of the drill cores. This is due to the larger abundance of secondary hydrous minerals. At Oymetox 1 one interval (33 to 33.8 m) has high LOI values in the pristine ore, resembling a harzburgite unit, which is strongly altered to serpentine. The large abundance of serpentine explains the higher LOI values, as well as the elevated concentrations of MgO and the low CaO. The more mafic zones at 24.8 to 27 m (Oy2-11 and -12) and at 43.5 m (Oy2-19) within Oymetox 2 also show elevated contents of LOI. Oymetox 3 has overall low LOI contents in the pristine part.

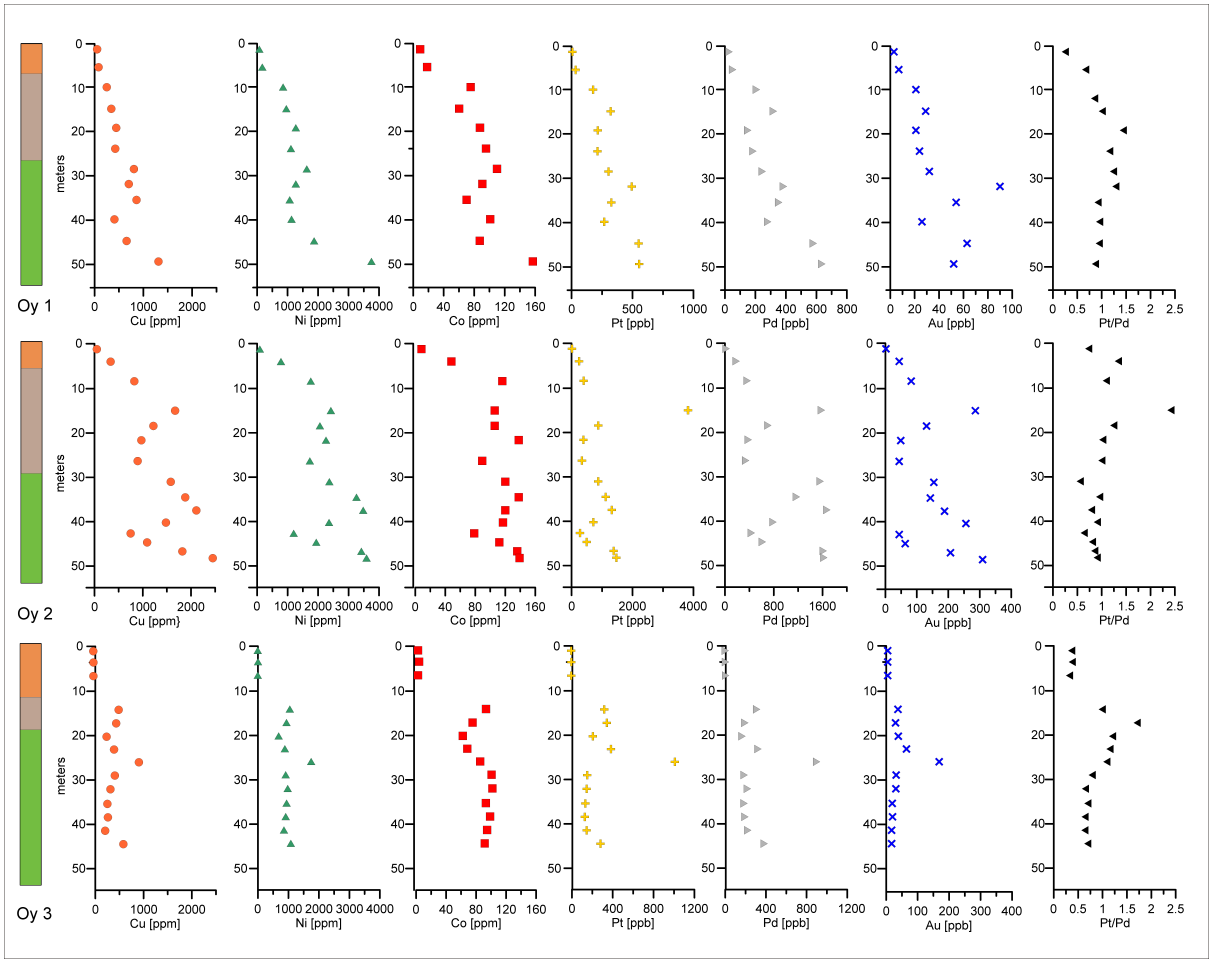

Figure 5.6 – Whole-rock variation of base metals, Pt, Pd, Au and the Pt/Pd ratio along the drill cores Oymetox 1, 2 and 3 of the composite procedure. Orange indicates the soil, brown the weathered and green the pristine ore (composite data).

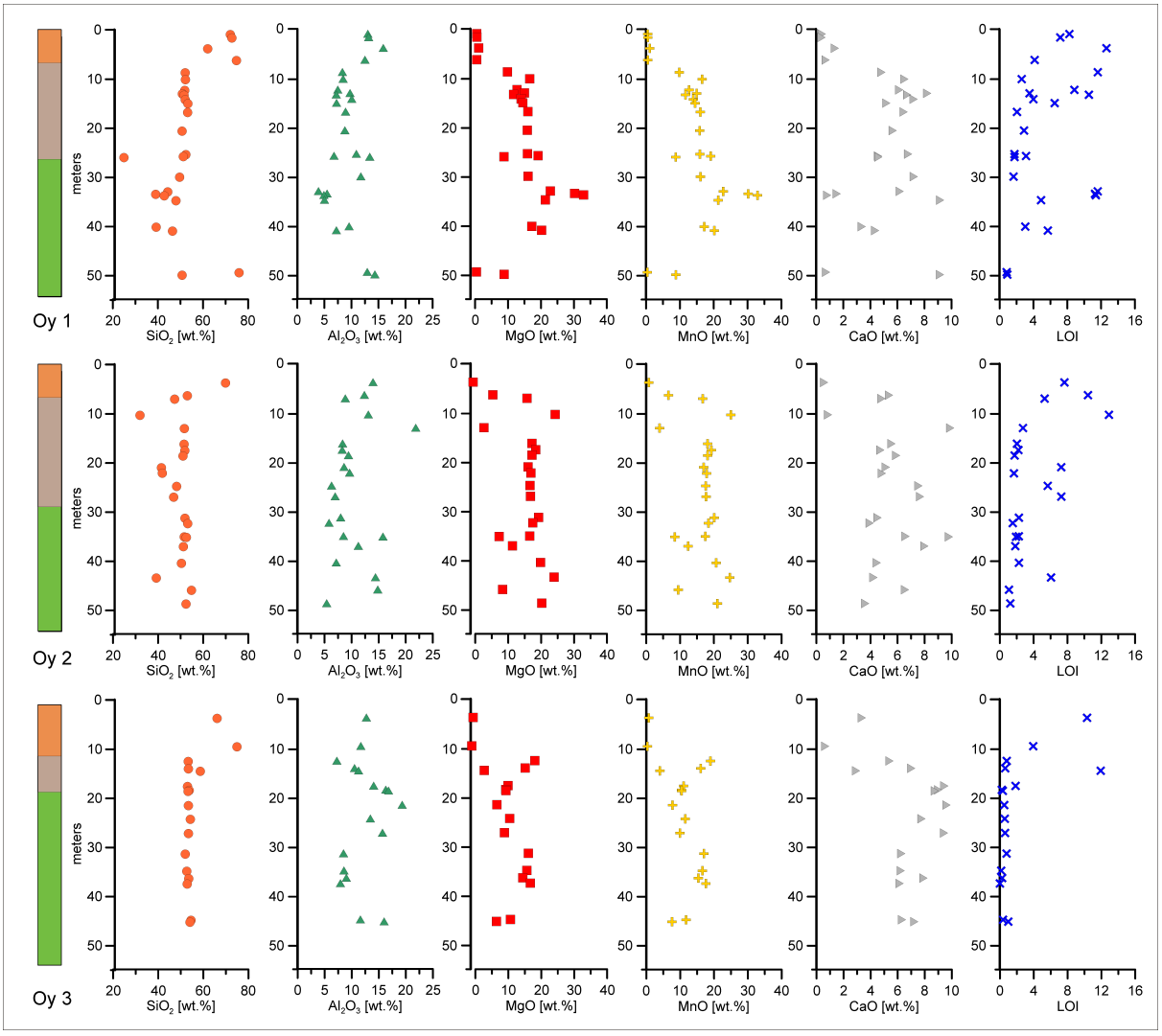

Figure 5.7 – Whole-rock variation of SiO_2, Al_2O_3, MgO, MnO, CaO and LOI along the drill cores Oymetox 1, 2 and 3. Orange indicates the soil, brown the weathered and green the pristine ore (selected data).

The Cu, Ni, Co, Pt, Pd, Au concentrations and the Pt/Pd ratio of the selective samples are plotted in Figure 5.8. The distribution patterns are usually parallel to the pattern of the composite sampling except that higher concentrations are detected in the selective sampling data. Again, Cu, Ni and Co are depleted in the soil horizons.

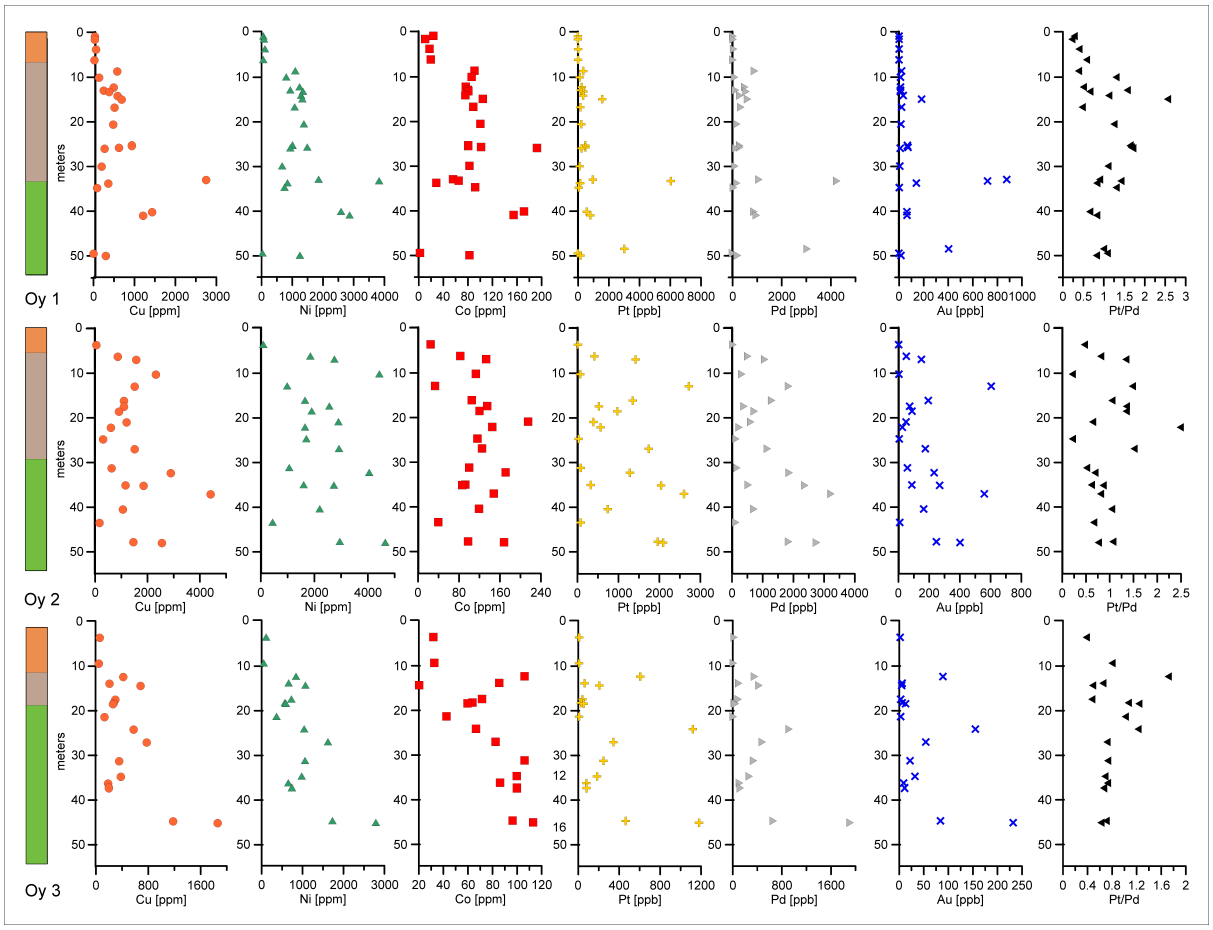

Figure 5.8 – Whole-rock variation of base metals, Pt, Pd, Au and the Pt/Pd ratio along the drill cores Oymetox 1, 2 and 3. Note for Oy1-19 (33.50 m) and Oy1-26 (48.50 m) Cu is >5000 ppm and for Oy1-26 Ni is >5000 ppm and Co is >500 ppm and Oy2-17 (37.10 m) Ni is >5000 ppm and Oy3-2 Au is <1 ppb. These values are not shown on the diagram. Orange indicates the soil, brown the weathered and green the pristine ore (selected data).

Figure 5.9 shows binary correlations diagrams for sulfur in pristine and weathered ores. Sulfur contents in the pristine ores are usually higher than 0.1 wt.%. Sulfides are largely destroyed during weathering processes causing the overall low concentrations of S in the weathered ores. Figure 5.9A plots the Pt/Pd ratio versus S and shows that the Pt/Pd ratios in the pristine ores vary between 0.8 to 1.0, whereas they show more scatter in the weathered ore. Figure 5.9B

shows the Ni versus S concentrations. In the pristine ore a good correlation exists but due to the S-loss during weathering no correlation is observed in the weathered ore. A similar observation can be made for Co (Figure 5.9C) and Cu (Figure 5.9D). In general the highest concentrations of S, Ni, Co and Cu were analyzed in Oymetox 2.

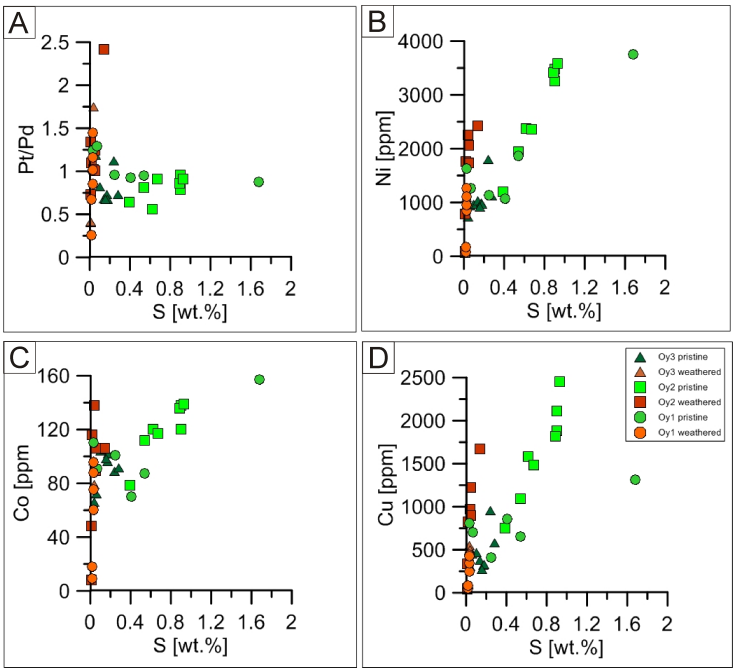

Figure 5.9 – Binary sulfur variation plots of the composite whole rock data. A. Pt/Pd ratio versus sulfur. B. Nickel versus sulfur. C. Cobalt versus sulfur. D. Copper versus sulfur.

In Figure 5.10 six binary correlation plots are shown. A good correlation exists between Pt and Pd in both pristine and weathered ore (Figure 5.10A). Furthermore, a good correlation between Cu and Pt+Pd exists. Large Cu concentrations coincide with the elevated Pt+Pd concentrations. A similar observation can be made for Ni, Co, Au and S (Figure 5.10C-F).

The Spearman rank correlation matrix in Figure 5.11 shows the data for the pristine feldspathic pyroxenite using the composite whole rock data. Positive correlation is observed for Pt, Pd, Au and Ag with S, Ni, Bi, Se and Cu, arguing for a sulfide control of Pt, Pd, Au and Ag. A further positive correlation is observed between Na, Al, K, Ca, Eu, Sr and Ba, interpreted as representing the composition of plagioclase. For Mg a negative correlation exists with Al, K, Eu, Sr and Ba, indicating orthopyroxene.

The Spearman rank correlation matrix in Figure 5.12 shows the data for the weathered feldspathic pyroxenite using the composite whole rock data. A positive correlation of Pd, Pt and

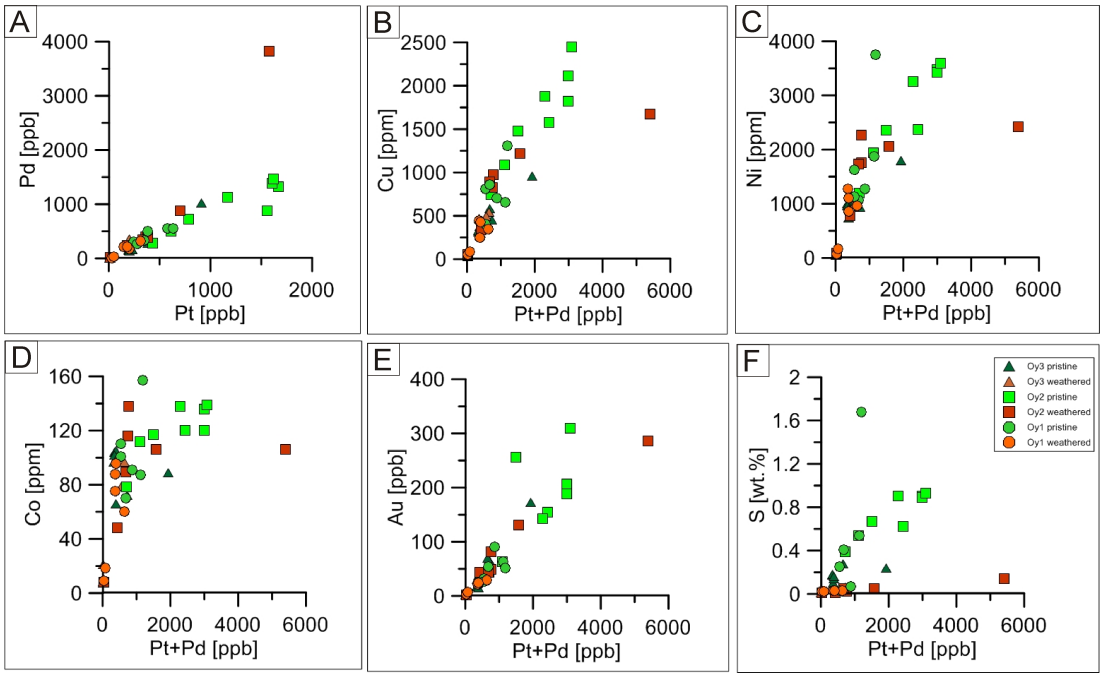

Figure 5.10 – Binary Pt and Pd variation plots. A. Palladium versus Pt. B. Cu versus Pt+Pd. C. Nickel versus Pt+Pd. D. Cobalt versus Pt+Pd. E. Gold versus Pt+Pd. F. Sulfur versus Pt+Pd.

	Au	Pt	Pd	S	Na	Mg	Al	K	Ca	V	Cr	Mn	Fe	Ni	Ag	Co	Eu	Bi	Se	Sr	Zr	Ba	Cu	Ti
Au	1																							
Pt	0.936	1																						
Pd	0.879	0.927	1																					
S	0.591	0.622	0.787	1																				
Na	0.058	0.019	-0.113	-0.225	1																			
Mg	0.036	0.070	0.241	0.617	-0.749	1																		
Al	-0.160	-0.184	-0.204	-0.208	0.918	-0.577	1																	
K	0.188	0.144	0.047	-0.037	0.917	-0.703	0.796	1																
Ca	-0.266	-0.359	-0.504	-0.563	0.522	-0.463	0.545	0.353	1															
V	-0.490	-0.548	-0.520	-0.445	0.540	-0.640	0.483	0.432	0.433	1														
Cr	-0.135	-0.222	-0.046	0.119	-0.221	0.037	0.109	-0.122	-0.348	0.167	1													
Mn	-0.431	-0.490	-0.313	0.071	-0.534	0.653	-0.258	-0.576	-0.109	-0.073	0.449	1												
Fe	-0.200	-0.249	-0.101	0.234	-0.068	0.228	0.125	-0.082	-0.323	0.100	0.781	0.599	1											
Ni	0.796	0.867	0.912	0.751	-0.205	0.276	-0.219	0.005	-0.603	-0.571	0.074	-0.234	0.045	1										
Ag	0.775	0.725	0.700	0.641	0.292	0.032	0.095	0.311	-0.270	-0.256	-0.217	-0.254	0.105	0.662	1									
Co	0.430	0.508	0.558	0.565	-0.126	0.210	-0.099	-0.016	-0.637	-0.404	0.412	0.026	0.540	0.732	0.544	1								
Eu	-0.001	-0.099	-0.213	-0.349	0.811	-0.650	0.816	0.743	0.639	0.372	-0.126	-0.513	-0.245	-0.308	0.035	-0.275	1							
Bi	0.861	0.865	0.917	0.763	-0.127	0.315	-0.166	0.039	-0.411	-0.651	0.043	-0.150	0.029	0.865	0.731	0.600	-0.135	1						
Se	0.770	0.839	0.903	0.829	-0.168	0.255	-0.158	0.033	-0.605	-0.489	0.121	-0.193	0.108	0.958	0.646	0.723	-0.306	0.843	1					
Sr	0.106	0.045	-0.139	-0.490	0.836	-0.804	0.800	0.742	0.667	0.362	-0.187	-0.645	-0.295	-0.213	0.122	-0.253	0.797	-0.106	-0.245	1				
Zr	-0.213	-0.262	-0.152	-0.038	0.130	-0.070	0.203	0.289	0.215	0.386	-0.008	0.032	-0.213	-0.206	-0.161	-0.367	0.305	-0.226	-0.204	0.000	1			
Ba	0.196	0.093	-0.072	-0.362	0.682	-0.600	0.574	0.609	0.591	0.175	-0.188	-0.534	-0.230	-0.126	0.163	-0.127	0.863	0.061	-0.217	0.818	0.037	1		
Cu	0.868	0.927	0.922	0.751	-0.144	0.262	-0.256	0.038	-0.520	-0.623	-0.093	-0.247	-0.059	0.938	0.767	0.648	-0.260	0.917	0.889	-0.153	-0.239	-0.063	1	
Ti	-0.314	-0.385	-0.275	-0.312	-0.267	-0.068	-0.110	-0.145	-0.182	0.279	0.510	0.097	0.192	-0.126	-0.496	-0.123	-0.089	-0.346	-0.130	-0.159	0.465	-0.152	-0.328	1

Figure 5.11 – Spearman rank correlation matrix for the pristine ore (whole rock composite data). The correlation coefficient above which it is considered statistically significant (99%) is 0.520 (Rollinson 1993). Positive correlation is marked in green and negative in red. The correlation matrix is based on 21 composite whole rock data.

Au exists with Ba. The weathered feldspathic pyroxenite is very heterogenous and due to the breakdown of minerals, elements are mobilized and lost from the system.

	Au	Pt	Pd	S	Na	Mg	Al	K	Ca	V	Cr	Mn	Fe	Ni	Ag	Co	Eu	Bi	Se	Sr	Zr	Ba	Cu	Ti
Au	1																							
Pt	0.927	1																						
Pd	0.944	0.845	1																					
S	0.626	0.693	0.636	1																				
Na	-0.122	0.045	-0.273	-0.049	1																			
Mg	0.149	0.127	0.182	0.399	0.000	1																		
Al	0.315	0.482	0.145	0.065	0.782	-0.164	1																	
K	0.469	0.564	0.329	0.016	0.667	-0.122	0.940	1																
Ca	0.332	0.382	0.273	0.856	0.200	0.455	0.091	-0.038	1															
V	-0.177	0.101	-0.303	0.190	0.673	0.679	0.488	0.410	0.421	1														
Cr	0.543	0.107	0.607	0.158	-0.536	0.679	-0.607	-0.395	0.250	-0.328	1													
Mn	0.280	0.136	0.282	0.244	0.000	0.691	-0.127	0.019	0.391	0.034	0.679	1												
Fe	0.376	0.345	0.327	0.065	-0.055	0.655	0.200	0.329	-0.009	0.101	0.536	0.455	1											
Ni	0.787	0.791	0.736	0.619	-0.082	0.573	0.227	0.357	0.400	0.185	0.464	0.445	0.736	1										
Ag	0.382	0.455	0.297	0.502	0.503	0.479	0.442	0.428	0.576	0.167	0.257	0.673	0.200	0.418	1									
Co	0.715	0.670	0.670	0.283	0.047	0.493	0.419	0.586	0.121	0.033	0.395	0.549	0.847	0.838	0.485	1								
Eu	0.094	0.179	-0.063	0.297	0.700	0.054	0.511	0.417	0.610	0.707	-0.071	0.386	-0.135	0.108	0.623	0.100	1							
Bi	0.771	0.765	0.728	0.570	0.129	0.314	0.397	0.504	0.424	0.135	0.393	0.553	0.415	0.784	0.718	0.783	0.463	1						
Se	0.720	0.666	0.594	0.326	0.102	0.378	0.486	0.659	0.270	0.103	0.544	0.450	0.726	0.870	0.234	0.835	0.235	0.750	1					
Sr	-0.122	0.009	-0.164	0.359	0.636	0.455	0.345	0.179	0.545	0.639	-0.500	-0.018	0.091	0.136	0.152	-0.028	0.377	-0.018	0.138	1				
Zr	0.399	0.426	0.227	0.168	0.388	-0.151	0.567	0.604	0.322	0.538	0.286	0.378	0.113	0.265	0.480	0.395	0.745	0.545	0.470	-0.123	1			
Ba	0.804	0.809	0.782	0.595	0.309	0.355	0.545	0.667	0.436	0.118	0.214	0.482	0.391	0.682	0.648	0.754	0.377	0.793	0.630	0.200	0.501	1		
Cu	0.892	0.909	0.845	0.782	0.000	0.445	0.300	0.414	0.564	0.135	0.464	0.491	0.482	0.909	0.612	0.763	0.296	0.876	0.762	0.091	0.445	0.855	1	
Ti	0.201	0.082	0.073	-0.147	-0.164	0.318	0.009	0.132	-0.036	0.185	0.768	0.427	0.736	0.509	-0.042	0.549	0.063	0.277	0.738	-0.164	0.350	0.018	0.245	1

Figure 5.12 – Spearman rank correlation matrix for the weathered ore (whole rock composite data). The correlation coefficient above which it is considered statistically significant (99%) is 0.745 (Rollinson 1993). Positive correlation is marked in green and negative in red. The correlation matrix is based on 11 composite whole rock data.

Figure 5.13 plots the relative gains and losses of selected elements during weathering using the spreadsheet "Easygrant" by López-Moro (2012) following the equation for the grain/loss calculations by Gresens (1967). The assumption for the calculation is that Al is strongly immobile. For the gain/loss calculation, whole-rock median values of the composite samples of weathered and pristine feldspathic pyroxenite are used. The rock densities estimated for the calculation are 3.3 g/cm^3 for the pristine and 2.9 g/cm^3 for the weathered ore. A strong loss is outlined for S (-86%) and intermediate loss by Na (-17%), Mg (-30%), Ca (-9%), Ag (-12%) and Au (-36%). Palladium shows a loss of -13% but Pt is slightly more enriched in the weathered ore (7%). Barium is the only element that gained by a large amount, e.g. +65%; this is explained by the liberation due to the breakdown of plagioclase and subsequent crystallization of barite. In general, it should be kept in mind that composite samples are used for the calculation of the diagram in Figure 5.13. These composite samples may include small amounts of harzburgite and chromitites. The nugget effect and the absolute values (close to the detection limit) of the elements are important to be considered. However, the general trends, in particular the strong loss of S and Pd is clearly observable.

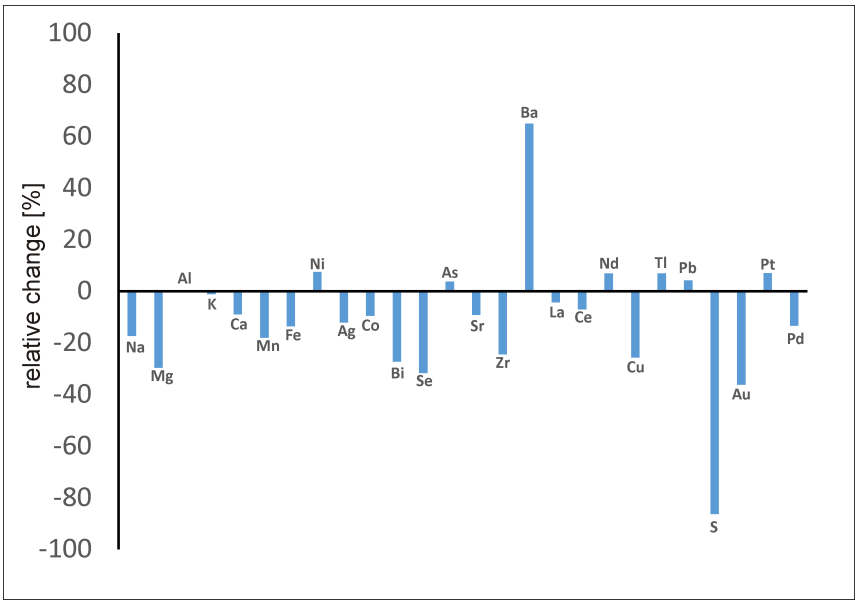

Figure 5.13 – Relative grains and losses following the equation of Gresens (1967) and using the spreadsheet by López-Moro (2012). Median values from weathered pyroxenite and pristine pyroxenite of the three drill cores.

5.3 Sulfide and platinum-group minerals

The sulfide mineralogy within the Platreef is described in Chapter 6 and is therefore only briefly covered here. Main sulfides at Overysel are pyrrhotite, pentlandite, chalcopyrite and pyrite. A list of the various proportions is given in the Appendix. The typical assemblage consists of large pyrrhotite grains (up to a few millimeter) with pentlandite and chalcopyrite along the rim (Figure 5.5A,B). Sulfides are typically disseminated but also occur more massive with dominant chalcopyrite with inclusions of pyrite and pyrrhotite at the rims of pyrite (Figure 5.5C). Secondary pyrite is observed in various sections and in particular in the chromite-rich parts (Figure 5.5D).

The PGE mineralogy is described in Chapter 6. Here, additionally a few analyses of (Pt,Pd)-germanides are shown. Figure 5.14 shows a ternary distribution plot of the composition of the analyzed (Pd,Pt)-germanides showing that its following $(Pd,Pt)_{2.0-2.33}Ge_{0.67-1.0}$. Armitage et al. (2002) and Holwell et al. (2006) were the first to show (Pt,Pd)-germanides in the Platreef. The only other published occurrences of (Pt,Pd)-germanides are from Noril'sk (Komarova et al. 2002) and $(Pd,Pb)_2Ge$ from the Burakovsk Layered Complex in the Karelia-Kola region (Grokhovskaya et al. 2005). In Chapter 9.1.1 the formation of these rare PGM are

discussed.

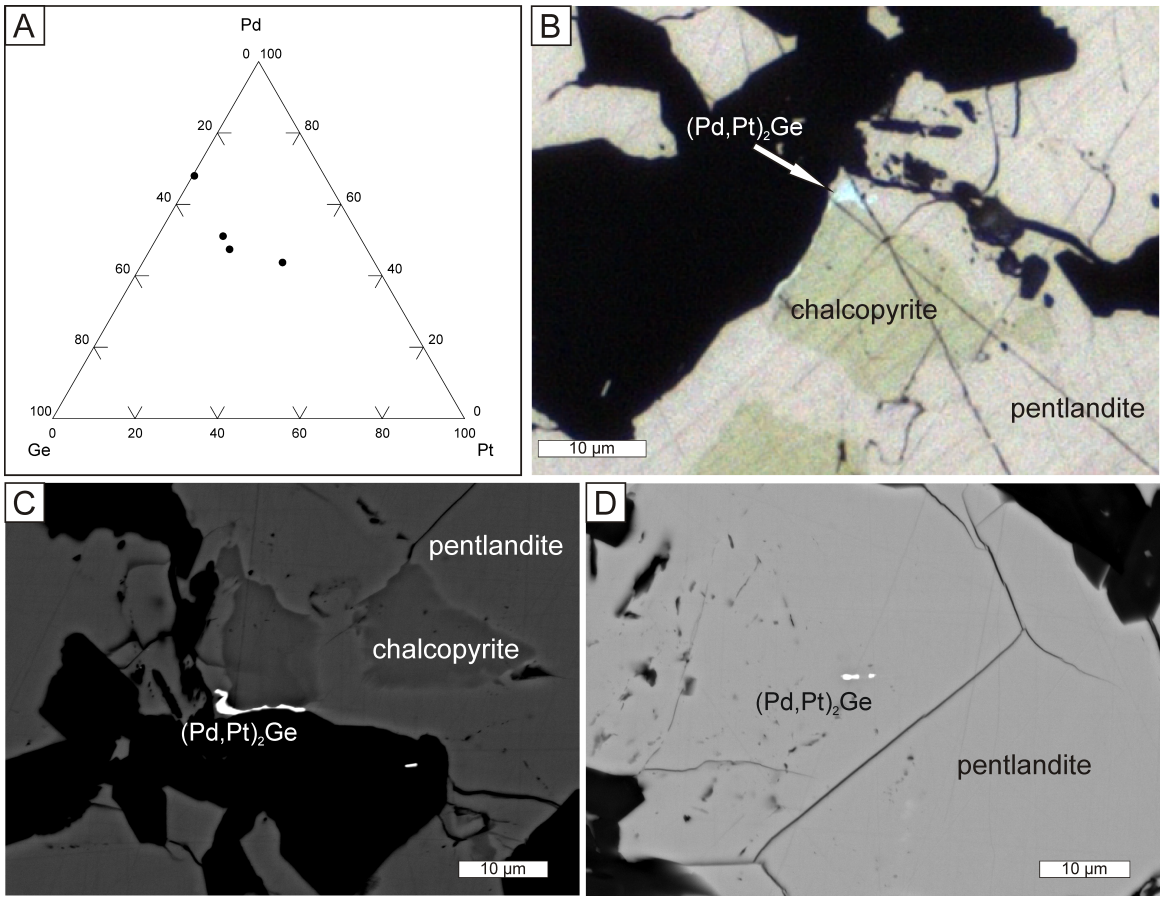

Figure 5.14 – A: Ternary plot showing the compositional data of the unnamed (Pt,Pd)-germanide in atomic%. B: Photomicrograph of $(Pd,Pt)_2$-germanide together with chalcopyrite and pentlandite [Pr-3]. C,D: Backscattered electron image of $(Pd,Pt)_2$-germanide with chalcopyrite and pentlandite [Pr-3].

Two samples were analyzed following electric-pulse disaggregation (EPD) and hydroseparation (HS), one from the weathered ore (Oy2-5, 233 g) and one from the pristine ore (Oy2-17, 192.3 g). Whole-rock geochemistry data for Oy2-5 are: Pt 2720 ppb, Pd 1840 ppb, Cu 1510 ppm, Ni 983 ppm and for Oy2-17: Pt 2600 ppb, Pd 3220 ppb, Cu 4410 ppm and Ni >5000 ppm.

The weathered ore was first crushed to <125 μm. Then the crushing product was subjected to wet-sieving producing three fractions: 125 to 80 μm, 80 to 40 μm and <40 μm. From each fraction a heavy mineral HS concentrate was produced, followed by monolayer polished sections. In total thirteen PGM grains are identified using SEM, of which eleven are completely liberated and two grains intergrown with goethite. The major identified PGM are cooperite and sperrylite.

The pristine ore was crushed to <71 μm. Then the crushing products were wet-sieved to the fractions 71 to 40 μm and <40 μm. The HS concentrates of heavy mineral grains were sieved again for both fractions. All HS concentrates are hand treated by wet magnetic separation. Monolayer polished sections were produced from all HS concentrates. Scanning electron microscope work identified the following PGM: cooperite, michenerite, sperrylite and moncheite and native gold. In the polished sections of the heavy mineral HS concentrates 60 to 80 grains of precious minerals are present.

5.4 Mineral chemistry of pentlandite

The mineral chemistry of pentlandite has been studied by various authors such as Cabri & Laflamme (1981), Todd et al. (1982), Cabri et al. (1984), Oberthür et al. (1997a, 2003), Gervilla et al. (2004), Godel et al. (2007), Holwell & McDonald (2010), Osbahr et al. (2013) and Osbahr et al. (2014) and is shown in Chapters 4 and 6. In this chapter additional EPMA data of pentlandite from the Bushveld Complex and the Great Dyke are presented.

Figure 5.15A,B is a Fe-Ni binary plot and shows EPMA analysis of pentlandite from the UG-2 chromitite (eastern and western Bushveld Complex), the Merensky Reef (eastern Bushveld Complex), the Platreef (Overysel, Nonnenwerth and Townlands) and the Great Dyke of Zimbabwe. The sulfur contents are roughly constant but the Fe-Ni ratio varies along a correlation line. The Fe-Ni ratios within one sample location are relatively homogenous but vary among different deposits. This relative constant Fe-Ni ratio for individual sample locations is also shown in Figure 5.15C where Co is added on one axis on the ternary plot. Cobalt concentrations vary from values below detection limit up to a few wt.% in pentlandite.

The compositional variation of pentlandite has been studied experimentally and by in-situ analysis of natural pentlandite (Kaneda et al. 1986). The metal to sulfur atomic ratio is approximately 9 to 8 but the ratio between Ni, Cu and Co may vary. Kaneda et al. (1986) studied the end-members of Co_9S_8 and $(Ni,Fe)_9S_8$ at different temperatures and showed that pentlandite forms a complete solid solution between Co_9S_8 and $(Ni,Fe)_9S_8$ in the temperature range of 600°C to 300°C (Figure 5.15D). At 200°C Kaneda et al. (1986) presumed that two separate phases exist. The pentlandite from the UG-2 chromitite (eastern and western Bushveld Com-

plex), the Merensky Reef (eastern Bushveld Complex), the Platreef (Overysel, Nonnenwerth and Townlands) and the Great Dyke of Zimbabwe plot in the low-Co 200°C field (Figure 5.15D). The distribution of PGE in pentlandite is further discussed in Chapter 9.1.2.

5.5 Sulfur isotopes versus S-Se ratio

Nickel-Cu-PGE deposits form when an immiscible sulfide melt migrates through a mafic- ultramafic magma collecting chalcophile elements - including PGE (Naldrett 2004a, 2011). Sulfur is present in mafic-ultramafic magmas but for some large Ni-Cu-PGE deposits it has been argued that externally derived sulfur from the country rocks triggered the generation of these deposits (Lesher & Groves 1986, Lesher & Burnham 2001, Li et al. 2002, Lightfoot & Keays 2005). Sulfur isotope studies provide information about the amount of externally derived sulfur in Ni-Cu-PGE deposits. The S content im mafic-ultramfic melts depends on temperature, fO_2 and fS_2 (Shima & Naldrett 1975, Naldrett & von Gruenewaldt 1989, Wallace & Carmichael 1992). Empirical studies and experimental data estimated sulfur concentrations in ultramafic melts of 0.3 up to 0.5 wt.% (Shima & Naldrett 1975, O'Neil & Mavrogenes 2002, Jugo et al. 2005, Li & Ripley 2005).

In Chapters 6 and 9 the sulfur isotope signature at the Platreef is presented. Here the application of the S/Se ratio from whole-rock data is discussed in comparison to the sulfur isotope data presented earlier. The S/Se ratio may indicate crustally derived S in magmatic Ni-Cu-PGE deposits (Smith et al. 2016). Selenium substitutes for S in base metal sulfides and within primary magmas the S/Se ranges from 3000 to 3500 (McDonough & Sun 1995, Lorand et al. 2003). The initial magmatic S/Se ratio can be shifted by various processes. In general it is assumed that S/Se ratios greater than mantle values are the result of contamination of the mantle-derived magma by S-rich sedimentary county rocks, whereas S/Se ratios lower than mantle values are assumed to be the result of S-loss during post-crystallization processes (Queffurus & Barnes 2015). Further processes effecting the S/Se ratio are hydrothermal alteration, high-grade metamorphism, serpentinization and S-loss due to supergene weathering (Queffurus & Barnes 2015). Sulfur is more mobile during alteration than Se which consequently causes a decrease in S/Se ratio during alteration. Figure 5.16 shows the S-Se and δ^{34}S data of the samples from

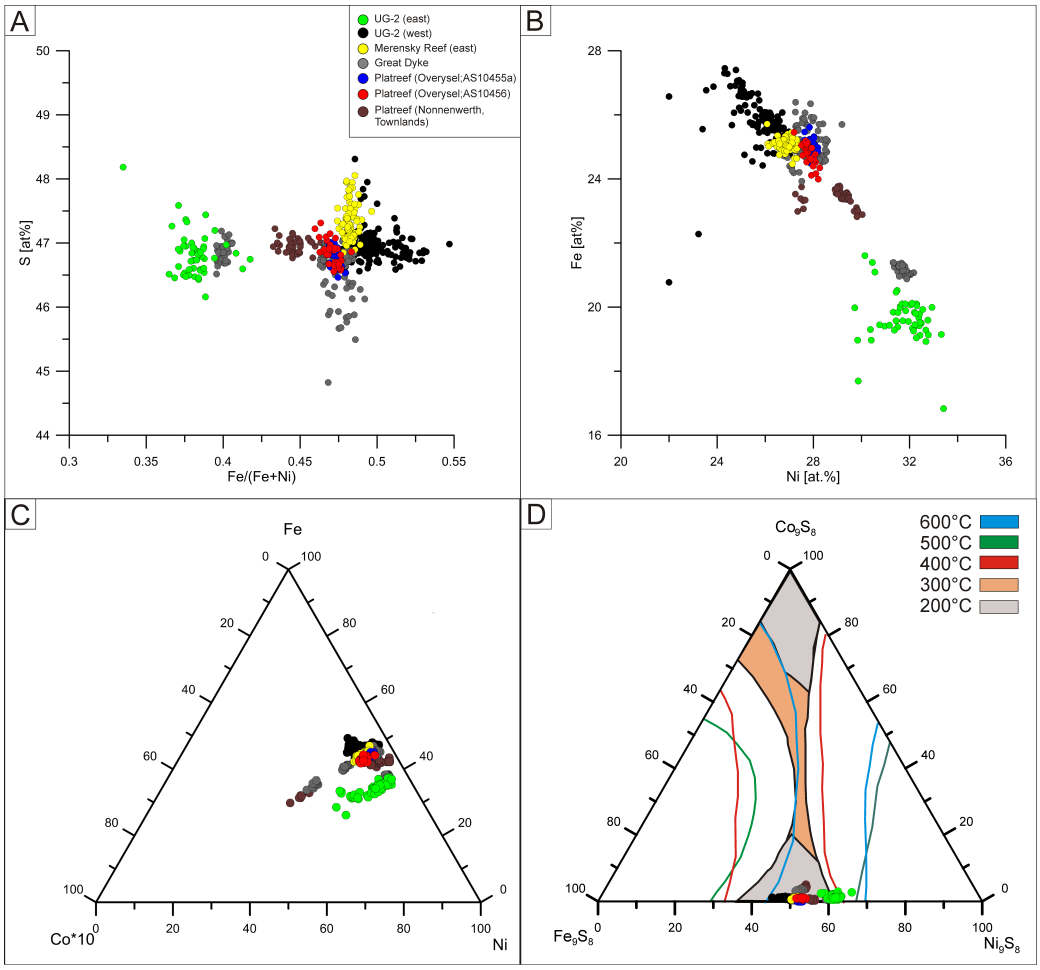

Figure 5.15 – Compositional diagrams of pentlandite chemistry from the eastern UG-2 chromitite (Kuhlmann et al. 2006) and western Bushveld Complex (Junge et al. 2014), from the eastern Merensky Reef (Ziaja et al. 2007), the Great Dyke, the Platreef and Townlands and Nonnenwerth (Manyeruke 2007) and the Platreef at Overysel from this study. A: Sulfur-Fe/(Fe+Ni) diagram showing nearly similar S contents. B: Fe-Ni diagram with varying Fe/Ni ratios of Fe-rich (27.5 at.%) endmember to Fe-poor (18.5 at%) endmember. Nickel varies from about 24 to 33 at% C: D: Ni-Fe-Co*10 diagram visualizing the variation in the Co concentrations within individual deposits. Note: Co is multiplied by 10: maximum Co concentrations are about 4 at% in this dataset. D: Pentlandite solid-solution fields in the Ni_9S_8, Co_9S_8 and Fe_9S_8 ternary diagram, at temperature of 600°C, 500°C, 400°C, 300°C, and 200°C. Modified after Kaneda et al. (1986).

the Mogalakwena and Tweefontein deposits. The heavy sulfur isotope signature at Tweefontein does not correspond with S/Se ratio lower than mantle values. The S/Se ratio alone can therefore not be used as an indicator of the amount of crustally derived S as higher S/Se ratio are expected for a heavier sulfur isotope signature. The lower S/Se ratio within the Mogalawena Mine is probably due to hydrothermal alteration as a S-loss by near surface weathering as the presented samples are from depth >30 m. Several processes may have affected the S/Se ratio at the Platreef: (1) The contamination with the country rock caused an increase in the S/Se ratio as well as the heavier δ^{34}S signature and a post-stage hydrothermal alteration lowered the overall S/Se ratio. (2) Alternatively, the S/Se ratio within the Platreef was initially lower than the mantle value but further increased due to the contamination with the country rock as indicated by the heavier isotope signature. However, differences in the fractionation between mss and iss can also affect the initial Se concentration in the sulfides and whole-rock data as Se is slightly incompatible with the mss and Se is therefore more enriched in the Cu-rich phase (Lorand & Alard 2001).

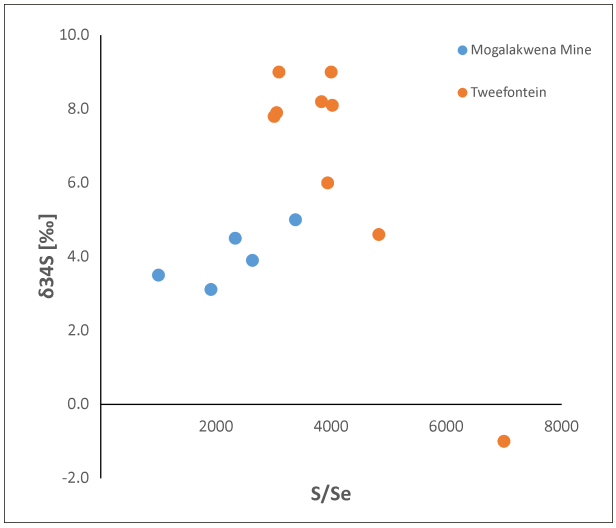

Figure 5.16 – S-Se ratio versus $\delta^{34}S$ data of the Mogalakwena and Tweefontein.

5.6 Conclusions

This chapter provides a detailed petrographic description and the whole rock geochemistry of the drill cores from the Mogalakwena Mine and additional results about PGM and the S/Se ratio. The main aspects of this chapter are:

1. The feldspathic pyroxenite from the Mogalakwena Mine typically consists of cumulus orthopyroxene and interstitial plagioclase. Sulfides occur disseminated, net-textured or massive and are mainly pyrrhotite, pentlandite, chalcopyrite and minor pyrite. Pristine ores usually contain sulfide aggregates of <1 cm in size but also blebs of a few centimeters are observed.

2. During weathering sulfides are largely destroyed and only relict sulfides are observed. Small cracks exist in the near-surface ore and allow the circulation of hydrous fluids and the breakdown of primary minerals and the formation of secondary minerals, carbonates and Fe-oxy/hydroxides. At larger degrees of weathering, orthopyroxene, clinopyroxene and plagioclase break down almost completely to serpentine, smectite and kaolinite and larger degrees of iron oxidation and the formation of Mn-oxides are observed.

3. Additionally to the typical PGM assemblage in the Platreef (mainly (Pt,Pd)- bismuthotellurides), analyses of (Pt,Pd)-germanides are presented. The only other published occurrences of (Pt,Pd)-germanides are from Noril'sk (Komarova et al. 2002) and $(Pd,Pb)_2Ge$ from the Burakovsk Layered Complex in the Karelia-Kola region (Grokhovskaya et al. 2005) and from the Platreef by Armitage et al. (2002) and Holwell et al. (2006). Germanium is very rare in mafic/ultramafic rocks and has a similar ionic radius as Si. Germanium can therefore replace Si in the lattice sizes of silicates. The formation of (Pd,Pt)-germanides in the Platreef may therefore be a result of a hydrothermal overprint where Ge-bearing silicates are destroyed and (Pt,Pd)-germanides formed. See also Chapter 9.1.1.

4. Pentlandite in ultramafic-mafic intrusions can hold elevated concentrations of PGE (in the 100s-ppm range and even up to a few wt.%). Also Co concentrations vary from values below detection limit up to a few wt.% in pentlandite. See also Chapter 9.1.2.

5. The S/Se ratio from whole-rock in comparison to the sulfur isotope data may indicate crustally derived S in magmatic Ni-Cu-PGE deposits. The lower S/Se ratio within the Mogalawena Mine is probably due to hydrothermal alteration.

Chapter 6

Distribution of PGE in pristine and near-surface Platreef ore, northern Bushveld Complex, South Africa

This chapter is to be submitted as: Junge, M., Oberthür, T., Kraemer, D., Melcher, F., Piña, R., Cassens, I., Manyeruke, T. and Strauß, H.: Distribution of PGE in pristine and near-surface Platreef ore, northern Bushveld Complex, South Africa. Chemical Geology.

6.1 Introduction

The 2,055 ± 3.9 Ma old (Scoates & Friedman 2008) Bushveld Complex of South Africa is the largest mafic-ultramafic layered intrusion on Earth covering an area of circa 66,000 km^2. The Bushveld Complex hosts the World's largest resources of platinum-group elements (PGE) occurring in three major ore bodies, namely the Merensky Reef, the UG-2 chromitite, and the Platreef. The Platreef is located north of the town of Mokopane in the northern limb of the Bushveld Complex (Fig. 6.1) and comprises an up to 400 m thick mineralized pyroxenite with sulfide contents of about 3% and PGE contents between 1 to 4 g/t (Verma 2007, McDonald & Holwell 2011). The Platreef lies on a granite-gneiss basement and on sediments of the Transvaal Supergroup: quartzites and shales of the Timeball Hill Formation, shales of the Duitschland Formation, the Penge banded iron formation, and dolomites of the Malmani Subgroup (Manyeruke

et al. 2005, Holwell et al. 2006, McDonald & Holwell 2011).

Weathering of the rocks in the area of the Bushveld Complex ranges down to 40 m below surface. Economic concentrations of PGE in the Platreef are mainly restricted to sulfide ores but are approximately similar in the weathered ore. However, near-surface oxidized Platreef ores are currently not processed although a potential ore resource of about 274 Mt containing 517 t of 4E (Pt, Pd, Rh and Au) was estimated by Buchholz & Foya (2015). Previous attempts to extract the PGE from oxidized PGE ore of the Main Sulfide Zone in Zimbabwe have proved to be uneconomic due to low PGE recovery rates («50%) achieved by conventional metallurgical methods (Prendergast 1988, Evans 2002, Locmelis et al. 2010, Oberthür et al. 2013a).

In order to investigate the behavior of PGE during weathering, three boreholes covering a sequence of oxidized and pristine Platreef ores from the Mogalakwena mine were studied by whole rock geochemistry, ore microscopy, scanning electron microscopy (SEM), mineral liberation analysis (MLA), electron microprobe (EPMA) and laser ablation-inductively coupled plasma-mass spectrometry (LA-ICP-MS). Further, conventional sulfur isotope analyses were used to obtain information about the source of the sulfur in the Platreef, deriving either primary from the magma or by assimilation with the country rock. The variation between sulfide and PGE mineralization along the strike of the Platreef is studied at Townlands, Tweefontein, Sandsloot, Overysel and Nonnenwerth.

6.2 Previous Work

The Platreef in the northern Bushveld Complex is 10 to 400 m thick consisting of pyroxenitic lithologies with PGE and base metal sulfide mineralization (Holwell et al. 2006, McDonald & Holwell 2011) with average PGE grades of 2 g/t (Cawthorn et al. 2002b). Variation in the mineralization has been assumed to be partly related to the assimilation of different floor rocks. Platinum-group elements occurring either as discrete platinum-group minerals or incorporated in sulfide minerals as described for different ultramafic-mafic complexes (Cabri et al. 1984, 2002, Cabri 1992, Oberthür et al. 1997a, 2003, Gervilla et al. 2004, Godel et al. 2007, Holwell & McDonald 2007, 2010, Hutchinson & McDonald 2008, Piña et al. 2012, Wirth et al. 2013, Osbahr et al. 2013, 2014, Junge et al. 2014, 2015b). The distribution of the PGE mineralization

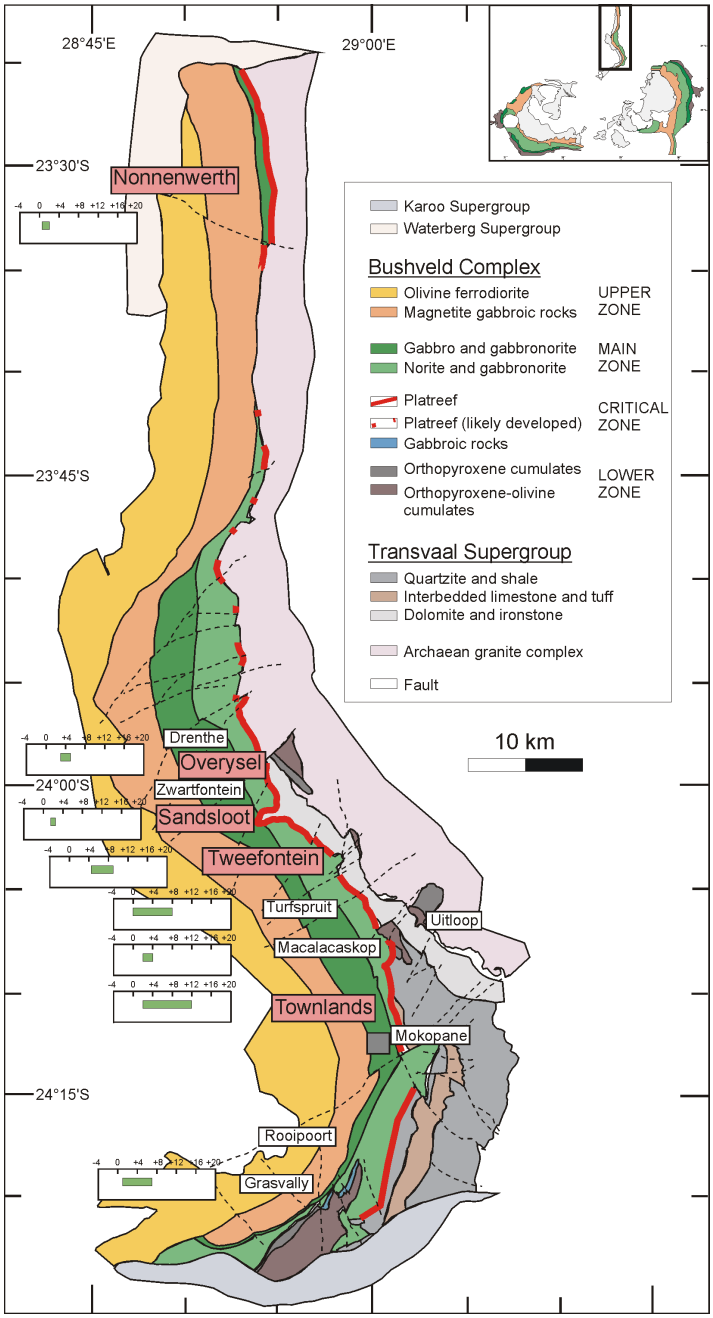

Figure 6.1 – Geological map of the northern Bushveld Complex with sample locations of the Platreef at the Mogalakwena Mine. Modified after Ashwal et al. (2005) and Maier et al. (2008). The range in $\delta^{34}S$ is shown next to the locations for Grasvally (Maier et al. 2008, Smith et al. 2016), Townlands (Manyeruke et al. 2005), Macalacaskop (Sharman-Harris et al. 2005), Turfspruit (Buchanan & Rouse 1984, Sharman-Harris et al. 2005), Tweefontein, Sandsloot and Overysel (all this study) and Nonnenwerth (Manyeruke 2007). All sulfur isotope compositions are calculated relative to Vienna Canon Diablo Troilite (VCDT) and are reported in standard.

in the Platreef has been studied at different locations along strike. Platinum-group minerals are mainly bismuthotellurides, sulfides and arsenides (Kinloch 1982, Viljoen & Schürmann 1998, Hutchinson & Kinnaird 2005, Holwell & McDonald 2006).

For the Platreef various sulfur isotope studies exists along strike. At the Grasvally Norite-Pyroxenite-Anorthosite (GNPA) member at the southern part of the Platreef, Maier et al. (2008) published δ^{34}S values ranging from +1.8‰ to +5.1‰. Smith et al. (2016) distinguished between two textural and paragenetic generations of sulfides at GNPA in which the primary sulfide assemblages (pyrrhotite, pentlandite and chalcopyrite) have δ^{34}S ranging from +1.6‰ to +4.0‰ and secondary sulfide assemblages (pyrite, millerite, pyrrhotite, pentlandite and chalcopyrite) from +0.9‰ to 6.8‰. At Rietfontein and Macalacaskop average δ^{34}S values are of +5.0‰ and 2.9‰, respectively (Sharman-Harris et al. 2005). On the farm Turfspruit Sharman-Harris et al. (2005) published two groups with an average δ^{34}S values of +1.4‰ and +5.2‰. Further north at Townlands, Manyeruke et al. (2005) provided δ^{34}S values of +2.6‰ to +9.1‰. Buchanan (1981) carried out sulfur isotope analysis of the Platreef at the farm Tweefontein ranging from +6.3‰ to +9.2‰. Holwell et al. (2007) studied sulfur isotope study on Zwartfontein, Sandsloot and Overysel with δ^{34}S values ranging from -0.6‰ to +1.9‰, 0‰ to +2.6‰ and +0.4‰ to +2.4‰ for primary sulfides, respectively. At Nonnenwerth, Manyeruke (2007) provided δ^{34}S values of +0.7‰ to +1.9‰ and at the base of the Platreef +5.2‰.

Oxidized PGE ores have been studied in the Great Dyke (Prendergast 1988, Evans 2002, Locmelis 2005, Locmelis et al. 2010, Oberthür et al. 2013a) and the UG-2 chromitite (Hey 1999). For oxidized ore of the Great Dyke, Oberthür et al. (2013a) estimated a total resource of 160 to 250 Mt with grades of 1.5 g/t. For the Bushveld Complex a potential resource of oxidized PGE ore was estimated to about 337 Mt containing 819 t of 4E (Buchholz & Foya 2015). Whole rock analysis of oxidized and pristine PGE ores showed that the Pt/Pd-ratio in the oxidized zone is higher than in the sulfide ore, proving that Pd more readily partitions into solution than Pt and can be transported out of the system (Wagner 1929, Hall 1932, Schneiderhöhn & Moritz 1939, Fuchs & Rose 1974, Hey 1999, Locmelis 2005, Locmelis et al. 2010). In oxidized ores from the Great Dyke and the UG-2 chromitite, PGE-oxides and PGE-hydroxides as weathering products from primary PGM and sulfide minerals were identified (Hey 1999, Locmelis 2005, Locmelis et al. 2010, Oberthür et al. 2013a). Based on Eh-pH relations, Fuchs & Rose (1974) showed in a

study on the geochemical behavior of Pt and Pd during weathering in the soils of the Stillwater Complex that Pd is mobile in acidic solutions, probably as chloride complexes but that Pt is only mobile under extremely acidic or highly chloridic conditions.

Processing of oxidized ore is currently uneconomic with conventional methods due to too low recovery rates. However, Kraemer et al. (2015) and Kraemer (2015) conducted leaching experiments with biomolecules on oxidized ores from the Great Dyke and obtained very promising PGE recovery rates of up to 80%.

6.3 Samples and Analytical Methods

This study focuses on the distribution of PGE in pristine and near-surface oxidized Platreef ore from the Mogalakwena mine (Overysel pit) in the northern Bushveld Complex, using ore microscopy, SEM, EPMA and sulfur isotope data (also Sandsloot pit and Tweefonein). Three drill cores of each up to 50 m long (Fig. 6.2), covering a sequence of oxidized to pristine ore were drilled at the Overysel open pit. Main rock type in these cores are feldspathic pyroxenites with mineralization present either as disseminated, massive and net-textured sulfide ore types. Sulfide grains range from a few millimeters up to several centimeters. Further, disseminated chromite grains and smaller chromitite bands occur as well as serpentinized harzburgitic rocks intercalated with the feldspathic pyroxenites. For a mineralogical comparison, sulfides and platinum-group minerals are additional studied in drill cores from Tweefontein (TN181), Townlands (TL01-3) and Nonnenwerth (NO2199).

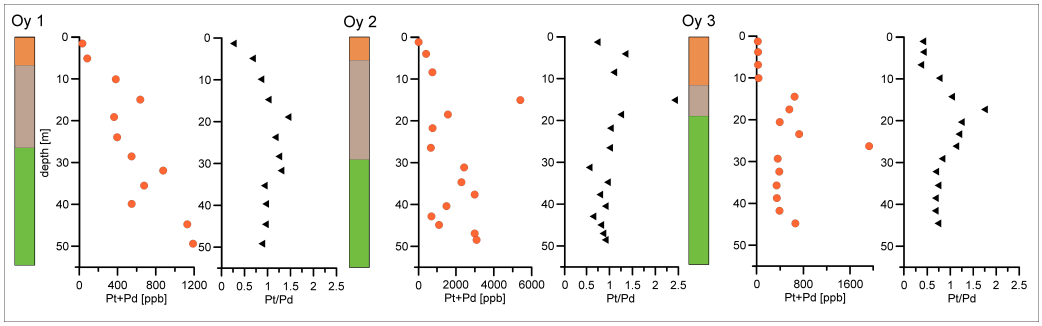

Figure 6.2 – Variation of Pt+Pd and the Pt/Pd ratio along the drill cores (Oy-1, Oy-2 and Oy-3). The sketch shows the soil (orange), weathered ore (brown) and pristine ore (green).

Sulfide grains and secondary silicates were analyzed with a CAMECA SX 100 electron

microprobe the following elements were analyzed: Si(Kα), S(Kα), Cr(Kα), Fe(Kα), Co(Kα), Ni(Kα), Cu(Kα), As(Lα), Se(Lα), Rh(Lα), Pd(Lα), Ag(Lα) and Pt(Lα). The analytical conditions for sulfides were: 20 kV acceleration voltage, 120 nA beam current, focused beam, and up to 190 s measuring time. Synthetic metals (Pd, Rh, Pt, Ag, Co, Cu, Se) and natural sulfides (pentlandite, chalcopyrite, pyrite) were used as standards. Mean detection limits were 75 ppm for Co, 100 ppm for Se, 120 ppm for Rh, 140 ppm for Pd, 160 ppm for Ag, and 300 ppm for Pt.

For the silicates in the oxidized ore the following elements were analyzed: Mg(Kα), Al(Kα), Si(Kα), S(Kα), Ca(Kα), Cr(Kα), Mn(Kα), Fe(Kα), Co(Kα), Ni(Kα), Cu(Kα), As(Lα), Se(Lα), Rh(Lα), Pd(Lβ), Ag(Lβ) and Pt(Lα). The analytical conditions employed for silicates were: 20 kV acceleration voltage, 120 nA beam current, focused beam, and up to 360 s measuring time. Synthetic metals (Rh, Pd, Ag, Pt, Se, Mn, Fe, Co, Ni, Cu, Se, Si), natural chromite (Al, Mg) and natural pentlandite (S) are used as standards. Mean detection limits were 130 ppm for Mg, 100 ppm for Al, 100 ppm for Si, 175 ppm for S, 130 ppm for Ca, 85 ppm for Cr, 160 ppm for Mn, 325 ppm for Fe, 100 ppm for Co, 145 ppm for Ni, 150 ppm for Cu, 90 ppm for Se, 85 ppm for Rh, 70 ppm for Pd, 325 ppm for Ag and 200 ppm for Pt.

Whole-rock analyses for major, minor and trace elements were conducted by ACTLABS, Canada, using instrumental neutron activation analysis, inductively coupled plasma mass spectrometry and inductively coupled plasma with optical emission spectroscopy.

The trace elements in sulfides were determined by LA-ICP-MS at LabMaTer, Universite du Quebec a Chicoutimi (UQAC), Canada, using a Resolution 193-nm Excimer laser with a M-50ablation cell and an Agilent7700 quadrupole mass spectrometer. An argon-helium gas mix was used as carrier gas. Samples and reference materials were placed in the chamber together, and the reference materials were run before and after each sample. The spectra were collected for 30 s with the laser switched off to determine the base line. Then, line scans across the grains were carried out using a beam size of 33 μm, a laser frequency of 15 Hz, a power of 0.5 mJ/cm^3, and a speed of lateral laser displacement of 5 Î¼m/s. The material was then analyzed using the mass spectrometer in time resolution mode using mass jumping and a dwell time of 10 ms/peak. The following isotopes were monitored: ^{29}Si, ^{33}S, ^{34}S, ^{57}Fe, ^{59}Co, ^{60}Ni, ^{61}Ni, ^{63}Cu, ^{65}Cu, ^{66}Zn, ^{75}As, ^{82}Se, ^{99}Ru, ^{101}Ru, ^{103}Rh, ^{105}Pd, ^{106}Pd, ^{107}Ag, ^{108}Pd, ^{111}Cd, ^{121}Sb, ^{125}Te, ^{187}Re, ^{189}Os, ^{191}Ir, ^{193}Ir, ^{195}Pt, ^{197}Au, ^{206}Pb, ^{208}Pb and ^{209}Bi. Data reduction was carried out using Iolite

software (Paton et al. 2011) and internal standardization was based on ^{57}Fe using the mean iron contents in the minerals as determined by electron microprobe. For the calibration of PGE and Au, the certified reference material Po727, a synthetic FeS doped with approximately 40 ppm of each PGE and Au provided by the Memorial University of Newfoundland, was employed. For the remaining elements, we used the certified reference material MASS-1, a (Zn-Fe-Cu-S) pressed power pellet provided by the United States Geological Survey (USGS) and doped with 50-70 ppm Ag, As, Co, Bi, Sb, Se and Te (Wilson et al. 2002). Two in-house reference materials, JB-MSS5 and UQAC-MSS-1, were used to monitor the accuracy of the calibration. Analyses of the in-house reference materials agreed with the certified and working values (Table 6.1). ^{101}Ru was corrected for ^{61}Ni^{40}Ar interference using UQAC-MSS1: the correction is equivalent to 0.8 ppm in pentlandite and less than the lower limit of detection in pyrrhotite, pyrite and chalcopyrite. The amount of Cu interference on ^{103}Rh and ^{105}Pd from ^{63}Cu^{40}Ar and ^{65}Cu^{40}Ar, respectively, was determined by running a (CuFe)S_2 blank at the beginning and end of each session. In all phases except chalcopyrite, the Cu corrections on Rh and Pd are below the lower limit of detection. The interference of Cu argide on 103Rh in chalcopyrite exceeds 50% of the Rh signal and thus Rh is not reported in chalcopyrite. Lower limit of detection for LA-ICP-MS analyses was calculated as three sigma background counts for the gas blank and each sulfide analysis.

Table 6.1 – Selected whole-rock PGE and Au contents of selected drill core samples from oxidized and pristine Overysel ore

Segment	Depth [m]	Os	Ir	Ru	Rh	Pt	Pd	Au	Pt/Pd
Oy1-26a	48.5	128	358	1080	2280	1480	3500	56	0.42
Oy2-05	13	<2	41.6	140	155	2660	2050	580	1.29
Oy2-06	16.2	<2	22	101	95	1410	1460	232	0.97
Oy2-12	27	<2	33.5	100	97.3	1120	1140	161	0.98
Oy2-14	32.4	<2	24.3	81	93.5	1010	2050	221	0.49
Oy2-17	37.1	<2	18.4	81	73.1	2060	2120	192	0.97
Oy2-18	40.5	24	35.6	111	158	2250	3390	395	0.66
Oy2-20	46	<2	26.6	105	99	1920	1900	215	1.01
Oy2-21	48.8	<2	45.5	205	197	2230	2820	441	0.79
Oy3-17	45.3	<2	16.6	63	85.9	1000	1910	180	0.52

Laser ablation-inductively coupled plasma-mass spectrometry measurements on secondary

minerals within the oxidized ore were carried out on a ThermoScientific Element XR (HR-ICP-MS) coupled to an UV-Femtosecond laser at the Leibniz University Hanover. The following isotopes were measured: ^{25}Mg, ^{27}Al, ^{29}Si, ^{34}S, ^{43}Ca, ^{47}Ti, ^{55}Mn, ^{57}Fe, ^{60}Ni, ^{63}Cu, ^{77}Se, ^{89}Y, ^{99}Ru, ^{101}Ru, ^{103}Rh, ^{105}Pd, ^{108}Pd, ^{111}Cd, ^{137}Ba, ^{139}La, ^{140}Ce, ^{147}Sm, ^{153}Eu, ^{172}Yb, ^{175}Lu, ^{185}Re, ^{189}Os, ^{193}Ir, ^{194}Pt, ^{195}Pt, ^{197}Au, ^{205}Tl. As reference materials the NIST610 glass (Jochum et al. 2011) and Lombard meteorite (Gilbert et al. 2012) were used. Beam size was about 40 μm. Analyses were carried out as 20 samples with 4 analysis spots at NIST610 and 4 on the Lombard followed by 12 on the sample. Ablation was done mostly as lines and smooth spectra were obtained. The raw data were exported to a data-handling software tool implemented in JAVA using the libraries JFreeChart (JFree 2009), commons Math (Commons 2009) and POI (POI 2009). A normalization of MgO, Al_2O_3, SiO_2, CaO, MnO, FeO to 100% was used, because these oxides comprise the major compounds of the analyzed phases.

Sulfur isotopic measurements (δ^{34}S) were carried out using a ThermoFinniganMat DELTA Plus mass spectrometer coupled with an elemental analyzer (Carlo Erba) at the Geologisch-Palaeontologisches Institut, Westfaelische Wilhelms-Universitaet Muenster, Germany.

6.4 Results

6.4.1 Pristine ores

6.4.1.1 Whole rock geochemistry

In the pristine ore, a good positive correlation between PGE and sulfides exists. Sulfur contents are maximum 2 wt.% and Pt+Pd concentrations average 1 to 3 ppm. Nickel and Cu concentrations average 1000 ppm and 500 ppm, respectively. Figure 6.2 plots the variation of Pt+Pd and the Pt/Pd ratio. Within the pristine ore the Pt/Pd ratio is close to unity.

6.4.1.2 Mineralogy - Sulfides and platinum-group minerals at Overysel (Oymetox)

In pristine ores at Overysel, the main sulfides are pyrrhotite (up to 75%), pentlandite, chalcopyrite and minor pyrite. These base metal sulfide assemblages can achieve sizes of up to several centimeters but are usually in the range of <10 millimeters. Pentlandite and chalcopyrite are

up to several millimeters large and mainly occur around the margins of pyrrhotite (Fig. 6.3A). Flame-like exsolutions of pentlandite in pyrrhotite can often be observed (Fig. 6.3A). Chalcopyrite also occurs in symplectic intergrowth with pyrite (Fig. 6.3B-D). In rare cases an alteration of chalcopyrite to covellite is observed (Fig. 6.3E) in close association with gold grains within pyrite (Fig. 6.4F). In the massive sulfide sequence, large grains of pyrite usually occur within chalcopyrite (Fig. 6.3F). Platinum-group minerals are mainly (Pt,Pd)-bismuthotellurides, cooperite-braggite [(Pt,Pd)S] and sperrylite [$PtAs_2$] and generally occur as individual grains in different shapes at the margins of the sulfide grains, in PGM assemblages (Fig. 6.4A-D) and as micrometer-sized inclusions in pyrrhotite. Laurite [RuS_2] is also observed as inclusions in chromite (Fig. 6.4E). (Pt,Pd)-bismuthotellurides occur often as a mineral assemblage with different Bi-Te and Pt-Pd ratios (Fig. 4D) and are in general Pt-dominated.

Mineral liberation analysis (MLA) of a flotation concentrate from the Mogalakwena Mine identified 402 grains of PGM (Figure 6.5). By number of grains (Pt,Pd)-bismuthotellurides are the most abundant PGM (33%), followed by zvyagintsevite [Pd_3Pb] (14%), sperrylite (11%), PGE-sulfarsenides (10%), laurite (8%), cooperite-braggite (7%), Pt-Fe-alloys (6%) and malanite (5%) (Fig.6.5A). PGE-sulfarsenides mainly belong to the solid-solution series of hollingworthite [RhAsS] and irarsite [IrAsS]. Cabri (2015) pointed out that looking at the PGM distribution based on number of grains may cause a misleading interpretation but plotting area percentage additionally give more detailed information about the PGM distribution. Figure 6.5B is based on the same database as Figure 6.5A but visualizes the PGM distribution in area percent. This distinct difference visualizes that (Pt,Pd)-bismuthotellurides have by far a larger influence to the bulk potential of PGM indicating that (Pt,Pd)-bismuthotellurides are the most abundant PGM.

Alteration features of sulfides comprise chemical replacement by amphibole at the margins of sulfide grains. In sulfide assemblages of pentlandite, chalcopyrite and pyrrhotite, secondary amphiboles mainly replace pentlandite and chalcopyrite but to a lesser extent pyrrhotite (Fig. 6.3A). Replacements often end at the grain boundary of pentlandite and pyrrhotite and generally grow perpendicular to the boundary of the sulfide grains. Replacement aureoles are several mm thick and are surrounding sulfide grains. Li et al. (2004) described similar replacements of sulfides from the UG-2 and the Merensky Reef by actinolite and tremolite.

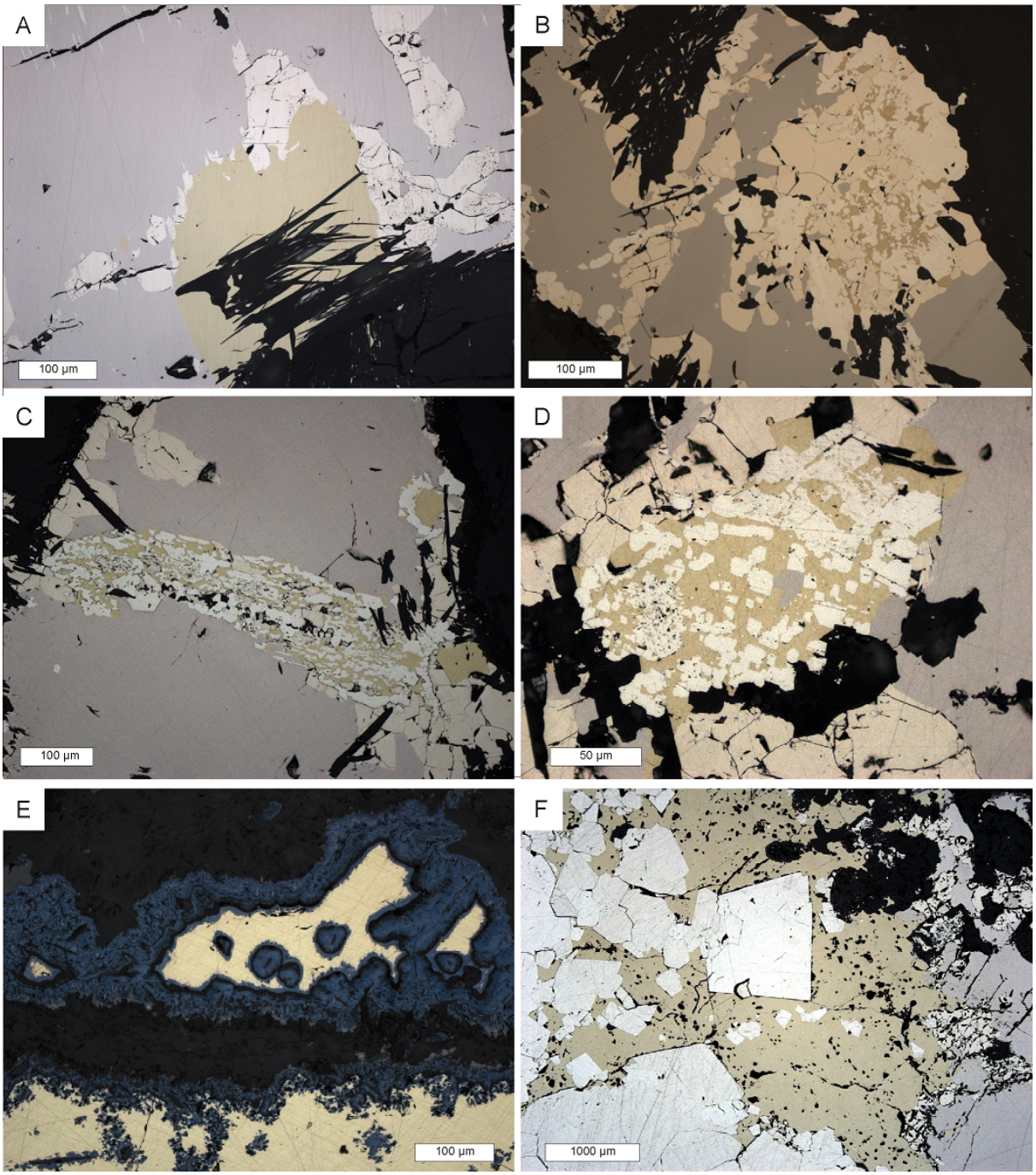

Figure 6.3 – Photomicrographs of sulfide assemblages at Overysel. A. Pyrrhotite (reddish brown), pentlandite (creme white), and chalcopyrite (yellow) with replacement of amphibole within chalcopyrite [AS10472]. B+C. Symplectic intergrowth of chalcopyrite with pyrite surrounded by pyrrhotite [AS10456]. D. Symplectic intergrowth of chalcopyrite with pyrite in pentlandite surrounded by pyrrhotite and pentlandite [AS10534]. E. Mineralization consisting of chalcopyrite with the formation of covellite (blue) [AS10429], F. Massive sulfide of pyrite (white), chalcopyrite and pyrrhotite [AS10533].

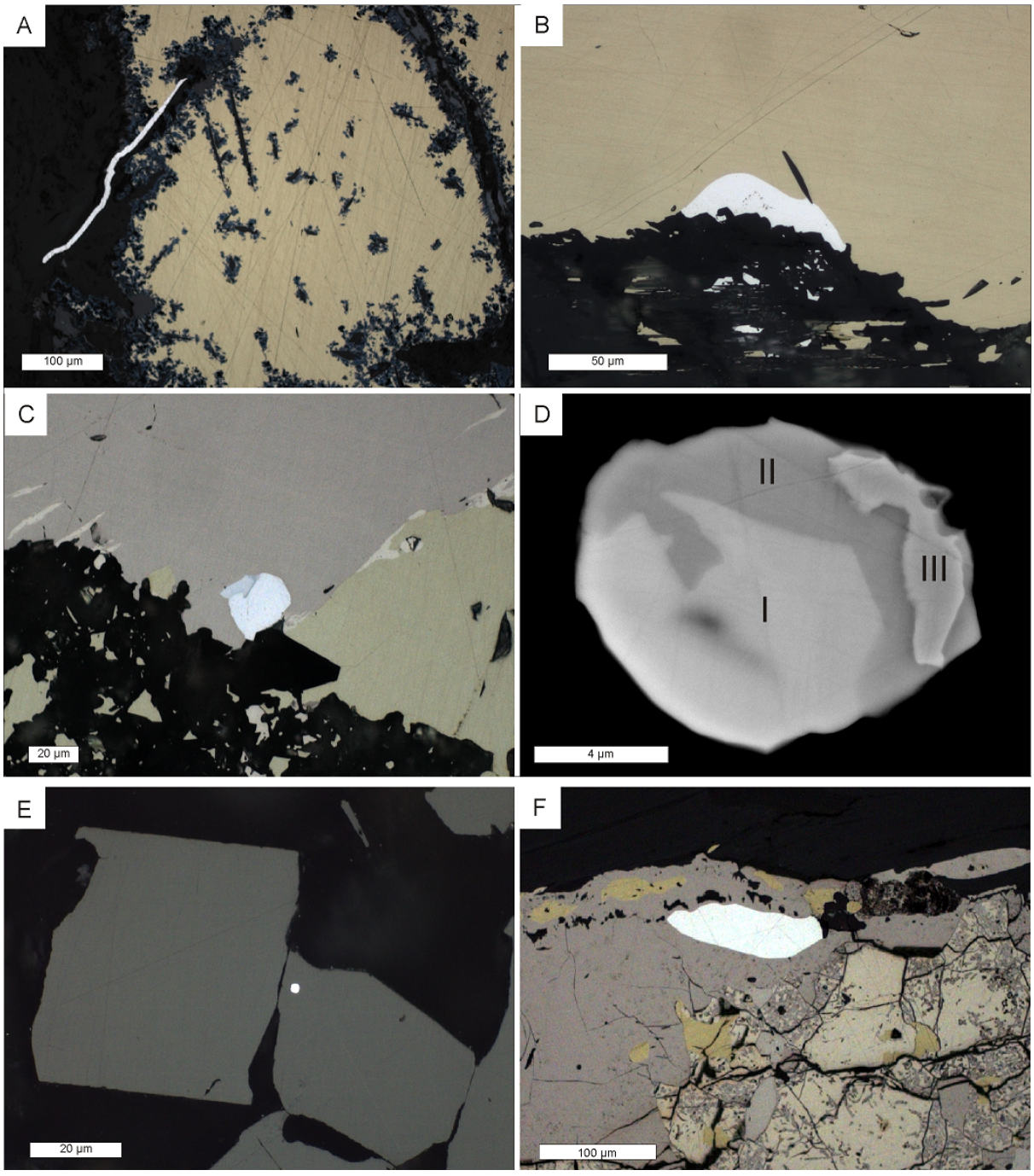

Figure 6.4 – Photomicrographs of PGM in air (A,B,F) and oil emission (C,E). A.Moncheite (white) [$Pt(Te,Bi)_2$] next to chalcopyrite (yellow), which is rimmed by covellite (blue) [AS10429]. B. Merenskyite [$Pd(Te,Bi)_2$] in chalcopyrite [AS10472]. C. Sperrylite (pale blue) [$PtAs_2$], merenskyite (white) [$Pd(Te,Bi)_2$] and hollingworthite (blue) [(RhIr)AsS] assemblage in pyrrhotite (reddish brown), next to chalcopyrite and pentlandite (creme white) [AS10451]. D: Backscattered electron image of a PGM assemblage consisting of I: moncheite, II: kotulskite [Pd(Te,Bi)] and III: tulamenite [Pt_2CuFe] [AS10716]. E. Laurite (white) [RuS_2] in chromite (grey) [AS10432a]. F. Merenskyite [$(Pd,Pt)(Te,Bi)_2$] in pyrrhotite next to chalcopyrite and pentlandite which is partly replaced to violarite [AS7381].

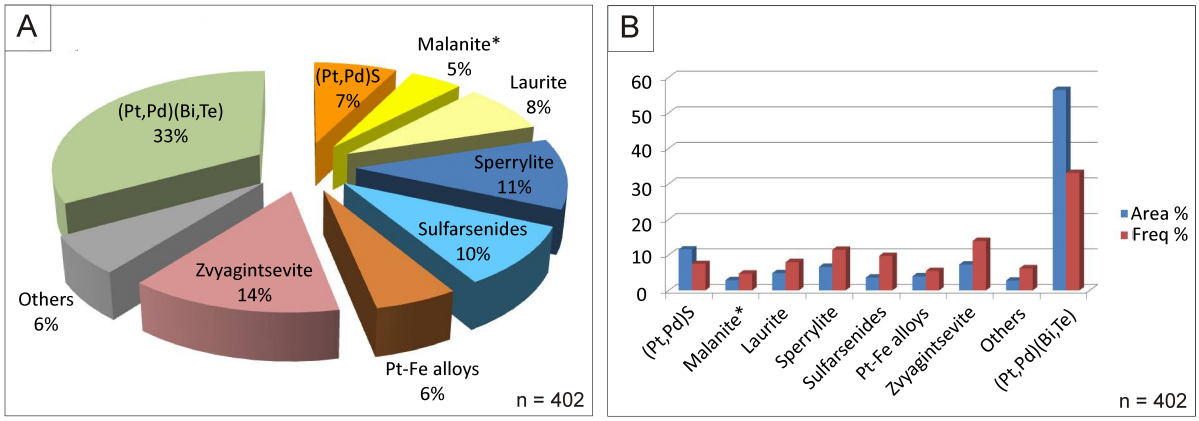

Figure 6.5 – Distribution diagrams of PGM based on MLA-data of a first flash concentrate of the Mogalakwena Mine with the distribution of PGM (n=402). A. Distribution of PGM based on frequency data (number of grains) showing that (Pt-Pd)-bismuthotellurides (33%) are the most dominant PGM followed by zvyaginsevite (14%), sperrylite (11%),(PGE)-sulfarsenides (10%), laurite (8%), and (Pt,Pd)-sulfides (7%), Pt-Fe-alloys (6%) and malanite (5%). Malanite represent the malanite-cuprorhodsite solid solution series. B. Column diagram visualizing the differences between frequency (number of grains) and area percentage of the PGM distribution indicating that (Pt,Pd)-bismuthotellurides are underestimated by looking at frequency data only as they make up 56% of the bulk PGM potential as they usually form larger grains. The clear dominance of (Pt,Pd)-bismuthotellurides is therefore emphasized by the PGM distribution in area percentage.

6.4.1.3 Mineralogy - Oxides and Silicates

Feldspathic pyroxenites are usually coarse-grained and consist of subhedral to euhedral cumulus orthopyroxene grains with grain sizes ranging from 1 to 3 mm and inter-cumulus plagioclase and clinopyroxene. Minor amounts of olivine, phlogopite, amphibole, chromite and ilmenite are also present.

6.4.1.4 Mineralogy - Sulfides and platinum-group minerals at Townlands, Tweefontein, Sandsloot and Nonnenwerth

The sulfide assemblage at Townlands consists of chalcopyrite, millerite, pyrrhotite, pyrite and pentlandite. Trace amounts of galena (in particular as submicrometer-sized inclusions in sulfide assemblages). At Townlands symplectic intergrowth of pyrite and chalcopyrite (Fig. 6.6A+C+F) and magnetite with pyrite (Fig. 6.6D+E) occurs. Millerite is frequently observed and can be associated with magnetite (Fig. 6.6B). At Townlands the PGM assemblage is dominated by Pd-rich (75%) bismuthotellurides, minor sperrylite (15%) and rare stibiopalladinite (5%) and

isomertieite (5%).

The sulfide mineralization Tweefontein is dominated by pyrrhotite, chalcopyrite and pentlandite. Pyrrhotite makes up 50 to 75% of the sulfides, whereas pentlandite and chalcopyrite occur in equal proportions. Pyrrhotite typically occurs as large grains rimmed by pentlandite and chalcopyrite (Fig. 6.7D+F). Chalcopyrite is partly observed as larger grains (Fig. 6.7E). Platinum-group minerals at Tweefontein are mainly Pd-bismuthotellurides and sperrylite.

The sulfide mineralization at Sandsloot is similar to Overysel with mainly pyrrhotite followed by pentlandite and chalcopyrite and minor amounts of pyrite. Sulfides occur as sizes of up to several centimeters but are usually in the range of smaller than 10 millimeters.

At Nonnenwerth the sulfides consist largely of pyrrhotite and chalcopyrite, pentlandite and traces of pyrite. Pyrrhotite is often intergrown with chalcopyrite and pentlandite. Flame-like exsolution of pentlandite occurs in pyrrhotite. Chalcopyrite and pentlandite mostly occur along the margins of pyrrhotite grains. Figure 7A shows pentlandite partly replaced by violarite [$FeNi_2S_4$]. Pyrite is observed to rim chalcopyrite and in some cases pyrrhotite is rimmed by chalcopyrite which is in turn rimmed by pyrite (Fig. 6.7B+C). The suite of PGM at Nonnenwerth is dominated by Pd-rich (69%) and Pt-rich (27%) bismuthotellurides and rare braggite and sperrylite.

The compositional variations of PGM of the Pt-Bi-Te and Pd-Bi-Te group are plotted in Figure 6.8 which shows that the Pt-Bi-Te group forms a solid-solution series between maslovite [PtBiTe] and moncheite [$PtTe_2$] but plot on the Te-rich part rather than close to the Bi-rich endmember (insizwaite) [$PtBi_2$]. The Pd-Bi-Te minerals of this study are kotulskite [PdTe] and michenerite [PdBiTe] and are therefore less enriched in the semimetals compared to the Pt-Bi-Te group. At the Mogalakwena Mine (Pt,Pd)-bismuthotellurides are Pt-dominated, whereas at Townlands are Pd-dominated and at Nonnenwerths both Pt and Pd-phases occur (Fig. 6.8A). Similarly, at Nonnenwerth (Pt,Pd)-bismuthotellurides are less Bi-dominated than at Mogalakwena.

6.4.1.5 PGE in sulfides

The scarcity of Pd- and Rh-bearing PGM in relation to relative large concentrations in the whole rock data, led to the assumption that these PGE are present in solid solution within sulfide minerals or occur as nanometer-sized PGM, especially in pentlandite, as outlined by a number of

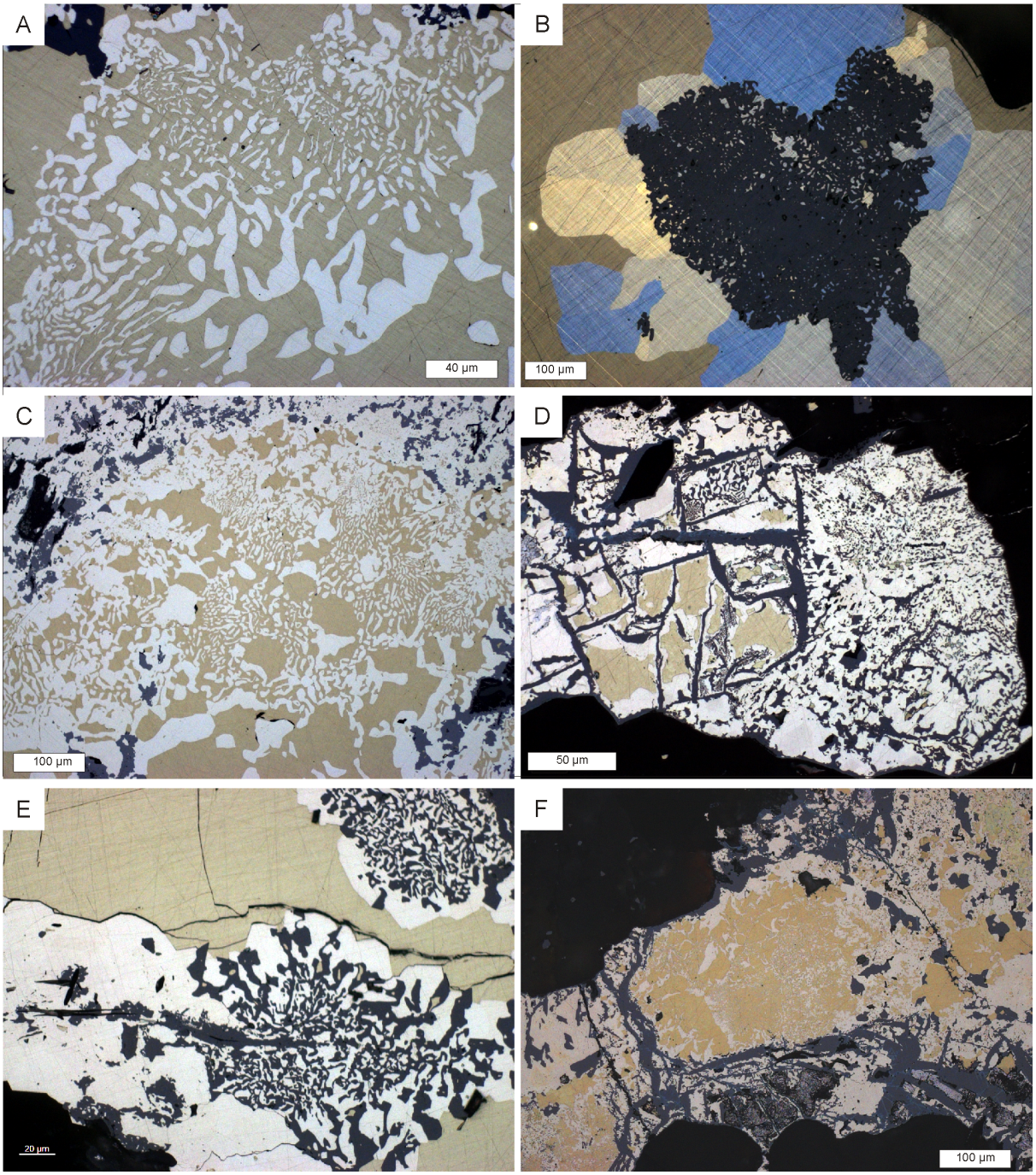

Figure 6.6 – Photomicrographs of sulfide assemblage at Townlands in oil emission. A. Symplectic intergrowth of pyrite and chalcopyrite [AS7385]. B. Magnetite intergrown with millerite [NiS] under crossed Nicols [AS7385]. C. Symplectic intergrowth of pyrite and chalcopyrite and magnetite at the rims [P106]. D. Pentlandite, chalcopyrite with veins of magneite [P2]. E. Symplectic intergrowth of pyrite and magnetite [AS7385]. F. Chalcopyrite and pentlandite surrounded by veins of magnetite [P2].

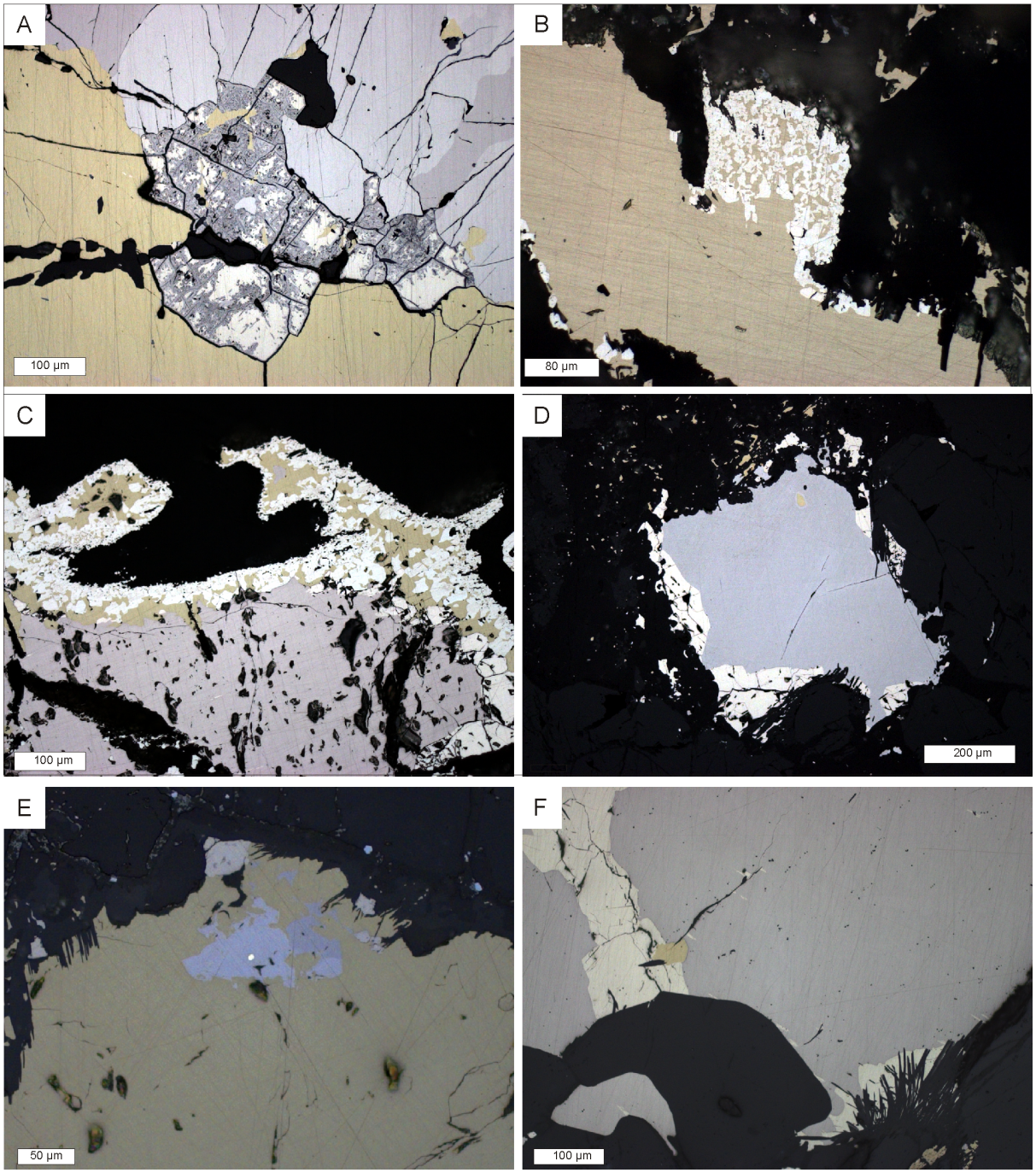

Figure 6.7 – Photomicrographs of sulfide assemblage at Nonnenwerth (A-C) and Tweefontein (D-F) in oil emission. A. Chalcopyrite, pyrrhotite and pentlandite which is partly replaced by violarite [AS7381]. B. Pyrite intergrown with chalcopyrite [M32]. C. Pyrrhotite with a rim of chalcopyrite with in turn has a rim of pyrite. [M32]. D. Sulfide assemblage consisting of a large core of pyrrhotite rimmed by pentlandite and chalcopyrite [AS7121] E Pyrrhitite with gold in chalcopyrite [AS7122] F Large grain of pyrrhotite with pentlandite at the rim which is partly replaced by amphiboles [AS7122].

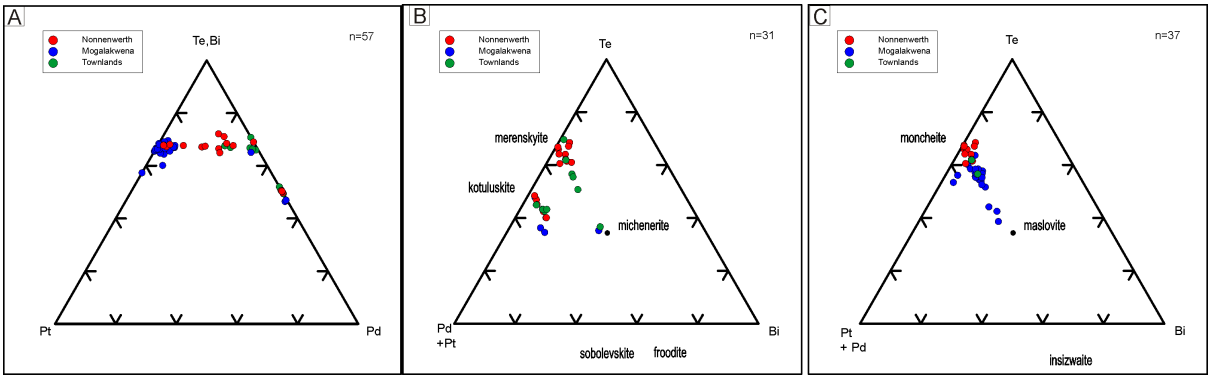

Figure 6.8 – Ternary plots of (Pt,Pd)-Bi-Te showing the solid solution between the of (Pt,Pd)-Bi-Te endmembers (EDX based data) [AS10716]. A:Plot of Pt-Bi-Te with up to 6 at% Pd (n=22). B. Plot of Pd-Bi-Te with up to 6 at% Pt (n=4).

authors in studies covering different ultramafic-mafic complexes worldwide (Cabri et al. 1984, 2002, Cabri 1992, Oberthür et al. 1997a, 2003, Gervilla et al. 2004, Godel et al. 2007, Holwell & McDonald 2007, 2010, Piña et al. 2012, Osbahr et al. 2013, 2014, Junge et al. 2014, 2015b, Klemd et al. 2016). The EPMA data of this study from Overysel showed that pentlandite (n=69) contains Pd concentrations ranging from <146 ppm to 681 ppm, but the concentrations of Rh are below the detection limit of 117 ppm. Concentrations of Pd and Rh in chalcopyrite (n=25), pyrrhotite (n=31) and pyrite (n=21) are all below the detection limit of Pd (146 ppm) and Rh (117 ppm). At Nonnenwerth median Pd t in pentlandite (n=27) are 180 ppm (max. 700 ppm). Platinum, Pd and Rh contents are below the detection limit in pyrrhotite (n=11) and pyrite (n=15) at Nonnenwerth. At Townlands Pt, Pd and Rh contents are below the detection limit in pentlandite (n=4), pyrrhotite (n=5) and pyrite (n=13).

LA-ICP-MS analysis of in pentlandite, chalcopyrite, pyrrhotite and pyrite was carried out to determine the concentrations of PGE, Co, Ni, and other trace elements (Table 6.2). The LA-ICP-MS data largely confirm the EPMA data and previous work on the distribution of PGE in pentlandite, as this is the major Pd-bearing sulfide. Pentlandite has low contents of IPGE and Pt (median values <0.4 ppm) and more elevated Rh (median 1.8 ppm; maximum 12.8 ppm) and Pd (median 22.3 ppm, maximum 185 ppm). Different Pd concentrations occur between pentlandite in the massive sulfide (median 11.2 ppm) and pentlandite in disseminated mineralization (median 180 ppm). Pyrrhotite shows slightly larger IPGE values than pentlandite (Os: 0.4 ppm, Ir: 0.7 ppm, Ru: 2.2 ppm). Platinum values are generally below the median detection limit of

0.1 ppm. The concentrations of Pd and Rh are lower in pyrrhotite than in pentlandite (median values of Rh 0.2 ppm and Pd are generally below the median detection limit of 0.5 ppm). Concentrations of all PGE in chalcopyrite are generally below the detection limit, except Ru which shows a median content of 0.3 ppm.

Several studies showed that pyrite can hold elevated concentrations of PGE (Dubrovsky & Rundqvist 2015, Piña et al. 2016). In general, pyrite occurs as a minor sulfide in Ni-Cu-PGE deposits and its origin is still under debate but may originate in different processes and timing of the mineralization as it often occurs as a secondary sulfide mineral. Pyrite shows the highest concentrations of Ru of all analyzed sulfides (median 7.3 ppm). In addition to the individual pyrite grains, two other types of pyrite were observed and analyzed within the massive sulfides (Oy1-26a): (i) pyrite hosted by chalcopyrite and (ii) pyrite hosted by pyrrhotite. Differences are evident in the distribution of Co, Ni, Pt, Pd, Ag and Re. Pyrite hosted by chalcopyrite (n=7) exhibits median Co contents of 17,580 ppm, mean Ni contents of 432 ppm and mean Pt contents of 12.9 ppm. Nickel correlates positively with Pd and Ag and negatively with Co, Pt and Re. Pyrite hosted by pyrrhotite (n=5) shows mean Co contents of 5170 ppm, mean Ni contents of 19,900 ppm and mean Pt contents of 0.9 ppm (Table 6.2). Cobalt correlates positively with Pt and Re and negatively with Ni, Ag and Pd.

Figure 6.9A shows the chondrite normalized data for the PGE contents in pentlandite and pyrrhotite. Pentlandite hosts the largest contents of Rh and Pd. The IPGE are relatively enriched in pyrrhotite compared to pentlandite. In Figure 6.9B, pyrite within chalcopyrite and pyrrhotite are plotted showing different PGE pattern exists. The IPGE contents in pyrite are similar. The PGE contents in chalcopyrite are usually below detection limit.

6.4.1.6 Sulfur isotopes

Sulfur isotope studies of Ni-Cu-PGE deposits are useful to obtain information about the source of sulfur in these deposits, provided that the isotopic composition is significantly different from mantle-derived (δ^{34}S 0$\pm$2‰) sulfur (Ripley 1999, McDonald & Holwell 2011). The addition of externally derived sulfur to the magma may have an effect on many Ni-Cu-PGE mineralization.

Sulfur isotope compositions are calculated relative to Vienna Canon Diablo Troilite (VCDT) and are reported in standard δ-notation. Samples for this sulfur isotope study originate from the

Table 6.2 – Median values and range of the composition of pentlandite, pyrrhotite, chalcopyrite, pyrite and the two pyrite groups hosted by chalcopyrite and pyrrhotite analyzed by LA-ICP-MS (all in ppm). $*$ = some analyses are below detection limits. $**$ = interference of CuAr on ^{103}Rh exceeds 50% of the Rh signal and thus Rh is not reported in chalcopyrite. N is number of analyses

[in ppm]		^{59}Co	^{61}Ni	^{189}Os	^{193}Ir	^{101}Ru	^{103}Rh	^{195}Pt	^{105}Pd
pentlandite in massive sulfide (n=6)	median	8,260	302,500	0.18	0.29	0.17*	1.15	0.87	11.2
	range	7,430-91,110	285,000-321,000	0.12-0.24	0.20-0.41	0.14-0.50	0.32-5.30	0.15-2.15	5.60-25.02
pentlandite in diss. sulfide (n=4)	median	7,252	303,500	0.43	0.46	1.55	7.16	0.11	180.1
	range	245-8,590	296,400-326,800	0.30-0.88	0.41-0.77	1.17-5.33	0.16-12.75	0.06-49.00	67.6-185.2
pyrrhotite (n=13)	median	110	5,200	0.4	0.7	2.2	0.2	0.1*	0.5*
	range	5-155	4,410-8,250	0.3-1.3	0.5-2.7	1.4-11.2	0.05-0.8	<0.08-0.3	<0.5-1.2
chalcopyrite (n=7)	median	2.6	813	0.1*	0.1*	0.3	**	0.1*	<d.l.
	range	0.8-20	719-1,100	<0.1-0.3	<0.06-0.5	0.2-0.5	**	<0.06-0.3	<0.003-0.6
pyrite (n=5)	median	10,660	13,820	0.97	1.7	7.3	5.3*	2	0.95
	range	128-14,910	460-118,000	0.8-1.2	1.2-2.1	4.8-8.3	<0.26-6.4	<0.025-5.9	0.2-26.7
pyrite hosted by chalcopyrite (n=7)	median	17,580	432	0.3	0.4	1.1	4.7	12.9	0.2*
	range	13,830-19,390	362-700	0.2-0.4	0.2-0.8	0.1-2.3	0.08-7.5	6.4-24.7	0.1-0.3
pyrite hosted by pyrrhotite (n=5)	median	5,170	19,900	0.3	0.5	1.3	2.3	0.9	1
	range	2,630-6,140	14,620-22,400	0.2-0.3	0.4-0.5	1.0-1.4	2.0-2.9	0.6-1.5	0.4-6.2

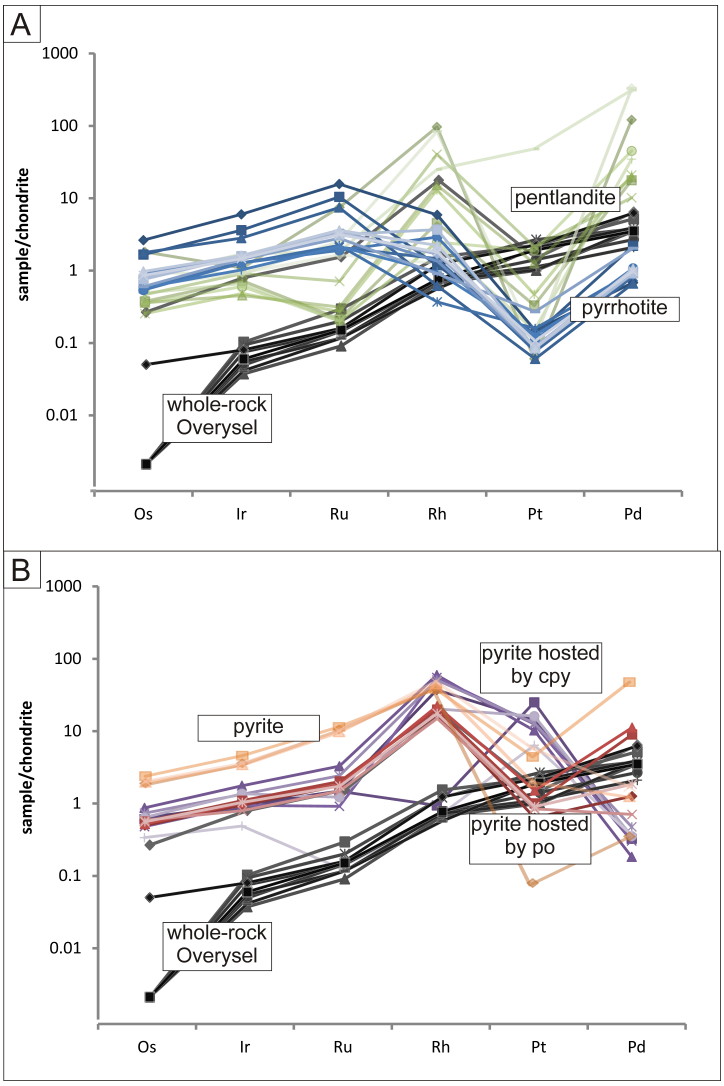

Figure 6.9 – Chondrite-normalized PGE distribution patterns. C1-chondrite values from McDonough & Sun (1995) A. Pentlandite (green), pyrrhotite (blue) and whole rock analysis of Overysel (black). B. Distribution pattern of pyrite hosed by chalcopyrite (purple), pyrite hosted by pyrrhotite (red) and whole-rock data of Overysel (black). Note: Os whole rock values are below the detection limit. The distribution of chalcopyrite is not plotted as the PGE values are generally close or below the detection limit.

Overysel and the Sandsloot open pit.

The results of the sulfur isotope study of the sulfides from Overysel showed mean values of δ^{34}S +3.75‰ for feldspathic pyroxenites, δ^{34}S +4.5‰ for massive sulfide samples and δ^{34}S +2.0‰ for the two Sandsloot samples (Table 6.3). The sulfur isotope signature of the pyroxenites at Tweefontein varies between +4.6‰ and +9.0‰. The floor rocks at Tweefontein are BIF and black shale with δ^{34}S of +9.0‰ and -1.0‰, respectively.

Table 6.3 – Sulfur isotope data and respective whole-rock Sulfur contents from Overysel, Sandsloot and Tweefontein.

Sample no.	Lithology	wt.% S	δ^{34}S‰ (‰ VCDT)
Overysel			
Oy1-19		2.18	3.1
Oy2-06	feldspathic pyroxenite	0.08	3.5
Oy2-14	feldspathic pyroxenite	1.58	3.9
Oy2-17	feldspathic pyroxenite	1.89	4.5
Oy1-26a	massive sulfide	>20	5
SA-2013-M-06	massive sulfide	>20	4.9
SA-2013-M-07	massive sulfide	>20	4.3
Mog-04	massive sulfide	>20	3.9
Sandsloot			
Pr3	feldspathic pyroxenite	0.05	2
Pr5	feldspathic pyroxenite	0.27	2
Tweefontein			
Plat R-4	feldspathic pyroxenite	1.83	8.2
Plat R-5	feldspathic pyroxenite	12.36	4.6
Plat R-6	feldspathic pyroxenite	15.21	6
Plat R-7	feldspathic pyroxenite	13.99	8.1
Plat R-8	feldspathic pyroxenite	1.45	7.8
Plat R-9	feldspathic pyroxenite	1.71	7.9
Plat R-10	feldspathic pyroxenite	8.07	9
Plat R-12	BIF	0.15	9
Plat R-13	black shale	0.42	-1

6.4.2 Oxidized ores

6.4.2.1 Whole rock geochemistry

In the oxidized ore, sulfur contents are generally below the detection limit. Selected whole-rock segments of the three drill cores were analyzed from both oxidized and pristine ore for the six PGEs and Au (Table 6.1).

The whole rock data indicate that in the oxidized Platreef, concentrations of Pt are grossly similar to those of the pristine ore but concentrations of Pd are lower, as evidenced by increases of the Pt/Pd ratio from 0.75 in the pristine ore to 1.15 in the oxidized ore (Fig. 6.10).

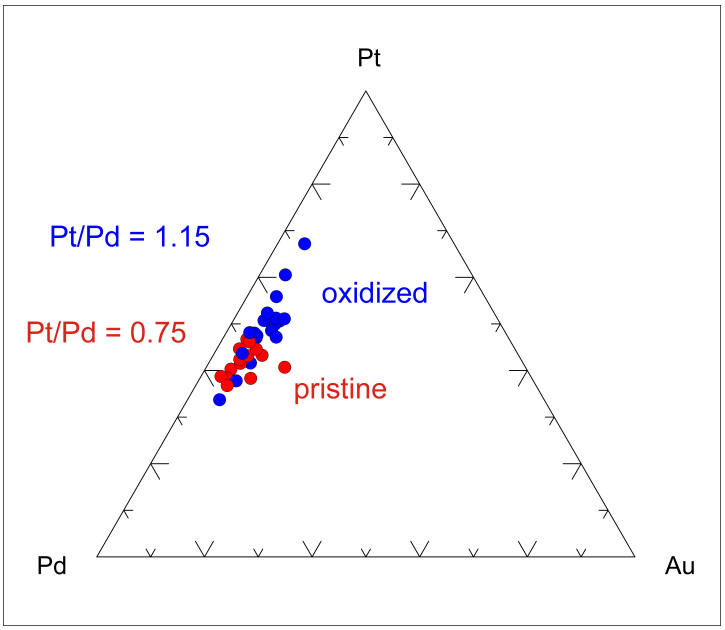

Figure 6.10 – Ternary diagram showing the whole rock data of Pt, Au and Pd contents of pristine (red circles) and oxidized Platreef ores (blue circles) and the average Pt/Pd ratio.

6.4.2.2 Mineralogy

In the oxidized ores, X-ray diffractometry (XRD) analysis showed that major minerals are secondary iron- and manganese oxides/hydroxides, clay minerals, smectite and vermiculite.

In the oxidized Platreef ore only relict sulfides and PGM were identified which are mainly sperrylite and cooperite-braggite, whereas (Pt,Pd)-bismuthotellurides were missing. Sulfide grains are partly to completely destroyed (Figure 6.11D). Barite is formed and is formed within

Fe-silicates (Figure 6.11A).

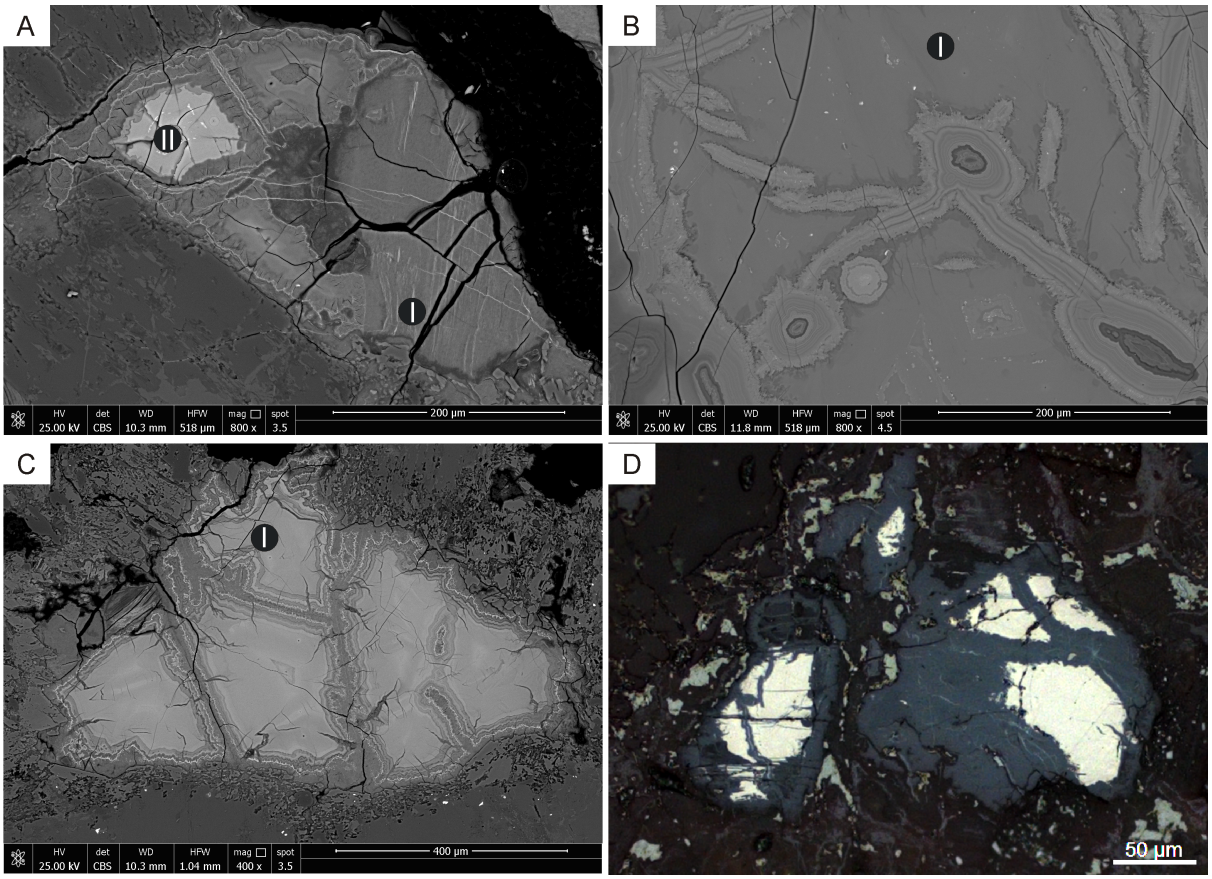

Figure 6.11 – Photomicrographs of minerals within the oxidized PGE ores. A: Secondary Fe-oxy-hydroxide with I: 118 ppm Pd and 208 ppm Pt and II: 196 ppm Pd and Pt below detection limit. B: Secondary Fe-oxy-hydroxide with I: 357 ppm Pd and Pt below detection limit. C: Secondary Fe-oxy-hydroxide with I: 192 ppm Pd and 214 ppm Pt. D. Partly weathered chalcopyrite.

Powder samples from the oxidized parts of the drill cores (Oy1-1 to Oy1-18; Oy2-1 to Oy2-13, Oy3-1 to Oy3-10) were analyzed using XRD. Main minerals identified by XRD are quartz, feldspar, vermiculite, orthopyroxene, talc, smectite, chlorite and kaolinite. In nine samples, swellable minerals are identified by adding glycerine (Figure 6.12). By adding glycerin to the sample it can be noted that the peak at 14.5Å (d-value: 6.1) is shifting to lower 2θ values, indicating that swellable minerals exist. Adding glycerin to the sample decreases 2θ and increases d-spaces according to Bragg's equation, showing that the mineral swells by adding larger cations in their interlayers.

Swellable minerals, such as smectite (montmorillonite), can be an excellent carrier for PGE

as they can attach large cations such as Pd^{2+} in the interlayer sites. Platinum-group elements may be adsorbed to clay minerals. Clay minerals have a negatively charged surface charge, where at the outer and inner surfaces by adsorbing cations these charges may be balanced. Non-swellable clay minerals can only absorb cations on the outer surface but swellable clay minerals also allow that cations, such as Pd^{2+}, occur in the inner layers of the clay minerals. The adsorption of different cations have a large effect on the structure of the clay minerals. The specific property of swelling allows that cations can be exchanged. The spacing in the crystal lattices may increase or decrease depending the size difference between the incorporating cations. In order to investigate the presence of PGE in these minerals, experiments for the cation exchange capacity were carried out.

Cation exchange capacity is used to determine the amount of PGE which are attached by adsorption to clay minerals. Physical and chemical factors, such as ionic radii and the hydration of ions influence the exchangeability of ions (Schollenberger & Simon 1945).

For the cation exchange capacity ammonium acetate CH_3COONH_4 was used. The solution was analyzed on an Agilent 7500 at the BGR in Hannover. Blanks were analyzed to monitor any analytical contamination of PGE. A selection of 10 fractions of the oxidized ores were analyzed. Samples were selected based on the presence of swellable material which was obtained from the XRD analysis.

Concentrations of Ru, Rh, Pd, Ir, Pt and Au are generally below detection limit after interaction of minerals from the oxidized ore with ammonium acetate (Table 6.4). Except for Pd which gives concentrations of up to 0.281 ppb. However, the overall concentrations are low, arguing that only limited amount of the PGE occur in the interlayers of swellable clay minerals.

On nine selected weathered ores, which showed swellable minerals using XRD, Fourier transform infrared spectroscopy (FTIR) was carried out. Figure 6.13 shows the infrared spectrum of a representative weathered ore sample (Oy1-5). All other analyzed weathered samples (Oy1-6, Oy1-7. Oy1-11, Oy1-18, Oy2-3, Oy2-6, Oy2-12 and Oy3-5) have a similar infrared spectrum. The peak in the non-dried sample indicated the presences of hydrous minerals, such as kaolinite, amphibole and chlorite. Also the small peak at a wavelength of 2900 cm^{-1} shows the presences of organic components. At the wavelength 1700 cm^{-1} smectite (nontronite) is indicated.

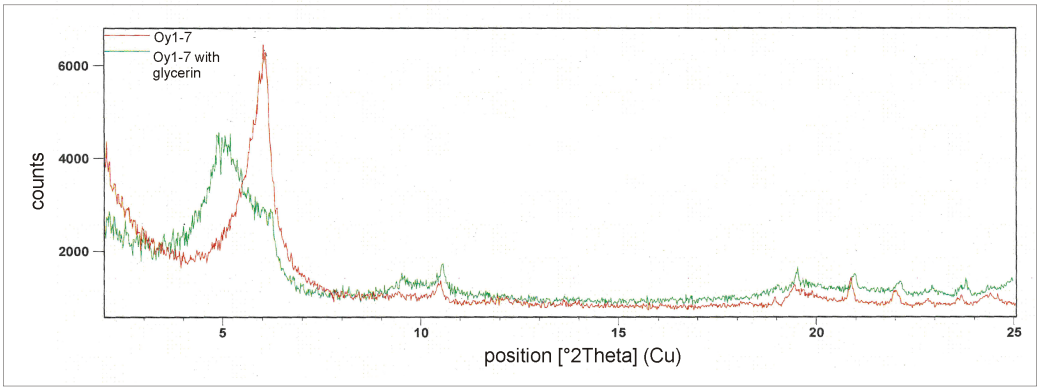

Figure 6.12 – X-ray Diffraction before and after glycerine showing the existence of swellable minerals with the weathered ore (Oy1-7).

Table 6.4 – Results of the cation exchange capacity. For each sample an aliquot of 1000 mg and 2000 mg was analyzed giving the range of two values. All in data is in ppb.

sample	^{99}Ru	^{103}Rh	^{108}Pd	^{191}Ir	^{194}Pt	^{197}Au
Oy1-5	<0.02	<0.02	0.04-0.045	<0.02	<0.02	<0.02
Oy1-6	<0.02	<0.02	<0.02	<0.02	<0.02	<0.02
Oy1-7	<0.02	<0.02	<0.02-0.03	<0.02	<0.02	<0.02
Oy1-11	<0.02	<0.02	0.033-0.0465	<0.02	<0.02	<0.02
Oy1-18	<0.02	<0.02	0.221-0.243	<0.02	<0.02	<0.02
Oy2-3	<0.02	<0.02	0.073-0.0665	<0.02	<0.02	<0.02
Oy2-5	<0.02	<0.02	0.088-0.0805	<0.02	0.034-0.049	<0.02
Oy2-6	<0.02	0.023-0.03	0.245-0.281	<0.02	<0.02	<0.02
Oy2-12	<0.02	<0.02-0.028	0.085-0.1145	<0.02	<0.02-0.021	<0.02
Oy3-5	<0.02	<0.02	<0.02	<0.02	<0.02	<0.02

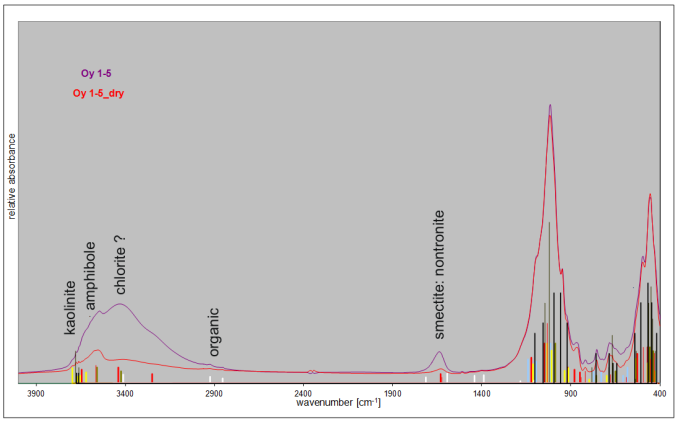

Figure 6.13 – Infrared spectrum of Oy1-5 indicating the presence of hydrous minerals such as amphibole, kaolinite and probably chlorite.

6.4.2.3 PGE-bearing secondary minerals - EPMA

In the oxidized Platreef ores, only relict PGM and sulfides are present and major minerals are secondary iron-oxides/hydroxides, manganese oxides/hydroxides and clay minerals such as smectite and vermiculite. The fine-grained secondary minerals are extensively intergrown, causing mixed EPMA analyses that are difficult to interpret. In general, PGE are polymodally distributed within the oxidized ore, as they are associated with relict PGM, iron- and manganese-oxides/hydroxides, and/or secondary silicates. This complex polymodal distribution of PGE in these ores is challenging for the recovery of PGE from supergene ore.

Figure 6.14 shows EPMA data of secondary minerals within the weathered ore and demonstrates concentrations of Rh (up to 135 ppm), Pd (up to 416 ppm), and Pt (up to 581 ppm). Silica concentrations vary between 0.5 to 53 wt.% in general. Electron microprobe data indicate that Fe oxy/hydroxides are often intimately intergrown with clay minerals causing mixed analysis values, indicated by a negative correlation between FeO and SiO_2 (Figure 6.14B). Manganese oxides/hydroxides have MnO_2 concentrations of 41 to 54 wt.% (Figure 6.14D). Silica contents are <15 wt.

6.4.2.4 PGE-bearing secondary minerals - LA-ICP-MS

In most of the analyses elevated concentrations of Y and Cu are detected. These concentrations have an effect on the ^{103}Rh and ^{105}Pd values due to Y-oxide and Cu argide. Figures 6.15A,B show the correlation between ^{103}Rh and ^{105}Pd with ^{63}Cu. Interference on ^{103}Rh are caused in Cu-rich analysis by ^{63}Cu-^{40}Ar and on ^{105}Pd by ^{65}Cu-^{40}Ar. Between ^{108}Pd and ^{63}Cu no interference is observed (Figure 13C) and ^{108}Pd is used for further processing.

Selenium is less mobile than S during weathering and therefore former sulfides show elevated Se concentrations as well as IPGE (Figure 6.15D). In total 37 spot and line analysis were carried out on secondary minerals within the weathered ore. Figure 6.16 shows BSE images of the secondary minerals after the LA-ICP-MS measurement with numbers of the individual analysis. Table 6.5 shows the median and maximum values of the LA-ICP-MS data of ^{99}Ru (up to 136 ppm), ^{103}Rh (up to 335 ppm), ^{108}Pd (up to 256 ppm), ^{189}Os (up to 19 ppm), ^{193}Ir (up to 32 ppm), ^{195}Pt (up to 803 ppm).

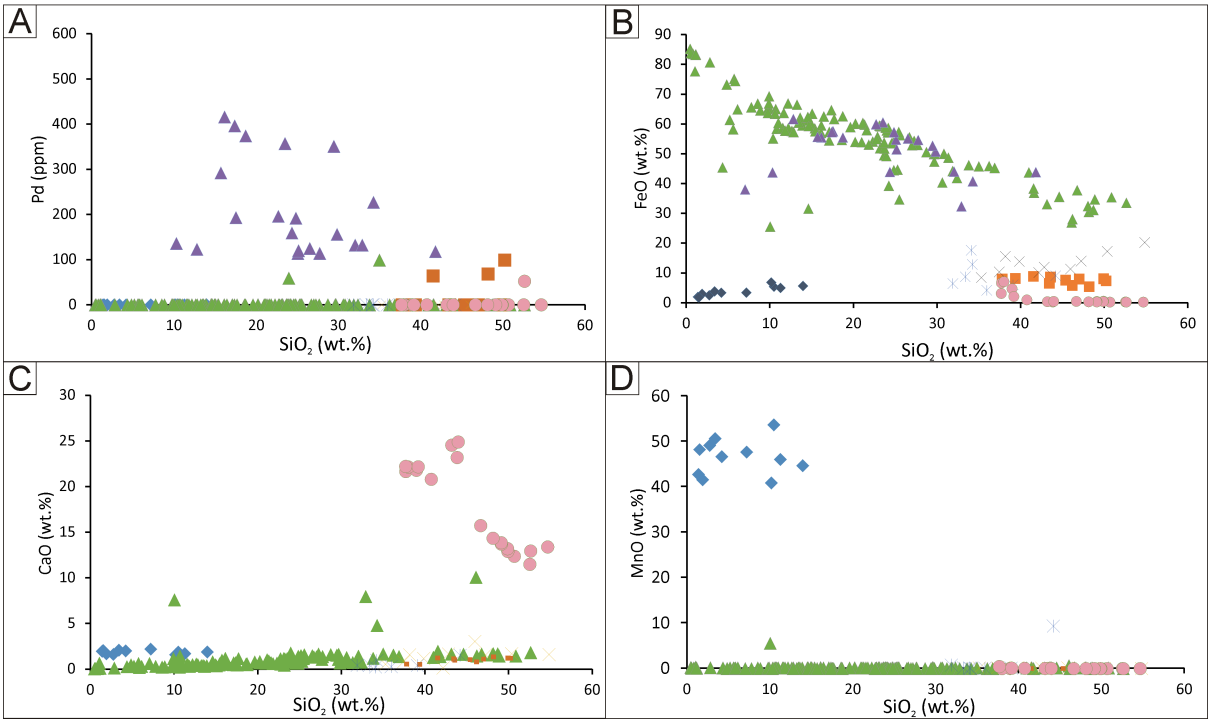

Figure 6.14 – Binary plots of EPMA data of secondary minerals. Triangles: FeO-rich (green) and Pd-rich phases. Blue diamonds: MnO-rich secondary phases. Red squares: CaO-rich phases. Orange squares: SiO_2-rich phases. A: Pd-SiO_2 diagram showing the Pd-rich minerals (100 to 500 ppm range; note median detection limit is about 90 ppm). B: FeO-SiO_2 diagram showing the large range of Fe-rich phases, partly containing elevated concentrations of Pd. C: CaO-SiO_2 diagram showing general low CaO concentrations, except one mineral group. D: MnO-SiO_2 diagram with overall low MnO contents except for one group.

Table 6.5 – LA-ICP-MS data of weathered Platreef ore. All in data is in ppm.

n=37	^{99}Ru	^{103}Rh	^{108}Pd	^{189}Os	^{193}Ir	^{195}Pt
Median	14	104	37	3	2	106
Max	254	335	256	55	79	803

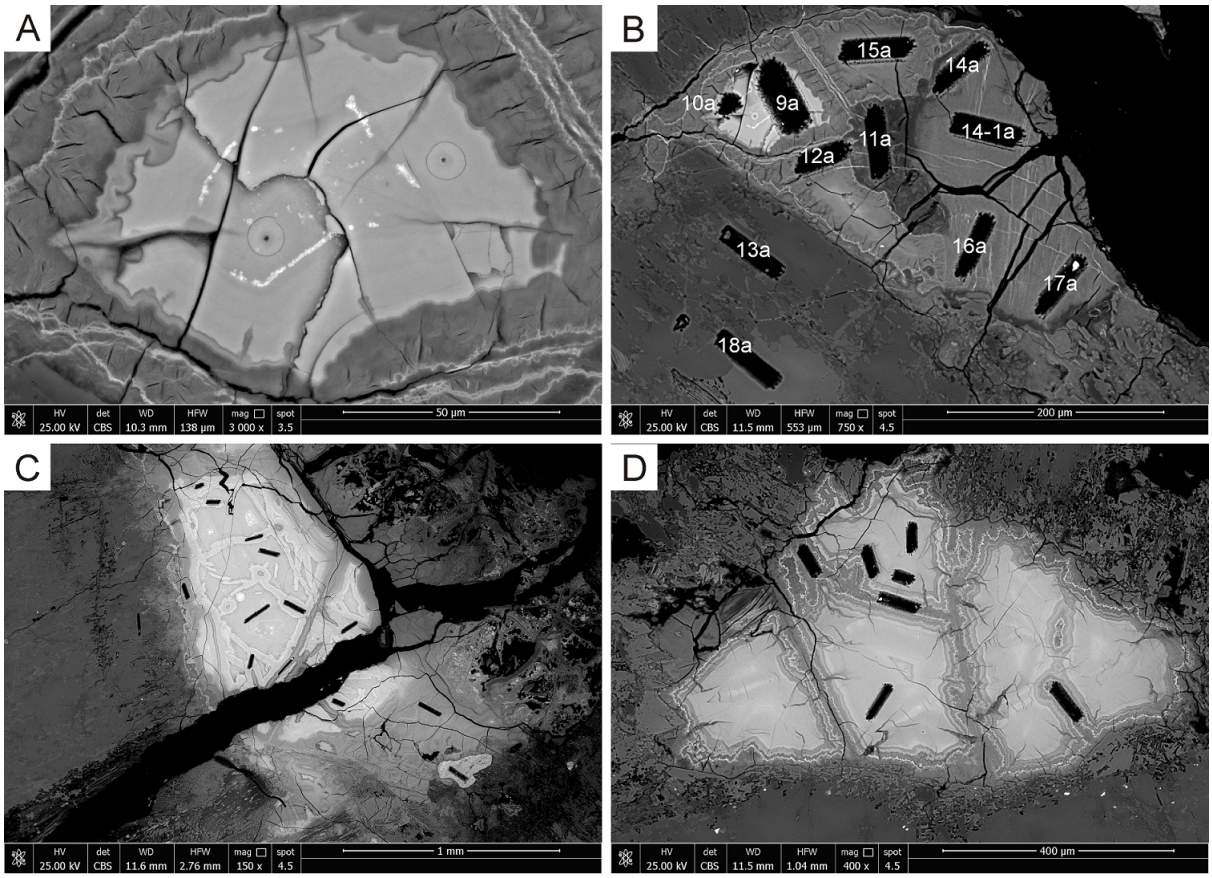

Figure 6.15 – Backscattered electron images after LA-ICP-MS measurement with sample numbers on AS10440a. A: Grain with previous EPMA measurement spots. B-D: Grains after LA-ICP-MS measurement.

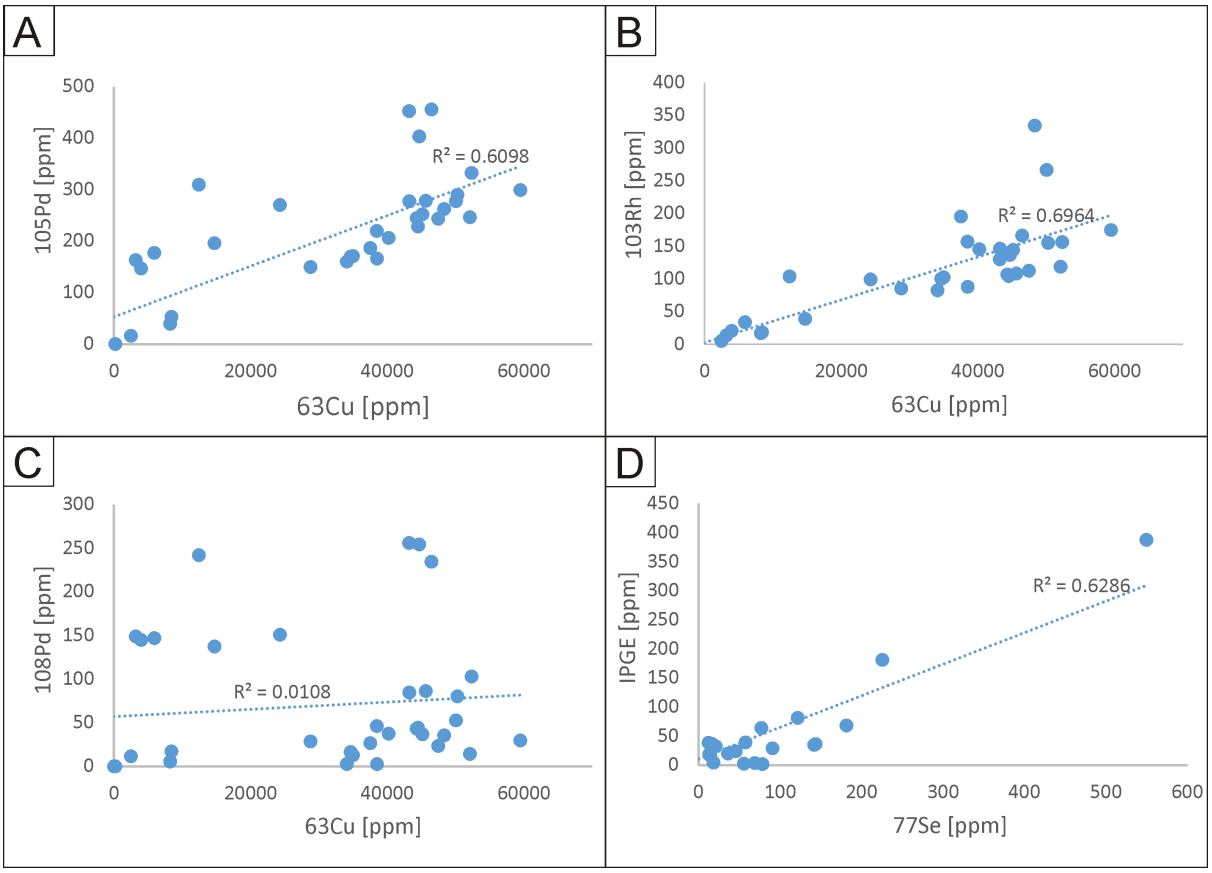

Figure 6.16 – Binary plots of LA-ICP-MS data of weathered ore. A: ^{105}Pd-^{63}Cu diagram showing a correlation between ^{105}Pd and ^{63}Cu due to ^{65}Cu-^{40}Ar. B: ^{103}Rh-^{63}Cu diagram with similar good correlation ^{105}Pd due to ^{63}Cu-^{40}Ar. C: No correlation between ^{105}Pd and ^{63}Cu. D: Correlation between the IPGE (^{99}Ru,^{189}Os,^{193}Ir) and ^{77}Se.

6.5 Discussion

6.5.1 Pristine ore

6.5.1.1 Effects of alteration and weathering on pristine mineralogy

Base metal sulfides at Overysel are mainly pyrrhotite, chalcopyrite, pentlandite and minor pyrite and the PGE mineralization in the pristine ore is commonly associated with sulfides. The PGM assemblage of Overysel is largely (Pt,Pd)-bismutotellurides. Elevated concentrations of PGE are presenet in sulfides (mainly pentlandite). Palladium is compatible in base metal sulfides as an exchange-substitution between Ni and Co with Pd can take place due to similar ionic radii. The ionic radii (in Å) of Pd, Fe, and Ni are Pd^{2+}=0.64, Fe^{2+}=0.63, and Ni^{2+}=0.55 (Shannon 1976). Substitution of Pd for Ni and/or Fe is possible as the ionic radii differ by less than 15% (Goldschmidt 1926). This compatibility explains the elevated concentrations of Pd in pentlandite in the 100s ppm range. However, PGE contents in pyrrhotite, as the major sulfide mineral in the ore, are below the detection limit of the EPMA. As shown by Junge et al. (2015b) concentrations of PGE in pentlandite can be both the result of solid solution by substitution of Ni and Fe by Pd and Rh in the pentlandite structure or as submicrometer-sized inclusions of discrete PGM.

Figure 6.3A shows alteration features of sulfides with replacement by amphibole at the margins of sulfide grains. Amphiboles mainly replace pentlandite and chalcopyrite but to a lesser extent pyrrhotite, since the replacement often ends at the grain boundary of pentlandite and pyrrhotite. These overprints generally develop perpendicular to the boundary of the sulfide grains. The addition of aqueous Ca, Mg, Si and H_2O, as well as the release of S, Fe and Ni or Cu is required for the replacement of sulfide by amphibole, although replacement of adjacent orthopyroxene may provide some of the required Mg and Si (Li et al. 2004). The fact that mainly chalcopyrite and pentlandite are replaced by amphibole and replacement usually ends at the contact to pyrrhotite indicates different stabilities of the sulfide minerals (Fig. 6.3A).

It was shown in Figure 6.3B that both at Overysel and at Townlands chalcopyrite may occur as symplectic-like intergrowth with pyrite. A similar observation was made by Naldrett (2009) at the UG-2, Holwell & McDonald (2010) for chromitites of the Platreef, by Piña et al. (2016) from the Great Dyke and by Lorand & Alard (2011) from Pyrenean peridotites. Further-

more, Gervilla & Kojonen (2002) described similar intergrowth in the Keivitsa ore assemblage in Finland, but these contain pentlandite intergrown with pyrite and locally chalcopyrite. This pyrite-chalcopyrite may represent a very late evolution at low temperatures of MSS causing the symplectic-like intergrowth as studies on phase relations in the Fe-Ni-S system at 230°C (Misra & Fleet 1973) and at <135°C (Naldrett 2009) showed that Ni-rich pentlandite coexists with pyrite.

At Townlands symplectic intergrowth of pyrite with magnetite was observed (Fig. 6.6E). This intergrowth argues for simultaneously growth of magnetite and pyrite at very specific fO_2 and fS_2. Figure 6.14 shows a projection of the $\log fO_2$ - $\log fS_2$ diagram for the Fe-O-S system at 127°C. The formation of the symplectic intergrowth occurred within a very limited range of fO2 and fS2 as these symplectites are closely associated with millerite and a symplectic intergrowth consisting of pyrite and chalcopyrite (Fig. 6.6A).

6.5.1.2 Variation of the sulfide and PGE mineralization along the strike of the Platreef

The sulfide and PGE mineralization was studied along the strike of the Platreef at Townlands, Tweefontein, Sandsloot, Overysel and Nonnenwerth. The major sulfide assemblage is similar along the strike with pyrrhotite, pentlandite and chalcopyrite, where the footwall consists of granites. However, variation in the sulfide mineralization and textures is observed in the southern part arguing that the difference in the floor rocks can affect the sulfide mineralization. At Overysel and Nonnenwerth the footwall consists of Archean granites and the sulfide mineralization resembles magmatic sulfide assemblage consisting of pyrrhotite, pentlandite and chalcopyrite. The dolomitic footwall at Sandsloot from the Malmani Subgroup did not largely affect the sulfide assemblage as at Sandsloot pyrrhotite, pentlandite and chalcopyrite occurs similar to Overysel and Nonnenwerth. The footwall at Tweefontein is ironstone (BIF) and black shale. At Townlands the floor rocks are hornfels, quartzite and calc-silicates belonging to the Silverton Formation. The large abundancy of millerite (Fig. 6.6B) and symplectitic intergrowth consisting of pyrite and chalcopyrite (Fig. 6.6A+C) as well as pyrite and magnetite (Fig. 6.6D+E) indicate different processes during the formation of the Platreef at Townlands compared to the northern part of the Platreef. The sulfide assemblage at Townlands consisting of millerite, pyrite, chal-

copyrite, pentlandite and trace amounts of galena and magnetite are probably formed under high fS2 and fO2 causing the breakdown of pentlandite and the formation of millerite and magnetite (Fig. 6.17).

The symplectic intergrowth of pyrite and magnetite in close association with millerite and magnetite gives a narrow fS_2 and fO_2 range (Fig. 6.17). Figure 6.8 plots the variation of (Pt,Pd)-bismuthotellurides at Nonnenwerth, at the Mogalakwena Mine and at Townlands. At Townlands (Pt,Pd)-bismuthotellurides are Pd-dominated, whereas at the Mogalakwena Mine the PGM are Pt-dominated. The late stage alteration of the primary magmatic sulfide assemblage under high fS2 and high fO2 conditions causing the formation of millerite can also have affected the PGE mineralization as pentlandite, as the main carrier of Pd was destroyed and Pd-bismuthotellurides crystallized. The low temperature alteration of the primary sulfide assemblages therefore also changed the distribution of PGM at Townlands. Assimilation with the floor rocks can also be assumed with the sulfur isotope data (Fig. 6.1, 6.2). At Townlands a large variation in δ^{34}S is observed with a heavy isotope signature (Manyeruke et al. 2005).

6.5.1.3 PGE in sulfides

Both EPMA and LA-ICP-MS data point to the fact that pentlandite is the main carrier for Pd (up to 185 ppm) and Rh (up to 12.8 ppm). Chalcopyrite has PGE concentrations generally below the detection limit of LA-ICP-MS.

Experimental studies showed that pyrite within magmatic sulfide deposits may form as exsolution from MSS at temperatures below 700°C (Naldrett et al. 1967, Kullerud et al. 1969). Another source of pyrite is the partial or total replacement of pre-existing sulfides, in particular pyrrhotite due to hydrothermal or metamorphic fluids (Djon & Barnes 2012, Piña et al. 2013, Smith et al. 2011, Holwell & McDonald 2014, Vukmanovic et al. 2014). In the massive sulfide two compositional different types of pyrite exist, i.e. pyrites hosted by chalcopyrite and pyrites hosted by pyrrhotite. For pyrites hosted by chalcopyrite Ni correlates positively with Pd and Ag and negatively with Co, Pt and Re. Pyrite hosted by pyrrhotite (n=5) shows mean Co contents of 5170 ppm, mean Ni contents of 19,900 ppm and mean Pt contents of 0.9 ppm (Table 6.2). For pyrites hosted by pyrrhotite Co correlates positively with Pt and Re and negatively with Ni, Ag and Pd. Substitution of trace elements into a solid phase depends on the nature of the bonding,

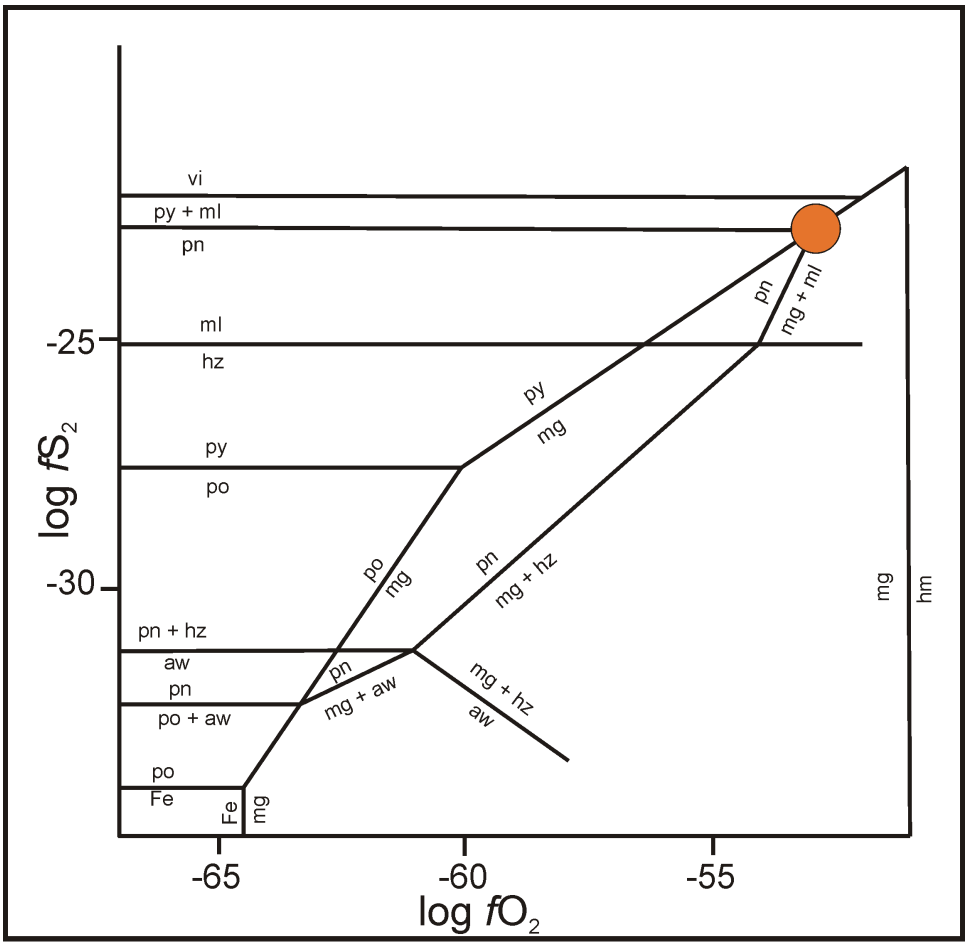

Figure 6.17 – Projection of the the log fO_2 - log fS_2 diagram for the Fe-O-S system at 127°C modified after Eckstrand (1975). The organge dot shows the position where the symplectic intergrowth of magnetite and pyrite can occur together. Similarly, the formation of millerite and magnetite out of pentlandite takes place at this point with high fO_2 and high fS_2 after assimilation of the sulfide assemblage due to late-stage overprint at the Platreef at Townlands.

the size of the lattice site, and the charge balance. The Fe atoms in the structure of pyrite lie on a face-centered cubic lattice and the S atoms on the trigonal axes of the cubic framework (Parker & Whitehouse 1932) with Fe occupying the tetrahedral site (Pauling & Huggins 1934). The ionic radii (in Å) of Fe, Ni, Co, Ag, Pd and Pt are: $^{IV}Fe^{2+}$ = 0.63, $^{IV}Ni^{2+}$ = 0.55, $^{IV}Co^{2+}$ = 0.58, $^{IV}Ag^{2+}$ 0.79, $^{IV}Pd^{2+}$=0.64 and IVPt^{2+}=0.6 (Shannon 1976). Median Ag concentrations in pyrites hosted by chalcopyrite are 0.22 ppm and for pyrites hosted by pyrrhotite 1.51 ppm (see electronic appendix). The high concentrations of Ni in the pyrite hosted by pyrrhotite (median: 2.0 wt.%) allows the incorporation of Ag^{2+} despite the large discrepancy of the difference in ionic radii more than 15% (Goldschmidt 1926). These pyrite grains can originate from an altering fluid which causes a replacement of chalcopyrite and pyrrhotite to form pyrite. The compositional differences in the pyrite mineral chemistry of the two types of pyrite is a result of the sulfide mineral which was replaced by the fluid. Differences for the formation of the massive sulfide segment is also evident in the relative low Pd concentrations in pentlandite (median 11.2 ppm compared to 180.1 ppm in the disseminated grains) as well as in the heavier sulfur isotope signature.

6.5.1.4 Sulfur isotopes

Assimilation of sulfur from the country rock can have an effect on the formation of magmatic Ni-Cu-PGE deposits (Keays 1995). Measurements of sulfur isotopes of Ni-Cu-PGE deposits are therefore useful to provide information about the source of sulfur in these deposits. Assuming that the sulfur isotopic composition in the country rocks differs from that of mantle derived sulfur (0 $\pm$ 2‰ VCDT), sulfur assimilation processes can be estimated using sulfur isotopic data (Ohmoto & Rye 1979). Low-sulfur Ni-Cu-PGE deposits, such as the J-M reef of the Stillwater Complex and the Merensky Reef of the Bushveld Complex, show little or no isotopic evidence for crustal contamination, whereas high-sulfur deposits, such as Noril'sk and the Duluth Complex, show strong isotopic evidence for contamination by sulfur from crustal origin (Ripley & Li 2003).

Different models exist for the formation of the mineralization of the Platreef. Buchanan (1981) argued that the mineralization of the Platreef is the result of an initially sulfur-rich magma which then incorporated additional sulfur from the assimilation of sulfur-bearing footwall rocks.

Holwell & McDonald (2007) carried out a detailed sulfur isotope study on different locations along strike of the Platreef and concluded that the sulfur saturation in the Platreef occurred before contamination and that assimilation of sulfides from the country rocks upgraded the sulfur contents on a local scale, as well as the introduction of sulfur from the country rock sulfates by hydrothermal leaching. For the Merensky Reef, the UG-2 chromitite and the Main Zone in the Bushveld Complex, Penniston-Dorland et al. (2012) carried out a multiple sulfur isotope study and observed a uniform positive sulfur isotope signature which they argue is caused by contamination with the country rock prior emplacement of the Platreef.

Table 6.3 displays that the sulfur isotopic data of the samples from Overysel have mean values of δ^{34}S +3.75‰ for feldspatic pyroxenites, δ^{34}S +4.5‰ for massive sulfide samples and δ^{34}S +2.0‰ for the two Sandsloot samples. The massive sulfide samples show slightly heavier signatures than the feldspatic pyroxenites of both Sandsloot and Overysel, which may indicate that the hydrothermal overprint may have caused a change in this pattern. The sulfur isotopic signatures at Overysel and Sandsloot show that the Platreef magma locally interacted with the country rock during emplacement, causing a slightly heavier sulfur isotopy signature at Overysel than on Sandsloot. Hydrothermal processes partly effected the distribution and re-distribution of PGE in the Platreef and Overysel as shown by irregular shaped PGM (Figure 6.4A). The data of slightly heavier δ^{34}S signature at Overysel indicates a possible post-magmatic hydrothermal redistribution, producing an intermediate sulfur isotopic signature. This redistribution only affected the samples from Overysel but not from Sandsloot. Alternatively or additionally to a hydrothermal overprint the slightly heavier isotope values at Overysel can also be the result of a larger degree of crustal contamination at Overysel. The conclusion regarding a more dominant late-stage hydrothermal overprint is in accordance with the multiple sulfur isotope data by Penniston-Dorland et al. (2008) and Sharman et al. (2013), who argue that local footwall-derived sulfur is not the significant reason to trigger the mineralization in the Platreef. At Tweefontein the floor rocks consist of BIF and black shale. The sulfur isotope signature of the pyroxenites at Tweefontein varies between +4.6‰ and +9.0‰ arguing for a crustal sulfur component.

6.5.2 Oxidized ore

Only relict PGM occur in the oxidized Platreef ore and are mainly sperrylite and cooperite-braggite, whereas (Pt,Pd)-bismuthotellurides are rare. This indicates different stabilities of PGM during the weathering processes. It can be concluded that (Pt,Pd)-bismuthotellurides are less stable than cooperite-braggite and sperrylite. Similar observations exist from placer studies of the Bushveld Complex and the Great Dyke (Oberthür et al. 2004, Melcher et al. 2005, Oberthür et al. 2013b) as well as a study of the altered gossan, overlying the Aguablanca deposit in Spain (Suárez et al. 2010) arguing for a surficial process and different stabilities of PGM.

6.5.3 Implications for the processing of oxidized PGE- ores

Near-surface oxidized PGE ores are ubiquitous in many PGE mining districts. Significant occurrences were not only reported for the Great Dyke Locmelis (2005), Locmelis et al. (2010), Oberthür et al. (2013a) and the Bushveld (this study), but also in weathered ultramafic sequences in Sierra Leone (Bowles 1987), in Cuba (Aiglsperger et al. 2016) and many other locations. These deposits have a large economic potential, but most recent attempts to extract the PGE from oxidized ore, especially with the oxidized reef-type ores, remained uneconomic due to low recovery rates («50%) with conventional metallurgical methods. Conventional processing of pristine reef-type PGE ores comprises froth flotation of the milled ore, matte smelting and subsequent chemical leaching of the base metal- and PGE-rich matte (Crundwell et al. 2011). One of the main issues faced with processing of near-surface oxidized PGE ores is the very heterogeneous PGE distribution covering several mineral phases, including dispersion of PGE in secondary silicates and in iron- and manganese oxides/hydroxides. Another reason for the notably very low recoveries is concentrate dilution during froth flotation due to the occurrence of naturally floating gangue (Bulatovic 2003, Becker et al. 2009) and lack of base metal sulfide association (Becker et al. 2014). Concentrate dilution during froth flotation is principally caused by the presence of talc-coated pyroxene grains, which express a different flotation behavior in comparison to uncoated pyroxene grains. We here showed that the Overysel near-surface oxidized PGE ores are rich in talc-like clay minerals (i.e., phyllosilicates like smectite, kaolinite and vermiculite) and hence both polymodal distribution of PGE and occurrence of NFG remain

the main issues faced with processing of the oxidized ores described in this study. Kraemer et al. (2015) showed that Pt and Pd can be significantly mobilized from oxidized Great Dyke PGE ores using a leach technique which involves specific PGE-affine biomolecules. However, the technique faced relatively heterogeneous recovery rates depending on the origin of the actual sample and the exact weathering state of the ore. These issues are basically related to the polymodal distribution of PGE, both spatially and in relation to oxidation/weathering of the ore with depth. Significant portions of the near-surface oxidized ores present in the Mogalakwena mine are already crushed, classified for 4E grades and stockpiled. Detailed mineralogical studies are necessary to understand the behavior of PGE during laboratory leaching tests. Process mineralogy in combination with novel hydrometallurgical techniques can significantly contribute to the successful and economic exploitation of oxidized near-surface PGE ores like those occurring in the Overysel open pit.

6.6 Conclusions

The present study of the Platreef at the Overysel and Sandsloot open pits showed that:

1) Whole rock data from the Platreef at Overysel showed that from pristine to oxidized ores the Pt/Pd ratio increases which is the result of a relative depletion of Pd over Pt. The relative depletion of Pd is due to its greater mobility during weathering.

2) EPMA and LA-ICP-MS data of sulfides indicate that pentlandite may contain elevated concentrations of Pd, whereas concentrations of Pd in pyrrhotite, chalcopyrite and pyrite are generally below the detection limit. Pyrite hosts the largest concentrations of IPGE in comparison to pentlandite, pyrrhotite and chalcopyrite. Differences in pyrite hosted by chalcopyrite and pyrrhotite are shown in Co, Ni and Pt contents.

3) Sulfur saturation at the Platreef - in particular at Overysel - is partly caused by contamination with the country rocks. The slightly heavier sulfur isotope signature in the massive sulfides may indicate a late stage hydrothermal redistribution.

4) Only relict PGM are present in the oxidized ore, being sperrylite and cooperite-braggite, whereas (Pt,Pd)-bismuthotellurides are less common. This variation in the PGM assemblages from pristine to oxidized ores indicates different stabilities of PGM during weathering processes,

i.e. (Pt,Pd)-bismuthotellurides are less stable than cooperite-braggite and sperrylite. These observations are similar to placer studies in the Bushveld Complex and the Great Dyke.

5) PGE are polymodally distributed in the oxidized ore, i.e. PGE occurring in relict PGM, in iron- and manganese-oxides/hydroxides, or in secondary silicates. Secondary silicates and iron- and manganese oxides/hydroxides contain concentrations of Pt, Pd and Rh in the 100s ppm range. This complex polymodal distribution of PGE in these ores is challenging for the recovery of PGE.

6) Near-surface oxidized PGE ores have a large potential, but attempts to extract the PGE by conventional metallurgical methods from this ore type have proved to be uneconomic due to low PGE recoveries («50%). A better understanding of the weathering processes affecting pristine Platreef ore may help to improve recovery rates of PGE from oxidized ores.

Chapter 7

Cryptic variation of chromite chemistry, platinum group-element and -mineral distribution in the UG-2 chromitite

This chapter is slightly modified after: Junge, M., Oberthür, T., Melcher, F. (2014): Cryptic variation of chromite chemistry, platinum group-element and -mineral distribution in the UG-2 chromitite - an example from the Karee Mine, western Bushveld Complex, South Africa. Economic Geology 109: 795-810.

7.1 Introduction

The Bushveld Complex in South Africa (Fig. 2.1) is the largest layered mafic-ultramafic intrusion on Earth, with an estimated areal extent of 66,000 km^2, and has been dated to ca. 2050 Ma (Wilson 1998, Scoates & Friedman 2008). It contains the largest resources of platinum group elements (PGEs) on Earth and hosts economically important reserves of Cr and V (Vermaak 1995). The formation of the layered sequence hosting the PGE-, Cr-, and V-rich layers still remains enigmatic and different models exist. Maier et al. (2013) argued that the cumulate rocks within the Bushveld Complex were generated by crystal sorting of slurries deposited on

the sloping floor of subsiding magma chambers.

Within the Bushveld Complex, PGE mineralization is mainly confined to a layered sequence of mafic-ultramafic rocks referred to as the Rustenburg Layered Suite, which is usually subdivided into the Marginal, Lower, Critical, Main, and Upper zones (Hall 1932). The economic PGE-bearing ore bodies within the Bushveld Complex are the Merensky Reef, the UG-2 chromitite, and the Platreef. Regional studies indicate that the Merensky Reef and the UG-2 are laterally continuous over hundreds of kilometers (Von Gruenewaldt et al. 1986, Hatton & von Gruenewaldt 1987, Scoon & Teigler 1994).

The UG-2 chromitite is the largest resource of PGEs on Earth (Vermaak 1995) and nowadays represents the predominant source of PGEs from the Bushveld Complex. It occurs in the Upper group of the Critical zone, between 15 and 400 m below the Merensky Reef, whereby the smallest vertical separation is in the western and the greatest in the eastern Bushveld (Lee 1996). The UG-2 chromitite has a general thickness of about 1 m, varying between 0.4 and 2.5 m (Schouwstra et al. 2000). The UG-2 layer is mainly a massive chromitite, consisting of 60 to 90 vol % of chromite with an average Cr/Fe ratio between 1.26 and 1.4, and 43.5% Cr_2O_3 (Lee 1996). Locally, the orebody consists of a number of smaller subsidiary seams that may bifurcate and merge with the main seam (Davey 1992, Penberthy & Merkle 1999, Maier & Barnes 2008, Voordouw et al. 2009, 2010). Generally, the footwall of the UG-2 consists of a pegmatoidal feldspathic pyroxenite, or anorthosite, and the hanging wall of a pyroxenite (Mondal & Mathez 2007). The PGE mineralization is generally limited to the UG-2 chromitite seam itself (Hiemstra 1985, 1986, Von Gruenewaldt & Worst 1986, Kinnaird 2005, Kuhlmann et al. 2006, Maier & Barnes 2008, Voordouw et al. 2009, Cawthorn 2011). PGE contents are up to 10 ppm $\sum$[PGE + Au] and Pt/Pd ratios close to unity. Copper and Ni contents are generally below 0.05%, and S is generally below 0.1% (Von Gruenewaldt et al. 1986, Lee 1996, Cawthorn 2011). Accordingly, the amount of accessory base metal sulfides is low.

In the present study, one drill core transecting the UG-2 chromitite of the Karee mine (LONMIN) in the western Bushveld Complex (Fig. 2.1) was studied in detail, using modern geochemical and mineralogical methods. The work centers on unraveling the fine-scale variation within the UG-2 chromitite regarding the distribution of PGEs (whole-rock data and concentrations in sulfides), platinum group minerals (PGMs), and the compositional variation of

chromite. The study shows that the UG-2 chromitite is composed of a number of chemically distinct chromitite sublayers. Various geochemical and mineralogical trends are established that provide new insights into the relationship of chromitite and PGE mineralization.

7.2 Previous Work

In the Bushveld Complex, the correlation between chromitite and PGEs is exceptionally well expressed, as all the chromitite layers have elevated levels of PGEs, and even the thinnest chromitite stringers tend to contain elevated PGE grades (Maier et al. 2013). The origin of the PGE enrichment in chromitite layers remains controversial partly because many of the most PGE-enriched seams tend to be very S poor (commonly <100 ppm S; Scoon & Teigler (1994) and the PGEs are thought to be predominantly hosted by PGMs (Hiemstra 1986). Von Gruenewaldt et al. (1986) and Naldrett & Lehmann (1987) proposed that the PGEs were originally hosted by PGE-rich magmatic sulfides and segregated in response to magma mixing, but that these sulfides were subsequently removed by late magmatic fluids and/or by reaction of sulfide with chromite.

The Bushveld chromitite seams show a progressive increase in PPGEs (Pt, Pd, Rh) higher in the stratigraphic layer, but only slight increases in IPGE (Os, Ir, Ru) contents (Naldrett & von Gruenewaldt 1989, Scoon & Teigler 1994), a trend also reported for the Great Dyke chromitites by Oberthür (2002, 2011). This trend coincides with decreasing Cr/Fe of the chromitites and has been interpreted to result from the combined effects of differentiation and progressively more vigorous magma mixing (Campbell et al. 1983).

Teigler & Eales (1993), Scoon & Teigler (1994), and Naldrett et al. (2009, 2012) studied compositional variation of chromite in the LG and MG chromitite layers of the Bushveld Complex. Teigler & Eales (1993) observed that Ti increases upward from LG-4 and showed a decrease in Mg# of chromites from the MG upward and a respective increase in Cr/Fe. Naldrett (2009) defined two compositional trends from LG-1 to UG-2/3: trend A is characterized by decreasing Mg# [Mg/(Mg + Fe)] combined with increasing Cr# [Cr/(Cr + Al)], interpreted as a result of the reciprocal exchange substitution of Cr and Fe^{2+} for Mg and Al between spinel and liquid, which affects the Mg-Fe^{2+} spinel-liquid Kd; trend B displays decreasing Mg# combined with decreasing Cr# and reflects a progressive increase in the chemical potential of Al_2O_3 as a

result of fractional crystallization of orthopyroxene (Naldrett 2009).

Vertical textural and compositional variations within the UG-2 were documented by Hiemstra (1985, 1986), Von Gruenewaldt & Worst (1986), Kuhlmann et al. (2006), Maier & Barnes (2008), Voordouw et al. (2009, 2010). Hiemstra (1985, 1986) performed whole-rock analyses on 2-cm segments of the UG-2 from the Western Platinum mine and noted three distinct cycles of PGE mineralization, starting with high total PGEs at the base, in the center, and at the top of the UG-2. Each cycle has its own discrete Pt/Pd value. Hiemstra (1986) also proposed that the PGEs are predominantly hosted by PGMs.

Von Gruenewaldt et al. (1986), Maier & Barnes (2008), Voordouw et al. (2009, 2010) demonstrated that the UG-2 often consists of one main seam and several smaller seams, mainly in the hanging wall, separated by mainly pyroxenite or anorthosite. Indeed, Voordouw et al. (2010) report up to nine separate chromitite layers forming the UG-2 in the Dwars river area of the eastern Bushveld. Von Gruenewaldt et al. (1986), Maier & Barnes (2008) also showed that the distribution of PGEs within the UG-2 seam is not homogeneous, but generally characterized by distinct peaks at the bottom and at the top of the main UG-2 seam.

Eales & Reynolds (1986) were the first to analyze chromite grains of the UG-2 by electron probe microanalysis (EPMA). These authors identified cryptic variation in one example of the main UG-2 layer, namely increasing Cr/Al ratios from bottom to top. Eales & Reynolds (1986) explained the increasing Cr/Al ratios due to the entry of plagioclase into the crystallization assemblage, with plagioclase failing to appear as a cumulus phase.

Naldrett et al. (2011, 2012) studied one core of the UG-2 from Waterval (western Bushveld) in segments of 3 cm and documented a progressive upward increase in the concentration of V, interpreted to be caused by a changing partition coefficient of V between spinel and magma.

PGMs in the UG-2 are dominated by cooperite-braggite [(Pt,Pd)S], laurite [RuS_2], Pt-Fe alloy, locally malanite-cuprorhodsite, and some rarer phases (McLaren & De Villiers 1982, Viljoen & Schürmann 1998, Schouwstra et al. 2000, Kuhlmann et al. 2006, Voordouw et al. 2010). PGE contents of sulfides of the UG-2 were measured by Kuhlmann et al. (2006), who found maximum values of 1.15 wt% Pd and 8.6 wt% Rh in pentlandite, and up to 4.23 wt% Rh in pyrite from the UG-2 of the eastern Bushveld (Lebowa mine) by EPMA. Josties (2012) and Osbahr et al. (2014), in their study of UG-2 samples from the Lebowa mine, found maximum

values of 1,009 ppm Pd and 421 ppm Rh in pentlandite by laser ablation-inductively coupled plasma-mass spectrometry (LA-ICP-MS).

7.3 Samples and Analytical Methods

Drill core DO-24 from the Karee mine (LONMIN) is 155 cm long and consists of three separate chromitite layers (Fig. 7.1). The main chromitite seam is 106 cm wide and is underlain by an altered, pegmatoidal pyroxenite that shows pervasive alteration to anthophyllite-rich rock. The main chromitite seam is overlain by pyroxenite (5 cm wide), a second chromitite layer (7.5 cm) or "leader seam," pyroxenite again (12 cm), and finally a third layer of chromitite (10 cm) on top. This sequence is overlain upward by some meters of pyroxenite.

The drill core was split into segments of 2.5 cm or 5 cm for whole-rock analyses (Fig. 7.1). One or two oriented polished sections each were prepared from each of these segments and were used for reflected light and scanning electron microscopy (SEM), electron probe micro-analysis (EPMA) and LA-ICP-MS. Whole-rock analyses for major, minor, and trace elements were conducted by ACTLABS, Canada, using instrumental neutron activation analysis (INAA) and ICP-MS.

PGMs were first identified using reflected light microscopy in polished sections followed by semiquantitative EDX analysis using an SEM (FEI Quanta 600 FEG ESEM). Chromite and pentlandite grains were analyzed with a CAMECA SX 100 electron microprobe using the following analytical conditions: for chromite analysis, 20-kV acceleration voltage, 30-nA sample current, and 10-s measuring time, electron beam diameter about 1 μm. The elements were calibrated against natural chromite (Cr, Al, Fe, Mg), rutile (Ti), and pure metals (V, Ni, Co, Zn). For Fe-Ni-Cu sulfides, 20 kV acceleration voltage, 120 nA sample current, and up to 180-s measuring time were employed. Synthetic metals (Pd, Rh, Pt, Ag, Co, Cu, Se) and natural sulfides (pentlandite) were used as standards. Detection limits were 75 ppm for Co, 100 ppm for Se, 120 ppm for Rh, 140 ppm for Pd, 160 ppm for Ag, and 300 ppm for Pt. Corrections were performed using the PAP program, and further interferences were corrected using a spreadsheet developed at the BGR, Germany.

In order to corroborate the EPMA results, the concentrations of the six PGEs, Co, Cu, and

Au in larger pentlandite grains (n = 170) of four polished sections (segments 5, 9, 18, and 26) were analyzed by LA-ICP-MS at the University of Erlangen, Germany. Analytical conditions and data corrections performed are identical to those described by Osbahr et al. (2013). The relatively wide laser beam (10-30 μm) led to a certain degree of "analytical contamination" from minerals adjacent to the sought-after pentlandite grains. This analytical problem was controlled by analyzing Si (silicates), Co (pentlandite), and Cu (chalcopyrite) at the same time and eliminating unreliable data from further consideration.

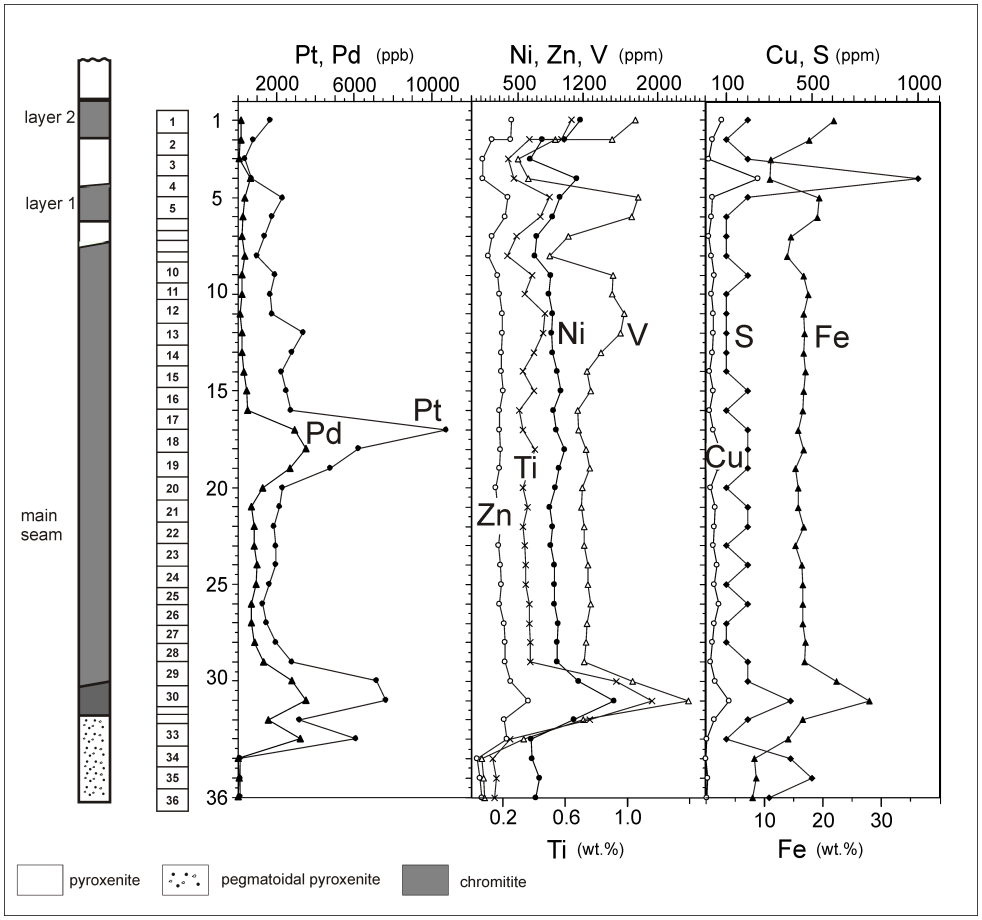

Figure 7.1 – Drill core DO-24 from the Karee mine, 155 cm long. Note three distinct layers of chromitite (main seam, layers 1 and 2) separated by pyroxenite, pegmatoidal pyroxenite at the bottom, and division of the drill core into the 36 segments (left side). Whole-rock element distribution of Pt, Pd, Ni, Zn, V, Ti, Cu, S, and Fe (right side).

7.4 Results

7.4.1 Geochemistry-distribution of Pt, Pd, Au and selected elements within the UG-2

The whole-rock data show a distinct covariance between Pt and Pd, with two overlapping peaks of Pt and Pd at the bottom and in the central part of the main UG-2 chromitite seam (Fig. 7.1). This distribution is largely consistent with previous UG-2 studies (McLaren & De Villiers 1982, Von Gruenewaldt et al. 1986, Davey 1992, Maier & Barnes 2008). Copper (mostly <50-100 ppm) and S contents (mostly <200 ppm) are low. Gold peak values coincide with the top Pt and Pd peaks in the center of the drill core and the top peaks of Cu and S at the top of the drill core.

Nickel, Zn, Fe, Ti, and V, elements compatible with chromite, illustrate a distinct covariance and have maxima in the massive chromitite at the bottom of the main seam (Fig. 7.1). Apart from this, no distinct vertical trends are obvious for these elements, except that the contents of vanadium are slightly higher in the upper UG-2 (sections 1-13) compared to the lower UG-2 (sections 14-30).

Selected segments were analyzed for the six PGEs and Au (Table 1; Fig. 7.2). The range of C1 chondrite-normalized distribution patterns largely corroborates earlier data on the UG-2 as published by Barnes & Maier (2002a).

Table 7.1 – PGE and Au contents (in ppb) as well as Pt/Pd ratios of six selected segments of core DO-24.

segment	Os	Ir	Ru	Rh	Pt	Pd	Au	Pt/Pd
2	47	95	523	192	746	220	5	3.39
17	150	481	1,900	1,870	12,100	3,410	29,2	3.84
18	61	195	779	790	4,250	2,290	8.1	1.86
30	100	331	1,440	1,030	4,720	1,950	1.6	2.42
31	200	676	2,000	2,060	8,770	3,960	6.8	2.21
35	55	208	417	536	1,810	977	1.2	1.85

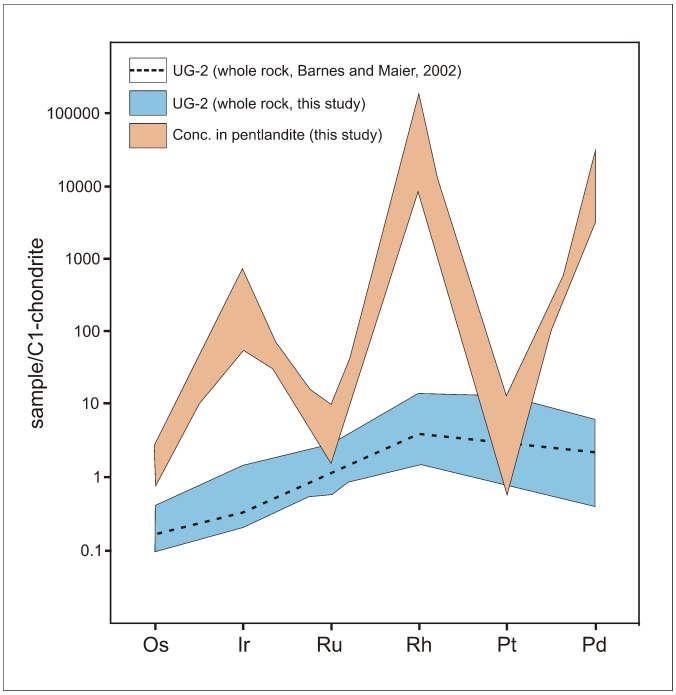

Figure 7.2 – Chondrite-normalized PGE distributions of average UG-2 of the western Bushveld (Barnes & Maier (2002a); stippled line), of DO-24 whole rock data (range in blue; see Table 1), and of PGE contents of pentlandite analyzed by LA-ICP-MS (range in orange). C1 chondrite values from McDonough & Sun (1995).

7.4.2 Mineralogy - oxides and chromite chemistry

Chromite grains are generally idiomorphic, optically homogeneous, and have grain sizes averaging 0.03 to 0.4 mm. The grains are disseminated or show point contacts within the main seam (Fig. 7.3A). At the base of the main seam, the chromite grains are annealed in more compact accumulations, often showing triple junctions. Here, the individual chromite grains often show oriented exsolution lamellae of ilmenite (Fig. 7.3B, C). Ubiquitous, individual rutile grains mainly occur in interstices of chromite grains at the base of the main seam (Fig. 7.3D).

Altogether, 1,455 chromite grains in 32 segments were analyzed by EPMA to investigate the distributions of Mg# (100*Mg/Mg + Fe) and Cr# (100*Cr/Cr + Al), and further elements (Ti, V, Ni, and Zn) in chromite. Between 30 and 50 chromite grains were measured along vertical profiles through the polished sections.

In Figure 7.4, a Cr# versus Mg# diagram, the chromite compositions fall into seven chemical groups, which partly express differences in host rock units. Group I represents the compo-

sitions of chromite grains in the altered pyroxenite at the base, from segment 36 to 33 (segment 35 measured). These chromite grains show the lowest Mg# (0-10) and the largest Cr# (80-93). These unusual compositions are interpreted to result from the hydrothermal alteration in the bottom part of the core that has led to an extreme enrichment of Fe and Cr and concomitant depletion of Mg and Al of the chromite grains. The trend continues into segment 32, the contact of the main chromitite seam (group II). Groups III, IV, and VII cluster tightly together; these groups represent the chromites of the main seam and of the two overlying top chromitite layers. Group 3 represents chromite grains at the base of the massive chromitite band, from segment 31 to 30. Group IV represents the composition of chromite in the main chromitite seam from segment 29 to 9, and in the first top layer (segments 6 and 5). Group VI chromites represent chromite schlieren in the first pyroxenite interlayer (segments 8 and 7). Group VII chromite grains are those in the upper chromitite layer (segments 2 and 1). Compositions of disseminated chromite grains in the second pyroxenite interlayer (segments 4 and 3) are represented by group VI. Apparently, these disseminated chromite grains have equilibrated to a certain degree with the surrounding country rock.

Figure 7.5 demonstrates the vertical variations in Cr#, Mg#, and TiO_2 contents in chromite grains, illustrated in box and whisker plots. Most obvious are the excursions at the bottom of the sequence (segment 35; see above), in the transition at the bottom of the main seam (segments 32-30), and in the pyroxenite interlayers (segments 8 and 7, 3 and 2). Chromite grains in the pyroxenite layers have generally lower Mg# and larger Cr# than chromite grains in the main seam. Closer inspection of the main seam (Fig. 7.5) resembles stepwise cryptic variations upward, as indicated by arrows. The basal sublayer shows increasing Mg#, decreasing Cr#, and increasing TiO_2 contents, followed by seven intervals of upward decreasing Mg# combined with increasing Cr# and increasing TiO_2 (equivalent to trend A of Naldrett (2009), Naldrett et al. (2012). From segment 29 to 9, Mg# varies from 44 to 52, Cr# from 57 to 67, and TiO_2 from 0.4 to 1.4 wt %. Top layer 1 displays a similar trend, whereas the trend in top layer 2 is somewhat obscure due to limited data.

Vertical profiles with variable distances between chromite grains were studied and more than 40 measurement points per polished section were analyzed along the profiles. These results demonstrate small-scale variations in Mg# and Cr# depending on the dominant host minerals

(Fig. 7.6A). Chromite grains, which are mainly surrounded by orthopyroxene, have generally lower Mg# and larger Cr# (Mg and Al distribute preferentially into orthopyroxene in the subsolidus stage) than chromite grains surrounded dominantly by plagioclase. However, these variations are on a minor scale compared to the overall trend as shown in Figure 7.6B and thus do not affect the general trends as described above.

In summary, 10 distinct chromitite sublayers (eight in the main seam plus the two separate top layers or leader seams) are distinguishable in the UG-2 sequence. Elevated PGE concentrations are mainly confined to sublayer 1 at the base and sublayer 6 in the center of the main chromitite seam. The interrelationship between chromitites and PGE mineralization will be followed up below.

7.4.3 Mineralogy - sulfides and PGMs

Sulfide grains and grain aggregates of pentlandite, chalcopyrite, rare pyrrhotite, and pyrite are found only in the interstices of chromite grains, often associated with silicates. Sulfide grain sizes range from <1 to 50 μm (mostly 10-20 μm). A mineral optically resembling violarite [$FeNi_2S_4$] often replaces pentlandite throughout the investigated UG-2 sequence (Fig. 7.3E, F). Microprobe analyses revealed that this compound is an unnamed iron-rich thiospinel of the greigite [Fe_3S_4]-polydymite [Ni_3S_4] series, approximating the composition [$NiFe_2S_4$] (Table 7.2).

PGMs generally occur in the interstices of chromite grains. The PGMs (grain sizes <5-20 μm) are locked within or, more commonly, occur at the peripheries of sulfide grains. PGMs within chromite are rare and in all cases consisted of laurite grains (Fig. 7.7A). Altogether, 356 discrete PGM grains were detected. Major PGMs are Pt-Fe alloy grains (30%), commonly displaying idiomorphic outlines (cubes; Fig. 7.7B), laurite [RuS_2] (29%; Fig. 7.7B), cooperite-braggite [(Pt,Pd,Ni)S] (26%; Fig. 7.7C), rarer zvyagintsevite [Pd_3Pb] (Fig. 7.7D), and potarite [PdHg] (Fig. 7.7E). Malanite [$CuPt_2S_4$], irarsite [IrAsS], platarsite [PtAsS], and sperrylite [$PtAs_2$] are rare. Notably, laurite always contains some Ir and Os (up to several wt %). In one instance, an inhomogeneous pentlandite grain (Fig. 7.7F; Table 7.2) shows exceedingly high contents of Rh (up to 12.5 wt %) and Pt (up to 2 wt %). The average composition (n = 2) is [$(Ni_{3.77}Fe_{3.59}Co_{0.09}Cu_{0.21}Rh_{0.93})_{8.59}S_8$] (Table 7.2). Cabri et al. (1981) measured Rh contents of

up to 14.1 wt % in pentlandite enclosed in Pt-Fe nuggets from Ethiopia and called this "rhodian pentlandite."

The study of polished sections revealed the presence of PGMs in all chromitite segments. In Figure 7.8, however, only those segments that contained more than 10 PGM grains are shown. The largest number of PGM grains was detected in the samples with the most elevated Pt and Pd contents (segments 17-19, 29-32). Figure 7.8, furthermore, demonstrates that the mineralogy of the PGMs changes vertically. At the UG-2 base, cooperite-braggite and laurite are most abundant, whereas Pt-Fe alloy is more dominant at the center part of the main seam. Zvyagintsevite and potarite only occur in the center of the main seam. In general, most of the PGMs are Pt-rich or IPGE-rich (laurite), whereas Pd- and Rh-bearing PGMs are rare. This raises the question on the mineralogical siting, especially of Pd and Rh in the ores, a matter that will be addressed below.

Table 7.2 – Compositions of pentlandite (in wt.%). (1) segment 5 (n=38), (2) segment 18 (n=37) and (3) segment 31 (n=38). Compositions of "violarite" (in wt.%). (4) segment 5 (n=5), (2) segment 18 (n=3) and (3) segment 31 (n=4). Compositions of Rh-rich pentlandite (in wt.%) from segment 18 (7 and 8). EPMA data.

		S	**Fe**	**Co**	**Ni**	**Rh**	**Pd**
1	median	33.25	31.64	0.65	34.15	0.03	0.05
	range	32.76-34.91	30.42-32.24	0.35-0.75	30.36-35.37	<0.01-0.32	<0.01-0.16
2	median	33.05	31.32	0.45	33.67	0.3	0.75
	range	32.64-33.62	29.43-32.14	0.20-0.61	32.73-34.98	0.10-3.00	<0.01-2.19
3	median	33.21	32.92	0.76	32.51	0.15	0.11
	range	32.91-33.48	31.82-34.03	0.58-0.94	28.71-34.00	<0.01-0.94	0.02-0.65
4	median	40.91	31.86	0.82	24.3	0.01	0.1
	range	39.71-41.10	31.44-32.74	0.81-0.84	22.41-25.10	<0.01-0.07	0.05-0.16
5	median	40.11	31.69	0.35	24.14	0.49	0.57
	range	39.90-40.16	30.71-33.05	0.29-0.54	21.63-25.51	0.20-0.90	0.29-1.47
6	median	40.64	34.36	0.88	20.7	0.08	0.15
	range	40.30-40.88	32.40-35.21	0.58-0.94	19.88-24.48	<0.01-0.23	0.09-0.34
7		30.45	22.81	0.63	25.4	12.49	0.02
8		30.68	24.96	0.62	27.36	10.34	0.05

7.4.4 PGEs in pentlandite - EPMA

The scarcity of Pd- and Rh-bearing PGMs led to the assumption that these PGEs are present in solid solution within sulfide minerals, especially pentlandite, as outlined by a number of authors

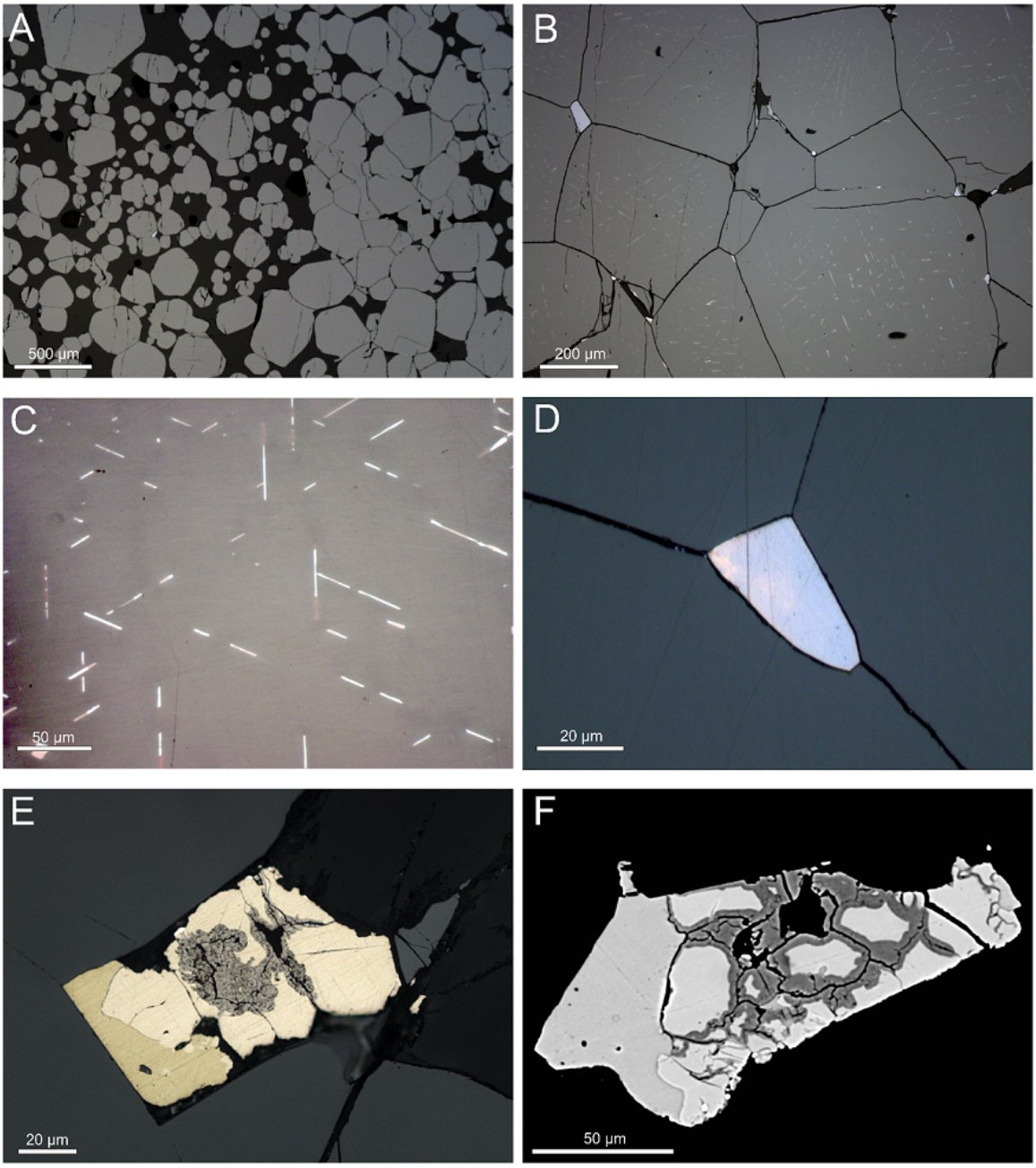

Figure 7.3 – Photomicrographs, polished sections, A-E reflected light, in air. F is backscattered electron image. (A) Disseminated to partly more massive chromite (gray). Segment 15 (AS 8915a). (B) Massive, annealed chromitite with exsolution lamellae of ilmenite and rutile grains. Segment 30 (AS 8930b). (C) Oriented exsolution lamellae of ilmenite (light gray) in chromite (medium gray). Segment 30 (AS 8930a). (D) Grain of rutile in interstice between chromite grains. Segment 30 (AS 8930b). (E) Sulfide aggregate squeezed between chromite (dark gray), consisting of chalcopyrite (yellow) and pentlandite (cream-white). Note replacement of pentlandite by darker compound ("violarite"). Segment 17 (AS 8917a). (F) Sulfide aggregate consisting of chalcopyrite (left; medium gray) and pentlandite (light gray). Note replacement of pentlandite by violarite (dark gray) along small channels leaving "islands" of pentlandite. Segment 18 (AS 8918b).

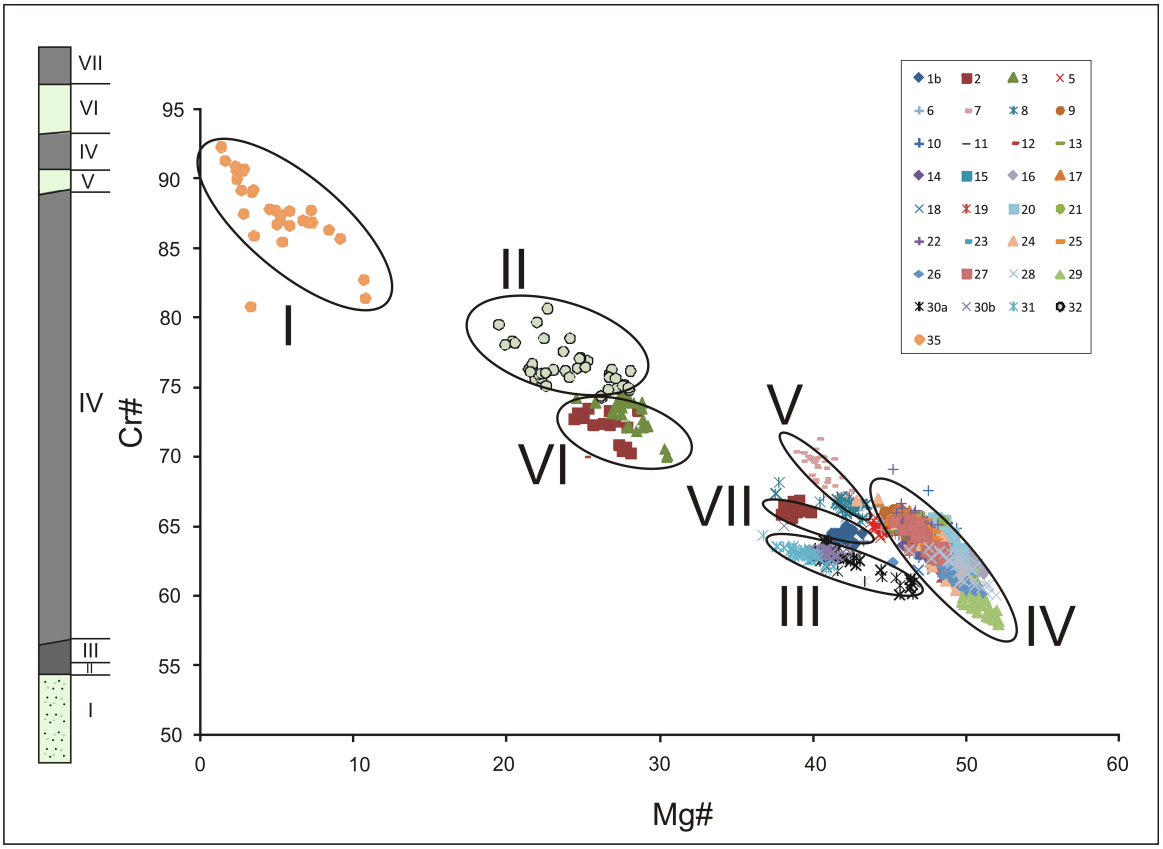

Figure 7.4 – Cr# versus Mg# diagram (EPMA data of all chromite grains analyzed in core DO-24), illustrating seven chemically different groups.

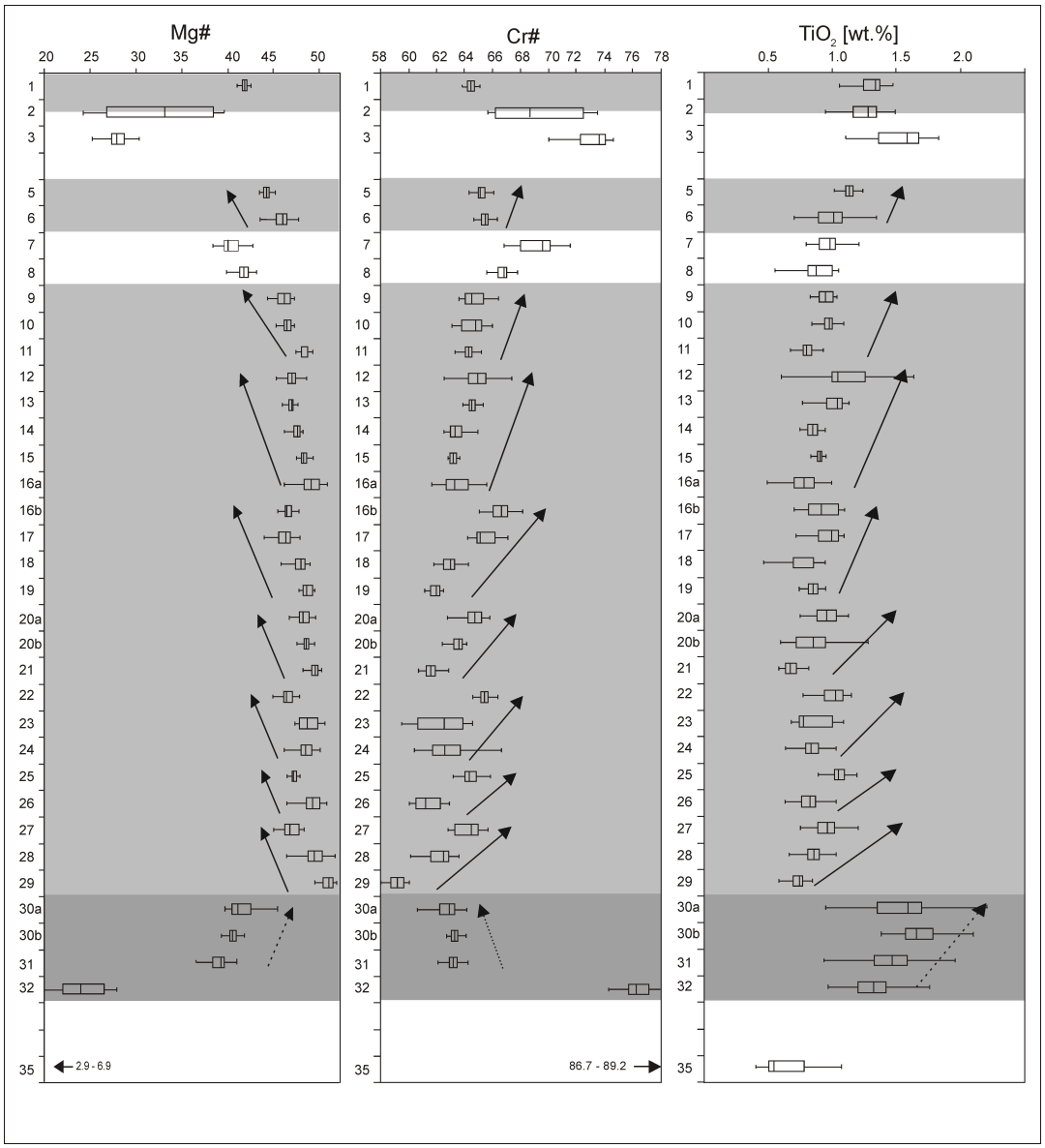

Figure 7.5 – Box-and-whisker plots illustrating the vertical distribution of Mg# and Cr# in chromite within the UG-2 main seam and the overlying pyroxenite and chromitite layers. Chromitites (pale gray), massive chromitite (segments 30-32; dark gray), and pyroxenite layers (segments 2-4, 7-8; white). Arrows indicate normal cyclic trends in Mg# and Cr#. Only from segment 30 to 32, at the bottom of the main chromitite seam, is the trend reversed.

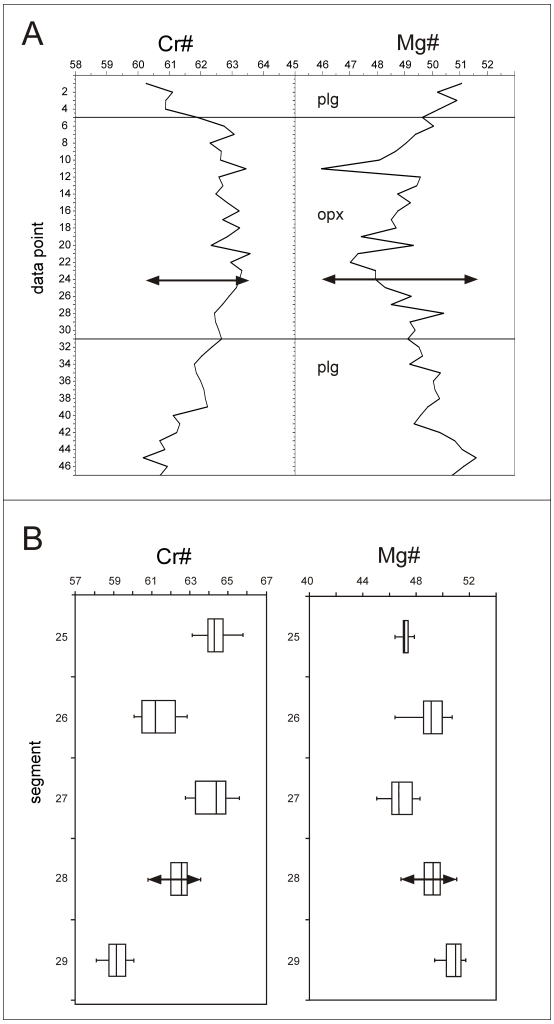

Figure 7.6 – Compositional variation of chromite grains surrounded by orthopyroxene or plagioclase. Arrows in Fig. 7A indicate variations of Cr# and Mg#, respectively, within segment 28. Arrows in Fig. 7B display the corresponding variation compared to the neighboring segments 27 and 29.

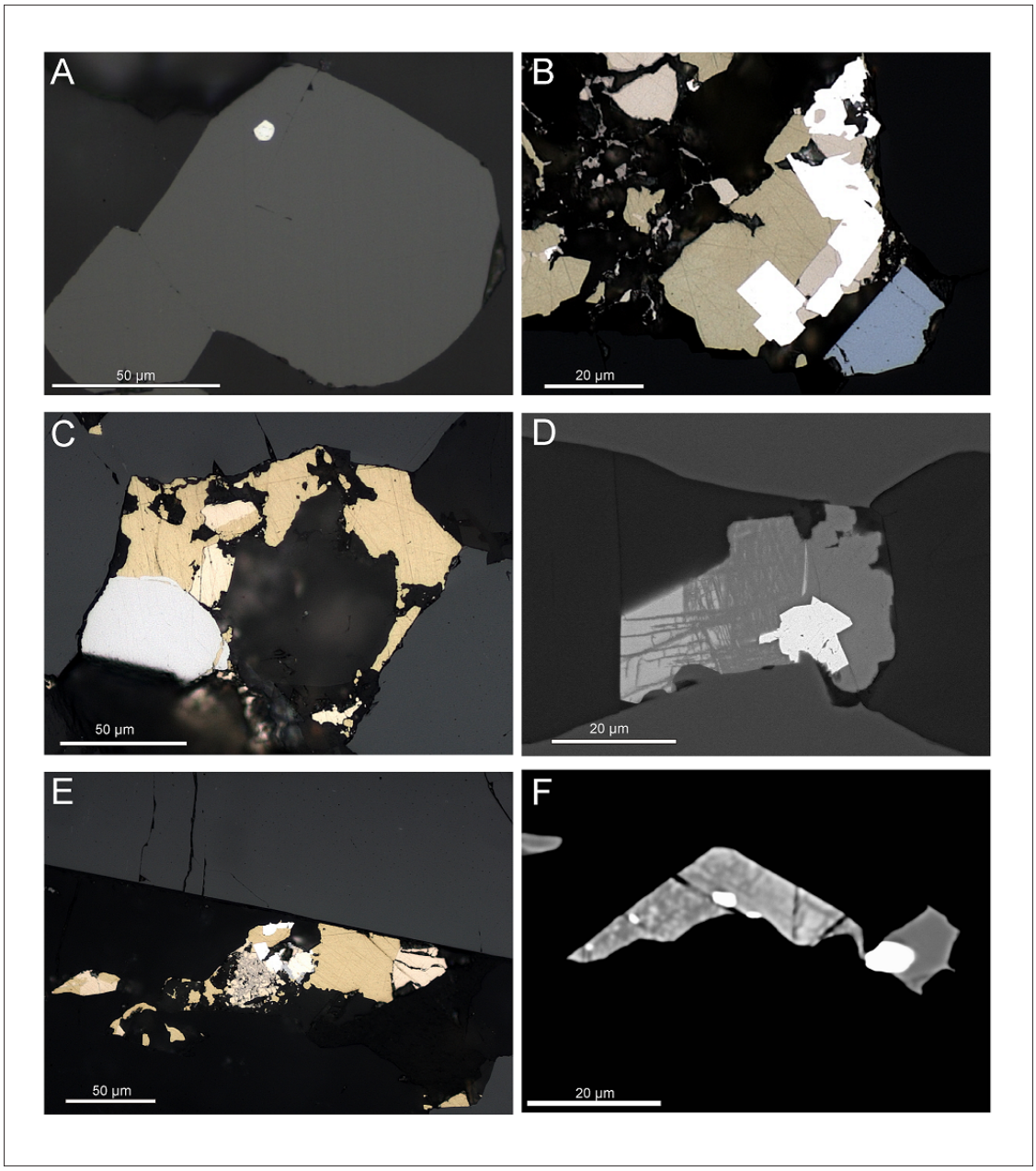

Figure 7.7 – Photomicrographs, polished sections. A and B are reflected light, in air. C and E are reflected light, in oil. D and F backscattered electron images. (A) Inclusion of laurite (white) in chromite grain (medium gray). Segment 17 (AS8917a). (B) Composite sulfide - PGM aggregate consisting of chalcopyrite (yellow), rarer pentlandite (cream-white), Pt-Fe alloy (white) and laurite (bluish, at bottom right). Segment 19 (AS 8919a). (C) Sulfide aggregate consisting of chalcopyrite and pentlandite, intergrown with braggite (light blue, to the left), surrounded by chromite. Segment 17 (AS 8917a). (D) Intergrowth of pentlandite (medium gray) with Pt-Fe alloy grain (lightest gray) and zvyagintsevite (light gray, to the left). Segment 18 (AS8918a). (E) Sulfide aggregate of chalcopyrite (yellow) and pentlandite (cream-white) intergrown with potarite (white). Chromite is medium gray. Segment 17 (8917a). (F) Rh-rich (max. 12 wt % Rh) pentlandite grain (light gray, mottled surface), "normal" pentlandite (medium gray, to the right) and smaller Pt-Fe alloy grains (white) attached to pentlandite. Segment 18 (AS8918b).

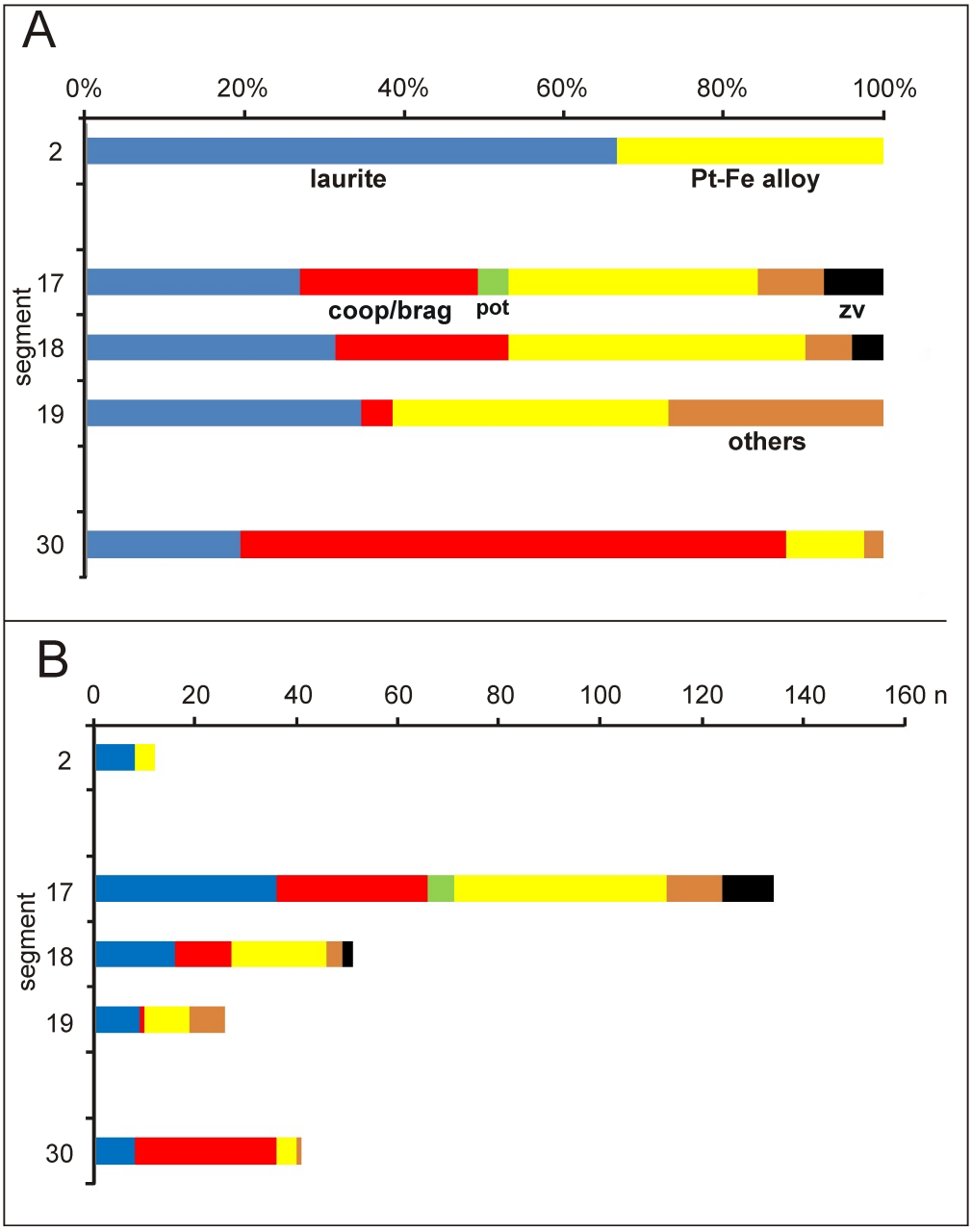

Figure 7.8 – Vertical distribution of PGMs within core DO-24 of the UG-2, concentrating on the segments with the highest PGE contents, 17, 18, 19, and 30). Fig. 9A is normalized to 100%, whereas Fig. 9B displays the number of PGMs per segment.

from different ultramafic-mafic complexes (Cabri et al. 1984, 2002, Cabri 1992, Oberthür et al. 1997a, 2003, Gervilla et al. 2004, Godel et al. 2007, Holwell & McDonald 2010). PGE data for Ni-Fe-Cu sulfides in the UG-2 are those of Kuhlmann et al. (2006) who identified up to 8.6 wt % Rh and 1.15 wt % Pd in pentlandite, and up to 4.23 wt % Rh in pyrite (EPMA). Josties (2012) and Osbahr et al. (2014) found maximum values of 1,009 ppm Pd and 421 ppm Rh in pentlandite by LA-ICP-MS. In the present study, concentrations of the PGEs in sulfide grains were measured using both EPMA (Pd, Rh, and Pt) and LA-ICP-MS (all PGEs).

Nickel, Fe, Co, S, Se, Pd, Pt, and Rh in pentlandite grains were first analyzed with EPMA (n = 153) in polished sections of segments 5, 18, and 31, representing the segments with elevated whole-rock PGE contents (Figs. 7.2, 7.9; Table 7.3). Nickel and Fe contents are relatively constant throughout the sequence (median values ranging from 32.51-34.15 wt % Ni and 31.32-32.92 wt % Fe). Median Co contents are 0.65, 0.45, and 0.76 wt % for pentlandite of segments 5, 18, and 31, respectively, whereas Se concentrations decrease from 178 to 114 ppm from bottom to top. Figure 7.10 shows little variation of Ni/(Ni + Fe) of pentlandite grains. Only the grains from the bottom part of the main chromitite seam (segment 31) and, in a very distinct manner, all altered grains ("violarite") tend to lower Ni/(Ni + Fe) ratios.

Elevated concentrations of Pd and Rh in pentlandite grains are the rule (hundreds of ppm), and no significant differences were encountered between Pd and Rh contents in pentlandite and "violarite" of the individual segments (Fig. 11). Palladium and Rh contents in pentlandite are comparatively low in segment 31, at the base of the main UG-2 seam (median = 1,084 ppm Pd and 1,520 ppm Rh), and also in segment 5, the first top chromitite layer (median = 456 ppm Pd and 319 ppm Rh). However, median values of 7,470 ppm Pd and 2,986 ppm Rh (max contents 2.2 wt % Pd and 3.0 wt % Rh) were detected in pentlandite of segment 18, which represents the area of the whole-rock Pt and Pd peaks, in the center of the main UG-2 seam (Fig. 7.10). The latter high values were confirmed by follow-up LA-ICP-MS work.

7.4.5 PGEs in pentlandite - LA-ICP-MS

Platinum group elements, Co, Cu and Au contents in sulfide grains (n = 73) were analyzed with LA-ICP-MS in polished sections of segments 5, 9, 18, and 26. Note that LA-ICP-MS work was only carried out in order to corroborate the EPMA results. The relatively wide laser beam (10-

Table 7.3 – Pd and Rh contents of pentlandite (in ppm) from segments 5, 18 and 31 (EPMA data).

Segment	Pd (ppm)			Rh (ppm)		
	Min	Median	Max	Min	Median	Max
5	<138	456	1627	<115	319	3245
18	<142	7470	21851	973	2986	29975
31	165	1084	6476	<117	1520	9429

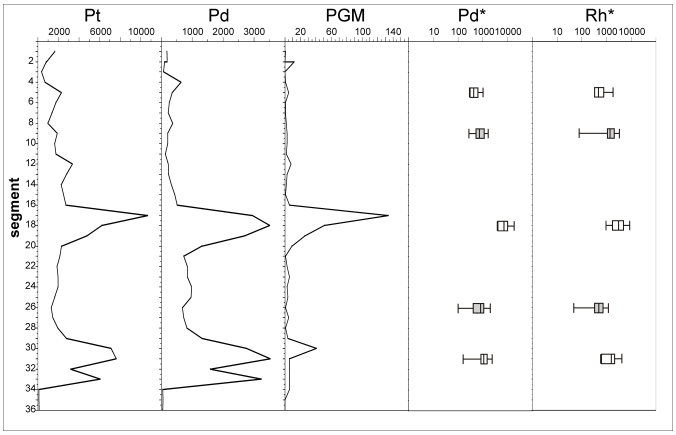

Figure 7.9 – Vertical distribution of Pt and Pd (whole-rock data, in ppb), PGMs (n = number of grains) as well as Pd and Rh contents of pentlandite (segments 5, 18, and 31: EPMA data; segments 9 and 26 (shaded): LA-ICP-MS data.

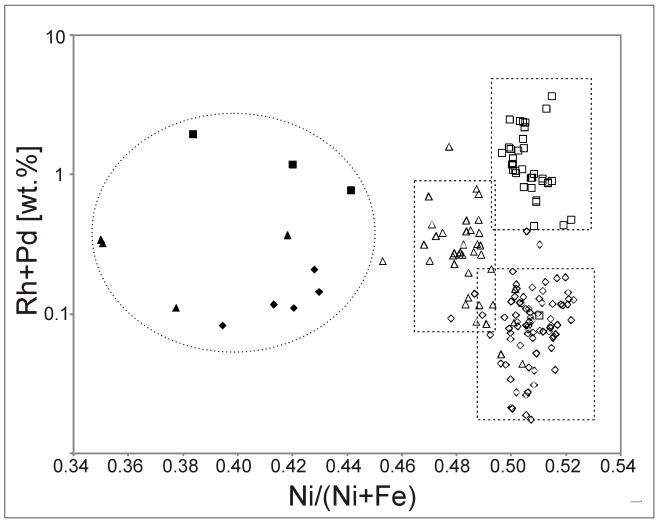

Figure 7.10 – Plot of (Rh + Pd) versus Ni/(Ni + Fe) in pentlandite (EPMA data). Note different, though slightly overlapping fields of analyses from segment 5 (open diamonds), segment 18 (open squares), and segment 31 (open triangles). Pentlandite from segment 31 has slightly lower Ni/(Ni + Fe) ratios. Filled symbols (segment 5, diamonds; segment 18, squares; and segment 31, triangles) represent analyses of "altered" pentlandite grains ("violarite"). These have distinctly lower Ni/(Ni + Fe) ratios whereas their Rh + Pd contents are grossly in the range of their pristine precursor grains.

30 μ diameter) led to a certain degree of "analytical contamination" from minerals surrounding the pentlandite grains. This analytical problem was controlled by analyzing Si (silicates), Co (pentlandite), and Cu (chalcopyrite) at the same time as the PGEs. Following, only the most reliable data (Cu <5,500 ppm, Co >1,500 ppm) were considered. Analytical contamination by silicates has a decreasing effect on maximum PGE contents in sulfide.

With respect to Pd and Rh, the LA-ICP-MS work largely confirmed the EPMA results. Maximum Pd and Rh contents (1.67 wt % Pd and 2.38 wt % Rh) were measured in pentlandite of segment 18 and much lower contents (still in the 100-ppm range) are persistently present in the other segments analyzed. Platinum contents are low and range from <0.2 to 56 ppm, and Au was generally below the detection limit (between 0.1 and 0.3 ppm). IPGE contents of pentlandite were constantly above the respective detection limit of the method (ca. 0.03-0.3 ppm), generally in the lower one digit ppm range. Notably, elevated contents of Ir (30 - ca. 130 ppm Ir), unparalleled by Os and Ru contents, were constantly encountered. Occasionally, coherent elevated values (up to several thousand ppm each) of the IPGEs (Ru, Os, Ir) and also Pt were detected. These are interpreted to signal discrete, PGM microinclusions or PGE clusters included within or attached to pentlandite (Wirth et al. 2013). Accordingly, the analyses (Os, Ru, Pt >60 ppm) were excluded from further consideration on the PGE contents of pentlandite.

Figure 7.2 illustrates that the range of analyses from core DO-24 closely corresponds to the average PGE data of the UG-2 as given by Barnes & Maier (2002a). However, the chondrite-normalized pattern obtained for the PGEs in pentlandite shows distinct enrichments of Rh and Pd, exceeding the whole-rock contents by far, and Ir also achieves elevated values. In contrast, Os, Ru, and Pt display characteristic minima. It is thought that the PGEs in pentlandite pattern largely reflects the capability of pentlandite to host Rh and Pd as well as some Ir in its crystal lattice. In contrast, as Pt is not compatible in pentlandite, this element forms discrete PGMs. Ruthenium and Os appear to have undergone a comparable fate to Pt as they are mainly found in laurite.

7.4.6 Weathering of UG-2 and the Merensky Reef

So far, only limited data exists about the oxidized UG-2 (Hey 1999). Whole-rock geochemistry of oxidized ores of the UG-2 chromitite is shown in Table 7.4. The Pt/Pd ratios are above unity

ranging from 1.1 to 16.1.

Sulfides are typically absent and are only rarely observed as inclusions in chromite. Chromite grains typically make up 60 to 70%. Relict grains of cumulus orthopyroxene and interstitial plagioclase are observed and often show alteration to secondary hydrous silicates and clay minerals (Figure 7.11A). Chromite grains typically have cracks caused by the volume change from pyroxene and feldspar to secondary hydrous minerals (Figure 7.11B,C). Deformation of chromite grains is pronounced in more massive chromite parts and cracks in particular originate where chromite grains are in contact to other chromite grains. Platinum-group minerals are mainly cooperite-braggite and laurite. Laurite grains are observed as inclusions within chromite or within silicates. Cooperite is observed at the grain boundaries of chromites grains with irregular shapes (Figure 7.12A) and within cracks of chromite grains (Figure 7.12B). At the rim of secondary Fe-Mg-Al-silicates, cooperite is observed together with Ir-Rh-sulfides. Within these secondary silicates inclusions of braggite has been analyzed (Figure 7.12C).

Table 7.4 – Whole rock data of oxidized UG-2 ore.

sample	location	reef type	Pt	Pd	Au
SA4011	Der Brochen	UG-2 chromitite	2520	1140	6
SA4013	Der Brochen	UG-2 chromitite (top 40 cm)	2570	462	29
SA4014	Der Brochen	UG-2 chromitite (bottom 40 cm)	1770	822	40
SA4019A	Driekop	UG-2 chromitite (0-20 cm)	3570	2800	190
SA4019B	Driekop	UG-2 chromitite (20-25 cm)	2650	2450	53
SA4056	Pit U9c (Lonmin)	UG-2 chromitite (2 m below surface)	4950	3440	80
SA4057	Pit U9c (Lonmin)	UG-2 chromitite (10 m below surface)	7420	462	<2

Limited work was done at the oxidized Merensky Reef (Korges 2014). Whole-rock geochemistry of oxidized ores of the Merensky Reef is shown in Table 7.5. The Pt/Pd ratios are above unity ranging from 2.2 to 11.9 in the Merensky Reef. Chromitite bands are typically not deformed but surrounded orthopyroxene and plagioclase are partly weathered to secondary silicated and clay minerals (Figure 7.11D,E). In rare cases inclusions of sulfide occur within orthopyroxene and are largely unaffected by weathering (Figure 7.11F). Platinum-group minerals are mainly cooperite-braggite and laurite. Cooperite-braggite is often found associated with secondary Cu-Fe-silicates (Figures 7.12D-F).

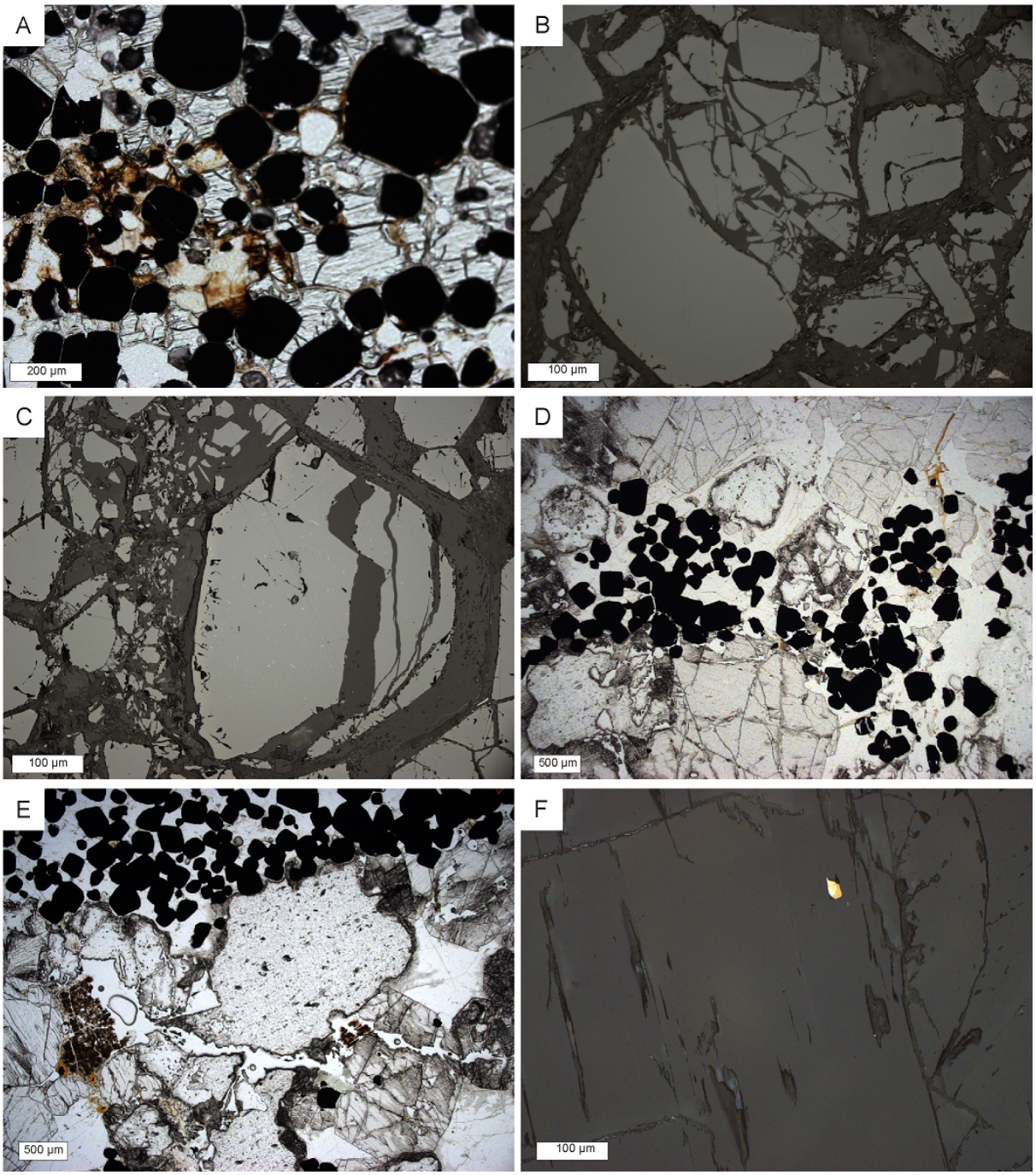

Figure 7.11 – Photomicrographs of oxidized UG-2 (A-C) and Merensky Reef (D-F). A: Chromite grains and partly weathered pyroxenes. Plane polarized transmitted light; SA4004. B-C: Deformed chromite grains surrounded by secondary hydrous silicates. Reflected light; AS11291. D-E: Chromitite band within the Merensky Reef suuround by partly weathered pyroxene and plagioclase. Plane polarized transmitted light; SA4024A. F. Relict sulfide assemblage (pentlandite, pyrrhotite and chalcopyrite) in orthopyroxene. Reflected light; AS11287.

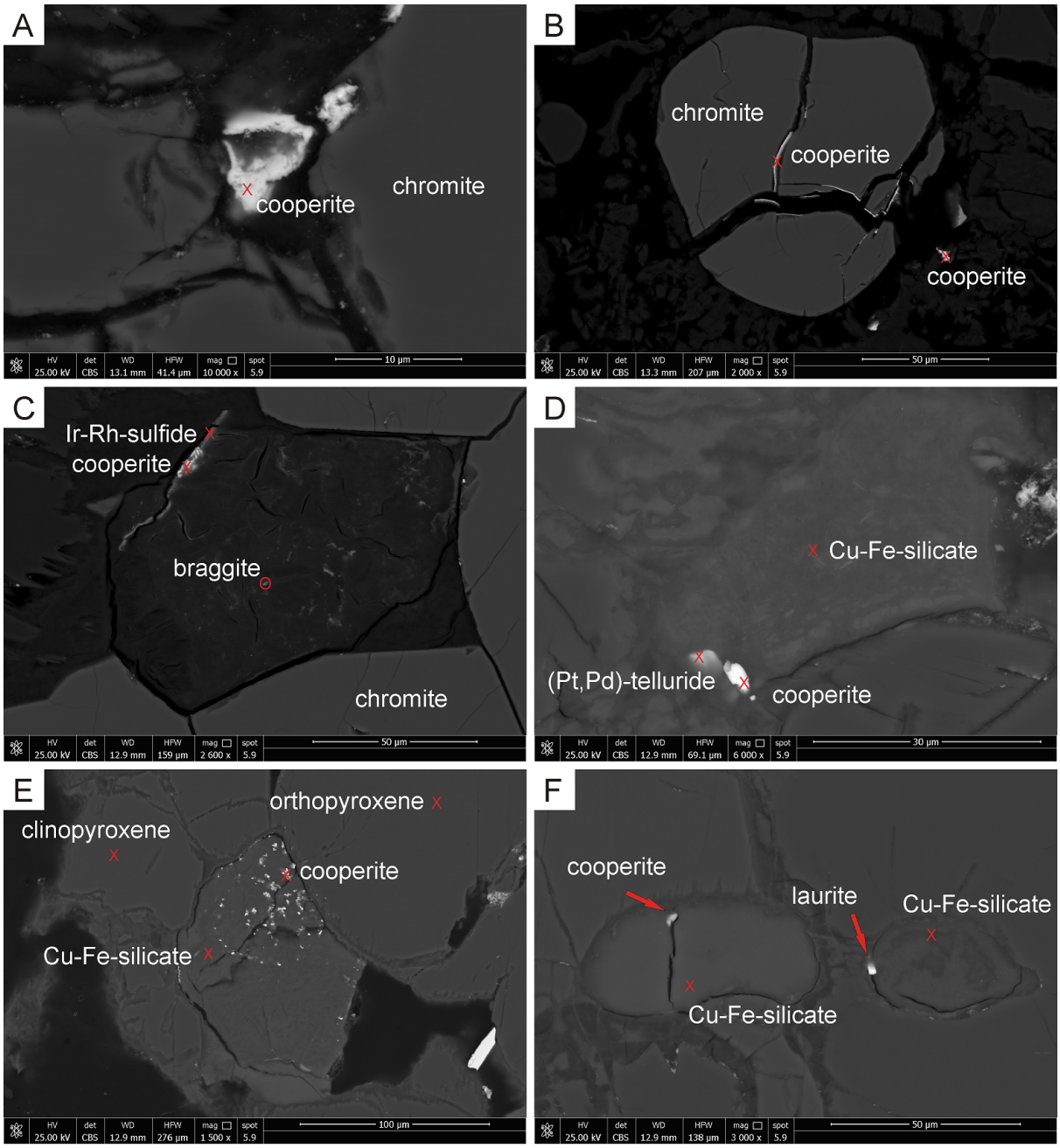

Figure 7.12 – Back-scattered electron (BSE) images of PGM in oxidized UG-2 and Merensky Reef. A-C: Oxidized UG-2 chromitite (2m below surface) from the Pit U9C/Lonmin (AS11290). D-F: Oxidized Merensky Reef (top part of the reef from Lebowa/Atok (AS11286)). A: Cooperite [PtS] grain in between chromite grains. B: Cooperite within the cracks of a chromite grain. C: Cooperite [PtS] together with Ir-Rh-sulfide at the rim of an Fe-Mg-aluminosilicate and braggite [PdS] within the Fe-Mg-aluminosilicate. D: Cooperite and (Pt,Pd)-telluride in Cu-Fe silicate. E. Several cooperite grains within Cu-Fe-silicate. F: Cooperite and laurite [RuS_2] within Cu-Fe-silicates.

Table 7.5 – Whole rock data of oxidized Merensky Reef.

sample	location	reef type	Pt	Pd	Au
SA4007	Driekop/Marula Mine	Merensky Reef	486	74.5	<2
SA4008	Driekop/Marula Mine	Merensky Reef	1120	217	62
SA4010	Driekop/Marula Mine	Merensky Reef (60 cm)	1040	358	5
SA4012	Der Brochen	Merensky Reef	3310	1500	14
SA4024A	Lebowa/Atok	Merensky Reef (0-20 cm)	1570	510	387
SA4024B	Lebowa/Atok	Merensky Reef (20-40 cm)	14200	1190	28
SA4058	Pit M9 (Lonmin)	Merensky Reef	9400	2520	426

7.5 Summary and Discussion

The UG-2 sequence of core DO-24 from the Karee Mine is characterized by the presence of a main chromitite seam at the base overlain by two chromitite layers ("leader seams"). This sequence is characteristic for the UG-2 at the Karee Mine and in general, where the UG-2 often consists of one main seam and several smaller layers or leader seams, mainly in the hanging wall (Von Gruenewaldt et al. 1986, Maier & Barnes 2008, Voordouw et al. 2009, 2010). Further, the distributions of Pt and Pd are characterized by enrichments at the base and in the center in the main chromitite seam, consistent with similar PGE distribution patterns described for the UG-2 by other authors (Hiemstra 1985, 1986, Von Gruenewaldt & Worst 1986, Kinnaird 2005, Kuhlmann et al. 2006, Maier & Barnes 2008, Voordouw et al. 2009, Cawthorn 2011).

Microprobe analyses revealed a distinct cryptic variation of chromite chemistry in the UG-2. Based on Cr#, Mg#, and TiO_2 contents, 10 distinct chromitite sublayers (eight in the main seam plus the two separate top layers) are distinguishable. Stepwise cryptic variations are obvious with intervals of upward decreasing Mg# combined with increasing Cr# and increasing TiO_2 (except the basal sublayer). The sublayers are interpreted to represent successive magmatic events (equivalent to trend A of Naldrett (2009), Naldrett et al. (2012) of chromite precipitation and accumulation following differentiation of the parent magma. The basal sublayer is an exception, showing an extreme enrichment of Fe and concomitant depletion of Mg and Al of the chromite grains toward the base. These unusual compositions are linked to either late-magmatic/hydrothermal alteration observed in the bottom part of the core (pegmatoidal pyroxenite showing pervasive anthophyllite alteration), or, alternatively, a first chromitite sublayer

that was chemically different (high-Cr-Ti-Fe) from the succeeding sublayers, and may have affected the underlying pyroxenite.

The 10 distinct chromitite sublayers suggest 10 subsequent pulses of chromitite input from a differentiating magma, whereby the main UG-2 seam is composed of eight initially separate sublayers which amalgamated to form the massive chromitite seam. Notably, Voordouw et al. (2010) describe UG-2 sequences consisting of up to nine chromitite layers separated by pyroxenite from the eastern Bushveld. Therefore, it would be worthwhile to study other UG-2 sequences in detail in order to show whether the "massive" chromitites are internally multilayered in general. The cryptic trends in mineral chemistry as unraveled in the present study point to differentiation in situ ("onstage"; Naldrett et al. (2011)) rather than accumulation of the chromitite layers by slurries (Maier et al. 2013) or injection as sills as suggested by Voordouw et al. (2009).

It is well known both from the Bushveld Complex (Naldrett & von Gruenewaldt 1989, Scoon & Teigler 1994, Lee 1996, Naldrett 2009) and the Great Dyke layered intrusions (Oberthür 2002, 2011) that the chromitite seams show a progressive increase in PPGEs (Pt, Pd, Rh) with height, but only slight increases in IPGEs (Os, Ir, Ru) contents. Indeed, strata-bound PGE mineralization in layered intrusions is related to either spinel-rich rocks, mainly chromitites, or to sulfide accumulations. Elevated PGE concentrations are a feature of chromite-rich rocks worldwide, regardless of their petrogenesis (Von Gruenewaldt et al. 1986). More specifically, chromitites are typically enriched in IPGEs relative to PPGEs (Lee & Parry 1988, Lee 1996). The mechanism of PGE concentration in chromitites, particularly whether the PGEs occur in solid solution in the chromite lattice or in associated sulfides, or as metal clusters, or as inclusions of discrete PGMs, is a continuing and unsolved matter of debate (Tredoux et al. 1995, Cawthorn 1999a, Mathez 1999, Maier 2005, Finnigan et al. 2008, Mungall 2010). Whatever mechanism is relevant, the fact remains that chromitites provide an environment conducive to the concentration of PGEs, termed "chromitite control" and defined by Scoon & Teigler (1994) as "*a process thought to involve a combination of direct nucleation of PGMs and localized S saturation*." Equally, it is well established that magmatic sulfides concentrate PGEs due to the high partition coefficients (D) of the PGEs between sulfide and silicate liquid, which are of the order of at least 10^4 and possibly as high as 10^7 (Campbell et al. 1983, Fonseca et al. 2009).

Fractionated, steep positive normalized PGE patterns are characteristic of PGE concentrations attained by scavenging of the PGEs from mafic magmas by sulfide segregation (Naldrett 1993, 2004b, Maier 2005, Holwell & McDonald 2010).

Accordingly, a dual mechanism is envisaged for PGE enrichments in layered intrusions, namely "chromitite control" and "sulfide control". The major magmatic differentiation trend is paralleled by the progressive buildup of sulfur concentration in the magma. In the Bushveld Complex, significant sulfide saturation and segregation is only obvious from the LG-5 chromitite seam upward (Naldrett 2009). The PGE contents of the Lower Group chromitites, therefore, mainly reflect "pure" chromitite control as shown by the preponderant concentration of IPGEs. This observation can also be interpreted in a way that the termination of chromitite formation, at the level of UG seam formation, immediately preceded, and was related to the commencement of sulfur saturation which initiated major sulfide segregation fixed in the overlying Merensky Reef. Accordingly, sulfide control took over from chromitite control once sulfides began to precipitate. Within the Karee Mine UG-2 sequence studied, elevated PGE concentrations are mainly confined to sublayer 1 at the base and sublayer 6 in the center of the main chromitite seam. Apparently, only during the first, initial event of chromitite deposition (sublayer 1) and accompanying an intermediate event (sublayer 6), elevated proportions of sulfides enriched in PGE coprecipitated with and were trapped in the interstices of chromite grains.

Gain (1985), Von Gruenewaldt et al. (1986), Naldrett & Lehmann (1987) and Naldrett et al. (2012) commented on the UG-2 and its high PGE/S ratio, suggesting that originally PGE-rich magmatic sulfides segregated contemporaneously with chromite, but that these sulfides were subsequently removed by late magmatic fluids and/or by reaction of sulfide with chromite. Our observations (e.g., that pyrrhotite and pyrite are nearly missing) corroborate this proposal and rather contradict the idea of Hiemstra (1979) of PGMs settling in a piggyback fashion on chromite grains. However, one should not generalize the PGMs as a group, as it is possible that some early-formed Os- and Ir-bearing laurite might behave in the manner as proposed by Hiemstra (1979).

Furthermore, the present results do not unequivocally lend support to the suggestion of Naldrett (2009) and Naldrett et al. (2012) that Pt and Pd were controlled by a different process than that responsible for the concentration of Rh, Ru, Os, and Ir. Naldrett (2009) and Naldrett

et al. (2012) contended that the segregation of sulfide liquid contributed Pt and Pd, some Rh, Ru, Ir, and Os, and chromite, but that the chromite grains themselves concentrated a significant proportion of the IPGEs, largely by encapsulating laurite and alloys that were present in the magma. In the present case of the UG-2, however, there are no obvious indications toward an IPGE-chromite coprecipitation, or a clear-cut separation of the various PGEs from each other. Instead, it is proposed that the primary control was coprecipitation of chromite and sulfide, the latter containing virtually all PPGEs at an early stage. Their fate down-temperature toward a bimodal distribution, contained in sulfide and hosted in discrete PGMs, will be described below.

Pentlandite holds elevated concentrations (hundreds of ppm, up into the percent range) of Pd and Rh, whereas Pt contents are extremely low. These concentrations account well for the Pd- and Rh-rich PGMs "missing" in the PGM assemblage. Indeed, Pd and Rh contents of pentlandite from the Merensky Reef vary between 200 and 1,750 ppm Pd and 40 and 1,000 ppm Rh (Paktunc et al. 1990, Ballhaus & Ryan 1995, Godel et al. 2007, Greß 2012, Osbahr et al. 2013). Maximum PGE contents reported for sulfides of the UG-2 from the eastern Bushveld (Kuhlmann et al. 2006, Josties 2012, Osbahr et al. 2014)) are 1.15 wt % Pd and 8.6 wt % Rh in pentlandite, and up to 4.23 wt % Rh in pyrite. Todd et al. (1982), Cabri et al. (1984), and Gervilla et al. (2004) detected contents of up to 3.3, 1.36, and 1.1 wt % Pd in pentlandite, respectively, from the Stillwater Complex. In the Main Sulfide zone of the Great Dyke, maximum concentrations of Pd and Rh in pentlandite are 2,506 ppm and 562 ppm, respectively (Oberthür et al. 1997a, 2003). Accordingly, elevated contents of Pd in pentlandite are known from a number of PGE mineralization, where Pd^{2+} substitutes for Ni^{2+} in the pentlandite lattice. The Pd and Rh contents in pentlandite (max 2.2 and 3.0 wt %, respectively) identified in the present study represent the highest PGE contents analyzed in pentlandite from the UG-2 of the western Bushveld Complex. The fact that pentlandite is able to carry high concentrations of Pd and Rh in its crystal lattice suggests that a large proportion of the PGEs were introduced bound in sulfides that co-segregated with chromite. It is postulated that all PGEs were primarily scavenged by sulfide in the magmatic stage due to their high partition coefficients in favor of sulfide (Mungall & Naldrett 2008). This suggestion is supported by experimental data of Ballhaus & Ryan (1995), who stated that the entire PGE content (500 ppm) of the sulfide fraction of the Merensky Reef can easily be accommodated in solid solution in base metal sulfides at temperatures as low as

500°C.

Naldrett et al. (2012) noted a special problem with Rh in chromitites, namely a preferred mineralogical concentration of this element in the relatively early-formed PGM hollingworthite [RhAsS], related to higher concentrations of As in the Bushveld Complex magma. Indeed, Rh tends to form discrete PGMs like hollingworthite in a chromitite (Merkle 1992) or sulfide environment (Mostert et al. 1982, Oberthür et al. 2003), in the case that sufficient quantities of As are available in the system. However, our present study of the UG-2 revealed a near-complete absence of arsenides, indicating very low concentrations of this possible reaction partner. Therefore, Rh was forced to remain bound to the sulfide in the crystal lattice of pentlandite.

Upon cooling, the PGE-bearing sulfide droplets recrystallized, via monosulfide solid solution (mss) and intermediate solid solution (iss), as described, for example, by Naldrett (2004a) and Dare et al. (2010), to finally form aggregates of pyrrhotite, pentlandite, chalcopyrite, and subordinate pyrite. As suggested by Gain (1985), Von Gruenewaldt et al. (1986), Naldrett & Lehmann (1987), and Naldrett et al. (2012), part of these sulfides were subsequently removed by late magmatic fluids and/or by reaction of sulfide with chromite. The further development down temperature was accompanied by continuous subsolidus annealing of the sulfides and their internal crystal ordering, whereby the overwhelming proportions of Pd and Rh were taken up in the crystal lattice of pentlandite. In comparison with the Pd and Rh contents of pentlandite from the Merensky Reef (max values of 1,750 ppm Pd and 1,000 ppm Rh in pentlandite; Greß (2012); Osbahr et al. (2013), our data (max 2.2 wt % Pd and 3.0 wt % Rh in pentlandite) indicate 10- to 30-fold enrichment of these elements in "residual" pentlandite.

As Pt is incompatible with any of the sulfides forming (Barnes et al. 2006), this metal was expelled from the crystal lattices of the sulfides. Platinum released from sulfides during the annealing process readily formed PGMs such as cooperite-braggite and Pt-Fe alloy. In a similar manner, Ru formed laurite (Ir- and Os-bearing), probably early, under existing magmatic conditions (Brenan & Andrews 2001, Bockrath et al. 2004).

The PGEs are bimodally distributed in the UG-2. Large proportions of Pd and Rh are hosted in pentlandite, whereas Pt and the IPGEs are dominantly present in the form of discrete PGMs. The distribution patterns of the various PGMs suggest that a large quantity of the PGEs, primarily concentrated in sulfide at magmatic conditions, was redistributed following the crys-

tallization of sulfides in the subsolidus stage.

Disseminated, rare sulfides (mainly pentlandite and chalcopyrite; note near-absence of pyrrhotite and pyrite) are found in the interstices of chromite grains only. PGM grains are present in all chromitite sublayers, locked within, or more commonly, at the margins of sulfide grains. In accordance with earlier work on the UG-2 (Kinloch 1982, McLaren & De Villiers 1982, Viljoen & Schürmann 1998, Penberthy & Merkle 1999, Schouwstra et al. 2000, Voordouw et al. 2010), the major PGMs are Pt-Fe alloy, laurite, cooperite braggite, malanite-cuprorhodsite in varying proportions, and some rarer compounds. Notably, the present PGM assemblage from the Karee mine is dominated by Pt-Fe alloy, laurite, and cooperite-braggite. The largest numbers of PGM grains were detected in the samples with the most elevated whole-rock Pt and Pd contents. In general, the PGMs are Pt-rich (Pt-Fe alloy, cooperite-braggite) or IPGE-rich (laurite). Palladium- and Rh-bearing PGMs are infrequent, as these elements are mainly hosted in pentlandite. The mineralogical siting especially of the Pt- and IPGE-rich PGMs in the ores, within or at the peripheries of sulfide grains, indicates that they originally coprecipitated with sulfide and were later, down-temperature, expelled from the crystal lattice of the annealing sulfides. It is known that laurite may be a stable phase at magmatic temperatures and may have formed early (Brenan & Andrews 2001, Bockrath et al. 2004). Platinum is not compatible with any of the sulfides forming (Barnes et al. 2006) and therefore combined with available reaction partners, in our UG-2 case with sulfur or iron to form discrete PGMs (cooperite-braggite, Pt-Fe alloy).

7.6 Conclusions

1. Whole-rock data reveal that Pt and Pd are heterogeneously distributed within the UG-2 sequence. Elevated Pt and Pd concentrations are found at the base and in the center of the main UG-2 chromitite seam. Platinum and Pd show a distinct covariation, but are not linked continually with Cu, Ni, or S contents.

2. Chromite compositions show distinct cryptic variation, leading to the subdivision of the UG-2 chromitite sequence into 10 separate sublayers. With exception of the bottom sublayer, these are characterized by stepwise trends, from bottom to top, of decreases in Mg# concomitant with increases in Cr# and TiO_2 contents in chromite (trend A of Naldrett (2009) and Naldrett

et al. (2012). The cryptic trends in chromite chemistry point to differentiation in situ rather than accumulation of the chromitite layers by slurries (Maier et al. 2013) or injection of chromitite seams as sills (Voordouw et al. 2009).

3. The bottom chromitite sublayer in contact with a pegmatoidal pyroxenite shows distinctly different trends in chromite chemistry, i.e., downward enrichment of Fe and Cr and concomitant depletion of Mg and Al in chromite. These unusual compositions are linked to the late-magmatic-hydrothermal alteration (pegmatoidal pyroxenite showing pervasive anthophyllite alteration). Alternatively, the first chromitite sublayer was chemically different (high-Cr-Ti-Fe) from the succeeding sublayers, and may have metasomatized the underlying pyroxenite.

4. Within the UG-2 chromitite, sulfides (mainly pentlandite and chalcopyrite) are scarce and occur mainly interstitial to chromite grains.

5. The PGEs are bimodally distributed in the UG-2. Platinum, Ru, and Os are dominantly present in the form of discrete PGMs, whereas large proportions of the Pd and Rh (and also Ir) are hosted in pentlandite.

6. PGMs are almost always associated with sulfides. The main PGMs are Pt-Fe alloy (30%), laurite (29%), and cooperite-braggite (26%). PGMs are mainly Pt- or Ru- and Os-rich, whereas Pd- and Rh-bearing PGMs are scarce.

7. Large proportions of Pd and Rh are hosted in pentlandite (max 2.2 wt % Pd and 3.0 wt % Rh), whereas Pt and IPGE contents in pentlandite are low. The Pd and Rh contents of pentlandite demonstrate that a large proportion of the PGEs were introduced bound to sulfides which co-segregated with chromite.

8. The present study signifies that primarily, PGE-rich magmatic sulfides segregated contemporaneously with chromite. Subsequently, large proportions of these sulfides were removed mainly by reaction of sulfide with chromite. Upon cooling, the PGE-bearing sulfide droplets recrystallized, thereby leading to a bimodal distribution of the PGEs in the UG-2; the bulk of the Pd and Rh is hosted in pentlandite, whereas Pt, Ru, and Os, apparently incompatible in the residual sulfides, formed a distinct suite of discrete PGMs.

Chapter 8

Platinum-group elements and minerals in the Lower and Middle Group chromitites of the Bushveld Complex

This chapter is slightly modified after: Junge, M., Oberthür, T., Osbahr, I. and Gutter, P. (2016): Platinum-group elements and minerals in the Lower and Middle Group chromitites of the western Bushveld Complex, South Africa. Mineralium Deposita: 51, 841-852.

8.1 Introduction

The 2,050 Ma old (Scoates & Friedman 2008) Bushveld Complex in South Africa is the largest layered mafic-ultramafic intrusion on Earth and contains the largest resources of platinum-group elements (PGE) on Earth as well as economically important reserves of chromium and vanadium (Von Gruenewald 1977, Vermaak 1995, Zientek et al. 2014). The PGE mineralization in the Bushveld Complex is mainly confined to a layered sequence of mafic-ultramafic rocks referred to as the Rustenburg Layered Suite which is subdivided into the Marginal, Lower, Critical, Main and Upper Zones (Hall 1932). Today's economic PGE deposits are three major ore bodies, namely the Merensky Reef, the Platreef, and the UG-2 chromitite, the only chromitite layer in

the Bushveld Complex mined for PGE as the primary economic metal. However, all chromitite seams contain elevated PGE concentrations ranging from 0.5 to 9 g/t (Cawthorn 1999a, Naldrett et al. 2012). Sylvania Platinum Ltd. is reworking chromite dumps from the LG-6 and MG-1/2 chromitites from the eastern and western Bushveld Complex and successfully produces saleable concentrates of both PGE and chromite. The recovery of PGE as a byproduct from both active chromite mining operations and reworking of old chromite mine dumps from the Lower Group (LG) and Middle Group (MG) chromitites is therefore an excellent opportunity to add value to the primary chromite resources.

The samples of this study were obtained from the recovery plants of Sylvania Platinum Ltd. in the western Bushveld Complex (Fig. 8.1). The feed material for the PGE concentrates mainly originates from the chrome tailings dumps of the about 1-m-thick LG-6 chromitite at the Millsell and from the about 0.5-m-thick MG-2 chromitite at the Mooinooi operation, as well as from the recent mine production from the nearby Millsell and Mooinooi plants. The PGE-enriched concentrates from the flotation of the chrome dumps material from both plants were studied in detail to unravel the deportment of the PGE and the nature of the platinum-group minerals (PGM) in the ores.

This work is a complementary study to our earlier investigation on the LG/MG chromitites of the eastern Bushveld Complex (Oberthür et al. 2016a). The aims of the study are (i) to determine the distribution of the PGE in the LG-6 and MG-2 chromitites, (ii) to determine the PGM assemblages using automated mineralogical analysis, (iii) to acquire data on the concentrations of PGE in sulfides, and (iv) to compare the obtained data with published work on the eastern Bushveld Complex. So far, little information exists on the distribution of PGE and the PGM assemblage of the LG and MG chromitites. Automated mineralogy techniques as used in this study provide statistically robust data on the mode of occurrence of PGM in these chromitite seams which is also of value to the metallurgical treatment of the ores. The new information also conveys valuable knowledge on PGE fractionation processes in general, PGM assemblages in chromite environments, and the partitioning of semimetals between monosulfide solid solution (mss) and sulfide melt.

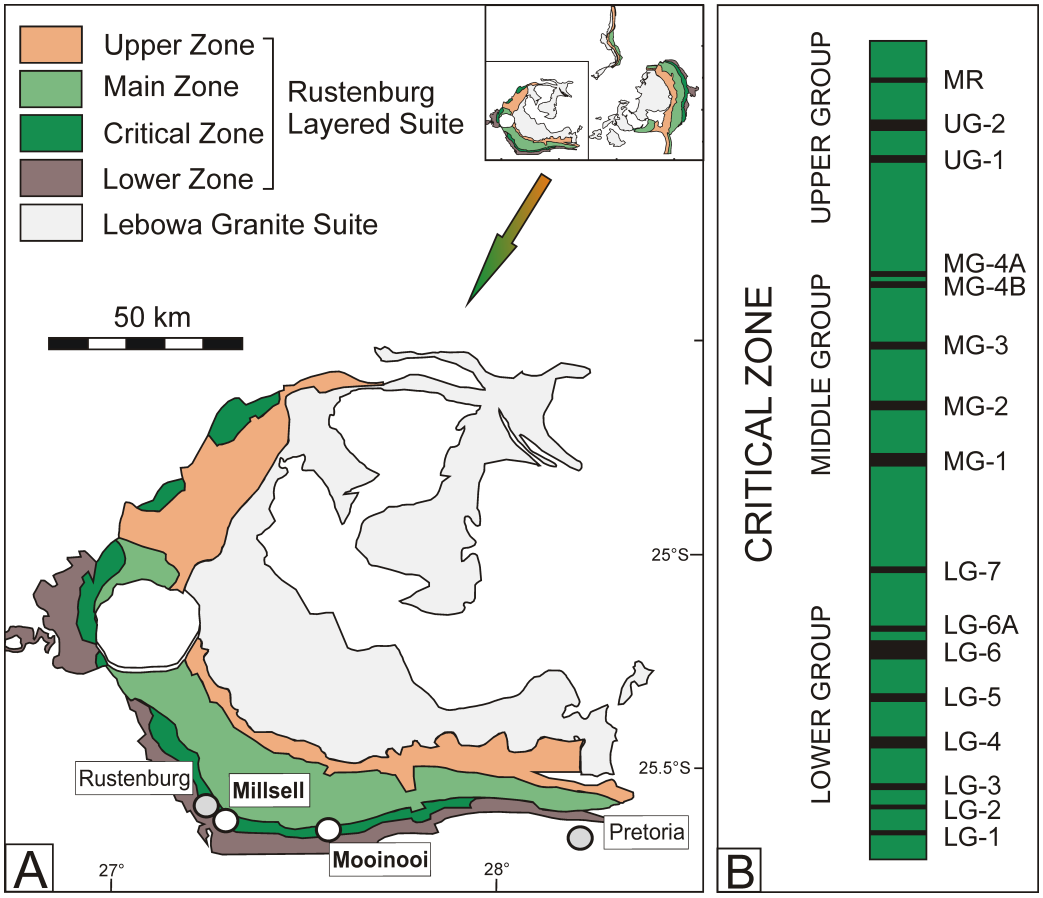

Figure 8.1 – Geological map of the western Bushveld Complex with the locations of the plants of Sylvania, Millsell and Mooinooi. B. Schematic stratigraphic column of the Critical Zone showing the chromitite seams and the Merensky Reef (MR). Modified after Oberthür et al. (2016a).

8.2 Previous work

The correlation between chromite and PGE is remarkably well expressed in the Bushveld Complex; even the thinnest chromitite stringers contain elevated concentrations of PGE (Maier et al. 2013). The UG-2 chromitite has been investigated in great detail (McLaren & De Villiers 1982, Gain 1985, Hiemstra 1985, 1986, Maier & Barnes 2008, Cawthorn 2011, Junge et al. 2014, 2015b, Osbahr et al. 2014), however, studies on the distribution of PGE and the mineralogical character of the PGM in the LG and MG chromitites are scarce Lee & Parry (1988), Merkle (1992), Teigler & Eales (1993), Naldrett et al. (2009, 2012), Kotzé & Gauert (2014) and Oberthür et al. (2016a).

Regarding PGE mineralogy, Lee & Parry (1988) identified laurite as the most common PGM in the MG chromitites, followed by cooperite-braggite, a PdRhCuS phase, PtFe alloys, and PtRhAsS associated with base metal sulfides. Kotzé & Gauert (2014) reported laurite, cooperite-braggite and Pt-Fe alloys as the major PGM in a sequence from LG to MG chromitites. A larger number of studies exist for the UG-2 chromitite, which generally agree that the main PGM are cooperite-braggite, laurite, Pt-Fe alloys, and minor malanite/cuprorhodsite (Kinloch 1982, McLaren & De Villiers 1982, Viljoen & Schürmann 1998, Schouwstra et al. 2000, Kuhlmann et al. 2006, Junge et al. 2014, Osbahr et al. 2014). Merkle (1992) studied a drill core covering chromitites of the MG of the western Bushveld Complex and showed that the PGM are dominantly sulfides, arsenides and sulfarsenides and that laurite typically occurs as inclusions in chromite. The PGE mineralogy in sulfide-rich systems such as the Merensky Reef and the Platreef in the Bushveld Complex, as well as the Main Sulfide Zone in the Great Dyke is typically dominated by (Pt,Pd)-bismuthotellurides, cooperite-braggite and minor sperrylite and sulfarsenides (Oberthür et al. 2003, Holwell & McDonald 2007, Osbahr et al. 2013, Junge et al. 2015a).

Oberthür et al. (2016a) studied the distribution of PGM in the LG-6 and MG-1/2 chromitites of the eastern Bushveld Complex and reported that the main PGM are various Pt-Pd-Rh sulfides (cooperite-braggite [(Pt,Pd)S] and malanite/cuprorhodsite [$CuPt_2S_4$]/[$CuRh_2S_4$]), laurite [RuS_2], the main carrier of the IPGE (Os, Ir, Ru), sulfarsenides [(Rh,Pt,Ir)AsS], sperrylite [$PtAs_2$], Pt-Fe-alloys, and a large variety of mainly Pd-rich PGM.

Palladium and Rh contents in sulfides (mainly pentlandite) may range up to thousands of ppm in ores associated with mafic-ultramafic intrusions (Cabri et al. 1984, Cabri 1988, Oberthür et al. 1997a, 2003, Osbahr et al. 2013, 2014, Junge et al. 2014, 2015b). In the base metal sulfides of the chromite layer of the Stillwater Complex, Barnes et al. (2016) reported concentrations of Pd, Rh and Ru in the 250 to 300 ppm range. Oberthür et al. (2016a) reported up to some hundred ppm of Pd in pentlandite from the LG and MG chromitites of the eastern Bushveld Complex.

8.3 Methodology, Samples and Analytical Methods

The flotation concentrates were obtained from the recovery plants of Sylvania Platinum Ltd. at Millsell (LG-6 chromitite) and at Mooinooi (MG-2 chromitite) in the western Bushveld Complex (Fig. 8.1). The feed at Millsell and Mooinooi originates both from current mining operations and from mine dumps. The dump feed at Millsell has an average grade of 1.8 g/t 4E (Pt, Pd, Rh, Au) and the production from the mining operations comprises 8,000 tonnes per month. On average the total feed at Millsell comprises 1.63 g/t 4E at a Cr_2O_3 content of 23%. Both recovery plants use gravity separation such as spirals and cyclones for the recovery of chromite as well as flotation of the chromite dumps material for the production of PGE concentrates. At Mooinooi and Millsell, a final chromite concentrate with 44% Cr_2O_3 is produced (Sylvania 2010). More details on the ore processing can be found at the Sylvania website (www.sylvaniaplatinum.com).

The concentrates were analyzed for PGE by ACTLABS, Canada, using nickel sulfide fire assay followed by instrumental neutron activation analysis (INAA). For the INAA method three different Merensky Reef reference materials from the African Mineral Standards (AMIS0254, AMIS0367 and AMIS0396) were used. Nickel and Cu concentrations are determined by ICP-MS and S contents by ICP after sodium peroxide fusion. For Ni and Cu a jasperoid (GXR-1) and a porphyry copper ore (GXR-4) from the US Geological Survey, and for S analysis a zinc-tin-copper-lead ore from Mount Pleasant mine (MP-1b) from the Canadian Certified Reference Materials Project were used as reference material. The results of the reference materials are given in the electronic appendix. Polished sections were prepared for reflected light microscopy, scanning electron microscope (SEM) and microprobe work at BGR in Hannover.

Quantitative mineralogical analysis using the Mineral Liberation Analyser (MLA) software

was carried out using a FEI-Quanta 650 F field emission scanning electron microscope (FE-SEM) equipped with two Bruker Quantax X-Flash 5030 energy dispersive X-ray spectroscopy (EDS) detectors and FEI's MLA suite 3.1.4 software for data acquisition, at the Helmholtz Institute Freiberg for Resource Technology, Germany. In-depth information on the MLA system and PGM identification can be found in Fandrich et al. (2007), Gu (2003) and Osbahr et al. (2015). In the present study, the sparse phase liberation (SPL)-Lite measurement mode was applied for the identification of PGM grains with high spatial resolution and accuracy (Fandrich et al. 2007). In this mode, a series of BSE images is collected and only mineral grains matching defined grey-scale ranges are analyzed by EDS. A summary of tangible instrumental parameters is given in Table 8.1. Polished sections of the concentrates were analyzed in a first run, then re-ground and re-polished and analyzed again in a second run.

Pentlandite grains were analyzed with a CAMECA SX 100 electron microprobe using the following analytical conditions: 20 kV acceleration voltage, 120 nA probe current and up to 180 s measuring time (backgrounds are half time of peak). The following elements were analyzed: Al (Kα), Si(Kα), S(Kα), Cr(Kα), Fe(Kα), Co(Kα), Ni(Kα), Cu(Kα), As(Lα), Se(Lα), Rh(Lα), Pd(Lα), Ag(Lα) and Pt(Lα). Synthetic metals (for Si, Cr, Pd, Rh, Pt, Ag, Co, Se), natural pentlandite (S, Fe, Ni), chalcopyrite (Cu), synthetic gallium-arsenide (As) and chromite (Al) were used as standards. Average detection limits were 75 ppm for Co, 100 ppm for Se, 120 ppm for Rh, 140 ppm for Pd, 160 ppm for Ag and 300 ppm for Pt. Corrections were performed using the PAP program supplied by CAMECA, and further interferences were corrected using a spreadsheet developed at BGR.

Table 8.1 – Summary of MLA parameters. Spot size of 5.704 equates to a ca 10 nm beam diameter.

SEM parameters		MLA parameters	
Voltage (kV)	25	Scan speed	16
Working distance (mm)	13	Resolution	1000 x 1000
Probe current (nA)	10	Pixel size (μm)	0.6
Spot size	5.704/5.9*	Acq. time (ms)	5
Horizontal Field Width (μm)	600	SPL BSE trigger	95-255
Brightness	93.77	Minimum grain size (px)	2
Contrast	19.40		
BSE calibration	Au 245		

8.4 Results

8.4.1 Geochemistry

Bulk analyses (PGE, Au, Ni, Cu and S) of the PGE flotation concentrates from Millsell (LG-6) and Mooinooi (MG-2) are presented in Table 8.2. The Pt/Pd, Pd/Ir and PPGE/IPGE (Rh,Pt, Pd/Os,Ir,Ru) ratios are similar at Millsell and Mooinooi and are all above unity. C-1 chondrite-normalized PGE distribution patterns of both the Millsell and the Mooinooi concentrates (Figure 8.2) display positive slopes from Os to Rh and a drop from Pt to Pd. These patterns are largely parallel to those of the chrome tailings dumps, the feed material for the PGE concentrates, from Millsell and Mooinooi, as well as to those of the LG-6, MG-1, MG-2 and UG-2 chromitites presented in the literature (Scoon & Teigler 1994, Junge et al. 2014) and the data of four concentrates of the LG-6 and MG-1/2 from the eastern Bushveld (Oberthür et al. 2016a), indicating that no apparent fractionation takes place during ore processing. The similar distribution pattern between the Millsell and Mooinooi concentrates with the respective tailing and literature data allows the comparison of the PGE and PGM distribution between the LG-6 and MG-1/2 chromitites.

8.4.2 Mineralogy

According to X-ray diffraction analysis, the main mineral components of both flotation concentrates (Millsell and Mooinooi) are talc and minor chlorite/vermiculite, calcite and orthopyroxene. Ore microscope and SEM studies showed that the sulfides (chalcopyrite, pentlandite, pyrite and rare millerite) and the PGM are largely liberated in the concentrates and occur as single grains or in grain aggregates (Fig. 8.3). Sulfide grain aggregates range in size from <1 to about 60 μm.

8.4.3 Mineral Liberation Analysis (MLA)

Our MLA application subdivides major groups of PGM into PGE-sulfides (malanite, cooperite, braggite, laurite, and vysotskite), PGE-sulfarsenides (irarsite and hollingworthite), Pt-Fe-alloys

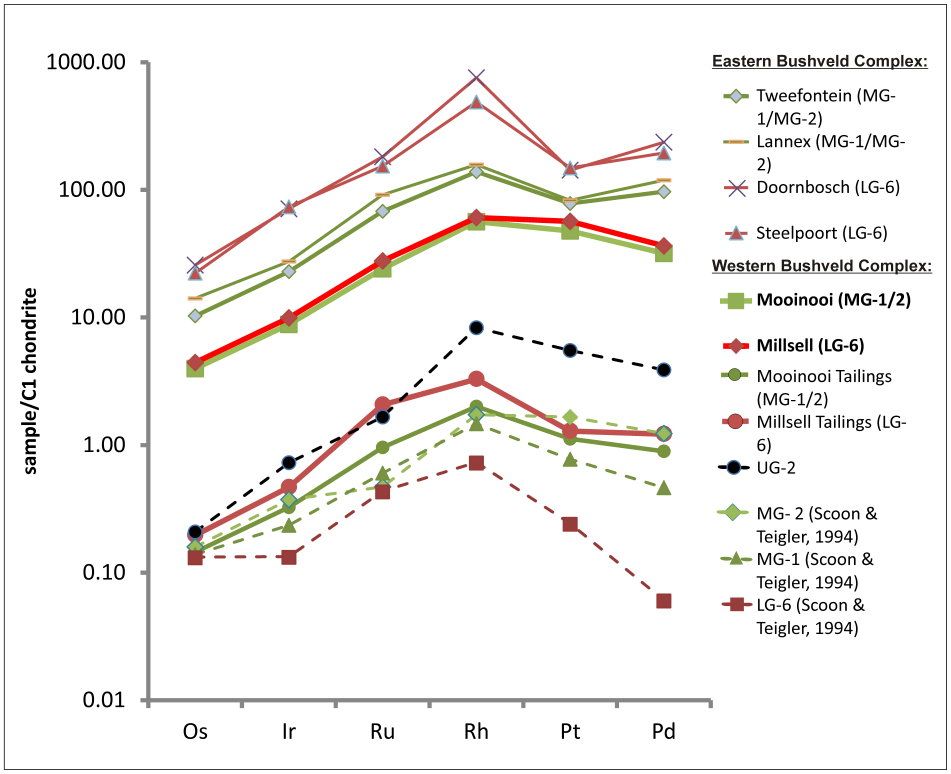

Figure 8.2 – Chondrite normalized PGE-distribution pattern of Millsell (LG-6) and Mooinooi (MG-2) of the western Bushveld Complex. For comparison flotation concentrate PGE data from processing plants of the LG-6 and MG-1/2 of the eastern Bushveld Complex (Oberthür et al. 2016a) and whole-rock data from the LG-6, MG-1, MG-2 (Lee & Parry 1988) and UG-2 (Junge et al. 2014) from the literature is plotted. C1-chondrite values are taken from McDonough & Sun (1995).

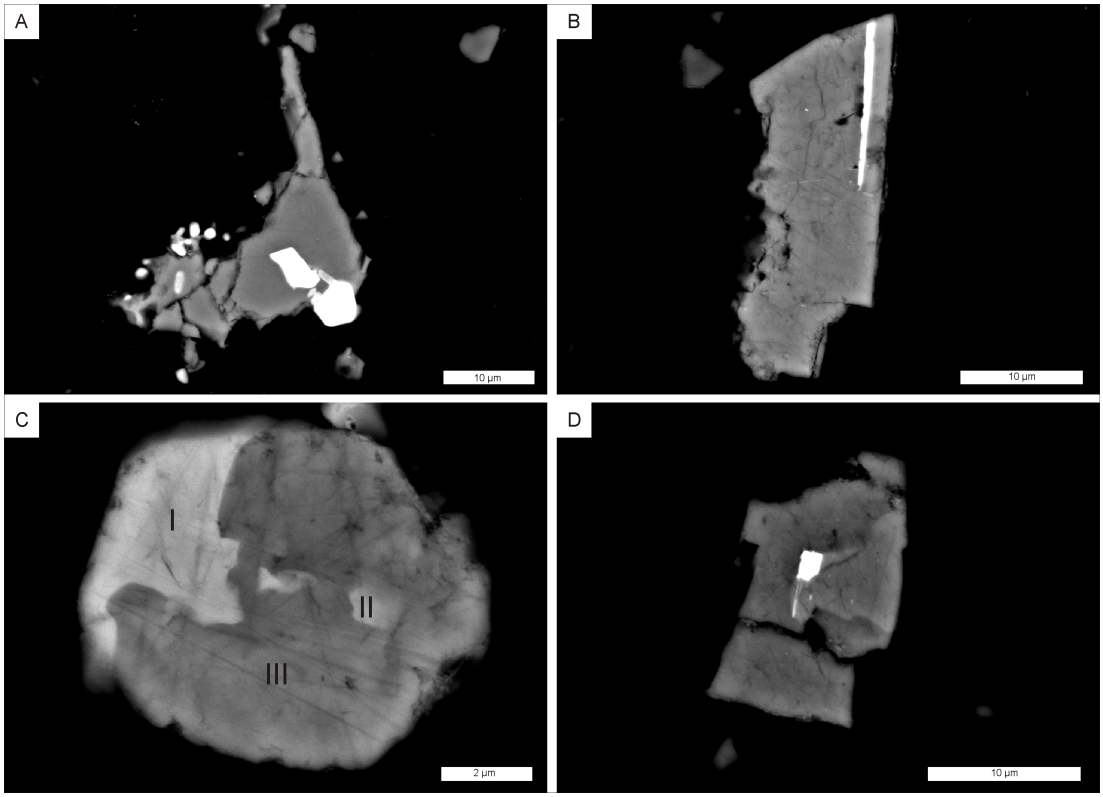

Figure 8.3 – Back-scattered electron images of sulfide and PGM grains. A: Grains of hollingworthite (white) in pyrite (gray). B: Malanite (white) in pentlandite (gray). C: Sperrylite (I), stibiopalladinite (II) and hollingworthite (III). D: Malanite (white) in pentlandite (medium gray) and pyrite (dark gray).

Table 8.2 – Bulk analysis data of PGE, Au, Ni, Cu and S, as well as Pt/Pd and PPFE/IPGE ratios of flotation concentrates of Millsell and Mooinooi from the plants of Sylvania Platinum Ltd (analyzed by ACTLABS, Canada).

	Millsell (LG-6)	Mooinooi (MG-2)
Os [ppb]	2170	1950
Ir [ppb]	4520	4010
Ru [ppb]	19,700	17,100
Rh [ppb]	7890	7320
Pt [ppb]	57,200	48,200
Pd [ppb]	20,000	17,500
Au [ppb]	145	145
Ni [ppm]	1790	1690
Cu [ppm]	1010	863
S [wt.%]	0.33	0.37
Pt/Pd	2.86	2.75
Pd/Ir	4.42	4.36
PPGE/IPGE	3.22	3.16
PGE [ppm]	111.5	96.1

(iso- and tetraferroplatinum), zvyagintsevite and sperrylite. Cooperite, braggite and vysotskite are grouped as PGE-sulfides [(Pt,Pd)S] in the following, and the members of the malanite-cuprorhodsite solid solution series as malanite (Fig. 8.4).

The number of grains, the areas occupied in square micrometers, and grain sizes are important factors in describing the PGM and their distribution in the ores. In the LG-6, grain sizes of the PGM range from 2 to 20 μm), and laurite may reach up to 35 μm). In the MG-2, the PGM show similar grain sizes (up to 15 μm)), however, Pt-Fe-alloys represent the biggest grains with up to 45 μm) in diameter.

Mineral proportions of the PGM (number of grains and areas, in %) in the Millsell (LG-6) and Mooinooi (MG-2) concentrates are shown in Figure 8.5. By number of grains, malanite is the most dominant phase (25 to 29%) both at Millsell and Mooinooi, followed by PGE-sulfarsenides (18 to 20%). Common are laurite (14 to 16%) and [(Pt,Pd)S] (Millsell 13%, Mooinooi 11%, respectively), and sperrylite makes up 9% and 10% at Millsell and Mooinooi, respectively, whereas Pt-Fe-alloys comprise 3% and 4%, respectively. Zvyagintsevite [Pd_3Pb] and stibiopalladinite [$Pd_{5+x}Sb_{2-x}$] are minor constituents (<2%). Other PGM like moncheite [$PtTe_2$], potarite [PdHg] and atokite [Pd3Sn] together represent around 10%.

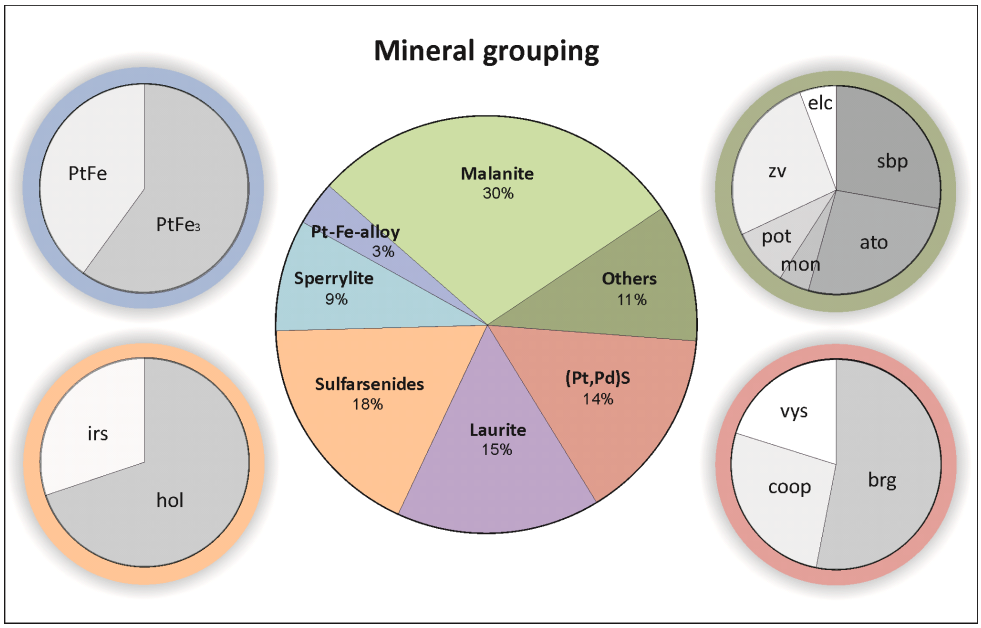

Figure 8.4 – Structure of mineral grouping of PGM. Example based on grain count data from the LG-6 (Millsell). Abbreviations: irarsite (irs), hollingworthite (hol), zvyagintsevite (zv), potarite (pot), moncheite (mon), atokite (ato), stibiopalladintite (sbd), electrum (elc), vysotskite (vys), cooperite (coop), braggite (brg).

Considering area %, laurite is the most dominant phase at both locations (24% at Millsell and 28% at Mooinooi), followed by malanite (22 and 20%), [(Pt,Pd)S] (12 and 16%), PGE-sulfarsenides (12%) and sperrylite (11 and 8%).

It has to be kept in mind that the concentrates have experienced various stages of crushing, milling, sieving and finally flotation. Also due to this fact, a large number of grains show free surfaces, namely 52% in the MG-2 and even 67% in the LG-6. Laurite is often observed as inclusions in chromite (Merkle 1992, Penberthy et al. 2000, Junge et al. 2014, Oberthür et al. 2016a). A certain proportion of these laurite grains is liberated during ore processing of the chromitite and show free surfaces in the concentrate. The amount of PGM associated with chromite in the original ore is therefore probably larger than shown in the concentrates. As at least part of the free surfaces represents cracks from crushing, only the remaining PGM grains were taken into consideration in discussing mineral associations. These PGM are mostly associated with silicates (54 and 60% in the LG-6 and MG-2, respectively), followed by sulfides (37 and 32% in the LG-6 and MG-2, respectively). Rarer associations are with chromite (2%) or other PGM (5 to 7%). Less than 1% of the PGM are associated with carbonates, Fe-oxides or

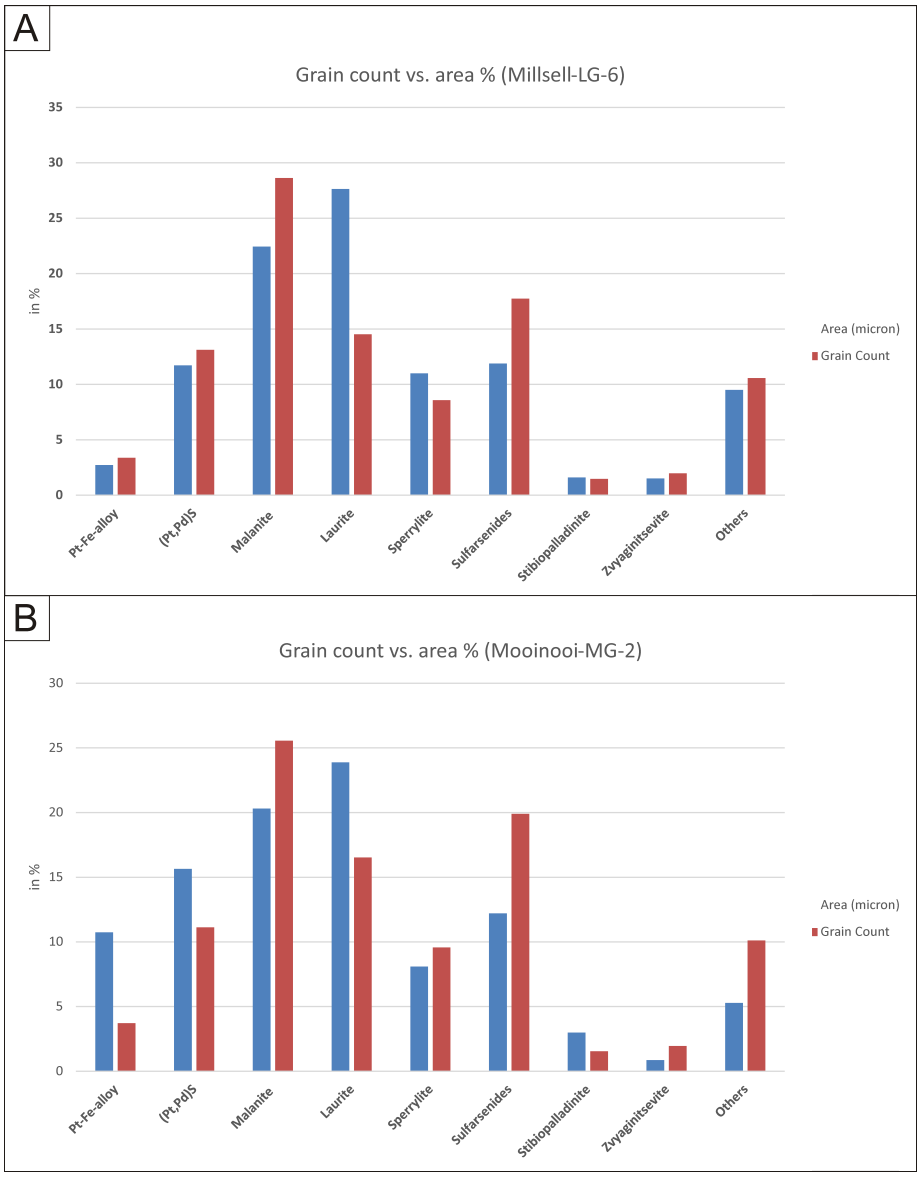

Figure 8.5 – Number of grains in % from A. Millsell and B. Mooinooi. Area in μm^2 normalized to 100% PGM.

rutile (Fig. 8.6).

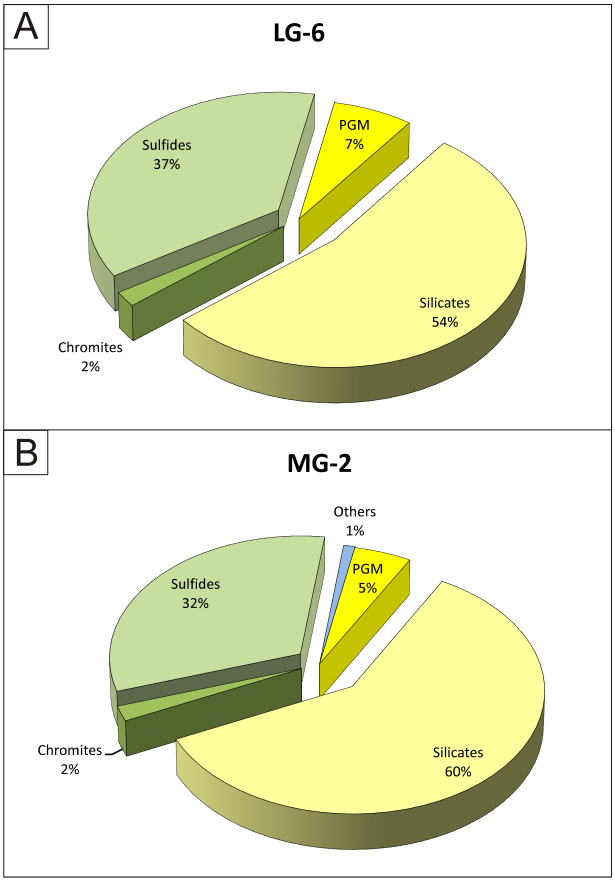

Figure 8.6 – Mineral association proportions based on MLA data. A. PGM concentrate from Millsell (LG-6).: B. PGM concentrate from Mooinooi (MG-2) Mineral associations without free surface are normalized to 100%.

8.4.4 PGE in sulfides

The presence of elevated concentrations of Pd and Rh in sulfides (mainly pentlandite) ranging from some 100 ppm to a few wt% was shown in PGE ores from the Bushveld Complex (Godel et al. 2007, Holwell & McDonald 2007, 2010, Osbahr et al. 2013, 2014, Junge et al. 2014, 2015b). In the present study of pentlandite grains from Millsell (LG-6) and Mooinooi (MG-2) (both n=13), average contents of 385 and 1005 ppm Pd, respectively, were determined. Maximum contents in pentlandite were 7730 ppm Pd and 6020 ppm Rh. Furthermore, for the first time PGE contents were analyzed in some rare thiospinel grains of the polydymite-linnaeite-greigite series. In a grain with composition close to siegenite [$Ni_{1.5}Co_{1.2}Fe_{0.4}S_4$] 1430 ppm Pt

were detected, and a grain with the composition [$Ni_{2.2}Fe_{0.5}Cu_{0.3}S_4$] had 5370 ppm Rh and 1460 ppm Pd.

8.4.5 Mineral chemistry of chromite

Chromite grains within MG-2 chromitite of the western Bushveld Complex at Thaba Mine were analyzed for PGE and trace elements concentrations. A normalisation of MgO, Al_2O_3, TiO_2, V_2O_5, Cr_2O_3, MnO, FeO, NiO and ZnO to 100% was used, because these oxides comprise the major oxides.

Laser ablation-inductively coupled plasma-mass spectrometry measurements on chromite were carried out on a ThermoScientific Element XR (HR-ICP-MS) coupled with an femtosecond laser. The following isotopes were measured: ^{25}Mg, ^{27}Al, ^{29}Si, ^{34}S, ^{43}Ca, ^{47}Ti, ^{51}V, ^{53}Cr, ^{55}Mn, ^{57}Fe, ^{60}Ni, ^{63}Cu, ^{66}Zn, ^{67}Zn, ^{77}Se, ^{89}Y, ^{99}Ru, ^{101}Ru, ^{103}Rh, ^{105}Pd, ^{108}Pd, ^{111}Cd, ^{137}Ba, ^{139}La, ^{140}Ce, ^{147}Sm, ^{153}Eu, ^{172}Yb, ^{175}Lu, ^{185}Re, ^{189}Os, ^{193}Ir, ^{194}Pt, ^{195}Pt, ^{197}Au, ^{205}Tl. As reference materials the NIST610 (Jochum et al. 2011) and Lombard (Gilbert et al. 2012) were used. Beam size were about 40 μm and chromite grains are analyzed with a grid over the largest part of the grain. Analyses were carried out as 20 samples with 4 analysis spots at NIST610 and 4 on the Lombard followed by 12 on the sample.

The ablation spectrum was typically flat and no inclusions of laurite were identified (Figure 8.7). All PGE are below the detection limit but ^{99}Ru shows median values (n=18) of 264 ppb (total range from 171 to 365 ppb). In-situ LA-ICP-MS measurements of komatiitic chromite grains carried out by Locmelis et al. (2011) showed that Ru has concentrations of 220 to 540 ppb. Pagé & Barnes (2016) showed similar values of Ru contents in chromites of the Bushveld Complex (maximum values of 548 ppb).

8.4.6 Weathering of LG and MG chromitites

This chapter briefly summarizes and discusses the distribution of PGE in the LG and MG chromitite in the weathered, near-surface ores.

In pristine LG and MG chromitites PGE contents can vary up to 4 g/t (Cawthorn 1999a). Similar concentrations are observed in chromitite seams close to the surface (Table 8.3). Pal-

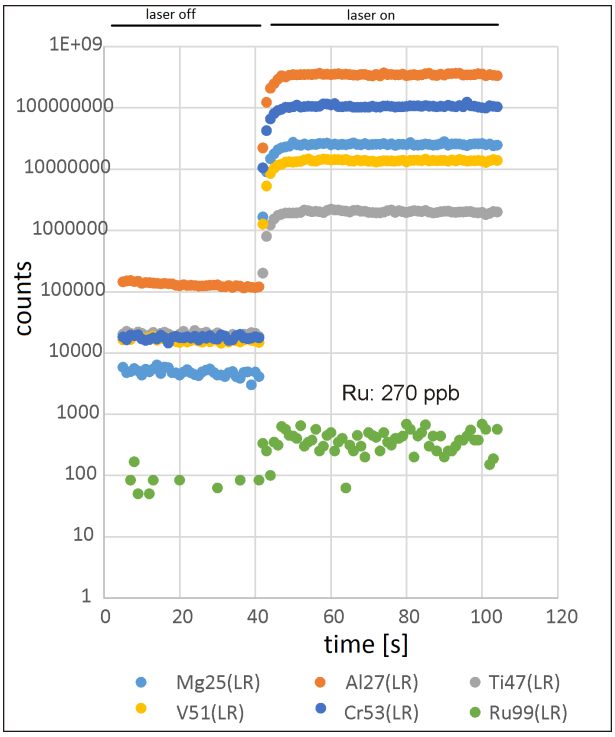

Figure 8.7 – Spectrum of chromite analysis (29jnd10).

ladium concentrations are typically lower than Pt, arguing for a larger mobility of Pd during weathering. Ruthenium contents are typically large, whereas Pt and Pd are lower in the near-surface ore than in the pristine ore. Laurite, as the main carrier of Ru, is often observed as inclusions within chromite grains. Chromite itself is also a carrier of Ru as shown in this study and by Locmelis et al. (2011) and Pagé et al. (2012). Therefore laurite grains within chromite are protected by the weathering processes. Smectite, vermiculite and carbonates are observed in weathered LG and MG chromitites. Mobilisation takes place both in hanging and footwall as elevated concentrations of Pt and Pd are observed as well as within smaller carbonate veins within the seams.

Table 8.3 – Whole-rock PGE and Au contents of LG-6, MG-1, MG-2, MG-3 and MG-4 from near surface ores at the Thaba Mine in the western Bushveld Complex. All in ppb.

	Os	Ir	Ru	Rh	Pt	Pd	PGE	Au
LG-6	60	76.5	642	27.9	91	57	954.4	5.1
MG-1	54	94.6	448	46.3	109	42	793.9	4.9
MG-2	31	80.7	640	68.7	157	41	1018.4	3.2
MG-3	71	143	522	86.2	395	80	1297.2	4.6
MG-4	< 2	12.5	150	8.1	716	54	940.6	6.8

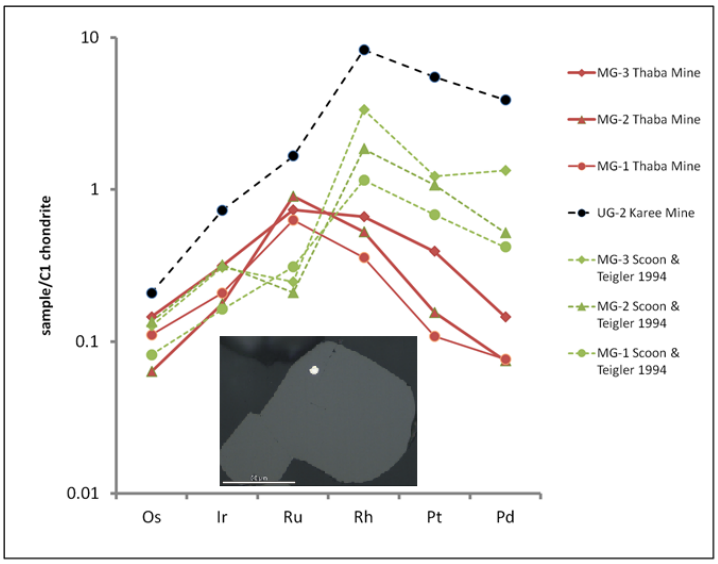

Figure 8.8 – Chondrite normalized PGE-distribution pattern of the LG-6, MG-1, MG-2, MG3 and MG-4 chromitite the western Bushveld Complex. For comparison whole-rock data from the LG-6, MG-1, MG-2 (Scoon & Teigler 1994) and UG-2 (Junge et al. 2014) from the literature is plotted. C1-chondrite values are taken from McDonough & Sun (1995). The relative constant IPGE concentrations are probably caused by the fact that inclusions of laurite in chromite are not submitted to weathering processes. Similarly, incorporation of IPGE in chromite are unaffected by weathering.

Figures 8.9 and 8.10 show BSE images of weathered LG-6 and MG-1 chromitites of the western Bushveld Complex at Thaba Mine. Chromite grains are partly zoned with Fe-rich core and -poor rim and with inclusions of ortho- and clinopyroxene (Figure 8.9A). Grains can be fractured or remain relatively unaffected but fracturing usually takes place at grain contacts of chromite grains, however, chromite grains within secondary silicates are typically intact (Figure 8.9B). Relict PGM are observed within silicates or as inclusions in chromite (mostly laurite) and often show cores of relict grains and rim of oxidized and typically without sulfur at the rims (Figure 8.9C,D). Irregular shaped grains are observed in secondary Fe-silicates, arguing for redistribution and neoformation of PGM (Figure 8.9AE,F). Larger grains of Pt-Fe are observed with weathered morphology (Figure 8.10A-D) which may be neoformed PGM. Former grains of PGM are observed in secondary Fe-silicates showing larger shapes but are locally redistributed (Figure 8.9E,F).

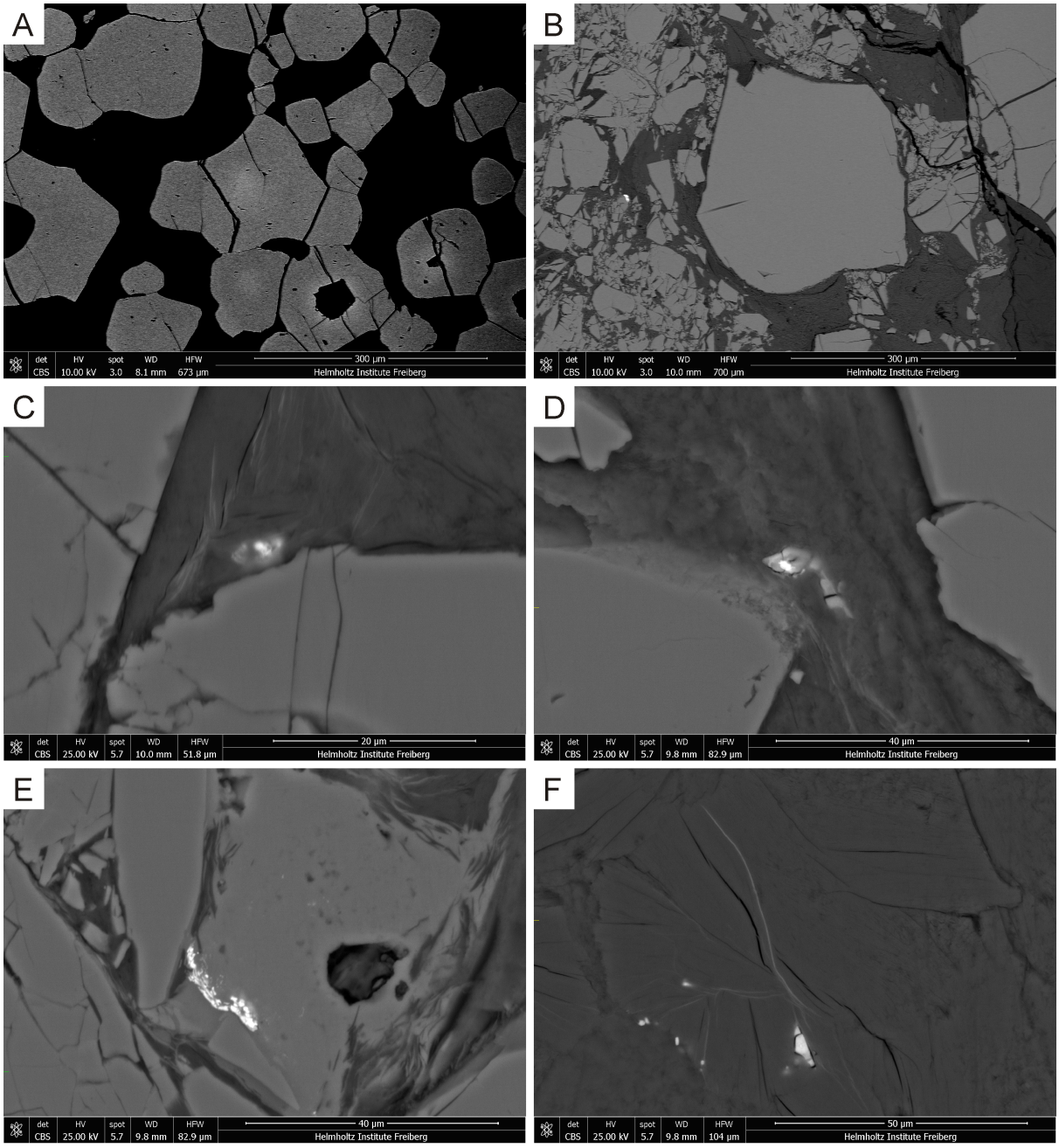

Figure 8.9 – Backscattered electron images of weathered chromitite seams of western Bushveld Complex (Thaba Mine). A: Slightly zoned chromite grains. LG-6 (AS11183). B: Larger alomst unaffected chromite grains surrounded by fractured chromite grains. MG-1 (AS11197). C: Weathered platarside (white core) surrounded by Pt-As-S-oxide. MG-1 (AS11197). D: Weathered hollingworthite surrounded by Rh-As-S-oxide. MG-1(AS11198). E: Platarside in secondary Fe-silicate. MG-1 (AS11198). F: Pt-Rh-Ir-phase in secondary Fe-silicate. MG-1 (AS11198).

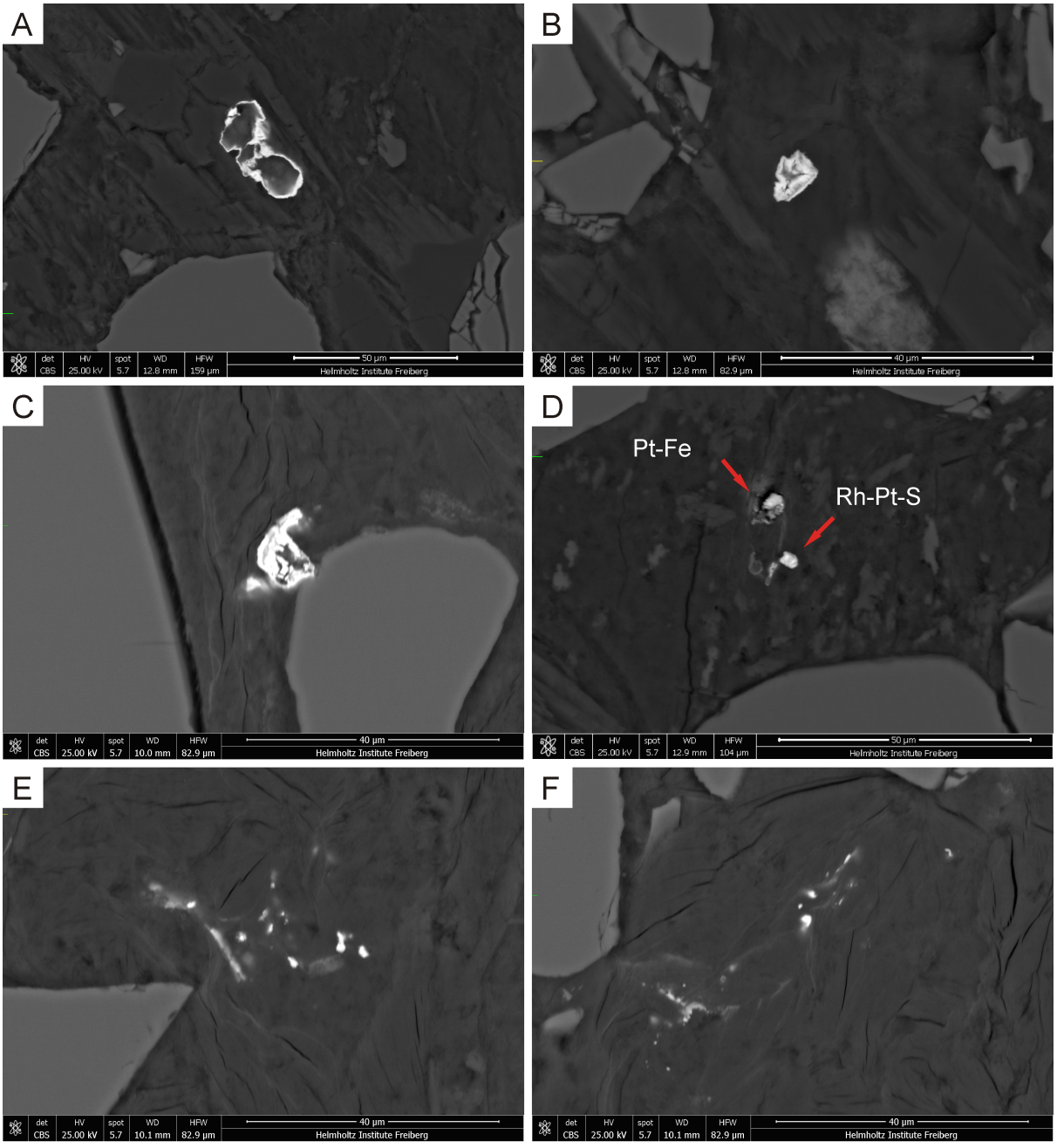

Figure 8.10 – A,B: Pt-Fe oxide in Fe-silicates. MG-1 (AS11199). C: Pt-Fe oxide in Fe-silicates next to chromite. MG-1 (AS11197. D: Weathered Pt-Fe alloy and Rh-Pt-sulfide. MG-1 (AS:11200). E,F: Stibiopalladinite in secondary Fe-silicate MG-1 (AS11197).

8.5 Summary and Discussion

The chondrite-normalized PGE distribution pattern of the flotation concentrates from the LG-6 and MG-2 chromitite, respectively chrome tailings material, from Millsell and Mooinooi and literature bulk-rock data of the LG-6 and MG-2 demonstrate that no preferential upgrade of any PGE has taken place during the flotation process, corroborating findings of Oberthür et al. (2016a) on concentrates of the eastern Bushveld Complex. This observation allows the comparison of PGE and PGM distribution of the LG-6 and MG-2 flotation concentrate with the chromitite seams on a statistical basis. LG-6 data of the literature show a negative slope from Rh to Pd which is less pronounced in tailings and concentrates of this study. This may indicate that Pt and Pd are relatively stronger enriched in the tailings and concentrates than Os, Ir, Ru and Rh.

Ore microscopy and SEM/MLA studies usually report the number of PGM grains only. However, modern analytical methods also allow determining area percentages of the various PGM. This important advance assists in the interpretation of data as one single large PGM grain can account for tens or hundreds of smaller PGM, and therefore large PGM would be underemphasized compared to more abundant but substantially smaller PGM although these have a minor impact on the bulk PGM content and the bulk metal budget (Cabri 2015). In our samples, the comparison of grain frequency and area percentage shows that e.g. laurite grains are on average larger than sulfarsenides, but there are relatively more grains of sulfarsenides . Laurite grains often occur as inclusions in chromite (Junge et al. 2014) and, as this PGM assemblage is based on flotation concentrates, small-sized laurite grains may not all be separated during processing.

Newly calculated area percentages of the PGM assemblages of LG and MG chromitites of the eastern Bushveld Complex presented by Oberthür et al. (2016a) are shown in the electronic supplementary appendix. Similar to Millsell and Mooinooi, the LG and MG chromitites of the eastern Bushveld Complex (LG-6: Doornbosch, Steelpoort and MG-1/2: Lannex, Tweefontein), laurite is overemphasized and sulfarsenides are underrated with respect to the area percentage. Further, malanite has a larger area percentage than frequency percentage data in the LG-6 than in the MG-1/2 chromitites, arguing that malanite has an even larger influence on the bulk potential

of PGM and the metal budget in the system in the LG-6 chromitites of the eastern Bushveld Complex than shown by frequency data only.

The PGM assemblages of the LG-6 and MG-2 chromitite samples from the western Bushveld Complex are very similar. However, in comparison with the data from the LG-6 and MG-1/2 chromitites of the eastern Bushveld (Oberthür et al. 2016a), the LG-6 and MG-2 chromitites of the western Bushveld generally contain more PGE-sulfarsenides compared to the seams (in particular the LG-6) of the eastern limb. With regard to arsenides and sulfarsenides, the PGM assemblages of Millsell and Mooinooi closely resemble those from Lannex and Tweefontein (both originating from the MG-1/2 chromitites) in the eastern Bushveld Complex.

A comparative summary of the PGM assemblages in LG/MG chromitites of the eastern and western Bushveld Complex is presented in Figure 8.11. Obviously, the differences in PGE mineralogy between LG and MG chromitites are less pronounced in the western than in the eastern Bushveld. The proportions of PGE-arsenides/sulfarsenides by number of grains in both the LG-6 and MG-1/2 are larger in the western (27 to 30%) than in the eastern Bushveld (11 to 26%), although low PGE-arsenides/sulfarsenides occur in the LG-6 of the eastern Bushveld. PGE-sulfides are less abundant in the LG-6 of the western (56%) than of the eastern Bushveld (68 to 69%). Also the amount of Pt-Fe alloys is less pronounced in the eastern (3 to 4%) compared to the western Bushveld Complex (7 to 12%). The area percentages show similar results and are given in the ESM.

Despite slight differences, the PGM assemblages of the LG and MG samples from the western Bushveld are akin to those from the eastern Bushveld (Oberthür et al. 2016a) and also show far-reaching similarities to samples from the UG-2 chromitite (Kinloch 1982, Penberthy et al. 2000, Voordouw et al. 2010, Junge et al. 2014, Osbahr et al. 2014). The PGM assemblages are dominated by PGE-sulfides (malanite, laurite, cooperite-braggite), followed by PGE-arsenides, PGE-sulfarsenides and Pt-Fe alloys. Voordouw et al. (2010) conducted a detailed study of the lateral variation of the PGM assemblage in the UG-2 chromitite and showed that the PGM are mostly cooperite-braggite, Pt-Rh-Cu sulfides (i.e. malanite-cuprorhodsite), laurite and Pt-Fe alloys. Notably, PGE-bismuthotellurides are nearly absent in the LG and MG chromitites, and also in the UG-2 chromitite (this study and Junge et al. (2014), Osbahr et al. (2014)). Penberthy et al. (2000) reported that the PGM in the UG-2 are either predominantly associated with base

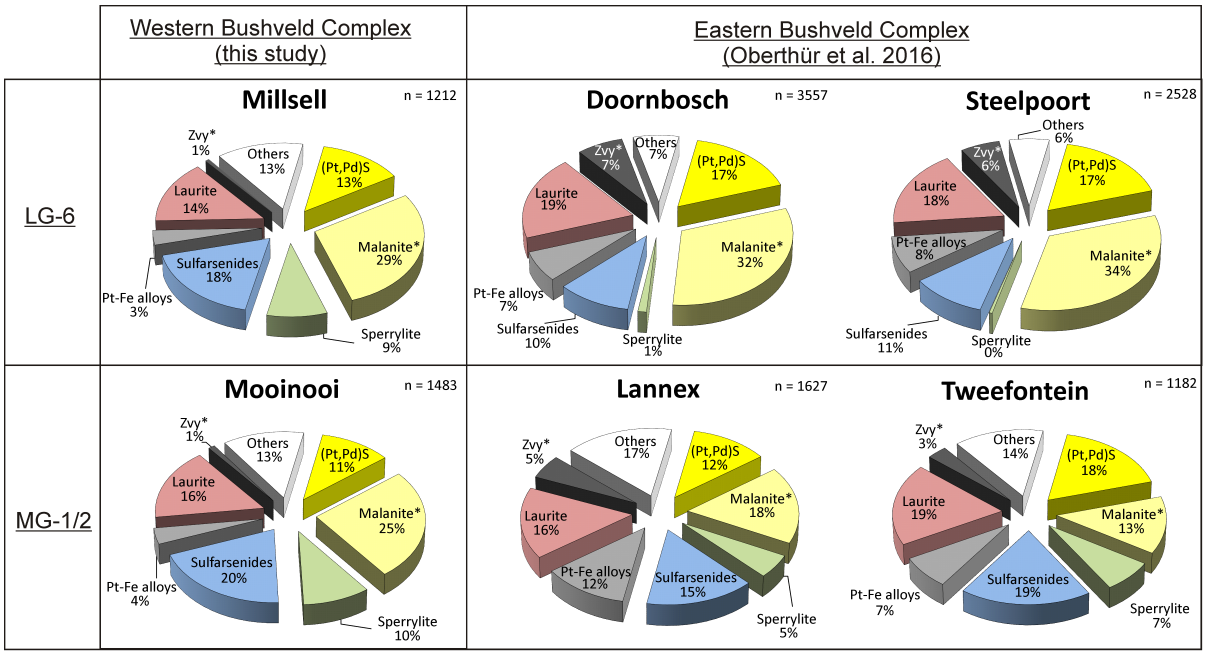

Figure 8.11 – Frequency percentage of PGM in the chromitite seams of Millsell and Mooinooi (this study) and for comparison of Doornbosch, Steelpoort, Lannex and Tweefontein (Oberthür et al. 2016a); n equals number of grains.

metal sulfides or are locked in chromite or silicate, or at grain boundaries between chromite and silicate.

In general, PGE mineralization is associated either with chromitites, or with sulfide-rich rocks, termed as "chromite control" and "sulfide control" (Scoon & Teigler 1994, Naldrett 2004a). Chromitites are typically enriched in IPGE over PPGE (Lee & Parry 1988, Naldrett 2004a). The mode of the occurrence of PGE in a chromite environment is still under debate, i.e. PGE occurring in solid solution in the chromite lattice, or in associated sulfides, or as discrete PGM (inclusions or free grains), or as metal clusters (Tredoux et al. 1995, Naldrett 2009, Naldrett et al. 2011, Locmelis et al. 2011, Pagé et al. 2012). It is well known that the PGE strongly partition into sulfide compared to silicate liquid due to the high partition coefficients of the PGE, which are on the order of 10^3 to 10^6 (Campbell et al. 1983, Mungall & Brenan 2014) or even 10^7 to 10^{11} for Pt between sulfide and silicate melt depending on fS_2 and fO_2 (Fonseca et al. 2009). In the Bushveld Complex, the IPGE contents are relatively constant in the chromitites of the Critical Zone, whereas the PPGE steadily increase from the LG-5 upwards (Naldrett & von Gruenewaldt 1989, Scoon & Teigler 1994). The abrupt change in PPGE con-

centrations points to the fact that sulfide control took over from chromite control from the LG-5 upwards (Oberthür et al. 2016a). The most abundant PGM within the LG-6 and MG-2 in the western Bushveld Complex is laurite (typically Os- and Ir-bearing). The appearance of laurite in chromite as well as experimental studies indicate that laurite may have been formed at magmatic conditions (Brenan & Andrews 2001, Bockrath et al. 2004).

Dominant PGM in Millsell and Mooinooi are sulfides (laurite, malanite-cuprorhodsite, cooperite-braggite and arsenides (sperrylite and sulfarsenides) totaling 83% and 82%, respectively, whereas PGE-bismuthotellurides are missing. PGE mineralization in a chromite environment is generally dominated by PGE-sulfides, PGE-arsenides and PGE-sulfarsenides. However, within sulfide-rich systems, PGE-bismuthotellurides are the dominant PGM besides cooperite-braggite and sperrylite. Elevated concentrations of As in the initial melt causes As to preferentially associate with PGE, forming PGE-As molecules or polyatomic clusters which are then stabilized during further cooling (Tredoux et al. 1995, Helmy et al. 2010). Besides the metal/sulfur ratio, the partition coefficients $D_{mss/melt}$ of As also strongly depends on fS_2. In relatively reduced sulfide melts, As may be incorporated in the mss or stabilize discrete arsenide minerals (Helmy et al. 2010). The mode of PGE occurrence in chromitites is therefore related to an initially more As-rich environment, allowing the formation of stable high-temperature arsenides and sulfarsenides. In base metal sulfide systems such as the Merensky Reef, the Great Dyke and the Platreef, PGM are typically (Pt,Pd)-bismuthotellurides (Oberthür et al. 2003, Holwell & McDonald 2007, Osbahr et al. 2013, Junge et al. 2015a). The elements Te and Bi are highly incompatible with mss and therefore strongly partition into the sulfide melt (Helmy et al. 2010). PGE-bismuthotellurides must therefore not have formed by solid state exsolution from crystallizing mss but rather may originate from droplets of immiscible Te-Bi-enriched melts (Helmy et al. 2007, 2010). The partition coefficient Dmss/melt of As, Te and Bi also largely depends on the atomic radii as Te and Bi have larger atomic radii than As and S. Within chromite environments only the semi-metals with smaller atomic radii occur, whereas in sulfide-rich systems the semi-metals with larger atomic radii and a higher incompatibility in mss form the dominant PGM species. The different PGM assemblages of a chromitite (PGE-sulfides, arsenides and sulfarsenides) versus a sulfide (PGE-bismuthotellurides, alloys) environment reflect the availability of the semimetals As, Te and Bi in the melt, the fS_2 and the partition coefficient Dmss/melt of

As, Te and Bi.

Pentlandite grains from Millsell (LG-6) and Mooinooi (MG-2) have average contents of 385 and 1005 ppm Pd, respectively, and maximum contents in pentlandite were 7730 ppm Pd and 6020 ppm Rh. PGE contents in thiospinel grains of the polydymite-linnaeite-greigite series were 1430 ppm Pt in a grain with a near-siegenite composition [$Ni_{1.5}Co_{1.2}Fe_{0.4}S_4$] and 5370 Rh and 1460 Pd in a grain with the composition [$Ni_{2.2}Fe_{0.5}Cu_{0.3}S_4$]. These concentrations are based on EPMA data and may reflect either solid solution in the sulfides or submicrometer-sized inclusions of PGM (see Junge et al. (2015b)).

In general, laurite is the dominant carrier of the IPGE and formed at magmatic conditions (Brenan & Andrews 2001, Bockrath et al. 2004). Hollingworthite, the main sulfarsenides, and malanite-cuprorhodsite are the major hosts of Rh. Palladium and Rh additionally occur within pentlandite.

8.6 Conclusions

(1) The chondrite-normalized PGE patterns of the LG-6 and MG-2 flotation concentrates from Millsell and Mooinooi are similar to the tailings of Millsell and Mooinooi, as well as to literature whole-rock data indicating no strong preferential upgrade of any PGE during the metallurgical processing of the ores and enabling the direct comparison of flotation concentrates with the respective chromitite seams.

(2) Sulfides (chalcopyrite, pentlandite, rare millerite) are scarce and pyrrhotite is largely missing.

(3) In both the Millsell (LG-6) and the Mooinooi (MG-2) PGM-concentrate samples, PGE-sulfides (cooperite-braggite, malanite, laurite) predominate, followed by PGE- sulfarsenides, sperrylite and Pt-Fe alloys. The LG-6 concentrate has slightly larger contents of PGE-sulfides. PGE-bismuthotellurides are typically missing. In general, laurite is the predominant PGM (area percentage) and the total number can increase as probably not all laurite grains occurring as small inclusions in chromite grains are recovered during flotation.

(4) The PGM assemblages of the LG and MG chromitites of the western and the eastern Bushveld Complex are very similar arguing for the same formation processes.

(5) The similar PGM assemblages of the LG and MG chromitites of the western and the eastern Bushveld Complex and the UG-2 chromitite appear to be "typical" of chromite-rich environments. The different PGM assemblages in a chromitite (PGE-sulfides, arsenides and sulfarsenides) and sulfide (PGE-bismuthotellurides, -sulfides, alloys) environment reflect differences in fS_2 and in the availability of the semimetals As, Te and Bi in the melt as well as differences in the partition coefficients Dmss/melt of As, Te and Bi.

(6) Platinum characteristically forms discrete PGM (cooperite-braggite and sperrylite). Palladium occurs in a variety of discrete PGM and incorporated in sulfide (pentlandite). Rhodium is mainly found in the form of discrete PGM (hollingworthite, cuprorhodsite) and is also hosted in pentlandite. The IPGE (Os, Ir and Ru) are mainly hosted in laurite (often as inclusions in chromite) and are also found in sulfarsenides.

(7) Pentlandite grains from Millsell and Mooinooi have average contents of 385 and 1005 ppm Pd, respectively, and maximum contents of 7730 ppm Pd and 6020 ppm Rh.

(8) PGE contents in thiospinel grains of the polydymite-linnaeite-greigite series showed 1430 ppm Pt in a grain with a near-siegenite- composition and 5370 Rh and 1460 Pd in a second grain. These concentrations are analyzed by EPMA and can be the result of both solid solution and submicrometer-sized inclusions of discrete PGM.

Chapter 9

General discussion

In the previous chapters the distribution of PGE in pristine and weathered Platreef ore, as well as within the UG-2 and the LG-MG chromitites has been described. In this chapter conclusions are further developed using additional aspects.

9.1 Distribution of PGE in the pristine ore

9.1.1 Platinum-group minerals

The combination between conventional (ore microscopy, SEM, EPMA and LA-ICP-MS) and follow-up high-resolution methods using combined techniques of FIB and TEM on pentlandite indicate that a continuum exists from discrete micrometer- to nanometer-sized PGM (nPGM). The nPGM represent early formed phases at temperatures of about 1200°C and may have been collected by the segregating sulfide liquid. Within sulfide, a variety of nPGM (Pt-bismuthides, Pt-tellurides, Pt-(Fe,Cu) alloy, Pd-Sn and Pt-Pd-Sn compounds) were detected. These nPGM do not display any orientation relationship to the host sulfide and therefore represent discrete phases which were trapped early during pentlandite growth and consequently do not represent exsolutions. The presence of nPGM in different PGE deposits are confirmed by Reid (2014), Gonzáles-Jiménez et al. (2015) and Gonzáles-Jiménez & Reich (2016).

In general, PGE mineralization is associated either with chromitites, or with sulfide-rich rocks, termed as "chromite control" and "sulfide control" (Scoon & Teigler 1994, Naldrett

2004a). Chromitites are typically enriched in IPGE over PPGE (Lee & Parry 1988, Naldrett 2004a). It is well known that the PGE strongly partition into sulfide compared to silicate liquid due to the high partition coefficients of the PGE, which are in the order of 10^3 to 10^6 (Campbell et al. 1983, Mungall & Brenan 2014) or even 10^7 to 10^{11} for Pt between sulfide and silicate melt depending on fS_2 and fO_2 (Fonseca et al. 2009). In the Bushveld Complex, the IPGE contents are relatively constant in the chromitites of the Critical Zone, whereas the PPGE steadily increase from the LG-5 upwards (Figure 2.4). The abrupt change in PPGE concentrations points to the fact that sulfide control took over from chromite control from the LG-5 upwards (Oberthür et al. 2016a).

The most abundant PGM within the LG-6 and MG-2 in the eastern and western Bushveld Complex is laurite - typically Os-and Ir-bearing (Junge et al. 2016, Oberthür et al. 2016a). The appearance of laurite in chromite as well as experimental studies indicate that laurite may have been formed at magmatic conditions (Brenan & Andrews 2001, Bockrath et al. 2004). Platinum-group element mineralization in a chromite environment is typically dominated by PGE-sulfides, PGE-arsenides and PGE-sulfarsenides in layered intrusions (Junge et al. 2014, Barnes et al. 2016) and in ophiolitic chromitites (Gonzáles-Jiménez et al. 2009) but PGE-bismuthotellurides are largely missing. Within sulfide-rich systems, PGE-bismuthotellurides are the dominant PGM, and minor amounts of zvyagintsevite. PGE-sulfides, -arsenides and -sulfarsenides are observed as well but do not have a large influence on the bulk PGE potential. Elevated concentrations of As in the initial melt causes As to preferentially associate with PGE, forming PGE-As molecules or polyatomic clusters which are then stabilized during further cooling (Tredoux et al. 1995, Helmy et al. 2010). However, besides the metal/sulfur ratio, the partition coefficient $D_{mss/melt}$ of As also strongly depends on fS_2. In more reduced sulfide melts, As may be incorporated in the monosulfide solid solution (mss) or stabilize discrete arsenide minerals (Helmy et al. 2010). The mode of PGE occurrence in chromitites is related to initially As-rich melts, allowing the formation of stable high-temperature arsenides and sulfarsenides. In base metal sulfide systems such as the Merensky Reef, the Great Dyke and the Platreef, PGM are typically (Pt,Pd)-bismuthotellurides (Oberthür et al. 2003, Holwell & McDonald 2007, Osbahr et al. 2013, Junge et al. 2015a) and only minor PGE-sulfides and -arsenides. The elements Te and Bi are highly incompatible with mss and therefore strongly partition into the sulfide melt (Helmy

et al. 2010). PGE-bismuthotellurides must therefore not have formed by solid state exsolution from crystallizing mss but rather may originate from droplets of immiscible Te-Bi-enriched melts (Helmy et al. 2007, 2010). The partition coefficient $D_{mss/melt}$ of As, Te and Bi also largely depends on the larger atomic radii of Te and Bi compared to As and S. Within chromite environments semi-metals with smaller atomic radii are frequent, whereas in sulfide-rich systems the semi-metals with larger atomic radii and a higher incompatibility in the mss form the dominant PGM species. The difference in the atomic radii of the semi-metals influences the compatibility in the sulfide melts. The different PGM assemblages in a chromitite environment (PGE-sulfides, arsenides and sulfarsenides) and sulfide environment (PGE-bismuthotellurides, alloys) reflect the availability of the semimetals As, Te and Bi in the melt, the fS_2 and the partition coefficient $D_{mss/melt}$ of As, Te and Bi. Experimental studies and observations on deposits have shown that chromite can act as a collector of PGE and chromitites are in particular enriched in IPGE (Brenan & Andrews 2001, Bockrath et al. 2004, Finnigan et al. 2008, Junge et al. 2014, Osbahr et al. 2014, Barnes et al. 2016, Pagé & Barnes 2016). Laurite represents the major inclusions of PGM in chromite (>90%). Based on a redox gradient produced by local reduction within the chromite-melt interface as a consequence of the selective uptake of trivalent Cr and Fe relative to the divalent species, PGM crystallize at the grain boundaries of chromite (Finnigan et al. 2008). Some chromite grains show differences in the mineral chemistry with Mg-rich core and Fe-rich rim (Figure 8.9A). This indicates that chromite records the evolution of the melt. During further cooling and chromite growth, PGM are trapped within the growing chromite grains. The formation of PGM is related to specific fO_2 conditions which are the result of steadily more reduced melts during chromite growth. The reduction of the melt surrounding the chromite grains allows the formation of a characteristic PGM assemblage in chromitite ores.

Figure 9.1 shows the atomic radii of S, As, Te, Bi and Pb and the fields of the dominant PGE mineralization in sulfide-rich systems (Platreef, Merensky Reef and Great Dyke) and chromite-rich systems (UG-2, LG/MG chromitites). In sulfide-rich systems dominant PGM are (Pt,Pd)-bismuthotellurides and zvyagintsevite, whereas in chromite-rich systems PGE-sulfides, -sulfarsenides and - alloys are the dominant phases (Melcher 2000a). Besides the atomic radii, the fO_2 and fS_2 are important parameters for the formation of the characteristic PGE mineralization. The fS_2 influences the partitioning coefficient between mss and sulfide liquid, and

therefore accounts for different availabilities of semi-metals which are necessary for the formation of discrete PGM.

Chromite, as a spinel, is a cubic close-packed array of anions, where one-eighth of the tetrahedral and one-half of the octahedral interstices are occupied by cations (Hill et al. 1979). The ionic radii (in Å) of Cr^{3+} and Fe^{3+} are for octahedral coordination $^{VI}Cr^{3+}$=0.615 and $^{VI}Fe^{3+}$=0.645 and Fe^{2+} and Mg^{2+} for the tetrahedral sites have ionic radii of $^{IV}Fe^{2+}$=0.63 and $^{IV}Mg^{2+}$=0.57 (Shannon 1976). For the PGE the ionic radii are as follows: $^{VI}Ru^{3+}$=0.68, $^{VI}Ir^{3+}$=0.68, $^{VI}Rh^{3+}$=0.665, $^{VI}Os^{4+}$=0.63, $^{VI}Pt^{2+}$=0.8, $^{VI}Pd^{2+}$=0.86, $^{VI}Pd^{3+}$=0.76. Substitution of Ru^{3+}, Ir^{3+} and Rh^{3+} for Cr^{3+} and/or Fe^{3+} in the chromite lattice on the octahedral sites is therefore possible as the ionic radii differ by less than 15% and the ionic charge is the same (Goldschmidt 1926). However, Pt, Pd and to a certain extent Os are not suitable for the incorporation in the chromite lattice because of differing ionic radius and charge. Concentrations of Ru in chromite in the 100s-ppm range are reported in komatiitic chromite grains (Locmelis et al. 2011) as well as in chromitite ores of the Bushveld Complex as shown in Chapter 8.4.5 and by Pagé & Barnes (2016).

Chapter 5.3 described the presences of unnamed (Pd,Pt)-germanides in the Platreef. This type of PGM was first reported from the Platreef by Armitage et al. (2002) and Holwell et al. (2006), as well as from Noril'sk (Komarova et al. 2002) and $(Pd,Pb)_2Ge$ from the Burakovsk Layered Complex in the Karelia-Kola region (Grokhovskaya et al. 2005). In general, the number of Ge-minerals is very limited and only 30 Ge-minerals are approved by the IMA (Melcher & Buchholz 2014, Hazen et al. 2015). Germanium ($^{IV}Ge^{4+}$) has a similar ionic radius as $^{IV}Si^{4+}$ (0.39 Å and 0.26 Å, respectively) as shown by Shannon (1976). Therefore Ge can replace Si in the lattice sizes of silicates (Goldschmidt & Peters 1933, Goldschmidt 1954, Bernstein 1985, Höll et al. 2006, Melcher & Buchholz 2014). Harris (1954) showed that Ge is is more concentrated in olivine and pyroxene than in quartz and feldspar. Germanium exhibits siderophile, lithophile, chalcophile and organophile character in different geological environments and generally tends to occur in hydrothermal sulfide deposits, and in pegmatites, greisens, and scarns but is rare in mafic/ultramafic rocks (Bernstein 1985, Höll et al. 2006). Mean Ge concentrations in ultramafic rocks are 0.9 ppm (Burton et al. 1959, Hörmann 1963, Baedecker & Wasson 1970, Bernstein 1985). The Ge/Si ratio in hydrothermal fluids is much higher than in crustal rocks and

increases with temperature (Pokrovski & Schott 1998). The formation of (Pd,Pt)-germanides in the Platreef may therefore be a result of a hydrothermal overprint where Ge-bearing silicates or sphalerite were dissolved and caused a redistribution of PGE and PGM and in particular the crystallization of (Pd,Pt)-germanides. Holwell et al. (2006) reported that the Pd-germanides are found as satellite grains around larger sulfides which are intergrown with amphiboles and are not bounded to unaltered sulfide minerals. Based on this observation Holwell et al. (2006) assumed that Pd-germanides are the result of hydrothermal overprint. Figure 5.14 shows photomicrographs and BSE images of Pd_2Ge in the Platreef at Overysel. The Pd_2Ge phases are typically associated with chalcopyrite and pentlandite and occur within or at the grain boundary of sulfides.

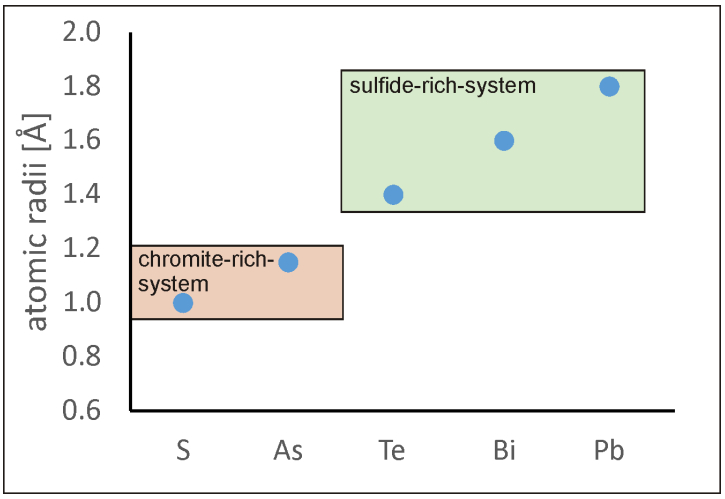

Figure 9.1 – Atomic radii of S, As, Te, Bi and Pb taken from Slater (1964) with the typical PGM assemblage in a sulfide-rich system (Platreef, Merensky Reef, Great Dyke) and chromite-rich systems (UG-2, LG-MG chromitites). Note: the dominant PGM assemblage is shown only. Within the sulfide-rich systems PGE-sulfides, -arsenides and -sulfarsenides are observed as well but do not have a large influence on the bulk PGE potential.

In summary, Pt characteristically forms discrete PGM (e.g. cooperite-braggite and sperrylite) in both chromite and sulfide-rich PGE ores. Palladium occurs in a variety of discrete PGM and incorporated in sulfide (pentlandite). Rhodium is mainly found in the form of discrete PGM (hollingworthite, cuprorhodsite) and is also hosted in pentlandite. The IPGE (Os, Ir and Ru) are mainly hosted in laurite (often as inclusions in chromite) and are also found in PGE-sulfarsenides. Small concentrations of Ru occur in chromite grains of the LG-6 with median values of 260 ppb (total range from 170 to 365 ppb) as presented in Chapter 8.4.5. Similar Ru

concentrations are shown for komatiitic chromite grains as well as other chromitite seams in the Bushveld Complex (Locmelis et al. 2011, Pagé & Barnes 2016). These observations are the result of the different characteristics of PGE and the fate of PGE during ore-forming processes.

9.1.2 PGE in Ni-Fe-sulfide minerals

Electron probe microanalysis and LA-ICP-MS work on sulfides from the Platreef, the UG-2 and LG and MG chromitites indicate elevated concentrations of PGE within pentlandite. Concentrations of Pd and other PGE in pyrrhotite, chalcopyrite and pyrite are generally below the detection limit of EPMA and mostly of the LA-ICP-MS as well. The important consideration for this observation is that the substitution of trace elements into a solid phase is controlled by the nature of the bonding, the size of the lattice site, and the charge balance. The pentlandite structure represents a pseudo-cubic closest packing with cations (Fe, Ni) occupying the octahedral and tetrahedral sites (Rajamani & Prewitt 1973, 1975). The ionic radii (in Å) of Pd, Fe, and Ni are $^{IV}Pd^{2+}$=0.64, $^{IV}Fe^{2+}$=0.63, and $^{IV}Ni^{2+}$= 0.55 (Shannon 1976), thereby allowing substitution of Pd for Ni and/or Fe as the ionic radii differ by less than 15% (Goldschmidt 1926). The same is true for $^{VI}Rh^{3+}$=0.665, $^{VI}Ir^{3+}$=0.68, $^{VI}Ni^{2+}$=0.69, and $^{VI}Fe^{2+}$=0.61. The ionic radius of $^{VI}Pd^{2+}$ is 0.86 Å and consequently too large to occupy the octahedral site in pentlandite. These features enable the homogenous distribution of Pd in pentlandite on the tetrahedral site as shown by TEM work (Chapter 4). Additionally to the homogenous distribution of Pd within pentlandite, Rh and Ir occur as a patchily distributed solid solution and ordered within the pentlandite crystal structure, substituting for Ni and/or Fe on the octahedral site. The absence of possible reaction partners (e.g., Bi, Te, As, and Sn) or appropriate fS_2 and fO_2 conditions necessary for the formation of discrete PGM forced Rh and Ir to remain in the crystal lattice of pentlandite. The data imply that a large proportion of the Pd, even at elevated concentrations, is present in homogenous solid solution within the crystal lattice of pentlandite. At very high concentrations of Rh (up to 12.3 wt%) and Pd (up to 0.6 wt%) within pentlandite, ordering of Rh and Ir within the pentlandite lattice takes place on the (111) plane, forming a superlattice (Junge et al. 2015b).

Table 9.1 summarizes the Pd and Rh concentrations in pentlandite from the Bushveld Complex, Great Dyke, Noril'sk-Talnakh, Lac Des Iles, Stillwater Complex, Sudbury and Agua-

blanca obtained by EPMA, LA-ICP-MS, PIXE and AMS (ultra-sensitive accelerator mass spectrometry). Comparison with different analytical methods showed good reproducibility of the data: PIXE with LA-ICP-MS (Ballhaus & Ryan 1995, Ballhaus & Sylvester 2000), EPMA with PIXE (Cabri et al. 1984, Cabri 1988, Gervilla et al. 2004) and EPMA with LA-ICP-MS (Junge et al. 2014, 2015b). The concentrations of Pd and Rh in pentlandite is highly variable both within one deposit and also comparing the different PGE reefs ranging from below the detection limit up to several wt.%. The largest concentrations of both Pd and Rh in pentlandite are generally presented for chromitite reefs (LG-6, MG-1/2, UG-2, Stillwater), whereas sulfide-rich ores show lower concentrations (Table 9.1). Differences in fS_2 and fO_2 between chromite and sulfide-environment allow either the formation of discrete PGM or that Pd and Rh remain in pentlandite. The distribution within one reef are very heterogenous and pentlandite grains rich in Pd and Rh can be in close association with grains containing low Pd and Rh contents. Therefore, the effect of Pd and Rh incorporation or the formation of discrete PGM can also be on a very local scale. In general, the IPGE are enriched more than Pt and Pd in most chromitite layers of the Bushveld Complex and the Great Dyke (Oberthür 2002, Naldrett et al. 2009) and collection by sulfide liquid alone would be expected to enrich the ores in all PGE and thus some other processes must be important to account for the IPGE enrichment (Barnes et al. 2016). These different processes probably also affect the distribution of Pd and Rh in pentlandite.

Experimental work showed that chalcophile elements fractionate during crystallization of MSS from the sulfide melt at temperatures of 1180 to 950°C (Distler et al. 1977, Li et al. 1996, Barnes et al. 1997, 2001, Brenan 2002, Mungall et al. 2005, Sinyakova & Kosyakov 2007). However, Pd is not compatible in MSS. Cooling time can also affect the distribution of PGE in pentlandite. Fast cooling would result in patches of PGE within pentlandite (Figure 9.2F), whereas slower cooling enables the crystallization of PGM at the grain boundaries of sulfides (Figure 9.2C). Subsolidus diffusion of Pd into pentlandite can also take place as proposed by (Barnes et al. 2006, Dare et al. 2010). Also a late stage hydrothermal overprint could lower the proportion of PGE in pentlandite. Therefore differences in the textures and association of pentlandite with hydrous minerals are important to differentiate. The availability of semi-metals is certainly crucial for the crystallization of discrete PGM or the incorporation of PGE within pentlandite.

Table 9.1 – Concentrations of Pd and Rh in pentlandite from the Bushveld Complex, Great Dyke, Noril'sk-Talnakh, Lac Des Iles, Stillwater, Sudbury and Aguablanca obtained by EPMA, LA-ICP-MS, PIXE and AMS (ultra-sensitive accelerator mass spectrometry). [1] Median of Mean values, [2] feldspathic pyroxenite, nA = not published, bdl = below detection limit.

	Pd [ppm]			**Rh [ppm]**			**method**	**reference**
	Min	Max	Median	Min	Max	Median		
Bushveld Complex								
UG-2 (east)	<378	11,470	1,180	<543	85,990	1,760	EPMA	Kuhlmann et al. (2006)
UG-2 (east)	52.1	1,003	222	<0.039	421	78.7	LA-ICP-MS	Osbahr et al. (2014)
UG-2 (west)	0.92	298	62.6	<0.033	218	77.7	LA-ICP-MS	Osbahr et al. (2014)
UG-2 (west)	<138	29,975	835	<115	21,851	7,470	EPMA	Junge et al. (2014)
UG-2 (west)	124	16,682	650	<0.13	23,817	628	LA-ICP-MS	Junge et al. (2014)
Merensky Reef (east)	nA	700	130	nA	55	15	LA-ICP-MS	Osbahr et al. (2013)
Merensky Reef (east)	<527	3,789	<527	<348	49,030	<527	EPMA	Ziaja et al. (2007)
Merensky Reef (west)	6.6	599	205	0.88	649	15	LA-ICP-MS	Godel et al. (2007)
Merensky Reef (west)	nA	500	183	nA	80	18	LA-ICP-MS	Osbahr et al. (2013)
Merensky Reef (west)[1]	144	757	233	27	67	40	LA-ICP-MS	Ballhaus & Sylvester (2000)
Merensky Reef (west)[1]	114	359	230	<3	99	26	PIXE	Ballhaus & Ryan (1995)
Merensky Reef	nA	nA	958	nA	nA	258	PIXE	Cabri (1988)
Merensky Reef	nA	nA	925	nA	nA	<200	EPMA	Cabri (1988)
Platreef (Nonnenwerth)	<360	746	<360	nA	nA	nA	EPMA	Manyeruke (2007)
Platreef (Overysel)	68.6	183	119	0.04	58	15	LA-ICP-MS	Holwell & McDonald (2007)
Platreef (Overysel)	<146	681	<146	<117	<117	<117	EPMA	this study
Platreef (Overysel)	49	332	130	<0.02	23.7	1.2	LA-ICP-MS	Klemd et al. (2016)
Platreef (Sandsloot)	67.7	143	102	8.2	46	25	LA-ICP-MS	Holwell & McDonald (2007)
Platreef (Sandsloot)	3.1	636	334	1.03	405	27	LA-ICP-MS	Klemd et al. (2016)
Platreef (Turfspruit)[2]	nA	nA	5.4	nA	nA	nA	LA-ICP-MS	Hutchinson & McDonald (2008)
Platreef (Townlands)[2]	<358	<358	<358	nA	nA	nA	EPMA	Manyeruke (2007)
Platreef (GNPA)	bdl	35	12	bdl	1.4	0.4	LA-ICP-MS	Smith et al. (2014)

LG-6 (east)	<133	5,292	180	<97	4,003	<97	EPMA	Oberthür et al. (2016a)
MG-1/2 (east)	<138	3,059	<138	<103	11,366	<103	EPMA	Oberthür et al. (2016a)
LG-6 (west)	<72	7,731	250	<141	1,831	<141	EPMA	Junge et al. (2016)
MG-2 (west)	<73	2,306	1,109	<143	6,023	<143	EPMA	Junge et al. (2016)
Great Dyke								
Hartley Mine	44.5	227.9	nA	nA	127.9	nA	LA-ICP-MS	Piña et al. (2016)
Ngezi, Unki, Mimosa	4.7	271	nA	nA	<1	nA	LA-ICP-MS	Piña et al. (2016)
Hartley Mine	nA	2,236	nA	nA	259	nA	PIXE	Oberthür et al. (1997a)
Hartley Mine	nA	2,506	nA	nA	562	nA	EPMA	Oberthür et al. (2003)
Mimosa	181	2,045	419	nA	nA	nA	EPMA	Gervilla et al. (2004)
Mimosa	141	1,909	336	nA	nA	nA	PIXE	Gervilla et al. (2004)
Noril'sk Talnakh								
Oktyabr'sky	<5	284	nA	nA	nA	nA	PIXE	Czamanske et al. (1992)
Medvezhy Creek	203	2,540	nA	nA	nA	nA	PIXE	Czamanske et al. (1992)
Komsomolsky mine	127	254	nA	nA	nA	nA	PIXE	Czamanske et al. (1992)
Medvezhy Creek	402	1,052	534	12	75	40	LA-ICP-MS	Barnes et al. (2006)
Lac Des Iles								
Roby and Twilight	257	3,262	649	0.07	23	0.27	LA-ICP-MS	Djon (2010),Djon & Barnes (2012)
Roby and Twilight	0.4	785	18.3	0.013	1.41	0.058	LA-ICP-MS	Duran et al. (2016)
Stillwater Complex								
Mountain view/ Benbow	nA	nA	261	nA	nA	269	LA-ICP-MS	Barnes et al. (2006)
sulfide concentrates	955	10,929	3,723	nA	nA	nA	EPMA	Gervilla et al. (2004)
sulfide concentrates	789	11,204	3,443	nA	nA	nA	PIXE	Gervilla et al. (2004)
West Fork adit	1,868	13,648	5,450	<26	110	nA	PIXE	Cabri et al. (1984)
West Fork adit	2,992	14,220	5,243	nA	nA	nA	EPMA	Cabri et al. (1984)
East Boulder Mine[1]	2,992	21,720	5,207	11	319	103	LA-ICP-MS	Godel & Barnes (2008)

Sudbury								
Creighton deposit	0.275	2.71	0.825	0.006	0.13	0.01	LA-ICP-MS	Dare et al. (2010)
Cooper Cliff	<1.2	<3	nA	nA	nA	nA	PIXE	Cabri et al. (1984)
Strathcona	0.3	2.1	nA	nA	nA	nA	AMS	Li et al. (1993)
Kelly Lake	0.04	3.86	0.8	<0.003	0.103	0.019	LA-ICP-MS	Huminicky et al. (2005)
Aguablanca								
Semi massive ore	0.466	5.2	2.2	0.03	0.15	0.065	LA-ICP-MS	Piña et al. (2012)
Penikat								
Ala-Penikat-reef	nA	nA	957	nA	nA	12.1	LA-ICP-MS	Barnes et al. (2008)
Paasivaara-reef	nA	nA	133	nA	nA	0.133	LA-ICP-MS	Barnes et al. (2008)

9.1.3 Model for the distribution of PGE in ultramafic-mafic intrusions

Figure 9.2 summarizes the general processes taking place during formation of PGE deposits. Immiscible droplets of sulfide liquid migrate through a pile of magma collecting PGE and other chalcophile elements from the surrounding melt due to the high partition coefficients between sulfide and silicate melt, which are in the order of 10^3 to 10^6 (Campbell et al. 1983, Mungall & Brenan 2014). Turbulent migration of the sulfide liquid through the silicate melt allows interaction with sulfide droplets and silicate melts, i.e. a high R-factor as described by Campbell & Naldrett (1979). The sulfide droplets collect PGE and early formed nPGM acting as embryos for further PGM growth. At very high concentrations of PGE in the sulfide liquid and low metal-sulfur ratios of potential reaction partners for the formation of PGM, the PGE remain in the sulfide structure, forming superlattices within sulfide at high concentrations. Regional associated crystallization of chromite causes the formation of laurite and its incorporation into further grown chromite grains due to the preferential uptake of trivalent Fe and Cr over divalent, causing local decrease in fO_2 (Finnigan et al. 2008). Ruthenium is compatible in chromite and shows concentrations up to a few hundreds ppb within the chromite lattice.

Platinum-group minerals may crystallize directly from a sulfide melt (Power et al. 2004, Barnes et al. 2006, Hutchinson & McDonald 2008); or from a immiscible As-Bi-Te melt (Helmy et al. 2007, Holwell & McDonald 2007); or due to the addition of As, Bi and Te from the country rock to the sulfide liquid (Hutchinson & McDonald 2008); or from exsolution of PGM during cooling (Makovicky et al. 1986, Makovicky 2002, Godel et al. 2007); or due to recrystallization during metamorphism (Barnes et al. 2008).

9.1.4 Genesis of the Platreef

Sulfur saturation at the Platreef is partly caused by contamination with the country rocks. The various country rocks along strike have a different influence on the sulfur saturation. At Townlands for instance the Platreef rests on dolomite and shows heavy sulfur isotope signatures (δ^{34}S values of +2.6‰ to +9.1‰). The slightly heavier sulfur isotope signature in the massive sulfides may indicate a late stage hydrothermal redistribution. Hydrothermal fluids certainly overprinted

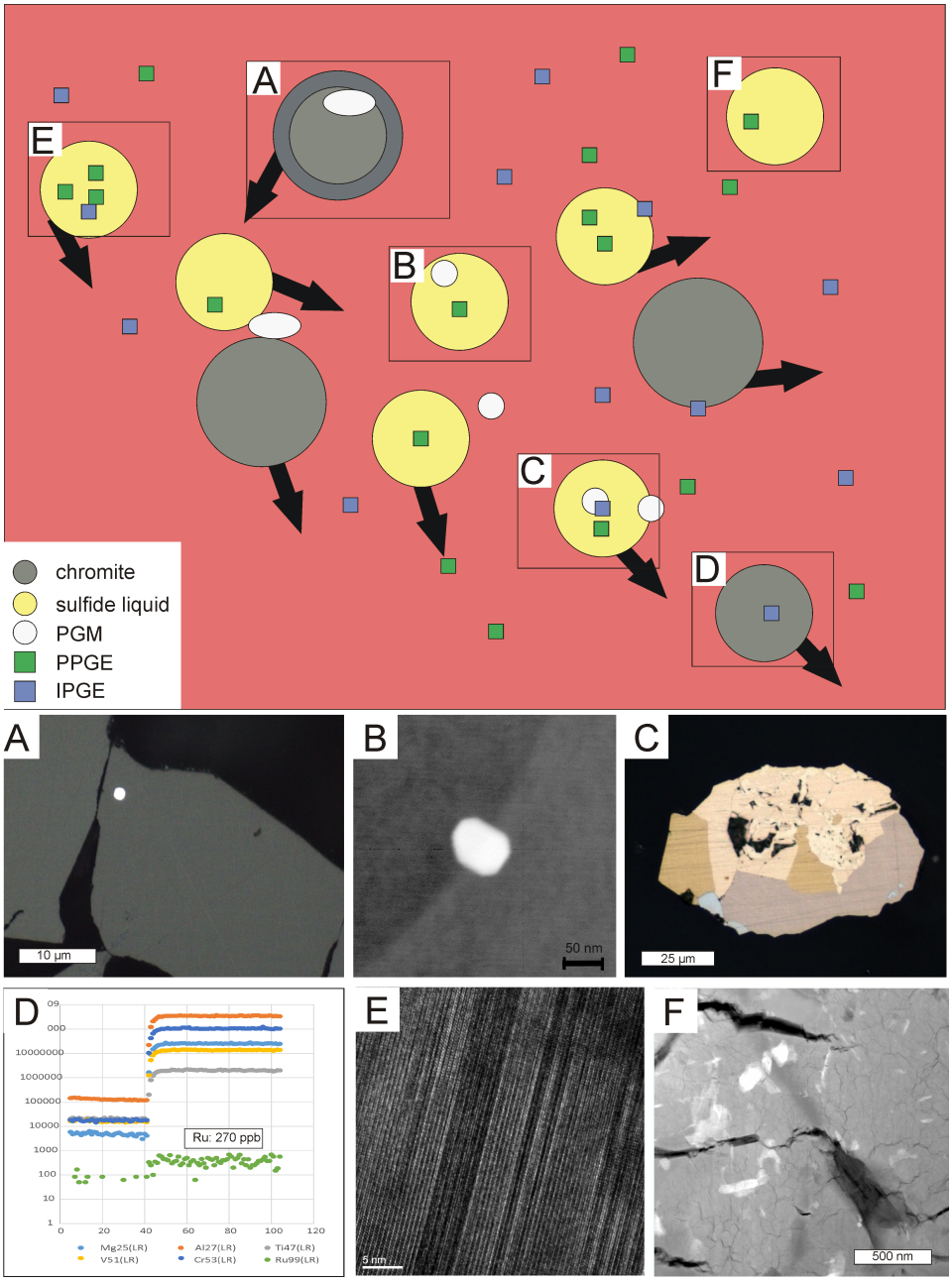

Figure 9.2 – Model for the distribution of PGE in pristine ores. In the pristine ore PGE occur as discrete PGM (all PGE), as well as in the crystal lattice of sulfide (Pd, Rh and Ir) and of chromite (Ru). In a chromite environment laurite [RuS_2] forms pre- and/or syn-chromite and thus occurs as inclusions in chromite. Early formed nanometersized PGM are trapped by sulfide droplets, acting as precursors for further PGM growth or remain as nPGM in the crystallizing sulfide. Sulfide droplets migrate turbulently through the silicate melt (high R-factor) collecting chalcophile elements (including PGE), which may later form discrete PGM, associated with the sulfide mineralisation or - when reaction partners are missing - remain in pentlandite. Palladium, Rh and Ir are compatible in the pentlandite structure forming solid-solution or superlattices. At high temperatures, Rh and Ir substitute for Fe^{3+} and Cr^{3+} in the chromite early during chromite growth.

the Platreef similar to most of the PGE deposits, also shown by the relatively high abundances of mica and amphiboles. The S/Se ratio at the Mogalakwena Mine further indicates that hydrothermal fluids slightly redistributed the ore.

The genesis of the Platreef began with sulfide droplets migrating through the Platreef magma and collecting PGE. During intrusion of the Platreef contamination with the country rock took place, which is indicated by the heavy sulfur isotope signature. However, sulfur saturation already occurred before the contamination. The contamination with the country rocks is rather an ore modifying than an ore-forming process as variation in δ^{34}S is observed along strike and crosscuts different country rocks. The interaction with the country rocks also caused the formation of hydrous fluids which additionally affected the ore, illustrated by S/Se ratios. The addition of aqueous Ca, Mg, Si and H_2O, as well as the release of S, Fe and Ni or Cu is required for the replacement of sulfide by amphibole, although replacement of adjacent orthopyroxene may provide some of the required Mg and Si (Li et al. 2004). Also the presence of (Pd,Pt)-germanides as shown in Chapter 5.3 and by Armitage et al. (2002) and Holwell et al. (2006) for the Platreef argues for local alteration and redistribution of the PGE-mineralogy in the Platreef by hydrothermal fluids. Redistribution of PGE took also place into the footwall and the transition zone of the Platreef as also shown by high PGE contents in calcsilicates (Klemd et al. 2016). Holwell et al. (2011) studied sulfide melt inclusions in chromite within the Platreef and compared these inclusions with fractionated sulfide blebs formed from the crystallization of an interstitial sulfide melt, open to contamination and upgrading or dilution of PGE and S during the cooling history of the Platreef. These trapped sulfide inclusions in chromite can hold information for the nature of the early sulfide liquid which includes the evidence of a highly PGE-rich sulfide liquid during the formation of the Platreef (Holwell et al. 2011). Therefore, within the Platreef, both the magmatic PGE-rich sulfide exist as well as externally derived sulfur due to the interaction with the country rock triggering sulfur saturation. Later redistribution of the PGE also effect the PGE mineralogy. Holwell et al. (2011) also showed elevated concentrations of Bi and Te in these melt inclusions in chromite arguing for the initial large availability of these semi-metals and allowing the later formation of discrete PGM.

9.2 Distribution of PGE in the weathered ore

Whole rock data from the Platreef at Overysel show that from pristine to oxidized ores the Pt/Pd ratio increases which is the result of a relative depletion of Pd over Pt. The relative depletion of Pd is due to its higher mobility during weathering.

As shown above, within the pristine ore, PGE are bimodally distributed, i.e. Pt and the IPGE typically form discrete PGM but Pd and Rh occur both as discrete PGM and incorporated in sulfides. Small concentrations of Ru occur in chromite grains. During weathering this characterstic distribution changes. Platinum-group elements are polymodally distributed in the oxidized ore, i.e. PGE occurring in relict PGM, in iron- and manganese-oxides/hydroxides, or in secondary silicates. Secondary silicates and iron- and manganese oxides/hydroxides contain concentrations of Pt, Pd and Rh in the 100s ppm range. This complex polymodal distribution of PGE in the ores is challenging for the recovery of PGE (Figure 9.3).

Palladium is more mobile than Pt. Platinum-group minerals and sulfides are largely destroyed during the oxidation process. Sulfides are the main host for Pd and Rh. Therefore, Pd and Rh are released during weathering of sulfides and are transported further away and later reprecipitated in the form of PGE-oxides/hydroxides or adsorbed or incorporated to clay minerals or lost completely from the system. Platinum and IPGE (primarily forming discrete PGM) occur in relict PGM or are associated with secondary minerals (clay minerals, Fe-oxy/hydroxides) in the weathered ore. The occurrences of relict PGM (mainly Pt-rich) account for the recovery rates of about 20%. During the flotation process only these relict PGM grains are recovered but no PGE associated with secondary minerals. Platinum and IPGE largely remain within the system as shown by whole-rock geochemical data. Experiments with CEC showed that PGE are not attached in the inter layers of clay minerals but rather occur incorporated in the structure.

Only relict PGM are present in the oxidized ore, mostly as sperrylite and cooperite-braggite, whereas (Pt,Pd)-bismuthotellurides are less common. This variation in the PGM assemblages from pristine to oxidized ores indicates different stabilities of PGM during weathering processes, i.e. (Pt,Pd)-bismuthotellurides are less stable than cooperite-braggite and sperrylite. These observations are similar to placer studies in the Bushveld Complex, the Great Dyke, and in other PGM placers, where the PGM assemblage mainly consists of sperrylite, and PGE-alloys

(Oberthür et al. 2004, Melcher et al. 2005, Oberthür et al. 2013b, 2014, 2016b).

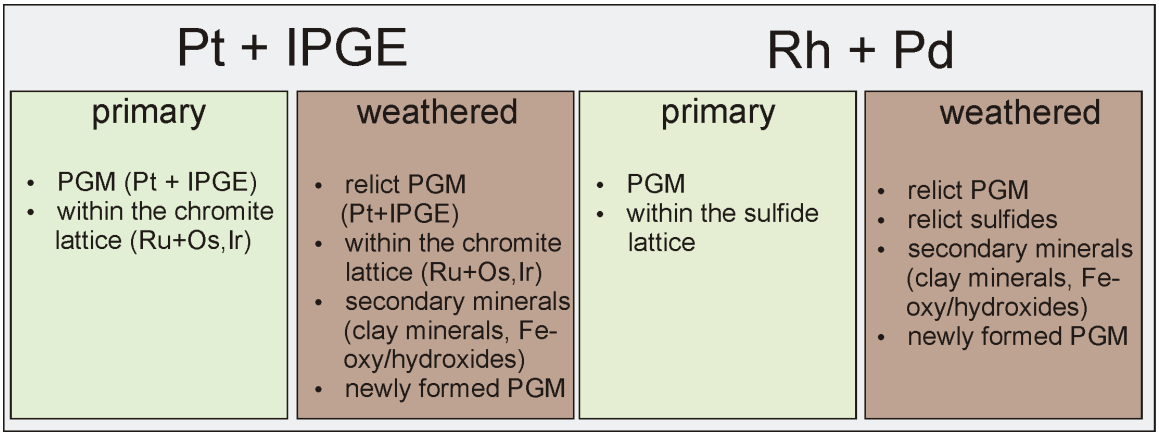

Figure 9.3 – Distribution of Pt and IPGE (Os, Ir, Ru) and Rh and Pd in the weathered and pristine ore. In the primary ore Pt and IPGE mainly occur as discrete PGM. Some 100s ppb of IPGE may occur in the chromite lattice. During weathering relict PGM may be preserved as well as IPGE retained in chromite. However, other fracations of Pt and IPGE occur in secondary minerals as well in newly formed PGM. Similarly Rh and Pd occur as discrete PGM but the main host for Pd and Rh are sulfides (mainly pentlandite) in the pristine ore. In the weathered ore relict PGM and sulfides contain Pd and Rh. Further concentrations occur similarly to Pt and IPGE associated with secondary minerals and newly formed PGM.

The presence of newly formed PGM in low-temperature and near-surface environments is still debated. Some studies argued that PGM are only formed under hypogene conditions (Cabri & Harris 1975, Brenan & Andrews 2001, Traore et al. 2006), whereas other authors propose that PGM can from in situ after the mobilisation and re-deposition of PGE (Wagner 1929, Augusthitis 1965, Cousins & Kinloch 1976, Bowles 1986, Kieser 1994, Bowles et al. 2000, Garuti et al. 2012). Traore et al. (2006) studied the effects of weathering on Pt and Pd in a supergene environment in New Caledonia. Using SEM and EPMA they argue that the PGM are residual and are affected by dissolution processes and not the result of neoformations. Wagner (1929) described the occurrence of newly formed PGM in supergene rocks overlying the Merensky Reef. Bowles (1986) and Bowles et al. (2000) suggested that PGE nuggets in alluvial deposits have grown in situ, partly as a result of precipitation from aqueous solutions. Figure 9.4 shows BSE images of PGM within the weathered ores. The weathering processes largely affected the shape, size and distribution of PGM. The various shapes argue for some dissolution and re-precipitation of PGM. Neoformation of PGM is therefore possible and PGM may grow under certain conditions within the weathered ore. The presences of PGE-oxides also argues

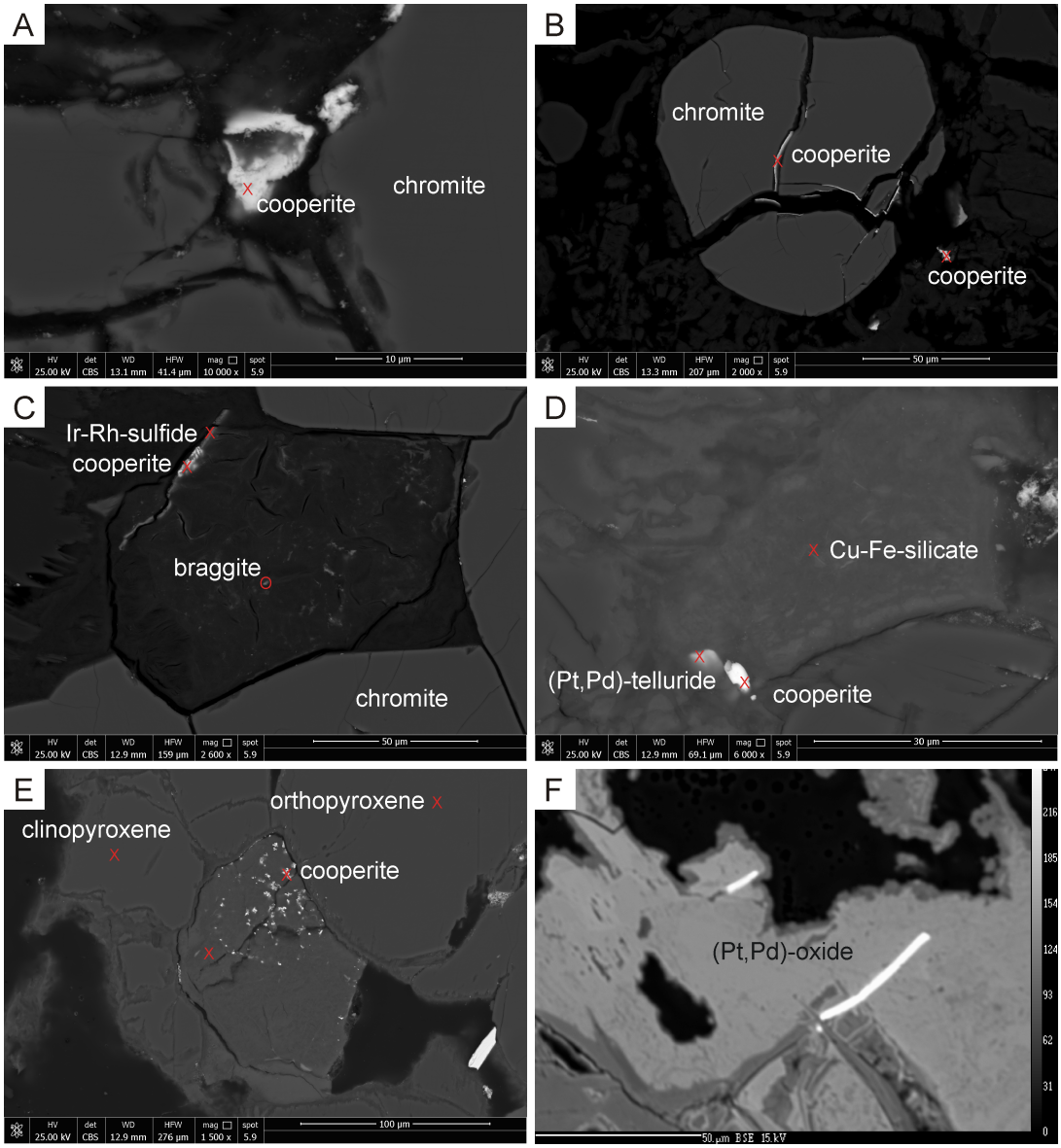

Figure 9.4 – Back-scattered electron (BSE) images of PGM in oxidized UG-2 and Merensky Reef. A-C: Oxidized UG-2 chromitite (2m below surface) from the Pit U9C/Lonmin (AS11290). D-E: Oxidized Merensky Reef (top part of the reef from Lebowa/Atok (AS11286)). F: Sandsloot open pit (AS7375). A: Cooperite grain surrounded by chromite. B: Cooperite within the cracks of a chromite grain. C: Cooperite [PtS] together with Ir-Rh-sulfide at the rim of an Fe-Mg-aluminosilicate and braggite [PdS] within the Fe-Mg-aluminosilicate. D: Cooperite and (Pt,Pd)-telluride in Cu-Fe silicate. E. Several cooperite grains within Cu-Fe-silicate. F: Pt,Pd oxide within secondary Fe-Al-silicate (AS7375-Pr10).

for some neoformation of PGM. The neoformation of PGM (dissolution and re-precipiation of PGM) is shown in Figure 9.4B,D. These PGM are certainly not of primary origin but are locally newly formed within the weathered ore.

The clear association of $BaSO_4$ and PGE enrichment argues for a transport of PGE in low-temperature near-surface conditions with sulfates. Thiosulfates can exist in relative large abundance during the oxidation of the sulfide ore body and may assist in dissolving and transporting PGE from sulfides into their present position in weathered ore.

9.3 Chromite composition

In Chapter 7 the cryptic variation of chromite chemistry in the UG-2 chromitite was presented and discussed and only some minor additional aspects about chromite chemistry are shown here. A large data set of the mineral chemistry of stratiform and podiform chromites exist as for example Dick & Bullen (1984), Arai & Yurimoto (1994), Stowe (1994), Zhou et al. (1996) and Barnes & Roeder (2001). The chromite chemistry is used as a petrogenetic indicator and chromites from different geological environments (e.g. podiform, stratiform) can be distinguished (Irvine 1965, 1967). Chromitite layers are particularly enriched in IPGE and Rh in ultramafic-mafic intrusions (Junge et al. 2014, Barnes et al. 2016) and ophiolites. However, the mineral chemistry can be affected during slow cooling, prograde or retrograde metamorphism, or hydrothermal alteration and the interpretation of the genesis should always be backed up by additional information (Melcher 2000b). Podiform chromite deposits, typically also carry low-grade PGE mineralization as for example in Albania (Kocks et al. 2007), Cuba (Gervilla et al. 2005), Greece (Augé 1985, Tsoupas & Economou-Eliopoulos 2008), Iran (Melcher et al. 2010, Jannessary et al. 2012), Kazakhstan (Melcher et al. 1994, 1997, 1999), Oman (Ahmed & Arai 2002), and Scotland (Prichard et al. 1986, Prichard & Lord 1993, Prichard et al. 1994). Plagioclase and orthopyroxene (Cameron 1975, 1977, Irvine 1977, Eales & Reynolds 1986), as well as olivine (Jackson 1969) surrounding chromite can influence the mineral chemistry, indicating a sub-solidus influence. Fine-scale differences of chromite surrounded by orthopyroxene and plagioclase was also observed in massive chromitite seams (Junge et al. 2014). Magmatic re-equilibration of chromite can therefore also take place with intercumulus liquids. Increases

in Vanadium concentrations (see Appendix) can, however, not be explained by intercumulus liquid and represent different influxes of magma, which can also be associated with the PGE mineralization.

Figure 9.5 shows a Cr# vs Fe# diagram with fields of the chromite chemistry from alpine-type and layered intrusions and the chromite chemistry from the MG-2 from the western Bushveld Complex (see Appendix) and UG-2 chromitite presented in Chapter 7. Fractional crystallization results in decreasing Mg# (increasing Fe#) upward in the stratiform complexes (Melcher 2000b). A general decrease in Mg# (increase in Fe#) from MG-2 to UG-2 is reported in Figure 9.5 and is in accordance with the observations in the Critical Zone of the Bushveld Complex by Naldrett (2009). However, Cr# vs Fe# are also influenced by the surround minerals and the interstitial liquids (Jackson 1969, Cameron 1975, 1977, Irvine 1977, Eales & Reynolds 1986).

9.4 Implications for the processing of weathered PGE ores

Near-surface weathered PGE ores have a large economic potential, but most recent attempts to extract the PGE from these near-surface ores are uneconomic due to low recovery rates («50%) with conventional metallurgical methods. Conventional processing of pristine PGE ores comprises froth flotation of the milled ore, and subsequent chemical leaching of the base metal- and PGE-rich matte (Crundwell et al. 2011). One of the main issues concerning the processing of near-surface weathered PGE ores is the very heterogeneous PGE distribution covering several mineral phases, including dispersion of PGE in secondary silicates and in iron- and manganese oxides/hydroxides. Another reason for the notably very low recoveries is the lack of base metal sulfide association (Becker et al. 2014). Kraemer (2015) and Kraemer et al. (2015) showed that Pt and Pd can be significantly mobilized from weathered PGE ores using a leach technique which involves specific PGE-affine biomolecules. However, the technique faced relatively heterogeneous recovery rates depending on the origin of the actual sample and the exact weathering state of the ore. Large scale processing with leach techniques as proposed by Kraemer (2015)

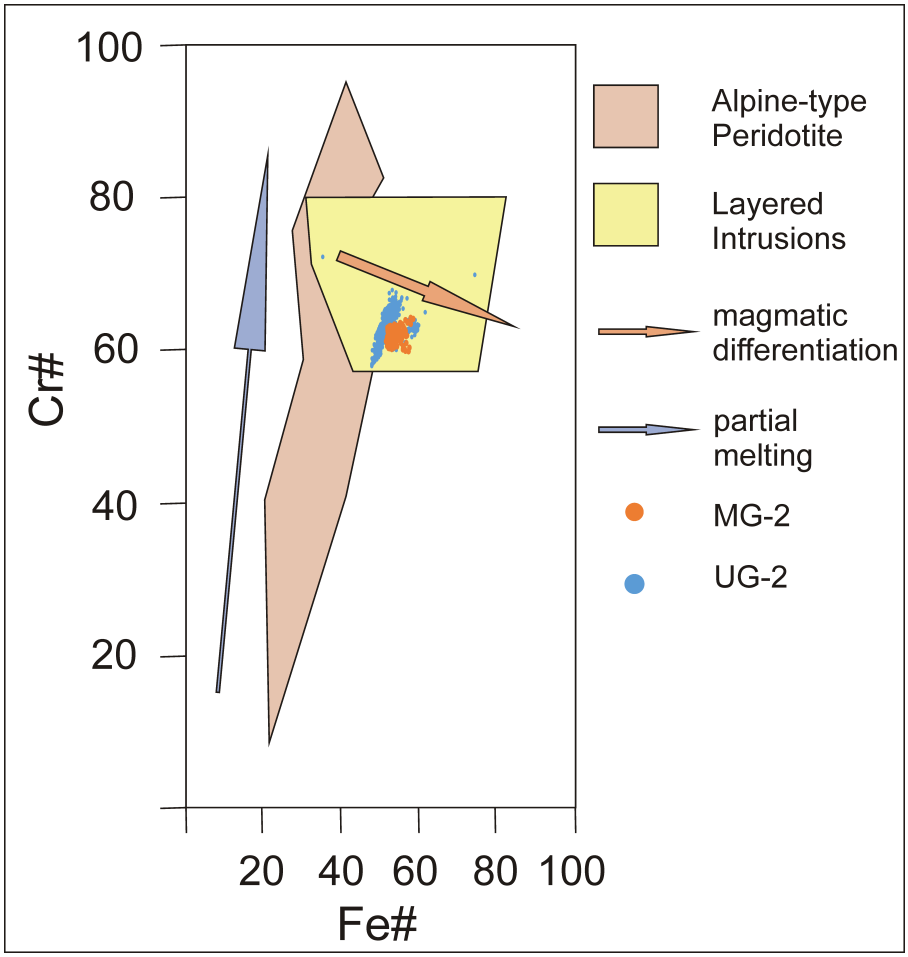

Figure 9.5 – Cr# vs Fe# diagram with fields from different geological environments (Dick & Bullen 1984). MG-2 from Thaba Mine western Bushveld Complex (this study, data see appendix), UG-2: Karee Mine western Bushveld Complex (Chapter 7). Modified after Melcher (2000b).

and Kraemer et al. (2015) can be a highly economic approach to process weathered PGE ores.

Chapter 10

Conclusions

The main conclusions of this study on pristine and weathered PGE ores in the Bushveld Complex are:

- In the pristine ore, PGE are bimodally distributed, occurring as discrete PGM or inside sulfide and chromite. Elevated concentrations of Pd occur within pentlandite, but are generally low in pyrrhotite, chalcopyrite and pyrite. Palladium and Rh are homogenously distributed within pentlandite and form superlattice at very high concentrations. Pyrite hosts the largest concentrations of IPGE in comparison to pentlandite, pyrrhotite and chalcopyrite but these concentrations are low in general. Pyrite is also a minor sulfide phase and therefore has only a minor contribution to the bulk PGE budget. Chromite hosts some hundreds of ppb of Ru. In general, Pt forms discrete PGM (cooperite-braggite, sperrylite, alloys). Palladium occurs in a variety of discrete PGM and is incorporated in pentlandite. Rhodium is found in the form of discrete PGM (hollingworthite, cuprorhodsite) but is also hosted in pentlandite. The IPGE (Os, Ir and Ru) are mainly hosted in laurite (often as inclusions in chromite) and in PGE-sulfarsenides (hollingworthite, irarsite, platarsite).

- Automated mineralogy techniques provide statistically robust data on the mode of occurrence of PGM in PGE ores. At the Platreef, by number of grains (Pt,Pd)-bismuthotellurides are the most abundant PGM, followed by zvyagintsevite, sperrylite, PGE-sulfarsenides, laurite, cooperite-braggite, Pt-Fe-alloys and malanite. In PGM-concentrates from the LG-6 and the MG-2 chromitites, PGE-sulfides (cooperite-braggite, malanite, laurite) predomi-

nate, followed by PGE- sulfarsenides, sperrylite and Pt-Fe alloys. PGE-bismuthotellurides are typically missing. In general, a continuum exists from discrete micrometer- to nanometer-sized PGM.

- The differences between typical PGM assemblages in chromite-rich (dominant PGE- sulfarsenides, -arsenides and -sulfides; (Pt,Pd)-bismuthotellurides are largely absent) and sulfide-rich (dominant (Pt,Pd)-bismuthotellurides) ores are explained by different behavior of Te, Bi, S, As during ore forming processes (fO_2 and fS_2, partition coefficient $D_{MSS/liquid}$), atomic radii).

- Sulfur saturation at the Platreef is partly caused by contamination with the country rocks. Late stage hydrothermal overprint is observed in the Platreef along strike.

- The sulfide mineralogy and textures vary along strike of the Platreef. In the central and northern part of the Platreef (Tweefontein, Sandsloot, Overysel and Nonnenwerth), where the footwall is dominated by Archean granite, gneiss and BIF, "typical" magmatic sulfide assemblages consist of pyrrhotite (dominant phase), pentlandite, chalcopyrite and minor pyrite (primary and secondary). At Townlands the footwall are sediments and the sulfide mineralogy consists of chalcopyrite, millerite, pyrrhotite, pyrite and pentlandite. Symplectic intergrowth of both pyrite with chalcopyrite and magnetite with pyrite are observed at Townlands.

- The PGE mineralogy at the Platreef is similar along strike and is largely dominated by (Pt,Pd)-bismuthotellurides, cooperite-braggite and laurite. It was observed that at Townlands (Pt,Pd)-bismuthotellurides are Pd-dominated, whereas at Mogalakwena Pt-rich phases are analyzed. Pentlandite from the Mogalakwena Mine hosts large concentrations of Pd, whereas Pd concentrations in pentlandite from Townlands, Sandsloot and Turfspruit is generally lower.

- Weathering takes place to a depth of about 25 m. The whole rock Pt and Pd contents remain in a similar range. Whole rock data from the Platreef at Overysel showed that from pristine to oxidized ores the Pt/Pd ratio increases which is the result of a relative

depletion of Pd over Pt. The relative depletion of Pd is due to its greater mobility during weathering.

- During weathering, sulfide and PGM are largely destroyed and pyroxene and plagioclase break down to secondary minerals, such as kaolinite, smectite and various clay minerals. Sulfides are the main host for Pd and Rh. Palladium and Rh are mobilized during weathering of sulfides and precipitate together with secondary minerals or are lost from the system. Platinum and IPGE (primarily forming discrete PGM) occur in relict PGM or are associated with secondary minerals (clay minerals, Fe-oxy/hydroxides). The recovery rates using the flotation process of a few 10% are explained by capture of relict PGM of a certain grain size only. Platinum and IPGE largely remain within the system as shown by whole-rock geochemical data.

- Only relict PGM are present in the oxidized ore, being sperrylite and cooperite-braggite, whereas (Pt,Pd)-bismuthotellurides are less common. This variation in the PGM assemblages from pristine to oxidized ores indicates different stabilities of PGM during weathering processes, i.e. (Pt,Pd)-bismuthotellurides are less stable than cooperite-braggite and sperrylite.

- Platinum-group elements are polymodally distributed in the oxidized ore, i.e. PGE occurring in relict PGM, in iron- and manganese-oxides/hydroxides, or in secondary silicates. Secondary silicates and iron- and manganese oxides/hydroxides contain concentrations of Pt, Pd and Rh in the 100s ppm range. This complex polymodal distribution of PGE in these ores poses a significant challenge to the recovery of PGE.

- Platinum-group elements are not loosely attached to interstitial sites of clay minerals but are rather incorporated in the mineral structure or form stronger bonds.

- Altered and newly formed PGM are observed within weathered Platreef, UG-2, Merensky Reef and LG-MG chromitites.

Chapter 11

Outlook

A few ideas are pointed out for further research related to pristine and weathered PGE ore.

11.1 Pristine ore

- In-situ sulfur isotope study of finely intergrown sulfides can obtain further information about the genesis of the PGE and associated sulfide mineralization in the Platreef. Comparing whole-rock sulfur isotope data with in-situ sulfur isotope using the SIMS may unravel information about differences between sulfides. The large abundances of pyrite may originate from a hydrothermal overprint and therefore change the overall whole-rock sulfur isotope data but the primary magmatic sulfides remain at mantle values. Secondary ion mass spectrometry is a good tool for the study of isotopes on the micrometer-scale. Additionally, a vertical sulfur isotope study is of interest in order to investigate differences in the contact and transition zone to the footwalls with respect to sulfides higher up in the Platreef stratigraphy.

- Similar to this thesis, several studies have indicated that pentlandite is the major host for Pd and Rh. The range of Pd and Rh concentrations range up to a few wt.%. As shown in this study these concentrations might be either the result of a substitution of Pd and Rh with Fe and Ni or as submicrometer-sized inclusions with the pentlandite. The question remains about how much Pd and Rh fit into the pentlandite lattice. By carrying out experi-

ments with different proportions of Pd with FeS and NiS as synthetic powder or by adding Pd to natural pentlandite, information can be obtained about to which extend (Pd,Ni)S and pentlandite are miscible and when do we observe two separate phases. Similar studies in the system Pd-Fe-Ni-S were carried out at higher temperatures by (Karup-Møller & Makovicky 1993, Makovicky & Karup-Møller 1993, Makovicky 2002) and at lower temperatures (Makovicky pers. com.) showing high solubility of Pd in Fe-Ni-sulfides.

- A more detailed focus on Co-rich pyrites which where shown to host the largest Pt contents in pyrite (mean 13 ppm) also in comparison with other Co-rich pyrites in layered intrusions as for e.g. by Dare et al. (2011) can help to study the different generations of pyrite and PGE redistribution in the pristine ores. Similarly, the Co contents in pentlandite and its variation could be studied also under consideration of the experiments by Eckstrand (1975).

- Transmission electron microscopy on chromite grains with elevated concentrations of Ru, Os and Ir will provide further information on the distribution of the IPGE in chromite. Similar to pentlandite, the elevated concentrations of IPGE in chromite can be a result of both solid solution and inclusions of nPGM. This data will help to understand the processes during chromite growth and the association with PGE and to discuss models as proposed for e.g. by Finnigan et al. (2008). For a detailed TEM study both natural chromite grains from layered intrusions and ophiolites as well synthetic chromite grains (e.g. synthesized by Brenan et al. (2012)) should be analyzed.

- Recent exploration drilling campaigns in the western part of the outcropping Platreef (Ivanhoe 2016) and in the newly discovered "Waterberg Deposit" in the north of the current Platreef operations (Platinum Group Metals 2016) could provide drill cores for the study of PGE and PGM as well as S-isotope study in order to investigate the effect of assimilation in the broader Platreef area. A more wide-ranging distribution of PGM assemblages (as shown in this thesis for Townlands, Tweefontein, Mogalakwena mine and Nonnenwerth) would increase the knowledge of PGM distribution west- and northwards of current Platreef activates.

- With respect to the study of the mineral chemistry of the UG-2 in the western Bushveld Complex which showed a cryptic variation with increasing Cr# and TiO_2 and decreasing Mg# upwards as well as shifts in the V_2O_3 concentrations, more similar work on chromitite seams would be useful to provide more information about the genesis of these seams. Kaufmann et al. (2014) already carried out a detailed EPMA study on the UG-2 in the eastern Bushveld Complex and made similar observation even though less sharp than in the UG-2 at Karee Mine. However, different faster methods such as the laser-induced breakdown spectroscopy or 2D micro-XRF analytical tools would be important for less-time consuming EPMA work. However, due to the small-scale variation in Cr#, Mg# and trace elements effort is needed for a method development. In addition to the chromite chemistry, associated minerals such as plagioclase, orthopyroxene, clinopyroxene and phlogopite should be analyzed as well.

- Additional to the distribution of PGE and PGM in the LG and MG ores as shown in this thesis and in Oberthür et al. (2016a), PGM concentrates from current Cr mines and the reprocessing of old LG and MG mine dumps at different locations in the Bushveld Complex would increase the statistics about the PGM distribution in LG and MG chromitites in the Bushveld Complex. At Tharisa Mine in the western Bushveld Complex, PGM concentrates are currently produced (Tharisa Mine 2016), which could be studied in detail for the PGE mineralogy. Mineral liberation analysis (free surfaces of PGM grains, grain size distribution, etc) together with leaching processes as shown by Kraemer et al. (2015) and Kraemer (2015) would help to increase recovery rates from currently 40% (Oberthür et al. 2016a) and would therefore increase the resource efficiency from active Cr mines as well as the reprocessing of old mine dumps.

- Mineral inclusions consisting also of amphiboles are observed in chromite grains of the LG and MG chromitites. A mineral chemistry study of these inclusions with respect to the Mg# of the inclusion in comparison to interstitial silicates can help to understand the formation processes of the chromitites.

11.2 Near-surface ore

- Experimental studies about the dissolution rates of the main minerals within the weathered ore can give further information about the fate of PGE during weathering. In the arid area of the Bushveld Complex different processes take place. Larger amounts of meteoric water and the interaction with sulfide will create sulfuric acids and therefore lower the pH. Platinum-group minerals and PGE-bearing phases can be dissolved at this stage. Afterwards, at changing conditions, certain minerals can precipitate and take up the PGE. Studies on natural minerals from the area can be used to estimate the dissolution rates in order to understand the kinetic processes taking place during weathering (dissolution and precipitation) of PGE ores.

- In order to obtain further information about the distribution of PGM in near-surface PGE ores and in soils overlying PGE ores and PGE-bearing chromitites, larger amounts of sample material can be processed by HS. The heavy mineral concentrates can then be further analyzed by MLA. This will give more detailed information about the shapes, mineral associations and chemistry of PGM in near-surface ores.

- The study of secondary minerals in the weathered ores by LA-ICP-MS already gave more robust information about the PGE distribution in secondary silicates than by EPMA due to the lower detection limits. More additional LA-ICP-MS work on secondary minerals in the weathered ores would be important for a larger database and would allow a mass balance calculations for the weathered ores.

- A synchrotron study (XAFS, XANES) on PGE-bearing secondary silicates and Fe-oxy/hydroxides can show the bonding and the charge of PGE within these mineral phases. This study can give further knowledge about the weathering processes of PGE ores and the incorporation or bonding of PGE to secondary minerals.

- Using field emission gun (FEG) electron beam methods (SEM and EPMA) more detailed information about the presence of PGE-oxides and weathering of PGM are possible due to the better resolutions of the more modern methods. Detailed FEG-SEM and EPMA stud-

ies would be possible on the distribution of PGE in Ni-laterites and ultramafic complexes similar to the work recently done by Aiglsperger et al. (2015b,a) on Ni-laterites from Falcondo (Dominican Republic) and on various other laterites as for example in Musongati (Burundi), Madagascar (McDonald et al. 1999a) or the Pirogues in New Caledonia (Augé & Legendre 1994). In order to produce PGM concentrates HS would be a useful tool. Cooperation with research groups in soils sciences, biomining and remote sensing in order to locate potential PGE bearing phases during drilling would be potential partners.

- Further CEC work on high-grade PGE ores using different substances besides ammonium acetate may support the ideas about the absorption of PGE on secondary minerals. Solutions containing different ions (e.g. $BaCl_2$, KCl, $MgCl_2$)) can be used for CEC experiments as well and may give additional information about the bonding of PGE to clay minerals.

Bibliography

Ahmed, A., Arai, S. (2002): Unexpectedly high-PGE chromitite from the deeper mantle section of the northern Oman ophiolite and its tectonic implications. Contributions to Mineralogy and Petrology 143, 263–278.

Aiglsperger, T., Proenza, J., Lewis, J., Labrador, M., Svojtka, M., Rojas-Purón, A., Longo, F., Durisova, J. (2016): Critical metals (REE, Sc, PGE) in Ni laterites from Cuba and the Dominican Republic. Ore Geology Reviews 73, 127–147.

Aiglsperger, T., Proenza, J., Lewis, J., Longo, F. (2015a): Multistage PGE Nugget Formation in Ni-Laterites: from Hpogene to Supergene, New Insights from Falcondo (Dominican Republic). Extended abstract 13th Biennial SGA Meeting Nancy, France 3, 1145–1148.

Aiglsperger, T., Proenza, J., Zaccarini, F., Lewis, J., Garuti, G., Labrador, M., Longo, F. (2015b): Platinum group minerals (PGM) in the Falcondo Ni-laterite deposit, Loma Caribe peridotite (Dominican Republic). Mineralium Deposita 50, 105–123.

Alapieti, T., Lahtinen, J. (2002): Platinum-group element mineralization in layered intrusions of the northern Finnland and the Kola peninsula, Russia. *In:* Cabri, L. (Ed.): The Geology, Geochemistry, Mineralogy and Mineral Beneficiation of Platinum-Group Elements, vol. 54 of *CIM Special*. Canadian Institute of Mining, Metallurgy and Petroleum, 507–546.

Andres, U., Timoshkin, I., Jirestig, J., Stallknecht, H. (2001): Liberation of valuable inclusions in ores and slags by electrical pulses. Powder Technology 114, 40–50.

Arai, S., Yurimoto, H. (1994): Podiform Chromitites of the Tari-Misaka Ultramafic Complex, Southwestern Japan, as Mantle-Melt Interaction Products. Economic Geology 89, 1279–1288.

Armitage, P., McDonald, I., Edwards, S., Manby, G. (2002): Platinum-group element mineralization in the Platreef and calc-silicate footwall at Sandsloot, Potgietersrus District, South Africa. Applied Earth Science (Transactions of the Institute of Mining and Metallurgy B) 111, B36–B45.

Armitage, P., McDonald, I., Tredoux, M. (2007): A geological investigation of the Waterberg hydrothermal platinum deposit, Mookgophong, Limpopo province, South Africa. Transaction of the Institution of Mining and Metallurgy 116, B113–B129.

Ashwal, L., Webb, S., Knoper, M. (2005): Magmatic stratigraphy in the Bushveld Northern Lobe: continuous geophysical and mineralogical data from the 2950 m Bellevue drillcore. South African Journal of Geology 108, 199–232.

Augé, T. (1985): Platinum-group mineral inclususions in ophiolitic chromitite from the Vourinos Complex, Greece. Canadian Mineralogist 23, 163–171.

Augé, T., Legendre, O. (1994): Platinum-Group element Oxides from the Pirogues Ophiolitic

Mineralization, New Caledonia: Origin and Significance. Economic Geology 89, 1454–1468.

Augusthitis, S. (1965): Mineralogical and geochemical studies of the platiniferous dunite-birbirite-pyroxenite complex of Yubdo, Birbir, W. Ethiopia. Chemie der Erde 24, 159–196.

Baedecker, P., Wasson, J. (1970): Gallium, Germanium, Indium, and Iridium in Lunar Samples. Science 167, 503–505.

Ballhaus, C., Ryan, C. (1995): Platinum-group elements in the Mereneky reef. I. PGE in solid solution in base metal sulfides and the down-teperature equilibration history of Merensky ores. Contributions to Minerlogy and Petrology 122, 241–251.

Ballhaus, C., Sylvester, P. (2000): Noble Metal Enrichment Processes in the Merensky Reef, Bushveld Complex. Journal of Petrology 41, 545–561.

Banfield, J., Welch, S., Zhang, H., Ebert, T., Penn, R. (2000): Aggregation-based crystal growth and microstructure development in natural iron oxyhydroxide biomineralization products. Science 289, 751–754.

Barnes, S., Roeder, P. (2001): The Range of Spinel Compositions in Terrestrial Mafic and Ultramafic Rocks. Journal of Petrology 42, 2279–2302.

Barnes, S.-J., Cox, R., Zientek, M. (2006): Platinum-group element, gold, silver, and base metal distribution in compositionally zoned sulfide droplets from the Medvezky Creek Mine, Noril'sk, Russia. Contributions to Mineralogy and Petrology 152, 187–200.

Barnes, S.-J., Maier, W. (1999): The fractionation of Ni, Cu and the noble metals in silicate and sulphide liquids. *In:* Keays, R., Lesher, C., Lightfoot, P., Farrow, C. (Eds.): Dynamic Processes in Magmatic Ore Deposits and Their Application to Mineral Exploration, vol. 13 of *Short Course Notes*. Geological Association of Canada, 69–106.

Barnes, S.-J., Maier, W. (2002a): Platinum-Group Element Distributions in the Rustenburg Layered Suite of the Bushveld Complex, South Africa. *In:* Cabri, L. (Ed.): The Geology, Geochemistry, Mineralogy and Mineral Beneficiation of Platinum-Group Elements, vol. 54 of *CIM Special*. Canadian Institute of Mining, Metallurgy and Petroleum, 431–458.

Barnes, S.-J., Maier, W. (2002b): Platinum-group Elements and Microstructures of Normal Merensky Reef from Impala Platinum Mines, Bushveld Complex. Journal of Petrology 43, 103–128.

Barnes, S.-J., Maier, W., Ashwal, L. (2007): Platinum-group element distribution in the Main Zone and Upper Zone of the Bushveld Complex, South Africa. Chemical Geology 208, 293–317.

Barnes, S.-J., Maier, W., Curl, E. (2010): Composition of the Marginal Rocks and Sills of the Rustenburg Layered Suite, Bushveld Complex, South Africa: Implications for the Formation of the Platinum-Group Element Deposits. Economic Geology, 105, 1491–1511.

Barnes, S.-J., Makovicky, E., Makovicky, M., Rose-Hansen, J., Karup-Møller, S. (1997): Partition coefficients for Ni, Cu, Pd, Pt, Rh and Ir between monoslulfide solid solution and sulphide liquid and the formation of compositionally zoned Ni-Cu sulphide bodies by fractional crystallization of sulphide liquid. Canadian Journal of Earth Science 34, 366–374.

Barnes, S.-J., Pagé, P., Prichard, H., Zientek, M., Fisher, P. (2016): Chalcophile and platinum-group element distribution in the Ultramafic series of the Stillwater Complex, MT, USA - implications for processes enriching chromite layers in Os, Ir, Ru, and Rh. Mineralium Deposita 51, 25–47.

Barnes, S.-J., Prichard, H., Cox, R., Fisher, P., Godel, B. (2008): The location of the chalcophile and siderophile elements in platinum-group element ore deposits (a textural, microbeam and whole rock geochemical study): implications for the formation of the deposits. Chemical Geology 248, 295–317.

Barnes, S.-J., Van Achterbergh, E., Makovicky, E., Li, C. (2001): Proton microprobe results of partitioning of platinum-group elements between monosulphide solid solution and sulphide liquid. South African Journal of Geology 104, 275–286.

Barrett, C., Massalski, T. (1980): Structure of Metals. International Series on Materials Science and Technology, Oxford, 3 edn., 654 pages.

Baumgartner, J., Dey, A., Bomans, P., Le Coadou, C., Frantzl, P., Sommerdijk, N., Faivre, D. (2013): Nucleation and growth of magnetite from solution. Nature Materials 12, 310–314.

Becker, K.-H., Wotruba, H. (2008): Aufbereitung von PGE-Oxiderzen. Berichte zur Lagerstätten- und Rohstoffforschung der Bundesanstalt für Geowissenschaften und Rohstoffe, 54 edn., 30 pages [in German].

Becker, M., Harris, P., Wiese, J., Bradshaw, D. (2009): Mineralogical characterisation of naturally floatable gangue in Merensky Reef ore flotation. International Journal of Mineral Processing 93, 246–255.

Becker, M., Ramonotsi, M., Petersen, J. (2012): Effect of alteration on the mineralogy and flotation performance of PPM platinum ore. *In:* Broekmans, M. (Ed.): Proceedings of the 10th International Congress for Applied Mineralogy (ICAM), vol. 10. Springer, 63–72.

Becker, M., Wiese, J., Ramonotsi, M. (2014): Investigation into the mineralogy and flotation performance of oxidized PGM ore. Minerals Engineering 65, 24–32.

Berg, G. (1928): Die neuen Platinvorkommen in Südafrika. Metallwirtschaft Special Print, 1–3 [in German].

Bernstein, L. (1985): Germanium geochemistry and mineralogy. Geochnica et Cosmochimica Acta 49, 2409–2422.

BGR (2016): Bundesanstalt fuer Geowissenschaften und Rohstoffe. `www.bgr.bund.de/`. [Online; accessed July-2016].

Bockrath, C., Ballhaus, C., Holzheid, A. (2004): Stability of laurite RuS2 and monosulfide liquid solution at magmatic temperatures. Chemcial Geology 208, 265–271.

Bowles, J. (1986): The development of plantinum-group minerals in laterites. Economic Geology 81, 1278–1285.

Bowles, J. (1987): Further studies of the development of platinum-group minerals in the laterites of the Freetown layered complex, Sierra Leone. *In:* Prichard, H., Potts, P., Bowles, J., Cribb, S. (Eds.): Geoplatinum ´87. London, Elsevier, 383–403.

Bowles, J. (1994): The mobility of the plantinum-group minerals in soils of the Freetown Peninsula, Sierre Leone. Canadian Mineralogist 32, 957–967.

Bowles, J., Gize, A., Vaughan, D. (1995): Organic controls on plantinum-group elements (PGE) solubility in soils: Initial data. Chronique de la Recherche Minière 520, 65–73.

Bowles, J., Lyon, I., Saxton, J., Vaughan, D. (2000): The origin of platinum group minerals from the Freetown Intrusion, Sierra Leone, inferred from osmium isotope systematics. Economic Geology 95, 539–548.

Brenan, J. (2002): Re-Os fractionation in magmatic sulphide melt by monosulfide solid solution.

Earth and Planetary Sciences Letters 199, 257–268.

Brenan, J., Andrews, D. (2001): High-temperature stability of the solubilty of laurite and Ru-Ir-Os alloy and their role on PGE fractionation in mafic magmas. Canadian Mineralogist 39, 341–360.

Brenan, J., Finnigan, C., McDonough, W., Homolova, V. (2012): Experimental constraints on the partitioning of Ru, Rh, Ir, Pt and Pd between chromite and silicate melt: The importance of ferric iron. Chemical Geology 302-303, 16–32.

Buchanan, D. (1981): The Genesis of Sulfide Mineralization in a Portion of the Potgietersrus Limb of the Bushveld Complex. Economic Geology 76, 568–579.

Buchanan, D., Rouse, J. (1984): Role of contamination in the precipitation of sulfides in the Platreef of the Bushveld Complex. *In:* Buchanan, D., Rouse, J. (Eds.): Sulfide deposits in mafic and ultramafic rocks, vol. 1 of *CIM Special*. Institution of Mining and Metallurgy, 141–146.

Buchholz, P., Foya, S. (2015): Investor's and Procurement Guide South Africa Part 2: Fluorspar, Chromite, Platinum Group Elements. DERA Rohstoffinformationen, 22 edn., 120 pages.

Bulatovic, S. (2003): Evaluation of alternative reagent schemes for the flotation of platinum group minerals from various ores. Minerals Engineering 16, 931–939.

Bulatovic, S. (2010): Handbook of Flotation Reagents Volume 2, Chemistry, Theory and Practice, Flotation of Gold, PGM, and Oxide Minerals. Elsevier, Amsterdam, 215 pages.

Burton, J., Culkin, F., Riley, J. (1959): The abundances of gallium and germanium in terrestrial materials. Geochimica et Cosmochimica Acta 16, 151–180.

Cabral, A., Beaudoin, G., Choquette, M., Lehmann, B., Polonia, J. (2007): Supergene leaching and formation of platinum in alluvium: evidence from Serro, Minas Gerais, Brazil. Mineralogy and Petrology 90, 141–150.

Cabri, L. (1976): Glossary of platinum-group minerals. Economic Geology 71, 1476–1480.

Cabri, L. (1981): Platinum-group minerals. *In:* Cabri, L. (Ed.): Platinum-group elements: mineralogy, geology, recovery, vol. 1. CIM Special Volume, 83–150.

Cabri, L. (1988): Applications of proton and nuclear microprobes in ore deposit mineralogy and metallurgy. Nuclear Instruments and Methods in Physics 30, 459–465.

Cabri, L. (1992): The distribution of trace precious metals in minerals and mineral products. Mineralogical Magazine 56, 289–308.

Cabri, L. (2002): The Platinum-Group Minerals. *In:* Cabri, L. (Ed.): The Geology, Geochemistry, Mineralogy and Mineral Beneficiation of Platinum-Group Elements, vol. 54 of *CIM Special*. Canadian Institute of Mining, Metallurgy and Petroleum, 13–129.

Cabri, L. (2013): Nanometer-sized platinum-group minerals (PGM) in base metal sulfides: new evidence for an orthomagmatic origin of the Merensky Reef PGE ore deposit, Bushveld Complex, South Africa: Discussion. Canadian Mineralogist 49, 817–819.

Cabri, L. (2015): Importance of sample preparation, representivity, and reporting methologies for quantitative evaluation of precious metal mineralogy. Joint Assembly meeting of the AGU-GAC-MAG-CGU abstract volume, 3–7 May 2015 in Montreal Canada.

Cabri, L., Blank, H., El Goresy, A., Laflamme, J., Nobiling, R., Sizgoric, M., Traxel, K. (1984): Quantitative trace-element analyses of sulfides from Sudbury and Stillwater by proton microprobe. Canadian Mineralogist 22, 521–542.

Cabri, L., Chryssoulis, S., De Villiers, J., Laflamme, J., Buseck, P. (1989): The nature of "invisible" gold in arsenopyrite. Canadian Mineralogoist 27, 353–362.

Cabri, L., Criddle, A., Laflamme, J., Bearne, G., Harris, D. (1981): Mineralogical study of complex Pt-Fe nuggets from Ethiopia. Bulletin de minéralogie 104, 508–525.

Cabri, L., Harris, D. (1975): Zoning in Os-Ir alloys and the relation of the geological and tectonic environment of the source rocks to the bulk Pt: Pt + Ir + Os ratio for placers. Canadian Minarlogist 13, 266–274.

Cabri, L., Harris, D., Weiser, T. (1996): Mineralogy and Distribution of Platinum-group Mineral (PGM) Placer Deposits of the World. Exploration and mining geology 5, 73–167.

Cabri, L., Kojonen, K., Gervilla, F., Oberthür, T., Weiser, T., Johanson, B., Sie, S., Campbell, J., Teesdale, W., Laflamme, J. (2002): Comparison of PGE trace analyses of pentlandite and some arsenides and sulfarsenides by EPMA and micro-PIXE. In: 9th International Platinum Symposium, Billings, Montana 21-25 July 2002, 73–80.

Cabri, L., Laflamme, J. (1981): Analyses of minerals containing platinum-group elements. *In:* Cabri, L. (Ed.): Platinum-group elements: mineralogy, geology, recovery, vol. 1. CIM Special Volume, 151–173.

Cabri, L., McDonald, A., Stanley, C., Rudashevsky, N., Poirier, G., Wilhelmij, H., Zhe, W., Rudashevsky, V. (2015): Palladosilicide, Pd_2Si, a new mineral from the Kapalagulu Intrusion, Western Tanzania and the Bushveld Complex, South Africa. Mineralogical Magazine 79, 295–307.

Cabri, L., Rudashevsky, N., Rudashevsky, V., Oberthür, T. (2008): Electric-Pulse Disaggregation (EPD), Hydroseparation (HS) and their use in combination for mineral processing and advanced characterization of ores. In: Canadian Mineral Processors 40th Annual Meeting Proceedings, Paper 14, 211–235.

Cameron, E. (1975): Postcumulus and subsolidus equilibration of chromite and coexisting silicates in the Eastern Bushveld Complex. Geochnica et Cosmochimica Acta 39, 1021–1033.

Cameron, E. (1977): Chromite in the central sector, eastern Bushveld Complex, South Africa. American Mineralogist 62, 1082–1096.

Cameron, E. (1978): The Lower Zone of the Eastern Bushveld Complex in the Olifants River Trough. Journal of Petrology 19, 437–462.

Cameron, E. (1980): Evolution of the lower Critical Zone, central sector, Eastern Bushveld Complex, and its chromite deposits. Economic Geology 75, 845–871.

Cameron, E. (1982): The Upper Critical Zone of the Eastern Bushveld Complex - precursor to the Merensky Reef. Economic Geology 77, 1307–1327.

Cameron, E., Hattori, K. (2005): Platinum Group Elements in Geochemical Exploration. *In:* Mungall, J. (Ed.): Exploration for platinum-group element deposits: Short Course Series, Oulu Finland, vol. 35. Mineralogical Association of Canada, 287–307.

Campbell, I., Naldrett, A. (1979): The influence of silicate:sulfide ratios on the geochemistry og magmatic sulfides. Economic Geology 74, 2248–2253.

Campbell, I., Naldrett, A., Barnes, S. (1983): A model for the origin of the platinum-rich sulfide horizons in the Bushveld and Stillwater Complexes. Journal of Petrology 24, 133–165.

Capobainco, C., Drake, M. (1990): Partioning of ruthenium, rhodium, and palladium between spinell and silcate metl and implications for platinum group element fractionation trends.

Geochmica et Cosmochimca Acta 52, 869–874.

Cawthorn, G., Lee, C., Schouwstra, R., Mellowship, P. (2002a): Relationship between PGE and PGM in the Bushveld Complex. The Canadian Mineralogist 40, 311–328.

Cawthorn, G., Webb, S. (2001): Connectivity between the western and eastern limbs of the Bushveld Complex. Tectonophysics 330, 195–209.

Cawthorn, R. (1996): Layered Intrusions. Developments in Petrology 15, Elsevier, 531 pages.

Cawthorn, R. (1999a): The platinum and palladium resources of the Bushveld Complex. South African Journal of Science 95, 481–489.

Cawthorn, R. (1999b): Platinum-group element mineralization in the Bushveld-Complex - a critical reassessment of geochemical models. South African Journal of Geology 102, 268–281.

Cawthorn, R. (2011): Geological interpretations from the PGE distribution in the Bushveld Merensky and UG2 chromitite reefs. The Journal of The Southern African Institute of Mining and Metallurgy 111, 67–79.

Cawthorn, R. (2015): The Bushveld Complex, South Africa. *In:* Charlier, B., Namur, O., Latypov, R., Tegner, C. (Eds.): Layered Intrusions, vol. 1. Springer, 517–587.

Cawthorn, R., Barnes, S., Ballhaus, C., Malitch, K. (2005): Platinum group element, chromium and vanadium deposits in mafic and ultramafic rocks. Economic Geology, 100th Anniversary Volume , 215–249.

Cawthorn, R., Barton Jr, J., Viljoen, M. (1985): Interaction of Floor Rocks with the Platreef on Overysel, Potgietersrus, Northern Transvaa. Economic Geology 80, 988–1006.

Cawthorn, R., Davies, G., Clubley-Armstrong, A., McCarthy, T. (1981): Sills associated with the Bushveld Complex, South Africa: an estimate of the parental magma composition. Lithos 14, 1–15.

Cawthorn, R., Merkle, R., Viljoen, M. (2002b): Platinum-Group Element Deposits in the Bushveld Complex, South Africa. *In:* Cabri, L. (Ed.): The Geology, Geochemistry, Mineralogy and Mineral Beneficiation of Platinum-Group Elements, vol. 54 of *CIM Special*. Canadian Institute of Mining, Metallurgy and Petroleum, 389–429.

Cawthorn, R., Walraven, F. (1998): Emplacement and crystallization time for the Bushveld Complex. Journal of Petrology 39, 1669–1687.

Charlier, B., Namur, O., Latypov, R., Tegner, C. (2015): Layered Intrusions. Springer, 531 pages.

Ciobanu, C., Cook, N., Utsunomiya, S., Pring, A., Green, L. (2011): Focussed ion beam-transmission electron microscopy application in ore mineralogy: bridging micro- and nanoscale observations. Ore Geology Reviews 42, 6–31.

Clarke, F. W., Washington, H. (1924): The composition of the Earth‘s crust. Washington Government Printing Office, 1 edn., 117 pages.

Coggon, J., Nowell, G., Pearson, D., Oberthür, T., Lorand, J.-P., Melcher, F., Parman, S. (2011): Application of the 190Pt-186Os system to dating platinum mineralization and ophiolite formation: an example from the Meratus Mountains, Borneo. Economic Geology 106, 93–117.

Coggon, J., Nowell, G., Pearson, D., Oberthür, T., Lorand, J.-P., Melcher, F., Parman, S. (2012): The 190Pt-186Os decay system applied to dating platinum-group element mineralization of the Bushveld Complex, South Africa. Chemical Geology 302-303, 48–60.

Commons, A. (2009): Commons-Math: The Apache Commons mathematics. `http://commons.apache.org/math/`. [Online; accessed July-2016].

Cousins, C., Feringa, G. (1964): The chromite deposits of the western belt of the Bushveld Complex. *In:* Haughton, S. (Ed.): The Geology of some Ore Deposits in Southern Africa, vol. 2. Geological Society of South Africa, 183–202.

Cousins, C., Kinloch, E. (1976): Some observations on textures and inclusions in alluvial planinoids. Economic Geology 71, 1377–1398.

Cowley, A. (2013): Platinum 2013 - Interim Review. Johnson Matthey Public Limited Company, 1 edn., 36 pages.

Crundwell, F., Moats, M., Ramachandran, V., Robinson, T., Davenport, W. (2011): Extractive Metallurgy of Nickel, Cobalt and Platinum-Group Metals. Elsevier Ltd, Oxford, 1 edn., 610 pages.

Czamanske, G., Kunilov, V., Zientek, M., Cabri, L., Likhachev, L., A.P.and Calk, Oscarson, R. (1992): A protron microprobe study of magmatic sulfide ores from the Noril'sk-Talnakh district, Siberia. Canadian Mineralogist 30, 249–287.

Daltry, V., Wilson, A. (1997): Review of platinum-group mineralogy: compositions and elemental associations of the PG-minerals and unidentified PGE-phases. Mineralogy and Petrology 60, 185–229.

Dare, S., Barnes, S.-J., Prichard, H. (2010): The distribution of platinum group elements (PGE) and other chalcophile elements among sulfides from the Creighton Ni-Cu-PGE sulfide deposit, Sudbury, Canada, and the origin of palladium in pentlandite. Mineralium Deposita 45, 765–793.

Dare, S., Barnes, S.-J., Prichard, H., Fisher, P. (2011): Chalcophile and platinum-group element (PGE) concentrations in the sulfide minerals from the McCreedy East deposit, Sudbury, Canada, and the origin of PGE in pyrite. Mineralium Deposita 46, 381–407.

Davey, S. (1992): Lateral variations within the upper Critical Zone of the Bushveld Complex on the farm Rooikoppies 297 JQ, Marikana, South Africa. South African Journal of Geology 95, 141–149.

Dick, H., Bullen, T. (1984): Chromian spinel as a petrogenetic indicator in abyssal and alpine-type peridotites and spatially associated lavas. Contributions to Mineralogy and Petrology 86, 54–76.

Distler, V., Malevsky, A., Laputina, I. (1977): Distribution of platinoids between pyrrhotite and pentlandite in crystallization of a sulphide melt. Geochemica International 14, 30–40.

Djon, M. (2010): Changement de la mineralogie des sulfures, des mineraux du groupe du platine et des textures avec le degree d'alteration des zones Roby, Twilight and high-grade du complexe du Lac-Des-Iles (Ontario, Canada). L'Universtité du Québec à Chicoutimi Comme exigence Partielle de La Maitrise en Sciences de la Terre, msc. thesis edn., 95 pages [in French].

Djon, M., Barnes, S.-J. (2012): Changes in sulfides and platinum-group minerals with the degree of alteration in the Roby, Twilight, and High Grade Zones of the Lac des Iles Complex, Ontario, Canada. Mineralium Deposita 47, 875–896.

Dubrovsky, M., Rundqvist, T. (2009): Petrology of the early Proterozoic plaintum-bearing massiv of Fedorov Tundrea, Kola peninusula. Geology of ore deposits 51, 577–587.

Dubrovsky, M., Rundqvist, T. (2015): Chalcophile and platinum-group element distribution in pyrites from the sulfide-rich pods of the Lac des Iles Pd deposits,Western Ontario, Canada: Implications for post-cumulus re-equilibration of the ore and the use of pyrite compositions in exploration. Journal of Geochemical Exploration 158, 223–242.

Duran, C., Barnes, S.-J., Corkery, J. (2016): Trace element distribution in primary sulfides and Fe-Ti oxides from the sulfide-rich pods of the Lac des Iles Pd deposits,Western Ontario, Canada: Constraints on processes controlling the composition of the ore and the use of pentlandite compositions in exploration. Journal of Geochemical Exploration 166, 45–63.

Eales, H., Marsh, J., Mitchell, A., de Klerk, W., Kruger, F. J., Fields, M. (1986): Some geochemical constraints upon models for the crstallization of the upper critical zone - main zone interval, Northwestern Bushveld Complex. Mineralogical Magazine 50, 567–582.

Eales, H., Reynolds, I. (1986): Cryptic Variations within Chromitites of the Upepr Critical Zone, Northwestern Bushveld Complex. Economic Geology 81, 1056–1066.

Eales, H. V., Cawthorn, R. G. (1996): The Bushveld Complex. *In:* Cawthorn, R. (Ed.): Layeres Intrusions. Amsterdam: Elsevier, 181–230.

Eckstrand, O. (1975): The Dumont Serpentinite: A Model for Control of Nickeliferous opaque mineral assemblages by alteration reactions in ultramafic rocks. Economic Geology 70, 183–201.

Ely, J., Neal, C., Kulpa, C., Schneegurt, M., Seidler, J., Jain, J. (2001): Implications of platinum-group element accumulations along U.S. roads from catalytic converter attrition. Environmental Science and Technology 35, 3816–2822.

European-Commission (2004): Report on critical raw materials for the EU. European Commission, 1 edn., 41 pages.

Evans, D. (2002): Potential for bulk mining of oxidized platinum-group element deposits. Applied Earth Science (Transactions of the Institute of Mining and Metallurgy B) 307, B81–B86.

Evans, R. (1966): An introduction to crystal chemistry. University Printing Home, Cambridge, 2 edn., 410 pages.

Fandrich, R., Gu, Y., Burrows, D., Moeller, K. (2007): Modern SEM-based mineral liberation analysis. International journal of mineral processing 84, 310–320.

Finnigan, C., Brenan, J., Mungall, J., McDonough, W. (2008): Experiments and models bearing on the role of chromite as a collector of platinum group minerals by local reduction. Journal of Petrology 49, 1647–1665.

Fleet, M., Chryssoulis, S., Stone, W., Weisener, C. (1993): Implications of the chromium budget of the Western Limb of the Bushveld Complex. South African Journal of Geology 115, 36–44.

Fleet, M., Crocket, J., Liu, M., Stone, W. (1999a): Laboratory partitioning of platinum-group elements (PGE) and gold with application to magmatic sulfide-PGE deposits. Lithos 47, 127–142.

Fleet, M., Liu, M., Crocket, J. (1999b): Partitioning of trace amounts of highly siderophile elements in the Fe-Ni-S system and their fractionation in nature. Geochmica et Cosmochimca Acta 63, 2611–2622.

Fleet, M., Stone, W. (1991): Partitioning of platinum-group elements in the Fe-Ni-S system and their fractionation in nature. Geochmica et Cosmochimca Acta 55, 245–253.

Fonseca, R., Campbell, I., O'Neill, H., Allen, C. (2009): Solubility of Pt in sulphide mattes:

Implications for the genesis of PGE-rich horizons in layered intrusions. Geochmica et Cosmochimca Acta 73, 5764–5777.

Fuchs, W., Rose, A. (1974): The geochemical behavior of platinum and palladium in the weathering cycle in the Stillwater complex, Montana. Economic Geology 69, 332–346.

Gain, S. (1985): The Geological Setting of Platiniferous UG-2 Chromitite layer on the Farm Maandagshoek, Eastern Bushveld Complex. Economic Geology 80, 925–943.

Gain, S., Mostert, A. (1982): The Geological Setting of the Platinoid and Base Metal Sulfide Mineralization in the Platreef of the Bushveld Complex in Drenthe, North of Potgietersru. Economic Geology 77, 1395–1404.

Garuti, G., Zaccarini, F., Proenza, J., Thalhammer, O., Angeli, N. (2012): Platinum-group minerals in chromitites of the Niquelandia Layered Intrusion (Central Goias, Brazil): Their Magnmatic Origin and Low-Temperature Reworking during serpentinization and lateritic weathering. minerals 2, 365–384.

Gebauer, D., Volkel, A., Cölfen, H. (2008): Stable prenucleation calcium carbonate clusters. Science 322, 1819–1822.

Genkin, A., Bortnikov, N., Cabri, L., Wagner, F., Stanley, C., Safonov, Y., McHahon, G., Friedl, J., Kerzin, A., Gamyanin, G. (1998): A multidisciplinary study of invisible gold in arsenopyrite from four mesothermal gold deposits in Siberia, Russian Federation. Economic Geology 93, 463–487.

Gervilla, F., Cabri, L., Kojonen, K., Oberthür, T., Weiser, T., Johanson, B., Sie, S., Campbell, J., Teesdale, W., Laflamme, J. (2004): Platinum group element distribution in some ore deposits: results of EPMA and Micro-PIXE analyses. Microchimica Acta 147, 167–173.

Gervilla, F., Kojonen, K. (2002): The platinum-group minerals in the upper section of the Keivitsansarvi Ni-Cu-PGE deposit, northern Finland. Canadian Mineralogist 40, 377–394.

Gervilla, F., Proenza, J., Frei, R., González-Jiménez, J., Garrido, C., Melgarejo, A., J.C. and. Meibom, Díaz-Martínez, R., Lavaut, W. (2005): Distribution of platinum-group elements and Os isotopes in chromite ores from Mayarí-Baracoa Ophiolitic Belt (eastern Cuba). Contributions to Mineralogy and Petrology 150, 589–607.

Gilbert, D., Danyushevsky, L., Robinson, P., Wohlgemuth-Ueberwasser, C., Pearson, N., Savard, D., Norman, M., Hanley, J. (2012): A Comparative Study of Five Reference Materials and the Lombard Meteorite for the Determination of the Platinum-Group Elements and Gold by LA-ICP-MS. Geostandards and Geoanalytical Research 37, 51–54.

Godel, B. (2015): Platinum-group element deposits in layered intrusions: recent advances onm the understanding of the ore forming proccesses. *In:* Charlier, B., Namur, O., Latypov, R., Tegner, C. (Eds.): Layered Intrusions, vol. 1. Springer, 379–432.

Godel, B., Barnes, S.-J. (2008): Platinum-group elements in sulfide minerals and th whole rocks of the J-M Reef (Stillwater Complex): Implication for the formation of the reef. Chemical Geology 248, 272–294.

Godel, B., Barnes, S.-J., Maier, W. (2007): Platinum-Group Elements in Sulphide Minerals, Platinum-Group Minerals, and Whole-Rocks of the Merensky Reef (Bushveld Complex, South Africa): Implications for the Formation of the Reef. Journal of Petrology 48, 1569–1604.

Godel, B., Barnes, S.-J., Maier, W. (2011): Parental magma composition inferred from trace

element in cumulus and intercumulus silicate minerals: An example from the Lower and Lower Critical Zones of the Bushveld Complex, South Africa. Lithos 125, 537–552.

Goldschmidt, V. (1926): Geochemische Verteilungsgesetze der Elemente - VII Die Gesetze der Kristallochemie. ASkrifter utgitt av det Norske Videnskaps Akademi i Oslo, 1: Matematisk - naturvidenskapelig klasse, University of Oslo, 117 pages [in German].

Goldschmidt, V. (1937): The principles of distribution of chemical elements in minerals and rocks. The seventh Hugo Müller Lecture, delivered before the Chemical Society 7, 655–673.

Goldschmidt, V. (1954): Geochemistry. At the Clarendon Press, 730 pages.

Goldschmidt, V., Peters, C. (1933): Zur Geochemie des Germaniums. Nachrichten von der Gesellschaft der Wissenschaften zu Goettingen, Mathematisch-Physikalische Klasse 1, 141–166 [in German].

Gonzáles-Jiménez, J., Gervilla, F., Proenza, J., Augé, T., Kerestedijan, T. (2009): Distribution of platinum-group minerals in ophiolitic chromitites. Applied Earth Science (Transactions of the Institutions of Mining and Metallurgy: Section B) 118, 101–110.

Gonzáles-Jiménez, J., Reich, M. (2016): An overview of the platinum-group element nanoparticles in mantle-hosted chromite deposits. Ore Geology Reviews actepted manuscripte, online.

Gonzáles-Jiménez, J., Reich, M., Camprubí, A., Gervilla, F., Griffin, W. L., Colás, V., O'Reilly, S., Proenza, J. A., Pearson, N., Centeno-García, E. (2015): Thermal metamorphism of mantle chromites and the stability of noble metal nanoparticles. Contributions to Mineralogy and Petrology 170, 1–20.

Good, N., Wit, M. (1997): The principles of distribution of chemical elements in minerals and rocks. Journal of the Geological Society, London 154, 93–97.

Gordon, R., Bertam, M., Graedel, T. (2006): Metal stocks and sustainability. Proceedings of the National Academy of Sciences of the United States of America 103, 1209–1214.

Greß, M. (2012): Platinum-group element (PGE) distribution in sulfides from the Merensky Reef (South Africa). University of Erlangen, unpublished bsc thesis edn., 32 pages.

Gresens, R. (1967): Composition-volume relationships of metasomatism. Chemical Geology 2, 47–65.

Grokhovskaya, T., Lapina, M., Ganin, V., Grinevich, N. (2005): PGE mineralization in the Burakovsk Layered Complex, Southern Karelia, Russia. Geology Ore Deposits 47, 283–308.

Gu, Y. (2003): Automated Scanning Electron Microscope Based Mineral Liberation Analysis. Journal of Minerals and Materials Characterization and Engineering 2, No.1, 33–41.

Gu, Y., Schouwsta, R., Rule, C. (2014): The value of automated mineralogy. Minerals Engineering 58, 100–103.

Gunn, G. (2014): Platinum-group metals. *In:* Gunn, G. (Ed.): Critical Metals Handbook, vol. 1. John Wiley and Sons, 284–311.

Hall, A. (1932): The Bushveld Igneous Complex in the central Transvaal. Geological Society of South Africa Memoir, 28 edn., 544 pages.

Hamilton, P. (1977): Sr isotope and trace element studies of the Great Dyke and Bushveld mafic phase and their relation to early Proterozoic magma genesis in southern Africa. Journal of Petrology 18, 24–52.

Hanley, J. (2005): The aqueous geochemistry of the platinum-group elements (PGE) in surfical, low-T hydrothermal and high-T magmatic hydrothermal environemnts. *In:* Mungall, J. (Ed.):

Exploration for platinum-group element deposits: Short Course Series, Oulu Finland, vol. 35. Mineralogical Association of Canada, 35–56.

Harris, C., Chaumba, J. (2001): Crustal contamination and fluid-rock interaction during the formation of the Platreef, Northern Limb of the Bushveld Complex, South Africa. Journal of Petrology 42, 1321–1347.

Harris, C., Pronost, J., Ashwal, L., Cawthorn, R. (2005): Oxygen and hydrogen isotope stratigraphy of the Rustenburg Layered Suite Bushveld Complex: constraints crustal contamination. Journal of Petrology 46, 579–601.

Harris, P. (1954): The distribution of germanium among coexisting phases of partly glassy rocks. Geochimica et Cosmochimica Acta 5, 185–195.

Hart, S., Kinloch, E. (1989): Osmium isotope systematics in Witwatersrand and Bushveld ore deposits. Economic Geology 84, 1651–1655.

Hatton, C., von Gruenewaldt, G. (1985): Chromite from the Swartkop Chrome Mine An Estimate of the Effects of SubsolidusR eequilibration. Economic Geology 80, 911–924.

Hatton, C., von Gruenewaldt, G. (1987): The geological setting and petrogenesis of the Bushveld chromitite layers. *In:* Stowe, C. (Ed.): Evolution of chromium ore fields. New York: Van Nostrand Reinhold Co., 109–143.

Hattori, K., Cameron, E. (2004): Using the high mobility of Palladium in Surface Media in Exploration for Platinum Group Element Deposits: Evidence from the Lac des Iles Region, Northwestern Ontario. Economic Geology 99, 127–171.

Hattori, K., Takahasi, Y., Augé, T. (2010): Mineralogy and origin of oxygen-bearing platinum-iron grains based on an X-ray absorption spectroscopy study. American Mineralogist 95, 622–630.

Hazen, R., Grew, E., Downs, R., Golden, J., Hystad, G. (2015): Mineral ecology: chance and neccessity in the mineral diversity of terrestrial planets. Canadian Mineralogist 52, 295–324.

Heinrich, C., Pettke, T., Halter, W., Aigner-Torres, M., Audétat, A., Günther, T., Hattendorf, B., Bleiner, D., Guillong, M., Horn, I. (2003): Quantitative multi-element analysis of minerals, fluid and melt inclusions by laser-ablation inductively-coupled-plasma mass-spectrometry. Geochimica et Cosmochimica Acta 67, 3473–3497.

Helmy, H., Ballhaus, C., Bermdt, J., Bockrath, C., Wolgemuth-Ueberwasser, C. (2007): Formation of Pt, Pd and Ni tellurides: experiments in sulfide-telluride systems. Contributions to Mineralogy and Petrology 153, 577–591.

Helmy, H., Ballhaus, C., Wirth, R. (2013): Noble metal nanoclusters and nanoparticles precede mineral formation in magmatic sulphide melts. Nature communications 4, 1–7.

Helmy, H., Ballhaus, C., Wolgemuth-Ueberwasser, C., Fonseca, R., Laurenz, V. (2010): Partitioning of Se, As, Sb, Te and Bi between monosulfide solid solution and sulfide melt - Application to magmatic sulfide deposits. Geochmica et Cosmochimca Acta 74, 6174–6179.

Hey, P. (1999): The effects of weathering on the UG-2 chromitite reef with special reference to the platinum-group minerals. South African Journal of Geology 102, 251–260.

Hiemstra, S. (1979): The role of collectors in the formation of platinum deposits in the Bushveld. Canadian Mineralogist 17, 469–482.

Hiemstra, S. (1985): The Distribution of Some Platinum-Group Elements in the UG-2 Chromitite Layer of the Bushveld Complex. Economic Geology 80, 944–957.

Hiemstra, S. (1986): The Distribution of Chalcophile and Platinum-Group Elements in the UG-2 Chromitite Layer of the Bushveld Complex. Economic Geology 81, 1080–1086.

Hill, R., Craig, J., Gibbs, G. (1979): Systematics of the Spinel Structure Type. Physics and Chemistry of Minerals 4, 317–339.

Höll, R., Kling, M., Schroll, E. (2006): Metallogenesis of germanium - a review. Ore Geology Reviews 30, 145–180.

Hoffman, E., Clark, J., Yeager, J. (1998): Gold analysis - fire assaying and alternative methods. Exploration Mining Geology 7, 155–160.

Hoffman, E., Dunn, B. (2002): Sample preparation and bulk analytical methods for PGE. *In:* Cabri, L. (Ed.): The Geology, Geochemistry, Mineralogy and Mineral Beneficiation of Platinum-Group Elements, vol. 54 of *CIM Special*. Canadian Institute of Mining, Metallurgy and Petroleum, 1–11.

Hoffman, E., Naldrett, A., Van Loon, J., Hancock, R., Manson, A. (1978): The determination of all the platinum group elements and gold in rocks and ore by neutron activation analysis after preconcentrating by a nickel sulphide fire-assay technique on large samples. Analytica Chimica Acta 102, 157–166.

Holwell, D., Armitage, P., McDonald, I. (2005): Observations on the relationship between the Platreef and its hangingwall. Applied Earth Science (Transactions of the Institute of Mining and Metallurgy B) 114, B199–B207.

Holwell, D., Armitage, P., McDonald, I. (2006): Platinum-group mineral assemblages in the Platreef at the Sandsloot Mine, northern Bushveld Complex, South Africa. Mineralogical Magazine 70, 83–101.

Holwell, D., Boyce, A., McDonald, I. (2007): Sulfur Isotope Variations within the Platreef Ni-Cu-PGE Deposit: Genetic Implications for the Origin of Sulfide Mineralization. Economic Geology 102, 1091–1110.

Holwell, D., McDonald, I. (2006): Petrology, geochemistry and the mechanisms determining the distribution of platinum-group element and base metal sulphide mineralisation in the Platreef at Overysel, northern Bushveld Complex, South Africa. Mineralium Deposita 41, 575–598.

Holwell, D., McDonald, I. (2007): Distribution of platinum-group elements in the Platreef at Overysel, northern Bushveld Complex: a combined PGM and LA-ICP-MS study. Contributions to Mineralogy and Petrology 154, 171–190.

Holwell, D., McDonald, I. (2010): A Review of the Behavior of Platinum Group Elements within Natural Magmatic Sulfide Ore Systems. Platinum Metals Review 64, 26–36.

Holwell, D., McDonald, I. (2014): A Review of the Behavior of Platinum Group Elements within Natural Magmatic Sulfide Ore Systems. Platinum Metals Review 64, 26–36.

Holwell, D., McDonald, I., Butler, I. (2011): Precious metal enrichement in the Platreef, Bushveld Complex, South Africa: evidence from homogenized magmaric sulfide melt inclusions. Contributions to Mineralogy and Petrology 161, 1011–1026.

Hörmann, P. (1963): Zur geochemie des germaniums. Geochimica et Cosmochimica Acta 27, 861–876.

Hulbert, L., Von Gruenwald, G. (1985): Textural and compositional features of chromite in the Lower and Critical Zone of the Bushveld Complex, South of Potgietersrus. Economic Geology 80, 872–865.

Huminicky, M., Sylvester, P., Cabri, L., Lesher, C., Tubrett, M. (2005): Quantitative mass balence of platinum-group elements in the Kelly Lake Ni-Cu-PGe deposit, Copper Cliff Offsett Sudbury. Economic Geology 100, 1631–1646.

Hutchinson, D., Kinnaird, J. (2005): Complex multistage genesis for the Ni-Cu-PGE mineralisation in the southern region of the Platreef, Bushveld Complex, South Africa. Applied Earth Science (Transactions of the Institute of Mining and Metallurgy B) 114, B208–BB224.

Hutchinson, D., McDonald, I. (2008): Laser ablation ICP-MS study of platinum-group elements in sulphides from the Platreef at Turfspruit, northern limb of the Bushveld Complex, South Africa. Mineralium Deposita 43, 695–711.

IMA (2016): IMA Database of Mineral Properties. `http://rruff.info/ima/`. [Online; accessed November-2016].

Institute for Mineralogy - University Hannover (2016): Analytical methods. `https://www.mineralogie.uni-hannover.de/`. [Online; accessed July-2016].

Irvine, T. (1965): Chromian spinel as a petrogenetic indicator, Part I. Theory. Canadian Jounral of Earth Science 2, 648–672.

Irvine, T. (1967): Chromian spinel as a petrogenetic indicator, Part 2. Petrologic applications. Canadian Jounral of Earth Science 4, 71–103.

Irvine, T. (1975): Crytallization sequences in the Muskox intrusion and other layered intrusions, II. Origin of chromitite layeres and similar deposits of other magmatic ores. Geochimica et Cosmochimica Acta 39, 991–1020.

Irvine, T. (1977): Origin of chromitite layers in the Muskox intrusion and other stratiform intrusions: A new interpretation. Geology 5, 273–277.

Ivanhoe (2016): Ivanhoe Platreef Project. `https://www.ivanhoemines.com/projects/platreef-project`. [Online; accessed October-2016].

Ivanov, O. (1996): Platinum mineralization of the Nizhniy Tagil concentric zoned pyroxenite-dunite massif. Izvestiya vysshikh uchebnykh zavedeniy Gorny zhurnal 3-4, 63–71.

Jackson, E. (1969): Chemical Variation in Coexisting Chromite and Olivine in Chromitite Zone of the Stillwater Complex. *In:* Wilson, H. (Ed.): Magmatic Ore Deposits. Economic Geology Monograph 4, 41–71.

Jannessary, M., Melcher, F., Lodziak, J., Meisel, T. (2012): Review of platinum-group element distribution and mineralogy in chromitite ores from southern Iran. Ore Geology Reviews 48, 278–305.

Jarvis, K., Parry, S., Piper, J. (2001): Temporal and spatial studies of autocatalyst-derived platinum, rhodium and palladium and selected vehicle-derived trace elements in the environment. Environmental Science and Technology 35, 1031–1036.

Jedwab, J. (1995): Oxygenated platinum-group element and transition-metal (Ti,Cr, Mn, Fe, Co, Ni) compounds in supergene environments. Chronique de la recherche de minière 520, 47–53.

JFree (2009): JFreeChart, Java chart library. `http://www.jfree.org/jfreechart/`. [Online; accessed July-2016].

Jochum, K., Weis, U., Stoll, B., Kuzmin, D., Yang, I., Q. Raczek, Jacob, D., Stracke, A., Birbaum, K., Frick, D., Günther, D., Enzweiler, J. (2011): Determination of Reference Values for NIST SRM 610 617 Glasses Following ISO Guidelines. Geostandards and Geoanalytical

Research 35, 397–429.

Johan, Z. (2002): Alaskan-type Complexes and Their Platinum-Group Element Mineralization. *In:* Cabri, L. (Ed.): The Geology, Geochemistry, Mineralogy and Mineral Beneficiation of Platinum-Group Elements, vol. 54 of *CIM Special*. Canadian Institute of Mining, Metallurgy and Petroleum, 669–719.

Johansson, C., Linde, J. (1925): Röntgenographische Bestimmung der Atomanordnung in den Mischkristallreihen Au-Cu und Pd-Cu. Ann Phys 383, 439–460.

Johnson Matthey (2016): Platinum Matthey Precious Metals Management. `http://www.platinum.matthey.com/`. [Online; accessed November-2016].

Josties, A. (2012): Petrological and geochemical investigations of the alteration in the UG-2 of the eastern Bushveld Complex, South Africa. University of Erlangen, diploma thesis edn., 72 pages.

Jugo, P., Luth, R., Richards, J. (2005): An Experimental Study of the Sulfur Content in Basaltic Melts Saturated with Immiscible Sulfide or Sulfate Liquids at 1300řC and 1.0 GPa. Journal of Petrology 46, 783–798.

Junge, M., Oberthür, T., Kraemer, D., Melcher, F. (2015a): Distribution of Platinum-Group Elements in Pristine and Near-Surface Ores from the Platreef, Northern Bushveld Complex, South Africa. Extended abstract 13th Biennial SGA Meeting Nancy, France 3, 955–958.

Junge, M., Oberthür, T., Melcher, F. (2014): Cryptic variation of chromite chemistry, platinum-group element and platinum group mineral distribution in the UG-2 chromitite: An example of the Karee Mine, western Bushveld Complex, South Africa. Economic Geology 109, 795–810.

Junge, M., Oberthür, T., Osbahr, I., Gutter, P. (2016): Platinum-group elements and minerals in the lower and middle group chromitites of the western Bushveld Complex, South Africa. Mineralium Deposita 51, 841–852.

Junge, M., Wirth, R., Oberthür, T., Melcher, F., Schreiber, A. (2015b): Mineralogical siting of platinum-group elements in pentlandite from the Bushveld Complex, South Africa. Mineralium Deposita 50, 41–54.

Kaneda, H., Takenouchi, S., Shoji, T. (1986): Stability of pentlandite in the Fe-Ni-Co-S system. Mineralium Deposita 21, 169–180.

Karup-Møller, S., Makovicky, E. (1993): The System Pd-Ni-S at 900°C, 725°C, 550°C, and 400°C. Economic Geology 88, 1261–1268.

Kaufmann, F., Bethke, M., Schannor, M., Manyeruke, R., Hecht, L. (2014): Variation in mineral chemistry across the UG2 chromitite layer, Eastern Bushveld Complex. *In:* Chetty, D., Andres, L., de Villiers, J., Dixon, R., Nex, P., Reimold, W., Richards, J., B., S., Smith, C., Verryn, S., Viljoen, F. (Eds.): 21st General Meeting of the IMA South Africa 2014. Geological Society of South Africa and the Mineralogical Association of South Africa, 235.

Keays, R. (1995): The role of komatiitic and picritic magmatism and S-saturation in the formation of ore deposits. Lithos 34, 1–18.

Kieser, N. (1994): In-situ modification of platinum-group minerals in Tonsina Ultramafic Complex, south-central Alaska: implcations for surfical dispersion and geochemical exploration. Applied Earth Science (Transactions of the Institutions of Mining and Metallurgy: Section B) 103, 45–51.

Kinloch, E. D. (1982): Regional trends in the platinum-group mineralogy of the Critical Zone of the Bushveld Complex, South Africa. Economic Geology 77, 1328–1347.

Kinnaird, J. (2005): Geochemical evidence for multiphase emplacement in the southern Platreef:. Applied Earth Science (Transactions of the Institute of Mining and Metallurgy B) 114, B225–B242.

Kinnaird, J., Hutchinson, D., Schurmann, L., Nex, P., de Lange, R. (2005): Petrology and mineralisation of the southern Platreef: northern limb of the Bushveld Complex, South Africa. Mineralium Deposita 40, 576–597.

Kinnaird, J., McDonald, I. (2005): An introduction to mineralization in the northern limb of the Bushveld Complex. Applied Earth Science (Transactions of the Institutions of Mining and Metallurgy: Section B) 114, B194–B198.

Kinnaird, J., Yudovskaya, M., Botha, M. (2014): The Waterberg extension of the Bushveld Complex. *In:* Anikina, E., Ariskin, A., Barnes, S.-J., Barnes, S., A.A., B., Evstigneeva, T., Kinnaird, J., Latypov, R., Li, C., Maier, W., Malitch, K., Melcher, F., Pushkarev, E., Ripley, E., Votyakov, S., Vymazalova, A., Yudovskaya, M., Zaccarini, F. (Eds.): 12th International platinum symposium, vol. 1 of *UB RAS*. Yekaterinburg: Institute of Geology and Geochemistry, 135–136.

Klemd, R., Junge, M., Oberthür, T., Herderich, T., Schouwstra, R., Roberts, J. (2016): Platinum-group element concentrations in base-metal sulphides from the Platreef, Mogalakwena Platinum Mine, Bushveld Complex, South Africa. South African Journal of Geology acepted, manuscript.

Kocks, H., Melcher, F., Meisel, T., Burgaht, K.-P. (2007): Diverse contributing sources to chromitite petrogenesis in the Shebenik Ophiolitic Complex, Albania: evidence from new PGE- and Os-isotope data. Mineralogy and Petrolgy 91, 139–170.

Komarova, M., Kozyrev, S., Simonov, O., Lulko, V. (2002): The PGE Mineralization of Disseminated Sulphide Ores of the Noril'sk-Taimyr Region. *In:* Cabri, L. (Ed.): The Geology, Geochemistry, Mineralogy and Mineral Beneficiation of Platinum-Group Elements, vol. 54 of *CIM Special*. Canadian Institute of Mining, Metallurgy and Petroleum, 547–567.

Korges, M. (2014): Supergene mobilisation and redistribution of platinum-group elements in the Merensky Reef, eastern Bushveld Complex, South Africa. Martin Luther University Halle-Wittenberg, msc. thesis edn., 116 pages.

Kotzé, E., Gauert, C. (2014): PGE-bearing minerals in chromitites of the Critical Zone (LG-6 to UG-3A) on Winterfeld 293KT, Eastern Bushveld Complex. IMA 2014 abstract volume, page 105.

Kozyrev, S., Komarova, M., Emelina, L., Oleshkevich, O., Yakovleva, O., Lyalimov, D., Maximov, V. (2002): The mineralogy and behavior of PGM during processing of the Noril'sk-Talnakh PGE-Cu-Ni ores. *In:* Cabri, L. (Ed.): The Geology, Geochemistry, Mineralogy and Mineral Beneficiation of Platinum-Group Elements, vol. 54 of *CIM Special*. Canadian Institute of Mining, Metallurgy and Petroleum, 757–791.

Kraemer, D. (2015): Mobility of High-Technology Metals in Earth's Surface Environment: A Study on Siderophore-Promoted Mobilization and Implications for the Extractive Hydrometallurgy of some Critical Metals. Jacobs University, phd. thesis edn., 151 pages.

Kraemer, D., Junge, M., Oberthür, T., Bau, M. (2015): Improving recoveries of platinum and

palladium from oxidized Platinum-Group Element ores of the Great Dyke, Zimbabwe, using the biogenic siderophore Desferrioxamine B. Hydrometallurgy 152, 169–177.

Kruger, F. (1990): The stratigraphy of the Bushveld Complex: a reappraisal of the Main Zone boundaries. South African Journal of Geology 93, 376–381.

Kruger, F. (1994): The Sr-isotopic stratigraphy of the Western Bushveld Complex. South Africa Journal of Geology 97, 393–398.

Kruger, F., Cawthorn, R., Walsh, K. (1987): Strontium isotopic evidence against magma addition in the Upper Zone of the Bushveld Complex. Earth and Planetary Science Letters 84, 51–58.

Kruger, F., Marsh, J. (1982): Significance of 87Sr/86Sr ratios in the Merensky Cyclic Unit of the Bushveld Complex. Nature 298, 53–55.

Kuhlmann, G., Oberthür, T., Melcher, F., Lodziak, J. (2006): Chromitithorizont - Mineralogisch-Geochemische Feinstratigraphie, Schwerpunkt Platinmetall-Verteilung. Bundesanstalt für Geowissenschaften und Rohstoffe (BGR), internal report tgb.-nr. 11327/06 edn., 162 pages [in German].

Kullerud, G., Yund, R., Moh, G. (1969): Phase relations in the Cu-Fe-S, Cu-Ni-S and Fe-Ni-S systems. *In:* Wilson, H. (Ed.): Magmatic Ore Deposits. Economic Geology Monograph 4, 323–343.

Lee, C. (1996): A Review of Mineralization in the Bushveld Complex and some other Layered Intrusions. *In:* Cawthorn, R. (Ed.): Layeres Intrusions. Amsterdam: Elsevier, 103–145.

Lee, C., Parry, S. (1988): Platinum-group element geochemistry of the Lower and Middle Group Chromitites of the eastern Bushveld Complex. Economic Geology 83, 1127–1139.

Lesher, C., Burnham, O. (2001): Multicomponent elemental and isotopic mixing in Ni-Cu-(PGE) ores at Kambalda, Western Australia. Canadian Mineralogist 39, 421–446.

Lesher, C., Groves, D. (1986): Controls on the formation of komatiite-associated nickelcopper sulphide deposits. *In:* Friedrich, G. (Ed.): eology and Metallogeny of Copper Deposits. Springer, Berlin, 43–62.

Li, C., Barnes, S.-J., Makovicky, E., Rose-Hansen, J., Makovicky, M. (1996): Partitioning of nickel, copper, iridium, rhenium, platinum, and palladium between monosulfide solid solution and sulfide liquid: Effects of composition and temperature. Geochmica et Cosmochima Acta 60, 1231–1238.

Li, C., Naldrett, A., Rucklidge, J., Kilius, L. (1993): Concentrations of platinum-group elements and gold in sulfides from the Strathconca deposit, Sudbury, Ontario. Canadian Mineralogist 30, 523–531.

Li, C., Ripley, E. (2005): Empirical equations to predict the sulfur content of mafic magmas at sulfide saturation and applications to magmatic sulfide deposits. Mineralium Deposita 40, 218–230.

Li, C., Ripley, E., Maier, W., Gomwe, T. (2002): Olivine and sisotopic compositions of the Uitkomst Ni-Cu sulfide ore-bearing complex, South Africa: evidence for S contamination and multiple magma emplacements. Chemical Geology 188, 149–159.

Li, C., Ripley, E., Merinio, E., Maier, W. (2004): Replacement of base metal sulfides by actinolite, epidote, calcite and magnetite in the UG2 and Merensky Reef of the Bushveld Complex, South Africa. Economic Geology 99, 173–184.

Li, J., Byrne, R. (1990): Amino acid complexation of palladium in seawater. Environmental Science and Technology 24, 1038–1041.

Liddell, K., McRae, L., Dunne, R. (1986): Process routes for benefication of noble metals from Merensky and UG-2 ores. Mintek Review 4, 33–44.

Lide, D. (2010): Handbook of Chemistry and Physics, 90th Edition. CRC Press/Taylor and Francis, Boca Raton, 2760 pages.

Lightfoot, P., Keays, R. (2005): Siderophile and chalcophile metal variations in flood basalts from the Siberian trap, Noril'sk region: implications for the origin of the Ni-Cu-PGE sulfide ores. Economic Geology 100, 439–462.

Lipin, B. (1993): Pressure increases, the formation of chromite seams, and the development of the ultramafic series in the Stilwater Complex, Montana. Journal of Petrology 34, 955–976.

Little, L., Becker, M., Wiese, J., Mainza, A. (2015): Auto-SEM particle shape characterisation: Investigating fine grinding of UG2 ore. Minerals Engineering online, 1–10.

Locmelis, M. (2005): The mineralogical siting of platinum-group elements in the oxidized Main Sulfide Zone at Hartlex Mine, Great Dyke, Zimbabwe. Federal Institute for Geosciences and Natural Resources (BGR) [internal report], 95 pages.

Locmelis, M., Melcher, F., Oberthür, T. (2010): Platinum-group element distribution in the oxidized Main Sulfide Zone, Great Dyke, Zimbabwe. Mineralium Deposita 45, 93–109.

Locmelis, M., Pearson, N., Barnes, S., Fiorentini, M. (2011): Ruthenium in komatiitic chromite. Geochmica et Cosmochimca Acta 75, 3645–3661.

Loferski, P. (2016): Platinum-group metals. *In:* USGS (Ed.): Mineral commodity summaries 2016. U.S. Geological Survey, 126–127.

Longerich, H. (2008): Laser ablation-inductively coupled plasma-mass spectrometry (LA-ICP-MS): An introduction. *In:* Sylvester, P. (Ed.): Laser Ablation ICP-MS in the Earth Scoences: Current Practices and Outstanding Issures. Mineralogical Association of Canada, Short Course Series 40, 1–18.

Lonzán, J. (1992): Angewandte Statistik für Naturwissenschaftler. Berlin, Parey Verlag, 237 pages.

Lorand, J.-P., Alard, O. (2001): Platinum-group element abundances in the upper mantle: New constraints from in situ and whole-rock analyses of Massif Central xenoliths (France). Geochmica et Cosmochimica Acta 65, 2789–2806.

Lorand, J.-P., Alard, O. (2011): Pyrite tracks assimilation of crustal sulfur in Pyrenean peridoites. Mineralium Deposita 101, 115–128.

Lorand, J.-P., Alard, O., Luguet, A., Keays, R. (2003): Sulfur and selenium systematics of the subcontinental lithospheric mantle: Inferences from the Massif Central xenolith suite (France). Geochmica et Cosmochimica Acta 67, 4137–4151.

López-Moro, F. (2012): EASYGRESGRANT- A Microsoft Excel spreadsheet to quantify volume changes and to perform mass-balance modeling in metasomatic systems. Computers and Geosciences 39, 191–196.

Macnamara, J., Thoede, H. (1950): Comparision of the isotopic constitution of terrestrial and meteoritic sulphur. Physical Review 46, 167–171.

Maier, W. (2005): Platinum-group element (PGE) deposits and occurrences: Mineralization styles, genetic concepts, and exploration criteria. Journal of South African Earth Science 41,

165–191.

Maier, W., Arndt, N., Curl, E. (2000): Progressive crustal contamination of the Bushveld Complex: evidence from Nd isotopic analyses of the cumulate rocks. Contributions to Mineralogy Petrology 140, 316–327.

Maier, W., Barnes, S., Groves, D. (2013): The Bushveld Complex, South Africa: Formation of platinum-palladium, chrome- and vanadium rich layers via hydrodynamic sorting of a mobilized cumulate slurry in a large, relatively slowly cooling, subsiding magma chamber. Mineralium Deposita 48, 1–56.

Maier, W., Barnes, S.-J. (2008): Platinum-group elements in the UG1 and UG2 chromitites, and the Bastard reef, at Impala platinum mine, western Bushveld Complex, South Africa: Evidence for late magmatic cumulate instability and reef constitution. South African Journal of Geology 111, 159–176.

Maier, W., de Klerk, L., Blaine, J., Manyeruke, T., Barnes, S.-J., M.V.A., S., Mavrogenes, J. (2008): Petrogenesis of contact-style PGE mineralization in the northern lobe of the Bushveld Complex: comparison of data from the farms Rooipoort, Townlands, Drenthe and Nonnenwerth. Mineralium Deposita 43, 255–280.

Makovicky, E. (2002): Ternary and Quaternary Phase Systems with PGE. *In:* Cabri, L. (Ed.): The Geology, Geochemistry, Mineralogy and Mineral Beneficiation of Platinum-Group Elements, vol. 54 of *CIM Special*. Canadian Institute of Mining, Metallurgy and Petroleum, 131–175.

Makovicky, E., Karup-Møller, S. (1993): The System Pd-Fe-S at 900°C, 725°C, 550°C, and 400°C. Economic Geology 88, 1269–1278.

Makovicky, M., Makovicky, E., Rose-Hansen, J. (1986): Experimental studies on the solubility and distribution of platinum-group elements in base metal sulphides in platinum deposits. *In:* Gallagher, M., Ixer, R., Neary, C., Pritchard, H. (Eds.): Metallurgy of basic and ultrabasic rocks, vol. 1. Institute of Mining and Metallurgy, London, 415–425.

Manyeruke, T. (2007): Compositional and lithological variation of the Platreef on the farm Nonnenwerth, northern lobe of the Bushveld Complex: Implications for the origin of Platinum-group elements (PGE) mineralization. University of Pretoria, phd thesis edn., 248 pages.

Manyeruke, T., Maier, W., Barnes, S.-J. (2005): Major and trace element geochemistry of the Platreef on the farm Townlands, northern Bushveld Complex. South African Journal of Geology 108, 381–396.

Mathez, E. (1999): On factors controlling the concentrations of platinum group elements in layered intrusions and chromitites. Geological Association of Canada Short Course Volume 13, 251–285.

McCandless, T., Ruiz, J. (1991): Osmium isotopes and crustal sources for platinum group mineralization in the Bushveld Complex, South Africa. Geology 19, 1225–1228.

McCandless, T., Ruiz, J., Adair, B., Freydier, C. (1999): Re-Os isotope and Pd/Ru variations in chromitites from the Critical Zone, Bushveld Complex SA. Geochimica et Cosmochimica Acta 63, 911–923.

McDonald, A., Pronza, J., Zaccarini, F., Rudashevsky, N., Cabri, L., Stanley, C., Rudashevsky, V., Melgarejo, C., Lews, J., Longo, F., Bakker, R. (2010): Garutiite, (Ni,Fe,Ir), a new hexagonal polymorph of native Ni from Loma Peguera, Dominican Republic. European Journal of

Mineralogy 22, 293–304.

McDonald, I., Holwell, D. (2011): Geology of the Northern Bushveld Complex and the Setting and Genesis of the Platreef Ni-Cu-PGE Deposit. *In:* Li, C., Ripley, E. (Eds.): Magmatic Ni-Cu and PGE Deposits: Geology, Geochemistry and Genesis, vol. 17 of *Review in Economic Geology*. Society of Economic Geologists, 297–327.

McDonald, I., Holwell, D., Armitage, P. (2005): Geochemistry and mineralogy of the Platreef and "Critical Zone" of the northern lobe of the Bushveld Complex, South Africa: implications for Bushveld stratigraphy and the development of PGE mineralisation. Mineralium Deposita 40, 526–549.

McDonald, I., Ohnenstetter, D., Ohnenstetter, M., Vaughan, D. (1999a): Palladium oxides in ultramafic complexes near Lavatrafo,Western Andriamena, Madagascar. Mineralogical Magazine 63, 345–352.

McDonald, I., Ohnenstetter, D., Rowe, J., Tredoux, M., Pattrick, R., Vaughan, D. (1999b): Platinum precipitation in the Waterberg deposit, Naboomspruit, South Africa. South Africa Journal of Geology 102, 184–191.

McDonough, W., Sun, S.-s. (1995): The composition of the Earth. Chemical Geology 120, 223–253.

McLaren, C., De Villiers, J. (1982): The Platinum-Group Chemistry and Mineralogy of the UG-2 Chromitite Layer of the Bushveld Complex. Economic Geology 77, 1348–1366.

Mei, Y., Etchmann, B., Liu, W., Sherman, D. M., Barnes, S., Fioretini, M., Seaward, T., Testemale, D., Brugger, J. (2015): Palladium complexation in chloride- and bisulfide-rich fluids: Insights from ab initio molecular dynamics simulations and X-ray absorption spectroscopy. Geochmica et Cosmochimica Acta 161, 128–145.

Melcher, F. (2000a): Base metal - platinum-group element sulides from the Urals and the Eastern Alps: characterization and significance for mineral systematics. Mineralogy and Petrology 68, 177–211.

Melcher, F. (2000b): Chromite and platinum-group elements as indicators of mantle petrogenesis. Montanuniversität Leoben, habilitation treatise edn., 406 pages.

Melcher, F., Buchholz, P. (2014): Germanium. *In:* Gunn, G. (Ed.): Critical Metals Handbook, vol. 1. John Wiley and Sons, 177–203.

Melcher, F., Grum, W., Simon, G., Thalhammer, T., Stumpfl, E. (1997): Petrogenesis of the Ophiolitic Giant Chromite Deposits of Kempirsai, Kazakhstan: a Study of Solid and Fluid Inclusions in Chromite. Journal of Petrology 38, 1419–1458.

Melcher, F., Grum, W., Thalhammer, T., Thalhammer, O. (1999): The giant chromite deposits at Kempirsai, Urals: constraints from trace element (PGE, REE) and isotope data. Mineralium Deposita 34, 250–272.

Melcher, F., Lodziak, J. (2007): Platinum-group minerals of concentrates from the Driekop platinum pipe, Eastern Bushveld Complex - Tribute to Eugen F. Stumpfl. Neues Jahrbuch fuer Mineralogie - Abhandlungen 183, 173–195.

Melcher, F., Lodziak, J., Jannessary, M., Meisel, T. (2010): Platinum-group element potential of chromite ores from southern Iran. 11th International Platinum Symposium, Sudbury, Canada, June 21-24, 2010, Ontario Geological Survey Miscellaneous Release-Data, 269.

Melcher, F., Oberthür, T., Lodziak, J. (2005): Modification of detrital paltinum-group minerals

from the eastern Bushveld Complex, South Africa. Canadian Mineralogist 43, 1711–1734.

Melcher, F., Stumpfl, E., Distler, V. (1994): Chromite deposits of the Kempirsai massif, southern Urals, Kazakhstan. Applied Earth Science (Transactions of the Institutions of Mining and Metallurgy: Section B) 103, 107–120.

Merensky, H. (1926): Die neuentdeckten Platinfelder im mittleren Transvaal und ihre wirtschaftliche Beudetung. Zeitschrift der Deutschen Geologischen Gessellschaft 7B, 296–314 [in German].

Merkle, R. (1992): Platinum-group minerals in the middle group of chromitite layers at Marikana, western Bushveld Complex:imdication for collection mechanism and postmagmatic modifications. Canadian Journal of Earth Science 29, 209–221.

Miller, J., Green, J., Severson, M., Chandler, V., Hauck, S., Peterson, D., Wahl, T. (2002): Geology and mineral potential of the Duluth Complex and related rocks of northeastern Minnesota. Minnesota Geological Survey Report of Investigations, 58 edn., 207 pages.

MinDat.org (2016): MinDat. `http://www.mindat.org/`. [Online; accessed October-2016].

Misra, K., Fleet, M. (1973): The chemical compositions of synthetic and natural pentlandite assemblagesx. Economic Geology 68, 518–539.

Mitchell, A. (1990): The stratigraphy, petrography and mineralogy of the Main Zone of the Northwestern Bushveld Complex. South African Journal of Geology 93, 818–831.

Mondal, S., Mathez, E. (2007): Origin of the UG2 chromitite layer, Bushveld Complex. Journal of Petrology 48, 495–510.

Mostert, A., Hofmeyr, P., Potgieter, G. (1982): The platinum-group mineralogy of the Merensky Reef at Impala Platinum Mines, Bophutatswana. Economic Geology 77, 1385–1394.

Mountain, B., Wood, S. (1988): Chemical Controls on the Solubility, Transport, and Deposition of Platinum and Palladium in Hydrothermal Solutions: Thermodynamic Approach. Economic Geology 83, 492–510.

Mudd, G. (2012): Key trends in the resource sustainability of platinum group elements. Ore Geology Reviews 46, 106–117.

Mungall, J. (2010): The association between chromite and PGE. International Platinum Symposium 11th, Sudbury, Canada, June 2010, Workshop notes.

Mungall, J., Andrews, D., Cabri, L., Sylvester, P., Tubrett, M. (2005): Partitioning of Cu, Ni, Au, and platinum-group elements between monosulfide solid solution and sulfie melt under controlled oxygen and sulfur fugacity. Geochmica et Cosmochimica Acta 69, 4349–4360.

Mungall, J., Brenan, J. (2014): Partitioning of platinum-group elements and Au between sulfide liquid and basalt and the origins of mantle-crust fractionation of the chalcophile elements. Geochmica et Cosmochimca Acta 125, 265–289.

Mungall, J., Naldrett, A. (2008): Ore Deposits of the Platinum-Group Elements. Elements 4, 253–258.

Nabrotsky, A. (2004): Energetic clues to pathways to biomineralization: precursors, clusters, and nanoparticles. Proceedings of the National Acadmie of Science 101, 12096–12101.

Naldrett, A. (1993): Models for the formation of strata-bound concentrations of platinum-group elements in layered intrusions. Geological Association of Canada Special Paper 40, 373–387.

Naldrett, A. (2004a): Magmatic Sulfide Deposits. Springer, 727 pages.

Naldrett, A. (2004b): South Africa‘s position in the world of magmatic sulfide deposits. Geo-

logical Society of South Africa Newsletter July.

Naldrett, A. (2009): Chromite composition and PGE content of Bushveld chromitites: Part 1 - the Lower and Middle Group. Applied Earth Science (Transactions of the Institutions of Mining and Metallurgy: Section B) 118, 131–161.

Naldrett, A. (2010): Secular variation of magmatic sulfide deposits and their source magma. Economic Geology 105, 669–688.

Naldrett, A. (2011): Fundamentals of Magmatic Sulfide Deposits. *In:* Li, C., Ripley, E. (Eds.): Magmatic Ni-Cu and PGE Deposits: Geology, Geochemistry and Genesis, vol. 17 of *Review in Economic Geology*. Society of Economic Geologists, 1–51.

Naldrett, A., Craig, J., Kullerud, G. (1967): The Central Portion of the Fe-Ni-S system and its bearing on pentlandite exsolution in Iron-Nickel Sulfide ores. Economic Geology 62, 826–847.

Naldrett, A., Gasparrini, E., Barnes, S., Von Gruenewaldt, G., Sharpe, M. (1986): The Upper Critical Zone of the Bushveld Complex and the origin of Merensky-type ores. Economic Geology 81, 1105–1117.

Naldrett, A., Hoffman, E., Green, A., Chou, C.-L., Naldrett, S. (1979): The composition of Ni-sulfide ores, with particular reference to their content of PGE and Au. Canadian Mineralogist 17, 403–415.

Naldrett, A., Kinnaird, A., J.and Wilson, Yudovskaya, M., Chunnett, G. (2011): Genesis of the PGE-enriched Merensky Reef and chromitite seams of the Bushveld Complex. *In:* Li, C., Ripley, E. (Eds.): Magmatic Ni-Cu and PGE Deposits: Geology, Geochemistry and Genesis, vol. 17 of *Review in Economic Geology*. Society of Economic Geologists, 235–296.

Naldrett, A., Kinnaird, J., Wilson, A., Chunnett, G. (2008): The concentration of PGE in the Earth's Crust with Special Reference to the Bushveld Complex. Earth Science Frontiers 15, 264–297.

Naldrett, A., Lehmann, J. (1987): Spinel non-stoichiometry as the explanation for Ni-, Cu-, and PGE-enriched sulphides in chromitites. *In:* Prichard, H., Potts, P., Bowles, J., Cribb, S. (Eds.): Geoplatinum ´87. London, Elsevier, 93–110.

Naldrett, A., von Gruenewaldt, G. (1989): Association of Platinum-Group Elements with Chromitite in layered intrusions and ophiolite complexes. Economic Geology 84, 180–187.

Naldrett, A., Wilson, A., Kinnaird, J., Chunnett, G. (2009): PGE Tenor and Metal Ratios within and below the Merensky Reef, Bushveld Complex: Implications for its Genesis. Journal of Petrology 50, 625–659.

Naldrett, A., Wilson, A., Kinnaird, J., Yudovskaya, M., Chunnett, G. (2012): The origin of chromites and related PGE mineralization in the Bushveld Complex: new mineralogical and pterological constraints. Mineralium Deposita 47, 209–232.

Nel, E., Theron, J. (2004): PGM ore processing at Impala's UG-2 concentrator in Rustenburg, South Africa. SGS Minerals Services Technical Paper 2004-02, 1–11.

Nielsen, H., Pilot, J., Grinenko, L., Grinenko, V., Lein, A., Smith, J., Pankina, R. (1991): Lithospheric sources of sulphur. *In:* Krouse, H., Grinenko, V. (Eds.): Stable Isotopes in the Assessment of Natural and Anthropogenic Sulphur in the Environment. Wiley and Sons, 65–132.

Normand, C., Wood, S. (2005): Effect of the trihydroxamate siderophores desferrioxamine-B and ferrichrome on the mobility of Pd, Pt, Rh and Ir. Annual Goldschmidt Conference

Abstracts 15, A329.

Nowell, G., Pearson, D., Parman, S., Luguet, A., Hanski, E. (2008): Precise and accurate 186Os/188Os and 187Os/188Os measurements by Multi-collector Plasma Ionisation Mass Spectrometry, part II: laser ablation and its application to single-grain Pt-Os and Re-Os geochronology. Chemical Geology 248, 394–426.

Oberthür, T. (2002): Platinum-group element mineralization of the Great Dyke, Zimbabwe. *In:* Cabri, L. (Ed.): The Geology, Geochemistry, Mineralogy and Mineral Beneficiation of Platinum-Group Elements, vol. 54 of *CIM Special*. Canadian Institute of Mining, Metallurgy and Petroleum, 483–506.

Oberthür, T. (2011): Platinum-group element mineralization of the main sulfide zone, Great Dyke, Zimbabwe. *In:* Li, C., Ripley, E. (Eds.): Magmatic Ni-Cu and PGE Deposits: Geology, Geochemistry and Genesis, vol. 17 of *Review in Economic Geology*. Society of Economic Geologists, 329–349.

Oberthür, T., Cabri, L., Weiser, T., McMahon, G., Müller, P. (1997a): Pt, Pd and other trace elements in sulfides of the Main Sulfide Zone, Great Dyke, Zimbabwe - a reconnaissance study. Canadian Mineralogist 35, 597–609.

Oberthür, T., Junge, M., Rudashevsky, N., de Meyer, E., Gutter, P. (2016a): Platinum-group minerals in the LG and MG chromitites of the eastern Bushveld Complex, South Africa. Mineralium Deposita 51, 71–87.

Oberthür, T., Melcher, F. (2005): PGE and PGM in the supergene environment: A case study of the persistence and redistribution in the Main Sulfide Zone of the Great Dyke, Zimbabwe. *In:* Mungall, J. (Ed.): Exploration for platinum-group element deposits: Short Course Series, Oulu Finland, vol. 35. Mineralogical Association of Canada, 97–111.

Oberthür, T., Melcher, F., Buchholz, P., Locmelis, M. (2013a): The oxidized ores of the Main Sulphide Zone, Great Dyke, Zimbabwe: turning resources into minable reserves - mineralogy is the key. The Journal of The Southern African Institute of Mining and Metallurgy 113, 191–201.

Oberthür, T., Melcher, F., Gast, L., Woehrl, C., Lodziak, J. (2004): Detrital platinum-group minerals in rivers draining the eastern Bushveld Complex. Canadian Mineralogist 42, 563–582.

Oberthür, T., Melcher, F., Goldmann, S., Wotruba, H., Gerdes, A., Dijkstra, A., Dale, C. (2016b): Mineralogy and mineral chemistry of detrital heavy minerals from the Rhine River in Germany as evidence to their provenance, sedimentary and depositional history: focus on platinum-group minerals and remarks on cassiterite, columbite-group minerals, and uraninite. International Journal of Earth Sciences 105, 637–657.

Oberthür, T., Melcher, F., Sitnikova, M., Rudashevsky, N., Rudashevsky, V., Cabri, L., Lodziak, J., Klosa, D., Gast, L. (2008): Combination of Novel Mineralogical Methods in the Study of Noble Metal Ores - Focus on Pristine (Bushveld, Great Dyke) and Placer Platinum Mineralisation. Ninth International Congress of Applied Mineralogy Brisbane, QLD, 8-10 September 2008, 187–193.

Oberthür, T., Weiser, T., Amanor, J., Chryssoulis, S. (1997b): Mineralogical siting and distribution of gold in quartz veins and sulfide ores of theAshanti mine and other deposits in the Ashanti belt of Ghana: genetic implications. Mineralium Deposita 32, 2–15.

Oberthür, T., Weiser, T., Gast, L. (1999): Mobility of PGE and PGM in supergene environemnt at Hartley Mine, Great Dyke, Zimbabwe - A case study. *In:* Stanley, C. (Ed.): Mineral deposits: processes to processing, vol. 1. Balkema, Rotterdam, 763–766.

Oberthür, T., Weiser, T., Gast, L., Kojonen, K. (2003): Geochemistry and mineralogy of platinum-group elements at Hartley Platinum Mine, Zimbabwe. Mineralium Deposita 38, 327–343.

Oberthür, T., Weiser, T., Melcher, F. (2014): Alluvial and eluvial platinum-group minerals from the Bushveld Complex, South Africa. South African Journal of Earth Sciences 117, 255–274.

Oberthür, T., Weiser, T., Melcher, F., Gast, L., Woehrl, C. (2013b): Detrital platinum-group minerals in rivers draining the Great Dyke, Zimbabwe. Canadian Mineralogist 51, 197–222.

O'Driscoll, B., Butcher, A., Latypov, R. (2014): New insights into precious metal enrichment on the Isle of Rum, Scotland. Geology today 30, 134–141.

Ohmoto, H., Rye, R. (1979): Isotopes of sulfur and carbon. *In:* Barnes, H. (Ed.): Geochemistry of hydrothermal ore deposits, vol. 2 of *London*. Wiley and Sons, 509–567.

O'Neil, H. S. C., Mavrogenes, J. (2002): The Sulfide Capacity and the Sulfur Content at Sulfide Saturation of Silicate Melts at 1400° and 1 bar. Journal of Petrology 43, 1049–1087.

Oppermann, L. (2016): PGE mobilty and distribution in oxidized soil from Thaba Mine, South Africa. Leibniz University Hannover, msc. thesis edn., 70 pages.

Osbahr, I. (2012): Platinum-group element distribution in base-metal sulfides of the Merensky Reef and UG2 from the eastern and western Bushveld Complex, South Africa. Friedrich-Alexander-Universitaet Erlangen-Nuernberg, phd. thesis edn., 168 pages.

Osbahr, I., Klemd, R., Oberthür, T., Brätz, H., Schouwstra, R. (2013): Platinum-group element distribution in base-metal sulfides of the Merensky Reef from the eastern and western Bushveld Complex, South Africa. Mineralium Deposita 48, 211–232.

Osbahr, I., Krause, M., Bachmann, K., Gutzmer, J. (2015): Efficient and Accurate Identification of Platinum-Group Minerals by a Combination of Mineral Liberation and Electron Probe Microanalysis with a New Approach to the Offline Overlap Correction of Platinum-Group Element Concentrations. Microscopy and Microanalysis 49, 1–15.

Osbahr, I., Oberthür, T., Klemd, R., Josties, A. (2014): Platinum-group element distribution in base-metal sulfides of the UG2 chromitite, Bushveld Complex, South Africa - a reconnaissance study. Mineralium Deposita 49, 655–665.

Ottemann, J., Ausustithis, S. (1967): Geochemistry and origin of "platinum nuggets" in lateritic covers from ltrabasic rocks and birbifites of W. Ethiopia. Mineralium Deposita 1, 269–277.

Pagé, P., Barnes, S.-J. (2016): The influence of chromite on osmium, iridium, ruthenium and rhodium distribution during early magmatic processes. Chemical Geology 420, 51–68.

Pagé, P., Barnes, S.-J., Bedard, J., Zientek, M. (2012): In situ determination of Os, Ir abd Ru in chromites formed from komatiite, tholeiite and boninite magmas: Implcations for chromite control of Os, Ir and Ru during partial melting and crystal fractionation. Chemical Geology 302-303, 3–15.

Paktunc, A., Hulbert, L., Harris, D. (1990): Partitioning of the platinum group and other trace elements in sulfides from the Bushveld Complex and Canadian occurrences of nickel-copper sulfides. Canadian Mineralogist 28, 475–489.

Parker, H., Whitehouse, W. (1932): An X-ray analysis of iron pyrites by the method of Fourier

Series. Philosophical Magazine 14, 939–961.

Paton, C., Hellstrom, J., Paul, B., Woodhead, J., Hergt, J. (2011): Iolite: freeware for the visualization and processing of mass spectrometric data. Journal of Analytical Atomic Spectrometry 26, 2508–2518.

Pauling, L., Huggins, M. (1934): Covalent Radii of atoms and interatomic distances in crystals containing electron-pair bonds. Contributions from Gates Chemical Laboratory, California Institute of Technolog 375, 205–238.

Penberthy, C., Merkle, R. (1999): Lateral variations in the platinum-group element content and mineralogy of the UG-2 Chrmoitite Layer Bushveld Complex. South African Journal of Geology 102, 268–281.

Penberthy, C., Oosthuyzen, E., Merkle, R. (2000): The recovery of platinum-group elements from the UG-2 chromitite, Bushveld Complex a mineralogical perspective. Mineralogy and Petrology 68, 213–222.

Penn, R., Banfield, J. (1998): Imperfect oriented attachment: dislocation generation in defect-free nanocrystals. Science 281, 696–971.

Penniston-Dorland, S., Mathez, E., Wing, B., Farquhar, J., Kinnaird, J. (2012): Multiple sulfur isotope evidence for surface-derived sulfur in the Bushveld Complex. Earth and Planetary Science Letters 337-338, 236–242.

Penniston-Dorland, S., Wing, B., Nex, P., Kinnaird, J., Farquhar, J., Brown, M., Sharman, E. (2008): Multiple sulfur isotopes reveal a magmatic origin for the Platreef platinum group element deposit, Bushveld Complex, South Africa. Geology 36, 979–982.

Piña, R., Gervilla, F., Barnes, S.-J., Oberthür, T., Lunar, R. (2016): Platinum-group element concentrations in pyrite from the Main Sulfide Zone of the Great Dyke of Zimbabwe. Mineralium Deposita online first, –.

Piña, R., Gervilla, F., Barnes, S.-J., Ortega, L., Lunar, R. (2012): Distribution of platinum-group and chalcophile elements in the Aguablanca Ni-Cu sulfide deposit (SW Spain): Evidence from a LA-ICP-MS study. Chemical Geology 302-303, 61–75.

Piña, R., Gervilla, F., Barnes, S.-J., Ortega, L., Lunar, R. (2013): Partition Coefficients of Platinum Group and Chalcophile Elements Between Arsenide and Sulfide Phases as Determined in the Beni Bousera Cr-Ni Mineralization (North Morocco). Economic Geology 108, 935–951.

Platinum Group Metals (2016): Platinum Group Metals - Waterberg Project. `http://www.platinumgroupmetals.net/projects/waterberg/default.aspx`. [Online; accessed November-2016].

Pohl, W. (2011): Economic Geology: Principals and Practice. Black Published Ltd., 663 pages.

POI, A. (2009): Apache POI - the Java API for Microsoft documents. `http://poi.apache.org/`. [Online; accessed July-2016].

Pokrovski, G., Schott, J. (1998): Thermodynamic properties of aqueous Ge(IV) hydroxide complexes from 25 to 350ŕC: Implications for the behavior of germanium and the Ge/Si ratio in hydrothermal fluids. Geochimica et Cosmochimica Acta 62, 1631–1642.

Pouget, E., Bomans, P., Goosl, J., Frederik, P., de With, G., Sommerdijk, N. (2009): The initial stages of templatecontrolled $CaCO_3$ formation revealed by cryo-TEM. The Canadian Mineralogist 323, 1455–1458.

Power, M., Pirrie, D., Jedwab, J., Stanley, C. (2004): Platinum-group element mineralization in an As-rich magmatic sulfide system, Talnotry, southwest Scotland. Mineralogical Magazine 68, 395–411.

Prendergast, M. (1988): The geology and economic potential of the PGE-rich Main Sulfide Zone of the Great Dyke, Zimbabwe. *In:* Prichard, H. (Ed.): Geoplatinum87. Elsevier, 281–302.

Prichard, H. M., Ixer, R. A., Lord, R. A., Maynard, J., Williams, N. (1994): Assemblages of platinum-group minerals and sulfides in silicate lithologies and chromite-rich rocks within the Shetland ophiolite. Canadian Mineralogist 32, 271–294.

Prichard, H. M., Lord, R. A. (1993): An overview of the PGE concentrations in the Shetland ophiolite complex. Geological Society, London, Special Publications 76, 273–294.

Prichard, H. M., Neary, C. R., Potts, P. J. (1986): Platinum group minerals in the Shetland ophiolite. *In:* Gallagher, M. J., Ixer, R. A., Neary, C. R., Prichard, H. M. (Eds.): Metallogeny of Basic and Ultrabasic Rocks. London: Institution of Mining and Metallurgy, 395–414.

Prichard, H. M., Sampson, J., Jackson, M. (2009): A further discussion of the factors controlling the distribution of Pt, Pd, Rh and Au in road dust, gullies, road sweeper and gully flusher sediment in the city of Sheffield, UK. Science of the total environment 407, 1715–1725.

Pronost, J., Harris, C., Pin, C. (2008): Relationship between footwall composition, crustal contamination, and fluid-rock interaction in the Platreef, Bushveld Complex, South Africa. Mineralium Deposita 43, 825–848.

Queffurus, M., Barnes, S.-J. (2015): A review of sulfur to selenium ratios in magmatic nickel-copper and platinum-group element deposits. Ore Geology Reviews 69, 301–324.

Rajamani, V., Prewitt, C. (1973): Crystal chemistry of natural pentlandites. Canadian Mineralogist 12, 178–187.

Rajamani, V., Prewitt, C. (1975): Thermal expansion of the pentlandite structure. American Mineralogist 60, 39–48.

Reid, D. (2014): Natural controls of platinum group mineral formation and distribution: new insights from recent advances in nanomineralogical analysis. IMA 2014 abstract volume, page 4.

Reisberg, L., Tredoux, M., Harris, C., Coftier, A., Chaumba, J. (2011): Re and Os distribution and Os isotope composition of the Platreef at the Sandsloot-Mogolakwena mine, Bushveld complex, South Africa. Chemical Geology 281, 252–263.

Reith, F., Zammit, C., Shar, S., Etschmann, B., Bottrill, R., Southam, G., Ta, C., Kilburn, M., Oberthür, T., Ball, A., Brugger, J. (2016): Biological role in the transformation of platinum-group mineral grains. Nautre geoscience online, doi:10.1038/ngeo2679.

Reuning, E. (1927): Verbandsverhältnisse und Chemismus der Gesteine des "Bushveld Igbeous Complex" Transvaals und das Problem seiner Enstehung. Neues Jahrbuch für Mineralogie 57, 631–664.

Reynolds, R. (1989): Principles of powder diffraction. *In:* Bish, L., Post, J. (Eds.): Reviews in Mineralogy and Geochemistry, volume 20. Mineralogical Society of America, 1–17.

Ridley, J. (2013): Ore Deposit Geology. Cambridge University Press, 1 edn., 398 pages.

Ripley, E. (1999): Systematics of Sulphur and oxygen isotopes in mafic igneous rocks and related Cu-Ni-PGE mineralization. *In:* Keays, R., Lesher, C., Lightfoot, P., Farrow, C. (Eds.): Dynamic processes in magmatic ore deposits and their application to mineral exploration.

Geological Association of Canada, Short Course 13, 133–158.

Ripley, E., Li, C. (2003): Sulfur isotope exchange and metal enrichment in the formation of magmatic Cu-Ni-(PGE) deposits. Economic Geology 98, 635–641.

Roelofse, F. (2012): Mineralogical, geochemical and isotopic constraints on the evolution of the lower Main Zone and Platreef on the northern limb of the Bushveld Complex. Council for Geosciences, Bulletin, 141 edn., 131 pages.

Rollinson, H. R. (1993): Using Geochemical Data: Evaluation, Presentation, Interpretation. Prentice Hall, 1 edn., 352 pages.

Rosman, K., Taylor, P. (1998): Isotopic compositions of the elements 1997. Pure and Applied Chemistry 70, 217–235.

Rudashevsky, N., Garuti, G., Anderesen, J., Kretser, Y., Rudashevsky, V., Zaccarini, F. (2002): Separation of accessory minerals from rocks and ores by hydroseparation (HS) technology: method and application to CHR-2 chromitite, Niquelandia intrusion, Brazil. Applied Earth Science (Transactions of the Institute of Mining and Metallurgy B) 111, B87–B94.

Rule, C. (1998): Hartley Platinum Mine - metallurgical processing. *In:* Prendergast, M. (Ed.): Guidebook, 8th International Platinum Symposium, Pre-Symposium Excursion to the Great Dyke of Zimbabwe, vol. 1. The Geological Society of South Africa and the South African Institute of Mining and Metallurgy, 20–22.

Salpéteur, I., Jezequel, J. (1992): Pt and Pd stream sediment geochemistry downstream from PGE-bearing ultramafics, West Andriamena area, Madagascar. Journal of Geochemical Exploration 43, 43–65.

Salpéteur, I., Martel-Jantin, B., Rakotomanana, D. (1995): Pt and Pd mobility in ferralitic soils of the West Andriamena area (Madagascar). Evidence of a supergene origin of some Pt and Pd minerals. Chronique de la Recherche Minère 520, 27–45.

Schmidt, M. (2015): Rohstoffrisikobewertung - Platingruppenmetalle. DERA, rohstoffinformationen 26 edn., 156 pages [in German].

Schneiderhöhn, H. (1931): Mineralische Bodenschätze im Südlichen Afrika. NEM-Verlag, 1 edn., 36 pages [in German].

Schneiderhöhn, H., Moritz, H. (1939): Die Oxydationszone im platinführenden Sulfidpyroxenit (Merensky-Reef) des Bushvelds in Transvaal. Zentralbl. Mineral. Geol. Paläontol. A, 1–19 [in German].

Schoenberg, R., Kruger, F., Nägler, T., Meisel, T., Kramers, J. (1999): PGE enrichment in chromitite layers and the Merensky Reef of the western Bushveld Complex; a Re-Os and Rb-Sr isotope study. Earth and Planetary Science Letters 172, 49–64.

Schollenberger, C., Simon, R. (1945): Determination of exchange capacity and exchangeable bases in soils in soil-ammonium acetate method. Soil Science 59, 13–24.

Schouwstra, R., Kinloch, E., Lee, C. (2000): A short review of the Bushveld Complex. Platinum Minerals Review 44, 33–39.

Scoates, J., Friedman, R. (2008): Precise age of the platinferous Mernenksy Reef, Bushveld Complex, South Africa by the U-Pb zircon chemical abrasion ID-TIMS technique. Econmomic Geology 103, 465–471.

Scoon, R., Mitchell, A. (2004): The platiniferous dunite pipes in the eastern limb of the Bushveld Complex: Review and comparison with unmineralized discordant ultramafic bod-

ies. South African Journal of Geology 107, 505–520.

Scoon, R., Teigler, B. (1994): Platinum element mineralization in the Critical zone of the Bushveld Complex: I. Sulfide-poor chromitites below the UG-2. Econmomic Geology 89, 1094–1121.

Seal, R. (2006): Sulfur Isotope Geochemistry of Sulfide Minerals. *In:* Vaughan, D. (Ed.): Sulfide Mineralogy and Geochemistry, vol. 61 of *Reviews in Mineralogy and Geochemistry*. Mineralogical Society of America, 633–677.

Shannon, R. (1976): Revised Effective ionic radii and systematic studies of interatomic distances in halides and chalcogenides. Acta Crystallography 32, 751–767.

Sharman, E. R., Pennigton-Dorland, S., Kinnaird, J., Nex, P., Brown, M., Wing, B. (2013): Primary origin of marginal Ni-Cu-(PGE) mineralization in layered intrusions Delta33S evidence from the Platreef, Bucheld, South Africa. Economic Geology 108, 365–377.

Sharman-Harris, E., Kinnaird, J., Harris, C., Horstmann, U., Wing, B. (2005): A new look at sulfide mineralization of the northern limb, Bushveld Complex: A stable isotope study. Applied Earth Science (Transactions of the Institute of Mining and Metallurgy B) 114, B252–B263.

Sharpe, M. (1985): Strontium isotope evidence for preserved density stratification in the Main Zone of the Bushveld Complex. Nature 316, 119–126.

Shima, H., Naldrett, A. (1975): Solubility of Sulfur in an Ultramafic Melt and the Relevance of the System Fe-S-O. Economic Geology 70, 960–967.

Shukolyukov, Y., Yakubovich, O., Mochalov, A., Kotov, A., Sal'nikova, E., Yakovleva, S., Korneev, S., Gorokhovskii, B. (2012a): New Geochronometer for the Direct Isotopic Dating of Native Platinum Minerals (^{190}Pt-^{4}He Method). Petrology 20, 491–505.

Shukolyukov, Y., Yakubovich, O., Yakovlava, S. Z., Sal'nikova, E., Kotov, A., Rytsk, E. (2012b): Geothermochronology Based on Noble Gases: III. Migration of Radiogenic He in the Crystal Structure of Native Metals with Applications to Their Isotopic Dating. Petrology 20, 1–20.

Sinyakova, E., Kosyakov, V. (2007): Experimental modeling of zoning in copper-nickel sulfide ore. Doklady Earth Sciecnes 417, 1380–1385.

Slater, J. (1964): Atomic radii in crystals. The Journal of Chemical Physics 41, 3199–3204.

Smith, J., Holwell, D., McDoanld, I. (2011): The mineralogy and petrology of platinum group element-bearing sulphide mineralisation within the Grasvally Norite-Pyroxenite-Anorthosite (GNPA) member, south of Mokopane, northern Bushveld Complex, South Afria. Applied Earth Science (Transactions of the Institute of Mining and Metallurgy B) 120, 158–174.

Smith, J., Holwell, D., McDoanld, I. (2014): Precious and base metal geochemistry and mineralogy of the Grasvally Norite-Pyroxenite-Anorthosite (GNPA) member, northern Bushveld Complex, South Africa: implications for a multistage emplacement. Mineralium Deposita 49, 667–692.

Smith, J., Holwell, D., McDoanld, I., Boyce, A. (2016): The application of S isotopes and S/Se ratios in determining ore-forming processes of magmatic Ni-Cu-PGE sulfide deposits: A cautionary case study from the northern Bushveld Complex. Ore Geology Reviews 73, 148–174.

Smith, K., Huyck, H. (1999): An overview of the Abundance, Relative Mobility and Human Toxicity of Metals. *In:* Plumlee, G., Logsdon, M. (Eds.): The Environmental Geochemistry

of Mineral Deposits, vol. 6A. Reviews in Economic Geology, 29–79.

South African Committee on Stratigraphy (1980): Straitgaphy of South Africa. Part 1. Lithostratigraphy of the Republic of South Africa, South West Africa(Namibia and the Republics of Botswana. Handbook of the Geological Survey of South Aftrica, 8 edn., 690 pages.

Stowe, C. (1994): Compositions and Tectonic Settings of Chromite Deposits through time. Economic Geology 89, 528–546.

Stumpfl, E., Tarkian, M. (1982): The Platiniferous Dunite Pipes of the Eastern Bushveld. Economic Geology 77, 1419–1431.

Subbotin, V., Korchagin, A., Savchenko, E. (2012): Platinum mineralization of the Fedorova-Pana ore node: types of ores, mineral compositions and genetic features. Vestnick of the Kola Science Center of the Russian Academy of Sciences, Apatity 1, 54–65 [in Russian].

Suárez, S., Prichard, H., Velasco, F., Fisher, P., McDonald, I. (2010): Alteration of platinum-group minerals and dispersion of platinum-group elements during progressive weathering of the Aguablanca Ni-Cu deposit, SW Spain. Mineralium Deposita 45, 331–350.

Sylvania (2010): Independent Metallurgical Statement for the Millsell Complex. Report 2nd December, 1–8.

Tabler, N. (2007): Mobilität von Platingruppenelementen in Böden. Universit Duisburg-Essen, phd. thesis edn., 207 pages [in German].

Tarkian, M., Bernhardt, H. (1984): A key-diagram for the optical determination of platinum-group minerals. Tschermaks Mineralogische und Petrographische Mitteilungen 33, 121–129.

Taylor, H. (1967): The zoned ultramafic complexes of southeastern Alaska. *In:* Wyllie, P. (Ed.): Ultramafic and related rocks. Willey and Sons Inc. New York-London-Sydney, 97–121.

Teigler, B., Eales, H. (1993): Correlation between chromite composition and PGE mineralization in the Critical Zone of the western Bushveld Complex. Mineralium Deposita 28, 291–302.

Teng, H. (2013): How ions and molecules organize to form crystals. Elements 9, 189–194.

Tharisa Mine (2016): Tharisa Mine. `http://www.tharisa.com/our-tharisa-mine.php`. [Online; accessed October-2016].

Todd, S., Keith, D., Le Roy, L., Schissel, D., Mann, E., Irvine, T. (1982): The J-M platinum-palladium reef of the Stillwater Complex,Montana: I. Stratigraphy and petrology. Economic Geology 77, 1454–1480.

Toth, R., Sato, H. (1962): Long period superlattice Cu3Au II. Journal of Applied Physics 33, 3250–3256.

Traore, D., Beauvais, A., Auge, T., Chabaux, F., Parisot, J., Cathelineau, M., Peiffert, C., Colin, F. (2006): Platinum and palladium mobility in supergene environment: The residual origin of the Pirogues River mineralization, New Caledonia. Journal of Geochemical Exploration 88, 350–354.

Tredoux, M., Lindsay, N., Davies, G., McDonald, I. (1995): The fractionation of platinum-group elements in magmatic systems, with the suggestion of a novel causal mechanism. South African Journal of Geology 98, 157–167.

Tsoupas, G., Economou-Eliopoulos, M. (2008): High PGE contents and extremely abundant PGE-minerals hosted in chromitites from the Veria ophiolite complex, northern Greece. Ore Geology Reviews 33, 3–19.

Ulmer, G. (1969): Experimental investigations of chromite spinels. *In:* Wilson, H. (Ed.): Magmatic Ore Deposits. Economic Geology Monograph 4, 114–131.

van Achterbergh, E., Ryan, C., Griffin, W. (2000): GLITTER. (version 3.0 on-line interactive data reduction for LA-ICPMS), Maquarie research Ltd.

Van der Merwe, M. (1976): The layered sequence of the Potgietersrus Limb of the Bushveld Complex. Economic Geology 71, 1337–1351.

VanTongeren, J., Mathez, E., Kelemen, P. (2010): A felsic end to Bushveld differentiation. Journal of Petrology 51, 1891–1912.

Veksler, I., Reid, D., Dulski, P., Keiding, J., Schannor, M., Hecht, L., Trumbull, R. (2015): Electrochemical Processes in a Crystal Mush: Cyclic Units in the Upper Critical Zone of the Bushveld Complex, South Africa. Journal of Petrology 56, 1229–1250.

Verma, H. R. (2007): Atomic and Nuclear Analytical Methods: XRF, Mössbauer, XPS, NAA and Ion-Beam Spectroscopic Techniques: XRF, Mossbauer, NAA and Ion-Beam Spectroscopy. Springer Berlin Heidelberg, 390 pages.

Vermaak, C. (1976): The Merensky Reef - Thoughts on its enivronment and genesis. Economic Geology 71, 1270–1298.

Vermaak, C. (1995): The Platinum-Group Metals - A global perspective. Mintek, 1 edn., 247 pages.

Viljoen, M. (1985): The distribution and main geologic features of discordant bodies of iron-rich ultramafic pegmatite in the Bushveld Complex. Economic Geology 80, 1109–1128.

Viljoen, M. (1999): The nature and origin of the Merensky Reef of the western Bushveld Complec based on geological facies and geophysical data. South African Journal of Geology 102, 221–239.

Viljoen, M., Schürmann, L. (1998): Platinum-group metals. *In:* Wilson, M., Anhaeusser, C. (Eds.): The Mineral Resources of South Africa, vol. 6 of *Cape Town*. Council for Geoscience, 532–568.

Von Gruenewald, G. (1977): The mineral resources of the Bushveld Complex. Minerals Science and Engineering 9, 83–95.

Von Gruenewald, G., Hatton, C. (1986): Geocongress 1986. Geological Society of South Africa, excursion 22a guidebook edn., 87 pages.

Von Gruenewaldt, G., Hatton, C., Merkle, R., Gain, S. (1986): Automated Scanning Electron Microscope Based Mineral Liberation Analysis. Economic Geology 81, 1067–1079.

Von Gruenewaldt, G., Hulbert, L., Naldrett, A. (1989): Contrasting platinum-group element concentration patterns in cumulates of the Bushveld complex. Mineralium Deposita 24, 219–229.

Von Gruenewaldt, G., Merkle, R. (1995): Platinum group element proportions in chromitites of the Bushveld complex: implications for fractionation and magma mixing models. South African Journal of Geology 21, 615–632.

Von Gruenewaldt, G., Worst, B. (1986): Chromite deposits at Zwartkop chrome mine, western Bushveld Complex. *In:* Anhaeusser, C., Maske, S. (Eds.): Mineral deposits of southern Africa, vol. 1. Geological Society of South Africa, 1217–1227.

Voordouw, R., Gutzmer, J., Beukes, N. (2009): Intrusive origin for Upper Group (UG1,UG2) stratiform chromitite seams in the Dwars River area, Bushveld Complex, South Africa. Min-

eralogy and Petrology 97, 75–94.

Voordouw, R., Gutzmer, J., Beukes, N. (2010): Zoning of platinum group mineral assemblages in the UG-2 chromitite determined through in situ SEM-EDS-based image analysis. Mineralium Deposita 45, 147–159.

Vorster, C. (2007): Mineral Map of the Bushveld Complex - South Africa with special reference to platinum and chrome. Council for Geoscinence.

Vukmanovic, Z., Reddy, S., Godel, B., Barnes, S., Fiorentini, M., Barnes, S.-J., Kilburn, M. (2014): Relationship between microstructures and grain-scale trace element distribution in komatiite-hosted magmatic sulphide ores. Lithos 184-187, 42–61.

Wager, L., Brown, G. (1968): Layered igneous rocks. Oliver and Boyd, Edingburg, 635 pages.

Wagner, P. (1925a): Notes on the platinum deposits of the Bushveld Igneous Complex. Transactions of the Geological Society of South Africa 28, 83–133.

Wagner, P. (1925b): The platinum deposits in the western part of the Lydenburg district, Transvaal. South African Journal of Industries 8, 90–113.

Wagner, P. (1926a): Occurrence of the platinum metals in South Africa - Part 1. Economic Geology 21, 109–134.

Wagner, P. (1926b): Occurrence of the platinum metals in South Africa - Part 2. Economic Geology 21, 243–270.

Wagner, P. (1929): The Platinum Deposits and Mines of South Africa. Oliver and Boyd, 326 pages.

Wallace, P., Carmichael, I. (1992): Sulfur in baslatic magmas. Geochimica et Cosmochimica Acta 56, 1863–1874.

Webb, S., Cawthorn, R., Nguuri, T., James, D. (2004): Gravity modeling of Bushveld Complex connectivity supported by South African seismic results. South African Journal of Geology 107, 207–218.

Weiser, T. (1991): The quantitative proof of the existence of PGE-oxides. 6th International Platinum Symposium Perth, 52.

Weiser, T. (2002): Platinum-group minerals in placer deposits. *In:* Cabri, L. (Ed.): The Geology, Geochemistry, Mineralogy and Mineral Beneficiation of Platinum-Group Elements, vol. 54 of *CIM Special*. Canadian Institute of Mining, Metallurgy and Petroleum, 721–756.

Wiese, J., Harris, P., Bradshaw, D. (2007): The response of sulphide and gangue minerals in selected Merensky ores to increased depressant dosages. Minerals Engineering 20, 986–995.

Wilson, M. (1998): A brief overview of the economic geology of South Africa. *In:* Wilson, M., Anhaeusser, C. (Eds.): The Mineral Resources of South Africa, vol. 6 of *Cape Town*. Council for Geoscience, 1–4.

Wilson, S., Ridley, W., Koenig, A. (2002): Development of sulfide calibration standards for laser ablation inductively-coupled mass spectrometry technique. Journal of Analytical Atomic Spectrometry 17, 406–409.

Wirth, R. (2004): Focused ion beam (FIB): a novel technology for advanced application of micro- and nanoanalysis in geosciences and applied mineralogy. European Journal of Mineralogy 16, 863–876.

Wirth, R. (2009): Focused Ion Beam (FIB) combined with SEMand TEM: advanced analytical tools for studies of chemical composition, microstructure and crystal structure in geomaterials

on a nanometer scale. Chemical Geology 261, 217–229.

Wirth, R., Reid, D., Schreiber, A. (2013): Nanometer-sized platinum-group minerals (PGM) in base metal sulfides: new evidence for an orthomagmatic origin of the Merensky Reef PGE ore deposit, Bushveld Complex, South Africa. Canadian Mineralogist 51, 143–155.

Wood, S. (1990): The interaction of dissolved Platinum with fulvic acid and simple organic acid analogues in aqueous solutions. Canadian Mineralogist 28, 665–673.

Wood, S. (1996): The role of humic substances in the transport and fixation of metals of economic interest (Au, Pt, Pd, U, V). Ore Geology Reviews 11, 1–31.

Wood, S. (2002): The aqueous geochemistry of the platinum-group elements with applications to ore deposits. *In:* Cabri, L. (Ed.): The Geology, Geochemistry, Mineralogy and Mineral Beneficiation of Platinum-Group Elements, vol. 54 of *CIM Special*. Canadian Institute of Mining, Metallurgy and Petroleum, 211–249.

Wood, S., Mountain, B., Pan, P. (1992): The aqueous geochemistry of Platinum, Palladium and Gold: recent experimental constraints and a re-evaluation of theoretical predictions. Canadian Mineralogist 30, 955–982.

Wood, S., Tait, C., Vlassopoulos, D., Janecky, D. (1994): Solubility and spectroscopic studies of the interaction of palladium with simple carboxylic acids and fulvic acid at low temperature. Geochimica et Cosmochimica Acta 58, 625–637.

Wood, S., Van Middlesworth, J. (2004): The influence of acetate and oxalate as simple organic ligands on the behavior of palladium in surface environments. Canadian Mineralogist 42, 411–421.

Wood, S., Vlassopoulos, D. (1990): The dispersion of Pt, Pd and Au in surfical media about two PGE-Cu-Ni prospects in Quebec. Canadian Mineralogist 28, 649–663.

Yakubovich, O., Mochalov, A., Kotov, A., Sluzhenikin, S., Okrugin, A., Danisik, M., McDonald, B., Evans, N., McInnes, B. (2015): 190Pt-4He dating of platium mineralization. Extended abstract 13th Biennial SGA Meeting Nancy, France 3, 663–665.

Yang, C.-J. (2009): An impending platinum crisis and its implications for the future of the automobil. Energy Policy 37, 1805–1808.

Yudovskaya, M., Kinnaird, J. (2010): Chromite in the Platreef (Bushveld Complex, South Africa): occurrence and evolution of its chemical composition. Mineralium Deposita 45, 369–391.

Yudovskaya, M., Kinnaird, J., Naldrett, A., Mokhov, A., McDonald, I., Reinke, C. (2011): Facies variation in PGE Mineralization in the central Platreef of the Bushveld Complex, South Africa. Canadian Mineralogist 49, 1349–1384.

Zeh, A., Ovtcharova, M., A.H., W., Schaltegger, U. (2015): The Bushveld Complex was emplaced and cooled in less than one million years - results of zirconology, and geotectonic implications. Earth and Planetary Science Letters 418, 103–114.

Zereini, F., Dirksen, F., Skerstupp, B., Urban, H. (1998): Sources of Anthropogenic Platinum-Group Elements (PGE): Automotive Catalysts versus PGE-Processing Industries. Environmental Science and Pollution Research 5, 224–230.

Zhou, M.-F., Robinson, P., Malpas, J., Li, Z. (1996): Podiform Chromitites in the Luobusa Ophiolite (SouthernTibet): Implications for Melt-Rock Interaction and Chromite Segregation in the Upper Mantle. Journal of Petrology 57, 3–21.

Ziaja, K., Melcher, F., Oberthür, T., Lodziak, J. (2007): CMineralogisch-geochemische Feinstratigraphie des Merensky Reefs (Lebowa Platinum Mines), Bushveld Komplex, Südafrika: Schwerpunkt Platinmetall-Verteilung. Bundesanstalt für Geowissenschaften und Rohstoffe (BGR), internal report 0127943 edn., 68 pages [in German].

Zientek, M., Causey, J., Parks, H., Miller, R. (2014): Platinum-Group Elements in Southern Africa-Mineral Inventory and an Assessment of Undiscovered Mineral Resources. U.S. Geological Survey Scientific Investigations, report 2010-5090-q edn., 126 pages.

MALTE JUNGE, M.SC.

UNIVERSITY EDUCATION

Since 09/2012	University, Hannover, Germany PhD student: “PGE-mobility in weathering processes”.
2010-2012	Utrecht University, the Netherlands M.Sc Geology (M.Sc: diploma 08/2012) Master thesis: “Distribution of Platinum-group elements and minerals in the UG-2 reef, Karee Mine, Western Bushveld Complex, South Africa”.
2007 - 2010	University Freiburg, Germany B.Sc Geosciences (B.Sc: diploma 08/2010) Bachelor thesis: “Symplectites in Gakkel Ridge Peridotites”.

WORK EXPERIENCE

Since 06/2015	research assistant at the BGR (Federal Institute for Geosciences and Natural Resources) Hannover, Germany on a third-party funded project (AMREP – PGE in the chromitite seams of the Bushveld Complex)
04/2015 – 05/2015	research assistant at the Leibniz University Hannover, Germany
09/2012 – 03/2015	research assistant at the BGR, Hannover, Germany (the fate of PGE during weathering processes of the Platreef, Bushveld Complex)
05/2012 – 08/2012	research assistant at the Department of Earth Sciences at Uppsala University, Uppsala, Sweden (supervisor: Prof. Dr. V. Troll)

LIST OF PUBLICATIONS

Kraemer, D., Junge, M. and Bau, M. (2017) Oxidized Ores as Future Resource for Platinum Group Metals: Current State of Research: Chemie Ingenieur Technik, v. 89, p. 1-12.

Derrey, I.T., Albrecht, M. Dupliy, E., Botcharnikov, R.E., Horn, I., Junge, M. Weyer, S. and Holtz, F. (2017) Experimental tests on achieving equilibrium in synthetic fluid inclusions: results for scheelite, molybdenite and gold solubility at 800°C and 200 MPa. American Mineralogist, v. 102, p. 275-283.

Klemd, R., Junge, M., Oberthür, T., Herderich, T., Schouwstra, R. and Roberts, J. (2016) Platinum-group element concentrations in base-metal sulphides from the Platreef, Mogalakwena Platinum Mine, Bushveld Complex, South Africa. South African Journal of Geology, v. 119, p. 623-638.

Junge, M., Oberthür, T., Osbahr, I. and Gutter, P. (2016) Platinum-group element and minerals in the Lower and Middle Group chromitites of the western Bushveld Complex, South Africa: Mineralium Deposita, v. 51, p. 841-852.

Oberthür, T., Junge, M., Rudashevsky, N., de Meyer, E. and Gutter, P., (2016) Deportment of platinoids in the LG and MG chromitites of the Bushveld Complex, South Africa: Mineralium Deposita, v. 51, p. 71-87.

Kraemer, D., Junge, M., Bau, M. and Oberthür, T. (2015) Improving recoveries of Platinum and Palladium from Oxidized Platinum-Group Element Ores of the Great Dyke, Zimbabwe, using the Siderophore Desferrioxamine B, Hydrometallurgy, v. 152, p. 169-177.

Junge, M., Wirth, R, Oberthür, T., Melcher, F. and Schreiber, A. (2015) Mineralogical siting of platinum-group elements in pentlandite from the Bushveld Complex, South Africa, Mineralium Deposita, v. 50, p. 41-54.

Junge, M., Oberthür, T. and Melcher, F. (2014) Cryptic variation of chromite chemistry, platinum-group-element and –mineral distribution in the UG-2 chromitite - an example from the Karee Mine, western Bushveld Complex, South Africa: Economic Geology, v. 109, p. 795-810.

And over 15 conference abstracts (not listed here)